Neural Plasticity

Neurological Disorders Related Neuronal Network Impairment: Function and Mechanism

Guest Editors: Sheng-tian Li, Yun Wang, and Masayuki Matsushita

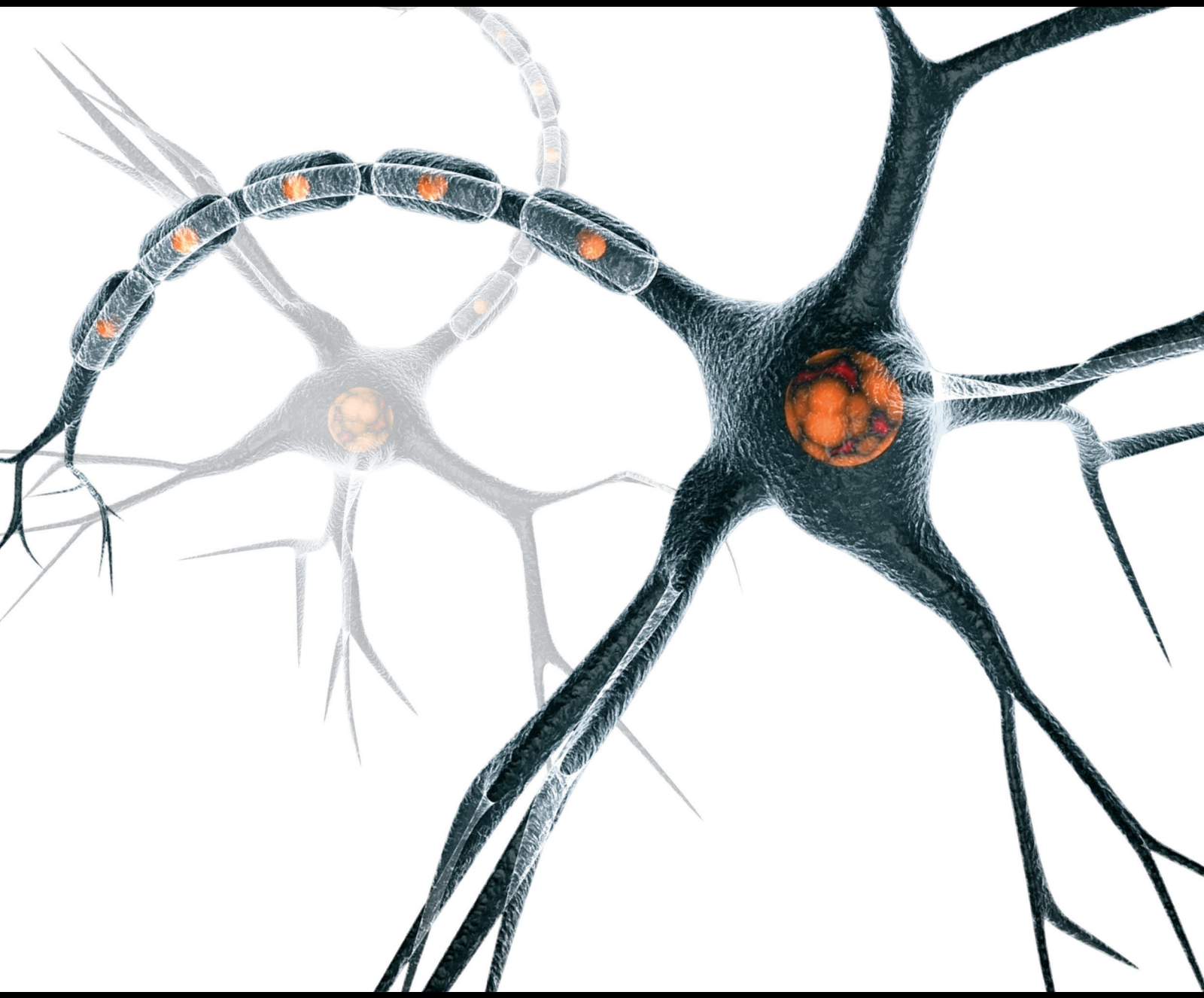

Neurological Disorders Related Neuronal Network Impairment: Function and Mechanism

Neural Plasticity

Neurological Disorders Related Neuronal Network Impairment: Function and Mechanism

Guest Editors: Sheng-tian Li, Yun Wang,
and Masayuki Matsushita

Editorial Board

Contents

Editorial

Neurological Disorders Related Neuronal Network Impairment: Function and Mechanism

Sheng-tian Li,[1] Yun Wang,[2] and Masayuki Matsushita[3]

[1] *Bio-X Institutes, Shanghai Jiao Tong University, Shanghai 200240, China*
[2] *Institutes of Brain Science and State Key Laboratory of Medical Neurobiology, Fudan University, Shanghai 200032, China*
[3] *University of the Ryukyus, 207 Uehara, Okinawa 903-0215, Japan*

Correspondence should be addressed to Sheng-tian Li; lstian@sjtu.edu.cn

Received 1 July 2014; Accepted 1 July 2014; Published 23 July 2014

Structural and functional neuronal networks provide the physiological basis for information processing and mental representations. Complex neurological disorders are characterized by structural and functional abnormalities in multiple brain areas involving several distinct brain systems. Recent advances in biology and medicine point to altered brain connectivity as a key feature of their pathophysiology. Knowledge and understanding of these deficits of neuronal networks have led to the development of animal models, successful therapies, and novel tools to characterize these clinical conditions and provide better care to patients. Inspired by the marked rise of scholarly research in these areas, this special issue attempts to provide timely collection of articles on neurological disorders, starting with recent findings on various deficits of neuronal networks and related signaling pathways in neurological disorders, and sheds light on the existing and emerging treatment concepts. The selected papers not only provide an overview of current open issues, but also identify potential lines for further research in the area of neurological disorders related neuronal network functions.

Epilepsy, particularly the temple lobe epilepsy (TLE), is a common neurological disorder worldwide; however, the underlying mechanism is still unknown. TLE is a most severe type of the epilepsy and with a high percentage becomes the untreatable seizure in clinic. In the current issue, we have three articles focused on the epilepsy study, in terms of the seizure origination in the neuronal network and functional abnormalities after the seizure. The papers by Y.-H. Li and colleagues and Y.-J. Shi and colleagues by using electrophysiological recording and mathematic modeling studied the brain structure relationship in generating the epileptiform activities during seizure initiation. They provide evidence that, in the seizure initiation period, the epileptiform activities are tended to spread from the thalamus to the hippocampus; in addition, the entorhinal cortex is not only a relay structure for epileptiform activities to the hippocampus, but also a more important brain structure in generating ictal discharges than hippocampus itself in generating epileptic seizure. Paper by S. Kong et al. further addresses the role of GABAergic inhibitory system in the chronic phase of the seizure. The paper described the phenomenon that, after a long silent period for seizure, the GABA synthetase, GABA transporters, and the GABA receptors are all significantly downregulated in the hippocampus, suggesting that the decreased GABAergic function directly contributes to the recurrent seizure occurrence.

Cognitive abilities rise steeply from infancy to young adulthood and then are either maintained or decline in older age. Brain activity studies have shown that healthy young adults develop better neurocognitive ability including working memory and attention. Evaluating working memory and attention in schizophrenia patients is usually based on traditional tasks and the interviewer's judgment. The article entitled "*A simple spatial working memory and attention test on paired symbols shows developmental deficits in schizophrenia patients*" by W. Song et al. reported a simple Spatial Working Memory and Attention Test on Paired Symbols (SWAPS). The SWAPS test has shown a plausible developmental pattern in healthy controls especially in difficulty load three and four, which developed well in the 20s group from the 10s group and then decline with the age increases.

In the spinal cord, the recurrent inhibitory circuit formed by Renshaw cells and motoneurons plays an important gated role in spinal motion loop. The dysfunction of Renshaw inhibition has been found to attribute to the cause of the motor neuron degeneration in various pathological conditions. The article entitled "*Reduced Renshaw recurrent inhibition after neonatal sciatic nerve crush in rats*" by L. Shu et al. is aimed to provide the relationships between peripheral nerve injury and spinal cord inhibitory circuit damage, particularly to the Renshaw recurrent inhibition pathway, during neonatal early development period, and discusses the possibility of Renshaw recurrent inhibition pathway being the target for neuroregeneration therapy.

Following stroke, a pathological neural plasticity termed postischemic long-term potentiation (i-LTP) often occurs over time, and emerging evidences from animal models suggest that such i-LTP plays important roles in ischemia. In their article "*Active calcium/calmodulin-dependent protein kinase II (CaMKII) regulates NMDA receptor mediated postischemic long-term potentiation (i-LTP) by promoting the interaction between CaMKII and NMDA receptors in ischemia,*" N. Wang et al. attempt to explore the mechanisms mediating i-LTP after stroke, especially in involvement of CaMKII activity and the enhancement of NMDA receptor mediated postsynaptic potentials.

The article entitled "*Enhanced expression of NR2B subunits of NMDA receptors in the inherited glaucomatous DBA/2J mouse retina,*" by L.-D. Dong et al. based on their observation of the relationships between increased expression of NMDA receptor subunit NR2B and the degeneration of retina ganglion cell in DBA/2J mice, the model for spontaneous secondary glaucoma proposed that progressive elevated intraocular pressure induced increase in NR2B expression may be associated with retina ganglion cells degeneration.

Vitamin B12 had been usually treated as sport nutrition, used to keep old people from getting anemic in past years. Recent studies have shown that vitamin B12 plays a key role in the normal functioning of the brain, nervous system, and the formation of blood. In their article entitled "*Methylcobalamin: a potential vitamin of pain killer*," M. Zhang et al. summarized recent findings about the analgesic effects and mechanisms of methylcobalamin, an activated form of vitamin B12, in clinical low back pain, neck pain, and diabetic neuropathic pain patients.

Childhood emotional trauma contributes significantly to certain psychopathologies, such as posttraumatic stress disorder (PTSD). The article entitled "*The effects of early-life predator stress on anxiety- and depression-like behaviors of adult rats,*" contributed by L.-J. Chen et al., investigated the relationships between early-life predator stress and the anxiety- or depression-like behaviors in adulthood. They showed that, in both Wistar rats and the genetic depression model of WKY rats, the early-life predator stress did not increase anxiety- or depression-like behaviors in adulthood. They propose that early-life predator stress, at least for rats, does not induce PTSD.

The selected articles capture some of the state-of-the-art research issues in neurological disorders related signaling pathways and network functions and aid in expanding our understanding of disease mechanisms. The editors hope that this issue will serve to illustrate and help future researchers on this topic.

Acknowledgments

The editors wish to express their sincere appreciation to all of those who helped in this project in one way or another. Very special thanks go to our anonymous referees for their professional and timely reviews. The editors are grateful to all authors for their scholarly contribution to this special theme issue.

Sheng-tian Li
Yun Wang
Masayuki Matsushita

Hindawi Publishing Corporation
Neural Plasticity
Volume 2014, Article ID 163908, 10 pages
http://dx.doi.org/10.1155/2014/163908

Research Article

The Effects of Early-Life Predator Stress on Anxiety- and Depression-Like Behaviors of Adult Rats

Lu-jing Chen,[1,2] Bing-qing Shen,[1,3] Dan-dan Liu,[1] and Sheng-tian Li[1]

[1] *Bio-X Institutes, Shanghai Jiao Tong University, Dongchuan Road 800, Shanghai 200240, China*
[2] *Zhiyuan College, Shanghai Jiao Tong University, Dongchuan Road 800, Shanghai 200240, China*
[3] *School of Life Science and Biotechnology, Shanghai Jiao Tong University, Dongchuan Road 800, Shanghai 200240, China*

Correspondence should be addressed to Sheng-tian Li; lstian@sjtu.edu.cn

Received 25 September 2013; Revised 12 February 2014; Accepted 12 February 2014; Published 15 April 2014

Academic Editor: Masayuki Matsushita

Childhood emotional trauma contributes significantly to certain psychopathologies, such as post-traumatic stress disorder. In experimental animals, however, whether or not early-life stress results in behavioral abnormalities in adult animals still remains controversial. Here, we investigated both short-term and long-term changes of anxiety- and depression-like behaviors of Wistar rats after being exposed to chronic feral cat stress in juvenile ages. The 2-week predator stress decreased spontaneous activities immediately following stress but did not increase depression- or anxiety-like behaviors 4 weeks after the stimulation in adulthood. Instead, juvenile predator stress had some protective effects, though not very obvious, in adulthood. We also exposed genetic depression model rats, Wistar Kyoto (WKY) rats, to the same predator stress. In WKY rats, the same early-life predator stress did not enhance anxiety- or depression-like behaviors in both the short-term and long-term. However, the stressed WKY rats showed slightly reduced depression-like behaviors in adulthood. These results indicate that in both normal Wistar rats and WKY rats, early-life predator stress led to protective, rather than negative, effects in adulthood.

1. Introduction

Many psychological diseases in adulthood are related to emotional traumas experienced during juvenility, especially depression and anxiety [1, 2]. For example, post-traumatic stress disorder (PTSD), also called post-traumatic stress reaction, is a severe anxiety disorder that develops after a person has experienced an acute, or chronic, stressor or traumatic event [3–5]. Examples of these types of stressors include natural disasters, such as floods, fires, and earthquakes. Also included are man-made traumatic events, such as physical assaults, motor-vehicle accidents, physical and sexual abuse, and witnessing violence, which produce intense negative feelings of fear or helplessness in the observer or participant [6]. Among the psychological traumas, childhood emotional trauma contributes significantly to some psychopathologies, such as PTSD. Epidemiological studies indicate that early-life stress, such as child abuse, is predominantly associated with a higher prevalence of a range of psychopathologies, particularly anxiety and depression [1, 7–12]. Therefore, it is important to study the effect of early-life psychological trauma on depressive and anxiety behaviors in adulthood.

Due to the ethical and practical limitations of applying psychological trauma on human beings, animal models are of great importance in studying the effects of psychological trauma. Over the past decades, a variety of valid animal models have been proposed for the study of stress and its effects [13–21]. Many different stressors were used in those studies, such as maternal separation, predator stress, and drug stimulation [18, 22, 23]. Predator stress is one of the most widely used stressors. Several reports have shown that rats and mice displayed anxiety- and depression-like behaviors in the short-term after exposure to predator scent or a predator per se [7, 13, 24–27]. Very few studies, however, have focused on long-term behavioral changes after predator stress. By using "cut-off behavioral criteria" (which allow for discrimination between clusters of behaviors analogous to anxious and depressive states), Tsoory et al. showed that cat urine exposure in juveniles induced anxiety- and depression-like behaviors in adulthood [7]. Miura et al. showed, however,

that predator stress could reduce the level of anxiety in both the short-term (one week) and long-term (four weeks) [12]. In Miura's research, rats were chosen as the predators of mice; thus, we cannot determine whether these outcomes resulted from the differences in the choice of predator (rat or cat). Thus, the effects of predator stress are still not clearly identified. In the current experiment, we focused on predator stress during juvenility. Since some key brain areas involved in emotion, such as the prefrontal cortex, hippocampus, and amygdale, are still undergoing significant maturation processes during this period [28], juvenile stress may affect brain development and may have significant effects even in adulthood. We modeled childhood psychological trauma by exposing juvenile Wistar rats to a feral cat to study whether or not predator stress contributes to anxiety- or depression-like behaviors in adulthood. In addition, it is known that WKY rats exhibit endogenous anxiety- and depression-like behaviors and have been proposed as an animal model for depression-like behavior [29–32]. However, the effect of predator stress on WKY rats has not been studied yet. Since Miura's research showed some protective effects of predator stress [12], we also exposed juvenile WKY rats to the same predator stress as Wistar rats to study whether early-life predator stress can affect the depression-like behavior of WKY rats.

2. Materials and Methods

2.1. Animals. All experiments were conducted according to the Health Guide for the Use and Care of Laboratory Animals of Shanghai Jiao Tong University. Male Wistar rats (3 weeks old) and male Wistar Kyoto (WKY) rats (3 weeks old) were purchased from Vital River Laboratory Animal Technology Co., Ltd., in Beijing. All rats were maintained on a 12-hr light-dark cycle with lights on at 12 a.m. and lights off at 12 p.m., at room temperature 22 ± 2°C, and at room humidity around 40%. Each rat was housed in a separate cage. WKY rats are required to be housed separately to induce the depression-like behavior; in order to reduce the effect caused by housing conditions, we housed Wistar rats separately as well. After one-week adaptation, rats (4 weeks old) were randomly divided into four groups: Wistar control, Wistar predator stress, WKY control, and WKY predator stress groups; each group consisted of 5 rats. The mean body weights of each group were 113.9 ± 2.3 g, 118.9 ± 4.6 g, 98.2 ± 2.5 g, and 96.8 ± 3.6 g, respectively. All the animals were treated alike except for the predator exposure between the control and stress groups. During the experiment, we recorded the body weight of each rat, both before and after predator stress. The percentage of weight change was calculated as (weight after predator stress—weight before predator stress)/weight before predator stress ∗ 100%.

2.2. Predator Stress. A healthy adult feral cat caught from our campus was used as the predator for rats. When being exposed to a predator, each rat was placed in a black cage, constructed by experimenters, with doors that can be opened toward the inside. Food was placed inside the cage, and the door was linked to a spring that kept the cage closed but could be opened when the cat pushed it to get the food. The door and the cage were not large enough to allow the cat entry; this avoided actual contact between the cat and the rats. After training, the cat could reach its claws into the cage to obtain the food. Before each stress, the rats were taken out for 30 min, and their weights were obtained. During the predator stress, an individual rat was put into each cage, and the cat was allowed to acquire the food inside the cages for 10 min (Figures 1(a1) and 1(a2)). Predator stress was given when the rats were 4 weeks old. The predator stress was applied 10 min per day during the dark cycle at room temperature 24 ± 1°C for 14 consecutive days. The exact time of each predator stress varied from day to day. All of the animals in the stress groups were exposed to the predator at the same time every day. The control animals were placed in another room under the same conditions except for the predator exposure.

2.3. Behavioral Tests. All behavioral tests were performed during the dark cycle at room temperature 24 ± 1°C. Each test started from around 6 p.m. and ended around 9 p.m. We performed a pre-open field test before predator stress to exclude some abnormal animals; an open field test and elevated plus maze test shortly following predator stress; and a light/dark transition test, open field test, elevated plus maze test, and forced swim test sequentially 4 weeks after the predator stress. The order of these tests is shown in Figure 1(d). Considering that the open field test would take a very long time if all of the animals were tested on the same day, we conducted an open field test on two consecutive days, with half of the control animals and half of the predator-stressed animals on each day. For all other experiments, we tested all of the animals on the same day. All the behavioral tests were recorded using a video camera and analyzed from the videotapes by using a motion tracking system (R.D, provided by MobileDatum Co., Ltd., Shanghai, China).

2.4. Open Field Test. The open field apparatus was a sound-proof box with an uncovered square box (40 × 40 × 45 cm) inside. The inside area of the apparatus was black, and testing was conducted under dim light. The rat was placed in the area with its head toward the inside of the box and allowed to behave freely for 10 min. During the test, rearing times and face-washing times were counted by the experimenters, while other data, including total distance and time in the center square, were analyzed by the motion tracking system. After each trial, the rat was returned to its home cage, and the square box was cleaned with 75% ethanol and dried with an air drier.

2.5. Elevated Plus Maze Test. The elevated plus maze consisted of two open arms (50 × 10 cm), two closed arms (50 × 10 cm), a central platform (10 × 10 cm), and 10 cm high walls that enclosed the closed arms. The four arms were 70 cm high from the floor, and the inside was completely black. A ceiling-mounted video camera recorded each trial. Each rat was placed into the center of the maze with its head toward the open arms and was allowed to freely explore for 5 min.

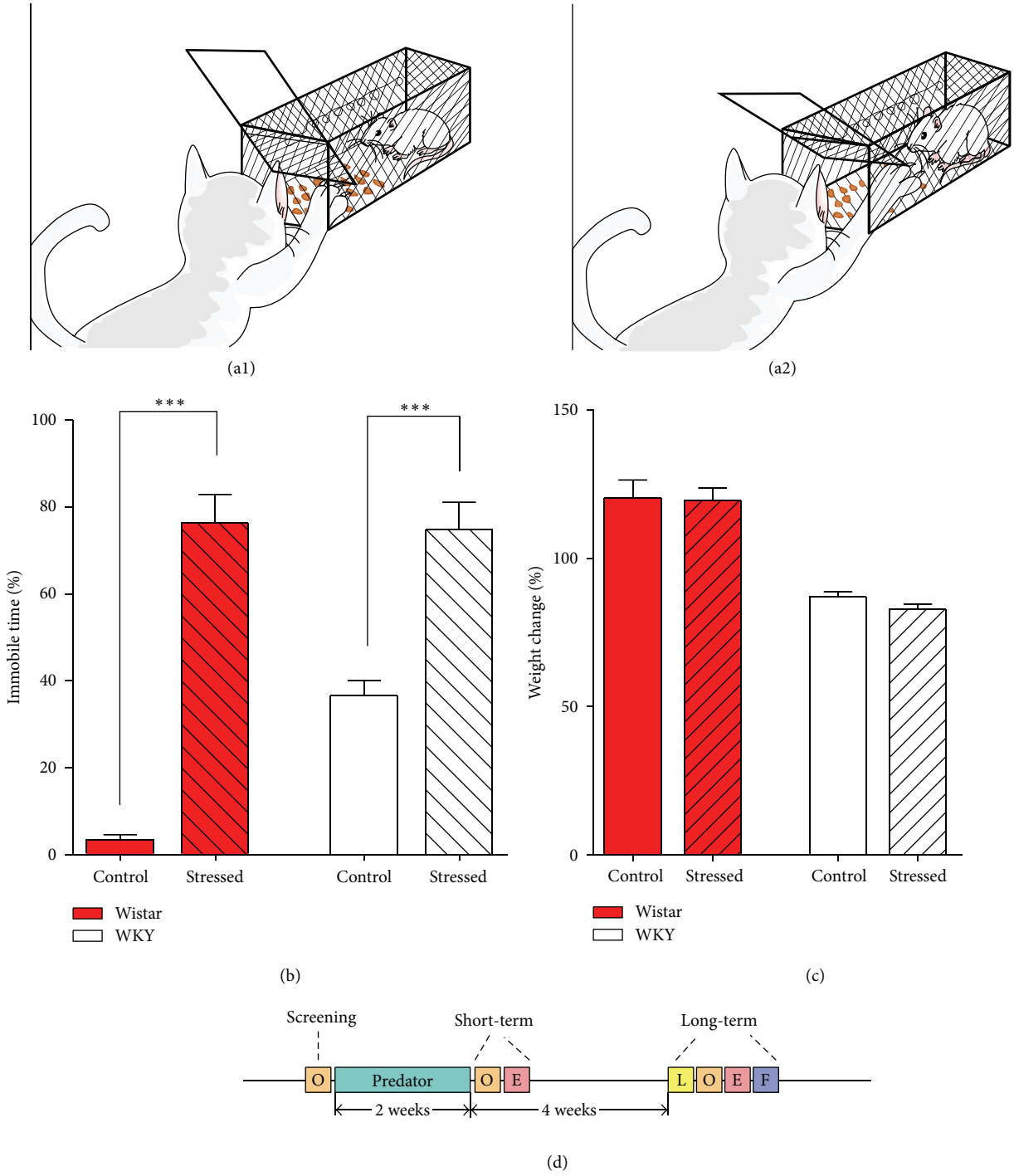

Figure 1: (a1) and (a2) procedure of predator stress. The feral cat could open the door to get the food inside, which intensely stressed the rat inside. The cage and the door were not large enough to allow the cat to fully enter, avoiding actual contact between the cat and the rat. Stimulations lasted for 10 min every day for 2 weeks. (b) Changes in the percent of freezing time of rats when exposed to predator stress. The percent of freezing time increased significantly while being exposed to a predator in both strains. Note that the control group of Wistar and WKY rats also showed differences in the percentage of freezing time. (c) Weight changes of rats before and after 2-week predator stress. Statistical differences only existed between the strains, not within the strains. Each bar indicates a group defined according to strains (Wistar rats and WKY rats) and predator exposure (red bar: Wistar rats; white bar: WKY rats; unshadowed bar: control group; shadowed bar: predator exposure). Values are shown as mean ± SEM. The results of t-test are shown. $^{***}P < 0.001$ for the effects of predator stress. (d) Procedure of experiment. O: open field test; E: elevated plus maze test; L: light/dark transition test; F: forced swim test; Predator: predator stress.

When more than half of a rat's body entered an arm, it was considered to be inside the arm. After each trial, the rat was returned to its home cage, and the floor and the walls of the maze were cleaned with 75% ethanol and dried with an air drier. Entry times to each arm and time spent on each arm were analyzed by the motion tracking system, as mentioned above. Entries into open arms (%) and time on open arms (%) were concomitantly calculated as the behavioral indexes of anxiety.

2.6. Light/Dark Transition Test. The apparatus consisted of a box (21 × 42 × 25 cm) and a video camera. A wall inside of the box separated the box into two rooms: the light box and the dark box. The two boxes were of the same size. The light box was illuminated by a white LED, while the dark box was illuminated by an infrared lamp. The roof of the apparatus could be opened in order to place the rat inside. At the beginning of the test, an individual rat was placed in the light box and was allowed to explore the boxes freely for 10 min. Behaviors were recorded by two infrared video cameras placed in the ceilings of the rooms. The latency of transmitting from the dark box to the light box, the time spent in each box, the number of transitions, and the total distance traveled were calculated and analyzed by the motion tracking system, as mentioned above. After each trial, the rat was returned to its home cage, and the two boxes were cleaned with 75% ethanol and dried with an air drier.

2.7. Forced Swim Test. The equipment of the forced swim test consisted of a cylindrical water tank (diameter = 30 cm and height = 45 cm) and a video camera placed horizontally on the side. During each trial, the tank was filled with 25 ± 1°C water up to 30 cm height. On the first day, an individual rat was placed in the water tank for 10 min to freely explore and dive. 24 h later, the rats were again placed in the water for 5 min, and the duration of immobility behavior (floating in the water without struggling) was measured by the motion tracking system mentioned above, as one of the indexes of depression-like behaviors. The rat was then removed from the water, dried with a towel, and returned to its home cage after each trial.

2.8. Statistical Analyses. Behavioral data were shown as mean ± SEM. Statistical comparisons between the control and stressed group in each strain were determined by using t-test with the alpha level set at 0.05. The differences between strains were determined by using 2 × 2 ANOVA test with the alpha level set at 0.05. All of the data were plotted using Prism software.

3. Results

3.1. Predator Stress. The open field test is well known to reflect anxiety- and depression-like behaviors of rats and mice [33]. Therefore, we used the open field test to screen all rats, in order to reduce individual variation prior to predator stress. The differences in total distance, rearing times, and face-washing times of all rats were analyzed. Results showed that only one Wistar rat's behaviors were abnormal in all of the indexes, although statistical differences did not exist between groups (see Supplemental Figure 1 in Supplementary Material available online at http://dx.doi.org/10.1155/2014/163908). Thus, we excluded this Wistar rat from further experiments.

The responses of rats to predator stress have often been evaluated by changes of self-directed behaviors, such as face-washing and sniffing [34]. Since the rats receiving predator stress in our experiment showed immobile response (an absence of obvious movements of the head and body) most of the time, we only calculated the percentage of immobile time during predator stress. The predator stress in our experimental condition did produce severe emotional stress in the rats, as indicated by the Wistar rats showing over 25 times the immobile behavior during predator stress compared to the same group before stress (Figure 1(b), before: 3.4 ± 1.2%, $N = 4$; stressed: 80.5 ± 6.5%, $N = 4$; $P < 0.001$). WKY rats, however, demonstrated two times the immobile behavior compared to the same group before stress (Figure 1(b), before: 36.6 ± 3.5%, $N = 5$; stressed: 74.8 ± 6.3%, $N = 5$; $P < 0.001$). We also calculated weight changes before and after the 2-week predator stress; no significant differences in weight were found between the control group and stressed group before and after stress in both Wistar (control: 120.3 ± 6.1%, $N = 5$; stressed: 119.7 ± 4.0%, $N = 4$; $P > 0.05$) and WKY rats (control: 87.0 ± 1.8%, $N = 5$; stressed: 82.9 ± 1.7%, $N = 5$; $P > 0.05$) (Figure 1(c)).

3.2. Short-Term Effects of Predator Stress. The short-term effects of predator stress on anxiety- and depression-like behaviors were evaluated by the open field test and the elevated plus maze test on the second day after the 2-week predator stress. Considering the high level of stress induced by the forced swim test per se, we did not perform it at this time in order to avoid a confounding effect on the adult rats' behaviors. In the open field test, predator-stressed Wistar rats showed significantly shorter total distance traveled compared to control Wistar rats (stressed Wistar, 2795.0 ± 319.7 cm, $N = 4$; control Wistar, 4024.0 ± 91.7 cm, $N = 5$; $P < 0.01$) (Figure 2(a)), while the rearing times, face-washing times, and the time spent in the central area remained unchanged (Figures 2(b)–2(d) and Supplemental Table 1). On the other hand, stressed WKY rats showed significantly less face-washing times compared to control WKY rats (Figure 2(c), stressed WKY rats, 3.6 ± 0.8, $N = 5$; control WKY rats, 6.6 ± 0.9, $N = 5$; $P = 0.0146$), while no significant differences were shown on other indexes (Figures 2(a)-2(b), 2(d), and Supplemental Table 1). In the elevated plus maze test, we calculated the percentage of time spent on the open arms and the percentage of entry times into the open arms; neither of the two indexes differed significantly between the control and the stimulated Wistar or WKY rats (Supplemental Table 2). In summary, 2-week predator stress decreased the total distance traveled of Wistar rats and face-washing time of WKY rats, respectively, in the open field test.

3.3. Long-Term Effects of Predator Stress. Early-life stress, such as child abuse, is predominantly associated with a higher

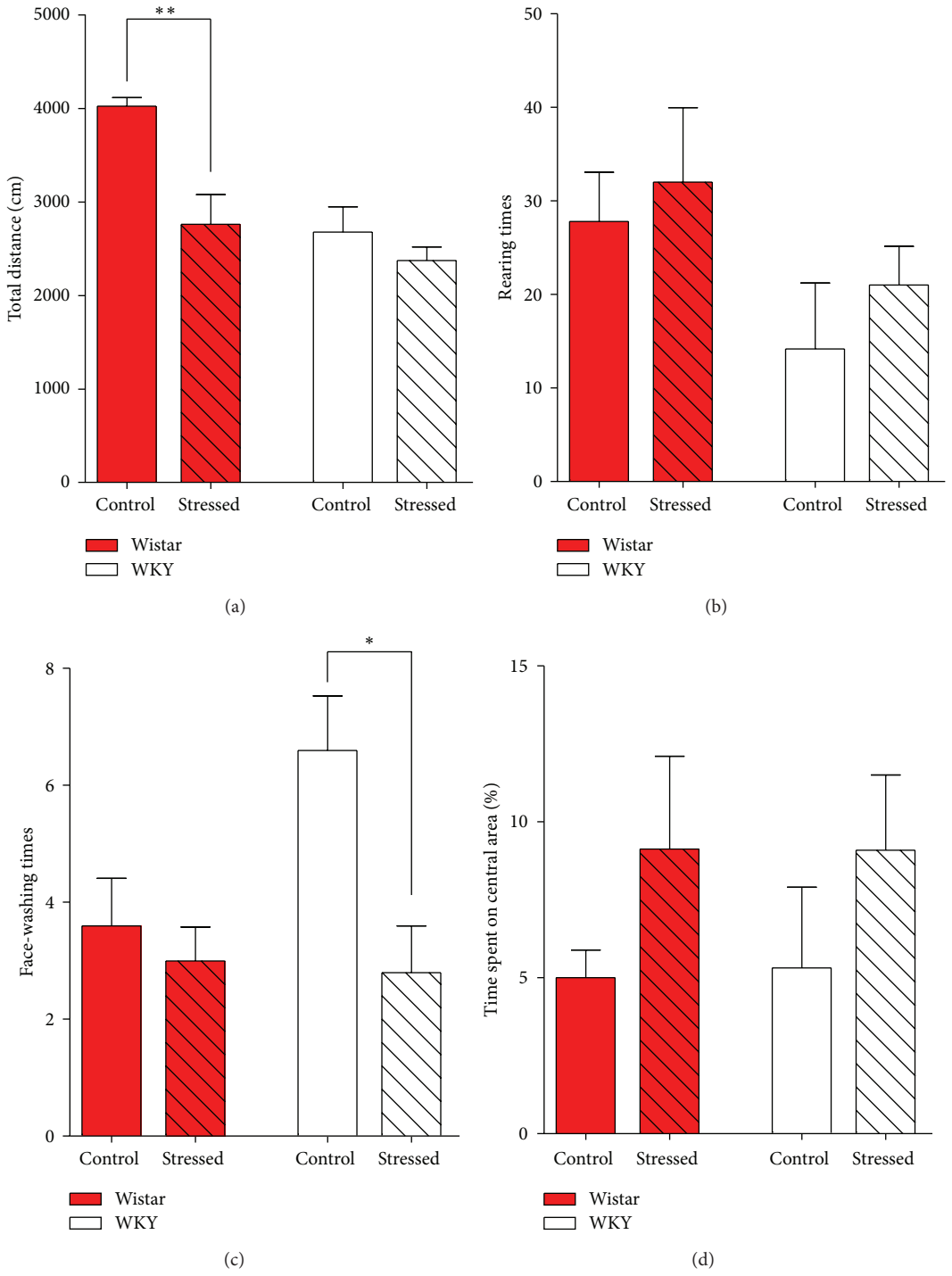

Figure 2: Total distance (a), rearing times (b), face-washing times (c), and percent of time spent on central area (d) in open field test in the short-term (two days) after 2-week predator stress. The stimulation decreased total distance traveled by Wistar rats (a) and face-washing times of WKY rats (c), respectively. Note that, compared to control Wistar rats, control WKY rats showed significantly decreased total distance (a) and increased washing times (c). Each bar indicates a group defined according to strains (Wistar rats and WKY rats) and predator exposure (red bar: Wistar rats; white bar: WKY rats; unshadowed bar: control group; shadowed bar: predator exposure). Values are shown as mean ± SEM. The results of t-test are shown. $^{*}P < 0.05$; $^{**}P < 0.01$ for the effects of predator stress.

prevalence of a range of psychopathologies, particularly anxiety and depression [1, 7–12]. Thus, we next examined the long-term effects of early-life predator stress on anxiety- and depression-like behaviors of both Wistar and WKY rats 4 weeks after the predator stress. The light/dark transition test, open field test, elevated plus maze test, and forced swim test were performed sequentially. The light/dark transition test is used to test anxiety-like behaviors of rats and mice by analyzing the latency to enter the light box, the percentage of time spent in the light box, the number of transitions, and the total distance traveled [35, 36]. As shown in Figure 3(a), Wistar rats that received early-life predator stress (34.0 ± 2.3, $N = 4$) showed significantly more transit times compared with control Wistar rats (23.6 ± 3.3, $N = 5$; $P = 0.0432$), whereas there were no obvious differences in the mean latency of entering into the light box, time spent in the light box, and total distance between stressed and control Wistar or WKY rats (Figures 3(b)–3(d) and Supplemental Table 3). Similarly, neither the open field test nor the elevated plus maze test showed statistical differences between control and stressed Wistar or WKY rats (Figures 4(a)–4(d) and Supplemental Tables 4-5). In the forced swim test, which is a canonical behavioral test used to assess depression-like behaviors of rats and mice [37, 38], the immobile time (floating without struggling) of stressed WKY rats (202.0 ± 7.8 s, $N = 5$) was significantly lower than that of control WKY rats (232.0 ± 7.5 s, $N = 4$; $P = 0.0295$), whereas Wistar rats showed no changes between the predator-stressed and control groups (Figure 5 and Supplemental Table 6). In summary, early-life predator stress increased the number of transitions of Wistar rats in the light/dark transition test and decreased immobile times of WKY rats in the forced swim test.

4. Discussion

4.1. Short-Term Effects of Predator Stress. In the current study, in order to investigate the effect of psychological trauma on anxiety- and depression-like behaviors, we applied 2-week predator stress (exposure to a feral cat) to rats (Wistar or WKY rats, 4 weeks old) and examined its effects immediately after the 2-week predator stress. Our results showed that predator stress decreased the total distance traveled by Wistar rats (Figure 2(a)) and reduced the face-washing times of WKY rats in an open field test (Figure 2(c)), respectively. This suggests that 2-week predator stress decreased spontaneous activities in Wistar rats immediately after stress but did not increase anxiety-like behaviors. Additionally, it has been reported that face-washing, as well as time spent in the central area in an open field test, represents anxiety-like behaviors [33, 39]. In addition to significantly reduced face-washing times, the predator-stimulated WKY rats also showed a tendency to increase time spent in the central area. However, no significant differences were shown in elevated plus maze test, the canonical test for anxiety-like behaviors, between control and stressed groups. This suggests that predator stress did not increase anxiety-like behaviors but had some slightly protective effects. These results differ from many previous reports [7, 13, 24–27] that have indicated that predator stress increased anxiety-like behaviors. One possible explanation for this discrepancy is the intensity of the predator stress. In our experiment, we trained the feral cat to be able to open the door of the cage and extend its paws deep into the cage, thereby intensely stressing the rat inside the cage; this was reflected by the Wistar rats showing an increase of over 25 times in immobile time during predator stress (from 3% to 80%, Figure 1(b)). Conversely, in previous research, mice showed more active behaviors, such as grooming and sniffing, rather than an immobile response, when exposed to a predator (rat) [34]. Thus, the discrepancy in the effects of predator stress on anxiety- and depression-like behaviors may be due to different intensities of predator stress.

4.2. Long-Term Effects of Predator Stress. The long-term effects of early-life predator stress on anxiety- and depression-like behaviors of both Wistar and WKY rats were examined 4 weeks after the end of the predator stress. Our results showed that early-life predator stress increased the number of transitions of adult Wistar rats in the light/dark transition test (Figure 3(a)) and decreased immobile time of adult WKY rats in the forced swim test (Figure 5). There were no obvious differences, however, in other indexes representing anxiety-like behaviors between control and predator-stimulated Wistar or WKY rats (Figures 3(b)–3(d), Figures 4(a)–4(d), and also Supplemental Tables 3–5). Taken together, these results indicate that early-life predator stress did not increase anxiety-like behaviors in adult Wistar rats and has some, although not large, protective effects. Predator stress also caused a slight decrease in the level of depression-like behaviors in adult WKY rats. Some reports have shown that predator stress could increase long-lasting (about three weeks) anxiety-like behaviors [13, 20, 21]. The most plausible explanation for the opposite long-term effect of predator stress is the intensity of predator stress, as discussed above. Interestingly, in some clinical studies, some people who suffered from psychological trauma showed posttraumatic growth [40]. Our research can be an example of posttraumatic growth on animals.

On the other hand, due to unforeseen loud noise caused by construction activity in our upstairs laboratory, all of the animals in our experiment unavoidably experienced stressful conditions from the 20th to 29th day after the end of the predator stress (it continued for 9 days before the final behavioral test battery) and may have affected the results of the behavioral tests. Nevertheless, our results still suggest that juvenile predator stress at least did not enhance depression- or anxiety-like behaviors and might provide some protective effects.

4.3. Different Effects of Predator Stress between Wistar and WKY Rats. In terms of the short-term effects, predator stress increased depression-like behaviors (decreased total distance traveled in the open field test) in Wistar rats, but not in WKY rats (Figure 2(a)). In contrast, regarding the long-term effects, predator stress relieved depression-like behaviors in the forced swim test only in WKY rats, but not in Wistar rats. Considering that WKY strain is a model for depression-like behaviors, we used two-way ANOVA to test the differences

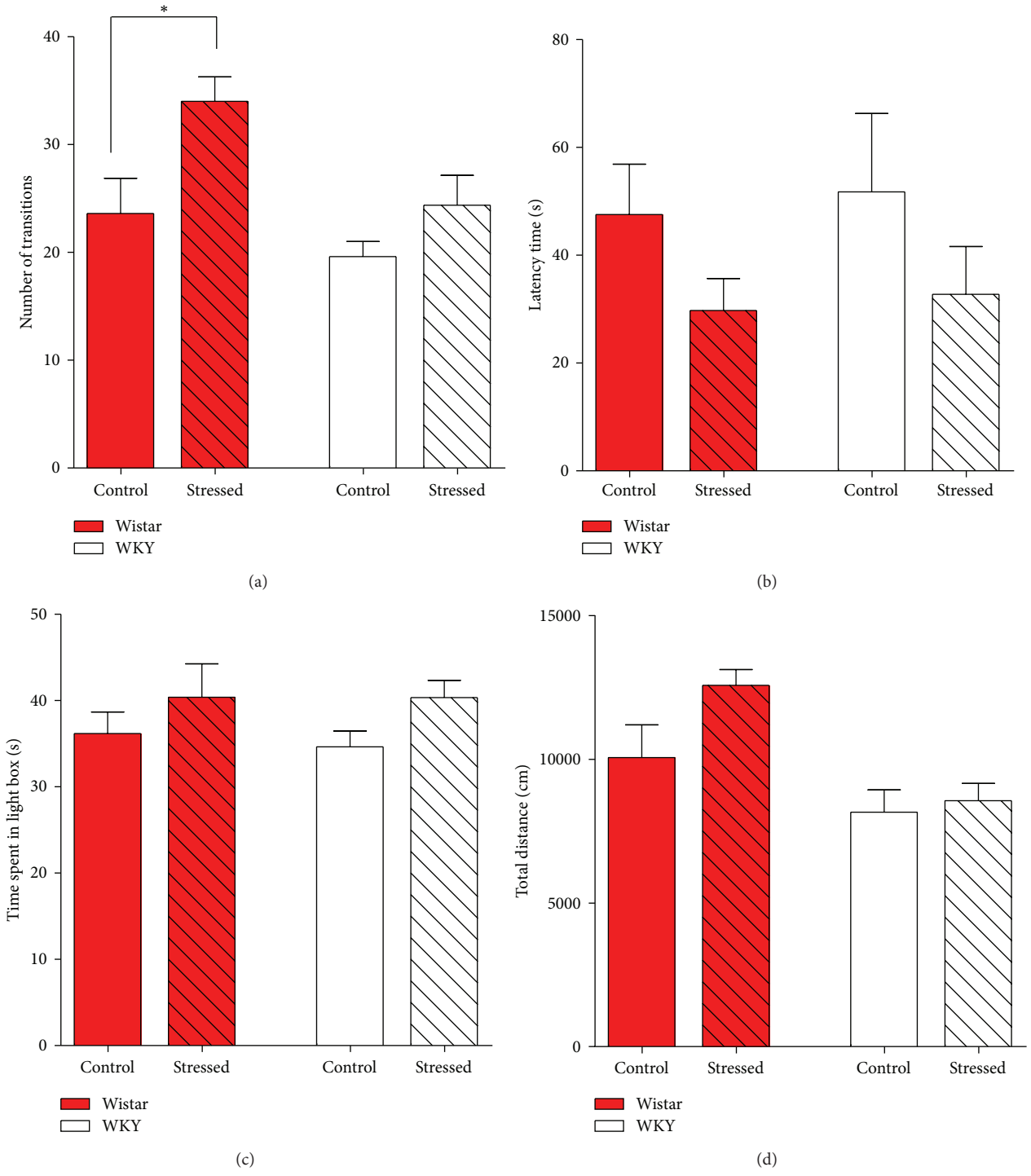

Figure 3: Behaviors of rats in light/dark transition test in the long-term (30 days) after 2-week predator stress. Wistar rats that received early-life predator stress showed significantly more number of transitions compared with control Wistar rats (a), while there were no obvious differences in latency (c), total time spent in the light box (d), and total distance between stimulated and control groups (b)–(d). Each bar indicates a group defined according to strains (Wistar rats and WKY rats) and predator exposure (red bar: Wistar rats; white bar: WKY rats; unshadowed bar: control group; shadowed bar: predator exposure). Values are shown as mean ± SEM. The results of t-test are shown. $^{*}P < 0.05$ for the effects of predator stress.

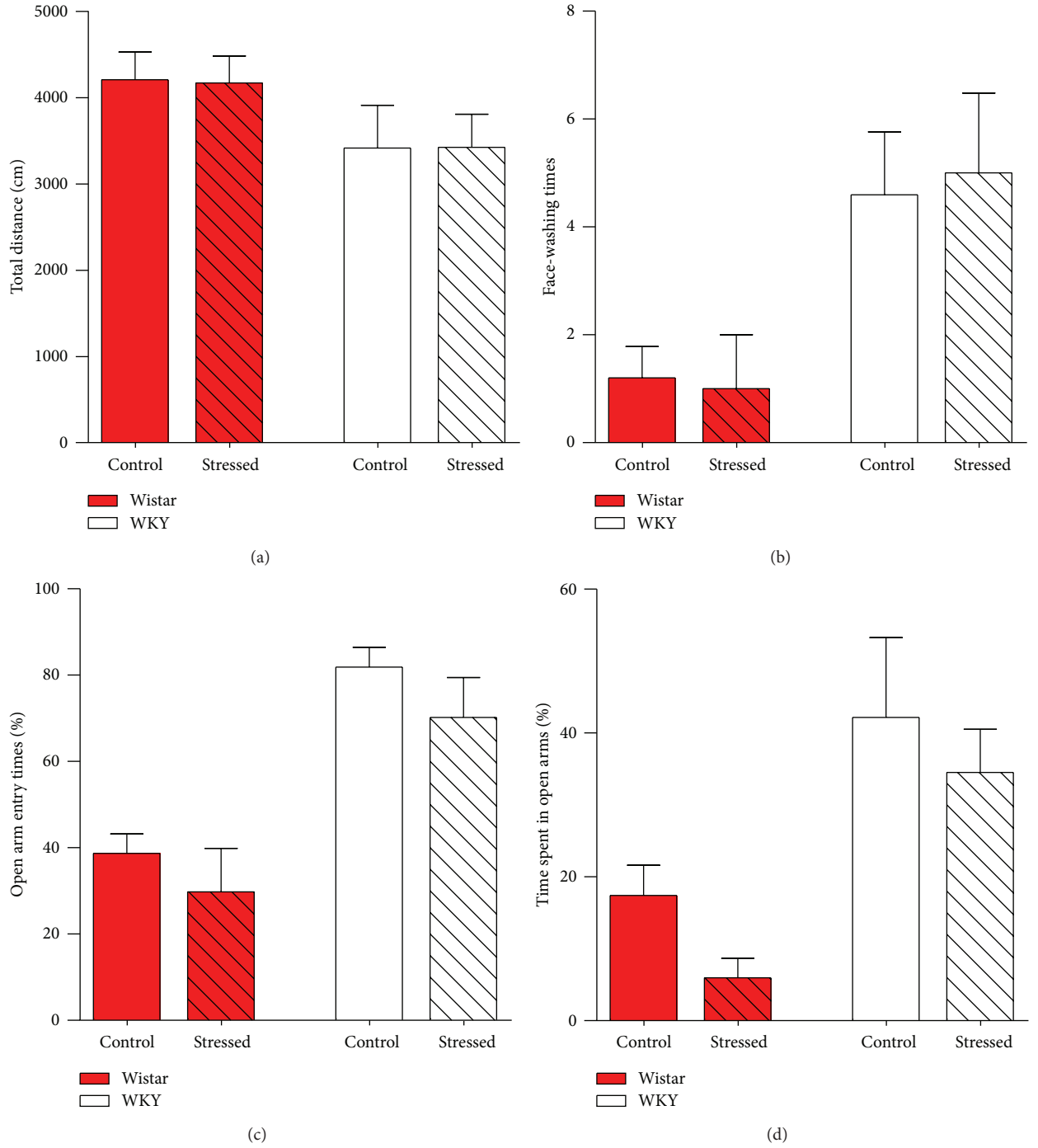

Figure 4: Behaviors of rats in open field test and elevated plus maze test in the long-term (30 days) after 2-week predator stress. (a) Total distance in open field test. (b) Face-washing times in open field test. (c) Percent of open arm entries in elevated plus maze test. (d) Percent of time spent on open arms in elevated plus maze test. No significant differences were found in the above tests between stimulated and control Wistar or WKY rats. Note that control WKY rats showed more face-washing times in open field test (b) and more open arms entry times in elevated plus maze test (c) compared with control Wistar rats. Each bar indicates a group defined according to strains (Wistar rats and WKY rats) and predator exposure (red bar: Wistar rats; white bar: WKY rats; unshadowed bar: control group; shadowed bar: predator exposure). Values are shown as mean ± SEM. The results of t-test are shown.

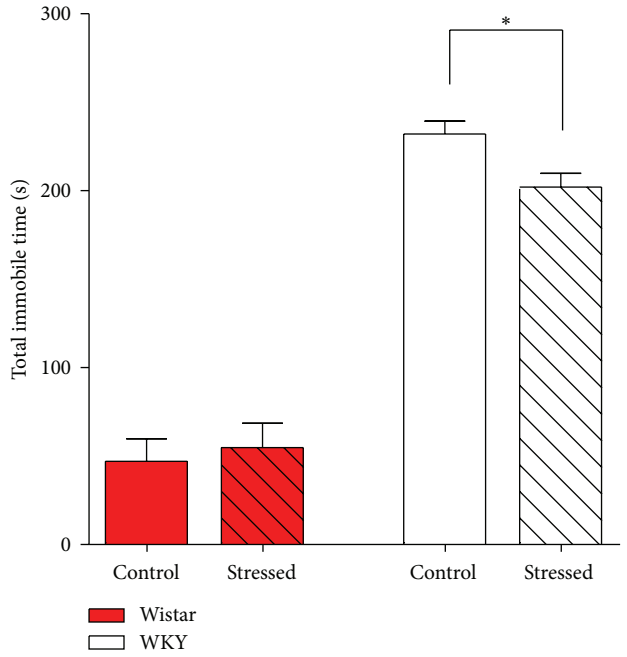

Figure 5: Immobile time of rats in forced swim test in the long-term (30 days) after 2-week predator stress. The immobile time (floating without struggling) of stimulated WKY rats was significantly lower than that of the control WKY rats, while Wistar rats showed no changes between predator-stimulated and control groups. Note that control WKY rats showed significantly longer immobile time than control Wistar rats. Each bar indicates a group defined according to strains (Wistar rats and WKY rats) and predator exposure (red bar: Wistar rats; white bar: WKY rats; unshadowed bar: control group; shadowed bar: predator exposure). Values are shown as mean ± SEM. The results of t-test are shown. $^{*}P < 0.05$ for the effects of predator stress.

between the two strains. Results showed that statistical differences exist between Wistar and WKY rats in many indexes (Supplemental Tables 7–9). These differences may contribute to the different results of behavioral tests between the two strains. Thus, the mechanisms underlying the different effects of predator stress on anxiety- and depression-like behaviors between Wistar and WKY rats require further study into the basis of the induction mechanism of depression in WKY rats.

5. Conclusions

In the current study, we show that, in Wistar rats, early-life predator stress decreased spontaneous activities in the short-term after the stimulation but did not increase anxiety- or depression-like behaviors in adulthood. In the genetic depression model rats, the WKY rats, the same early-life predator stress did not increase anxiety- or depression-like behaviors in adulthood as well. However, the predator stress slightly decreased anxiety-like behavior in Wistar rats and decreased depression-like behavior in WKY rats in adulthood. These results suggest that early-life predator stress, at least for rats, did not induce PTSD but may result in posttraumatic growth in adulthood. Further investigations are required to elucidate the neurobiological underpinnings of the effects of early-life predator stress on anxiety and depression-like behaviors.

Conflict of Interests

The authors declare that there is no conflict of interests regarding the publication of this paper.

Acknowledgments

This work was supported by Grants from the National Science Foundation of China (nos. 31271198, 81121001, and J1210047) and the Shanghai Committee of Science and Technology (no. 11ZR1415900). The authors express deep gratitude to Fei Yu, Yuhong Yang, Yifei Liu, and Jingyao Yuan for their invaluable assistance in designing and revising the experimental protocol.

References

[1] O. Agid, B. Shapira, J. Zislin et al., "Environment and vulnerability to major psychiatric illness: a case control study of early parental loss in major depression, bipolar disorder and schizophrenia," *Molecular Psychiatry*, vol. 4, no. 2, pp. 163–172, 1999.

[2] L. Arborelius, M. J. Owens, P. M. Plotsky, and C. B. Nemeroff, "The role of corticotropin-releasing factor in depression and anxiety disorders," *Journal of Endocrinology*, vol. 160, no. 1, pp. 1–12, 1999.

[3] American Psychiatric Association, *Diagnostic and Statistical Manual of Mental Disorders: DSM-IV*, American Psychiatric Association, Washington, DC, USA, 1994.

[4] D. S. Satcher, "Executive summary: a report of the Surgeon General on mental health," *Public Health Reports*, vol. 115, no. 1, pp. 89–101, 2000.

[5] A. Brunet, V. Akerib, P. Birmes, H. Merskey, and A. Piper, "Don't throw out the baby with the bathwater (PTSD is not overdiagnosed)," *Canadian Journal of Psychiatry*, vol. 52, no. 8, pp. 501–503, 2007.

[6] Mayo Clinic staff, "Post-traumatic stress disorder (PTSD)," Mayo Foundation for Medical Education and Research, 2011.

[7] M. Tsoory, H. Cohen, and G. Richter-Levin, "Juvenile stress induces a predisposition to either anxiety or depressive-like symptoms following stress in adulthood," *European Neuropsychopharmacology*, vol. 17, no. 4, pp. 245–256, 2007.

[8] C. Heim and C. B. Nemeroff, "The role of childhood trauma in the neurobiology of mood and anxiety disorders: preclinical and clinical studies," *Biological Psychiatry*, vol. 49, no. 12, pp. 1023–1039, 2001.

[9] C. Heim, P. M. Plotsky, and C. B. Nemeroff, "Importance of studying the contributions of early adverse experience to neurobiological findings in depression," *Neuropsychopharmacology*, vol. 29, no. 4, pp. 641–648, 2004.

[10] E. A. Young, J. L. Abelson, G. C. Curtis, and R. M. Nesse, "Childhood adversity and vulnerability to mood and anxiety disorders," *Depression and Anxiety*, vol. 5, pp. 66–72, 1997.

[11] R. Famularo, R. Kinscherff, and T. Fenton, "Psychiatric diagnoses of maltreated children: preliminary findings," *Journal of*

the American Academy of Child and Adolescent Psychiatry, vol. 31, no. 5, pp. 863–867, 1992.

[12] H. Miura, Y. Ando, Y. Noda, K. Isobe, and N. Ozaki, "Long-lasting effects of inescapable-predator stress on brain tryptophan metabolism and the behavior of juvenile mice," *Stress*, vol. 14, no. 3, pp. 262–272, 2011.

[13] R. E. Adamec and T. Shallow, "Lasting effects on rodent anxiety of a single exposure to a cat," *Physiology and Behavior*, vol. 54, no. 1, pp. 101–109, 1993.

[14] H. Cohen, J. Zohar, M. A. Matar, K. Zeev, U. Loewenthal, and G. Richter-Levin, "Setting apart the affected: the use of behavioral criteria in animal models of post traumatic stress disorder," *Neuropsychopharmacology*, vol. 29, no. 11, pp. 1962–1970, 2004.

[15] R. Adamec, "Transmitter systems involved in neural plasticity underlying increased anxiety and defense implications for understanding anxiety following traumatic stress," *Neuroscience and Biobehavioral Reviews*, vol. 21, no. 6, pp. 755–765, 1997.

[16] R. E. Adamec, P. Burton, T. Shallow, and J. Budgell, "NMDA receptors mediate lasting increases in anxiety-like behavior produced by the stress of predator exposure—implications for anxiety associated with posttraumatic stress disorder," *Physiology and Behavior*, vol. 65, no. 4-5, pp. 723–737, 1998.

[17] R. E. Adamec, T. Shallow, and J. Budgell, "Blockade of CCK(B) but not CCK(A) receptors before and after the stress of predator exposure prevents lasting increases in anxiety-like behavior: implications for anxiety associated with posttraumatic stress disorder," *Behavioral Neuroscience*, vol. 111, no. 2, pp. 435–449, 1997.

[18] H. Cohen, S. Friedberg, M. Michael, M. Kotler, and K. Zeev, "Interaction of CCK-4 induced anxiety and post-cat exposure anxiety in rats," *Depression and Anxiety*, vol. 4, pp. 144–145, 1996.

[19] H. Cohen, J. Benjamin, Z. Kaplan, and M. Kotler, "Administration of high-dose ketoconazole, an inhibitor of steroid synthesis, prevents posttraumatic anxiety in an animal model," *European Neuropsychopharmacology*, vol. 10, no. 6, pp. 429–435, 2000.

[20] H. Cohen, Z. Kaplan, and M. Kotler, "CCK-antagonists in a rat exposed to acute stress: implication for anxiety associated with post-traumatic stress disorder," *Depression and Anxiety*, vol. 10, pp. 8–17, 1999.

[21] H. Cohen, J. Zohar, and M. Matar, "The relevance of differential response to trauma in an animal model of posttraumatic stress disorder," *Biological Psychiatry*, vol. 53, no. 6, pp. 463–473, 2003.

[22] M. M. Sánchez, C. O. Ladd, and P. M. Plotsky, "Early adverse experience as a developmental risk factor for later psychopathology: evidence from rodent and primate models," *Development and Psychopathology*, vol. 13, no. 3, pp. 419–449, 2001.

[23] R. S. Duman and L. M. Monteggia, "A neurotrophic model for stress-related mood disorders," *Biological Psychiatry*, vol. 59, no. 12, pp. 1116–1127, 2006.

[24] F. Berton, E. Vogel, and C. Belzung, "Modulation of mice anxiety in response to cat odor as a consequence of predators diet," *Physiology and Behavior*, vol. 65, no. 2, pp. 247–254, 1998.

[25] D. C. Blanchard, R. J. Blanchard, and R. J. Rodgers, "Pharmacological and neural control of anti-predator defense in the rat," *Aggressive Behavior*, vol. 16, no. 3-4, pp. 165–175, 1990.

[26] H. Zangrossi Jr. and S. E. File, "Behavioral consequences in animal tests of anxiety and exploration of exposure to cat odor," *Brain Research Bulletin*, vol. 29, no. 3-4, pp. 381–388, 1992.

[27] A. Calvo-Torrent, P. F. Brain, and M. Martinez, "Effect of predatory stress on sucrose intake and behavior on the plus-maze in male mice," *Physiology and Behavior*, vol. 67, no. 2, pp. 189–196, 1999.

[28] L. P. Spear, "The adolescent brain and age-related behavioral manifestations," *Neuroscience and Biobehavioral Reviews*, vol. 24, no. 4, pp. 417–463, 2000.

[29] R. De La Garza II and J. J. Mahoney III, "A distinct neurochemical profile in WKY rats at baseline and in response to acute stress: implications for animal models of anxiety and depression," *Brain Research*, vol. 1021, no. 2, pp. 209–218, 2004.

[30] A. Lahmame, D. E. Grigoriadis, E. B. De Souza, and A. Armario, "Brain corticotropin-releasing factor immunoreactivity and receptors in five inbred rat strains: relationship to forced swimming behaviour," *Brain Research*, vol. 750, no. 1-2, pp. 285–292, 1997.

[31] A. Lahmame, C. Del Arco, A. Pazos, M. Yritia, and A. Armario, "Are Wistar-Kyoto rats a genetic animal model of depression resistant to antidepressants?" *European Journal of Pharmacology*, vol. 337, no. 2-3, pp. 115–123, 1997.

[32] C. López-Rubalcava and I. Lucki, "Strain differences in the behavioral effects of antidepressant drugs in the rat forced swimming test," *Neuropsychopharmacology*, vol. 22, no. 2, pp. 191–199, 2000.

[33] T. Miyakawa, M. Yamada, A. Duttaroy, and J. Wess, "Hyperactivity and intact hippocampus-dependent learning in mice lacking the M1 muscarinic acetylcholine receptor," *Journal of Neuroscience*, vol. 21, no. 14, pp. 5239–5250, 2001.

[34] M. Beekman, C. Flachskamm, and A. C. E. Linthorst, "Effects of exposure to a predator on behaviour and serotonergic neurotransmission in different brain regions of C57BL/6N mice," *European Journal of Neuroscience*, vol. 21, pp. 2825–2836, 2005.

[35] J. N. Crawley, "Exploratory behavior models of anxiety in mice," *Neuroscience and Biobehavioral Reviews*, vol. 9, no. 1, pp. 37–44, 1985.

[36] K. Takao and T. Miyakawa, "Light/dark transition test for mice," *Journal of Visualized Experiments*, no. 1, article e104, 2006.

[37] B. Petit-Demouliere, F. Chenu, and M. Bourin, "Forced swimming test in mice: a review of antidepressant activity," *Psychopharmacology*, vol. 177, no. 3, pp. 245–255, 2005.

[38] R. D. Porsolt, A. Bertin, and M. Jalfre, "'Behavioral despair' in rats and mice: strain differences and the effects of imipramine," *European Journal of Pharmacology*, vol. 51, no. 3, pp. 291–294, 1978.

[39] A. A. Walf and C. A. Frye, "The use of the elevated plus maze as an assay of anxiety-related behavior in rodents," *Nature Protocols*, vol. 2, no. 2, pp. 322–328, 2007.

[40] S. Joseph, D. Murphy, and S. Regel, "An affective-cognitive processing model of post-traumatic growth," *Clinical Psychology & Psychotherapy*, vol. 19, no. 4, pp. 316–325, 2012.

Hindawi Publishing Corporation
Neural Plasticity
Volume 2014, Article ID 786985, 11 pages
http://dx.doi.org/10.1155/2014/786985

Research Article

Reduced Renshaw Recurrent Inhibition after Neonatal Sciatic Nerve Crush in Rats

Liang Shu,[1] Jingjing Su,[1] Lingyan Jing,[2] Ying Huang,[1] Yu Di,[1] Lichao Peng,[2] and Jianren Liu[1]

[1] *The Department of Neurology, Shanghai Ninth People's Hospital Affiliated Shanghai Jiao Tong University School of Medicine, Shanghai 200011, China*
[2] *The Department of Anaesthesia, The Fifth People's Hospital of Shanghai, Fudan University, Shanghai 200240, China*

Correspondence should be addressed to Lichao Peng; plichao@foxmail.com and Jianren Liu; liujr021@vip.163.com

Received 11 December 2013; Accepted 11 February 2014; Published 23 March 2014

Academic Editor: Yun Wang

Renshaw recurrent inhibition (RI) plays an important gated role in spinal motion circuit. Peripheral nerve injury is a common disease in clinic. Our current research was designed to investigate the change of the recurrent inhibitory function in the spinal cord after the peripheral nerve crush injury in neonatal rat. Sciatic nerve crush was performed on 5-day-old rat puppies and the recurrent inhibition between lateral gastrocnemius-soleus (LG-S) and medial gastrocnemius (MG) motor pools was assessed by conditioning monosynaptic reflexes (MSR) elicited from the sectioned dorsal roots and recorded either from the LG-S and MG nerves by antidromic stimulation of the synergist muscle nerve. Our results demonstrated that the MSR recorded from both LG-S or MG nerves had larger amplitude and longer latency after neonatal sciatic nerve crush. The RI in both LG-S and MG motoneuron pools was significantly reduced to virtual loss (15–20% of the normal RI size) even after a long recovery period upto 30 weeks after nerve crush. Further, the degree of the RI reduction after tibial nerve crush was much less than that after sciatic nerve crush indicatig that the neuron-muscle disconnection time is vital to the recovery of the spinal neuronal circuit function during reinnervation. In addition, sciatic nerve crush injury did not cause any spinal motor neuron loss but severally damaged peripheral muscle structure and function. In conclusion, our results suggest that peripheral nerve injury during neonatal early development period would cause a more sever spinal cord inhibitory circuit damage, particularly to the Renshaw recurrent inhibition pathway, which might be the target of neuroregeneration therapy.

1. Introduction

Recurrent inhibition (RI) is a basic type of neuronal circuit throughout the central nervous system. In the spinal cord, Renshaw cell is the only interneuron in the spinal ventral horn that receives afferents directly from motoneurons and mediates recurrent inhibition back to the motoneuron themselves, through the corelased inhibitory neurotransmitters of glycine and GABA [1–7]. Renshaw cells and motoneurons thus form a recurrent inhibitory circuit that controls motor output. Individual Renshaw cell receives inputs from particular motor pools and spreads its inhibitory output to the same motoneurons, their synergists (i.e., motor pools exerting a similar action on the same joint), and sometimes selo ected motor pools across joints [2]. The RI is one of the important regulatory mechanisms synchronizing all muscles contract action [1–3], thus playing an important gated role in spinal motion loop [2, 8]. Renshaw inhibition dysfunction or even Renshaw cell loss has been attributed to the cause of the motoneuron degeneration in pathological conditions such as amyotrophic lateral sclerosis [4, 9, 10]. Sciatic nerve injury is a common disease of peripheral nerve in clinic with complex pathophysiological mechanism. Following nerve injury, the regenerated muscle and motoneuron were functionally disturbed, such as denervated amyotrophy and myoceptor degeneration [11]. These factors restricted functional recovery of the injured neurons. The findings that motoneuron was able to resubject muscle by regeneration and finally full or nearly full recovery in adult animals with sciatic nerve injury [12], but with reduced excitatory postsynaptic

potentials, indicated the plasticity of motoneuron central synapses after transiently losing a link between motoneuron and its controlled muscle [13–15]. The RI might act as a variable gain regulator at the motoneuronal level rather than modifying the pattern of motor activity. Studies on the cats primarily demonstrated that axon function degeneration makes injured motoneuron axon collateral die out [16, 17] and adjacent neuron transiently decreased after a part of peripheral nerve axon regenerated which had been cut off then back to normal upon nerve regeneration [18]. Therefore, we presumed that spinal motor reflex is enhanced due to weak motoneuron RI because of axon abscission [19].

Our own previous study indeed demonstrated that after sciatic nerve crush at adult, the RI after the subsequent nerve regeneration was likely permanent impaired, despite the fact that the injured spinal motoneurons and the related hindlimb muscles were fully recovered [20]. However, there were no reports, so far, about the influence on spinal RI by sciatic nerve injury during early neonatal period. Our current research further investigated the relationship between RI changes and the motoneuron functional self-regulation in adult rats after transient neonatal sciatic nerve crush injury, which had a significant meaning to identify mechanism of nerve regeneration.

2. Materials and Methods

2.1. Animals. Wistar rats were maintained on an ad libitum feeding schedule and kept on a 12 hr on/off light cycle at 22 ± 1°C. All animal experiments were approved by the local committee of Laboratory Animals of Jiao Tong University School of Medicine and carried out in accordance with Chinese National Science Foundation animal research regulation. At the end of the experiments, the rats were euthanized by anesthetic overdose.

2.2. Peripheral Nerve Crush Injury in 5-Day-Old Rats. The peripheral nerve crush model is the preferred model for mimicking the pathophysiology that occurs most commonly in humans [21]. The basic principle of the nerve crush model is to use an injury device to deliver a force that can be adjusted to control the contusion severity. Thus, in 5-day-old baby rats, under ice cold anesthesia, the left hindlimb was exposed in the middle of the thigh and the sciatic nerve was then crushed with fine watchmaker forceps for five seconds in the popliteal fossa. In some preparations, nerve crush was carried out on tibial (Tib) nerve where the nerve crush site was below the branching point of the peroneal and tibial nerves and above the branching point of gastrocnemius-soleus nerves; thus, the crush site on the tibial nerve was about 3 mm away from the point where nerve enters into the gastrocnemius-soleus muscles (Figure 5(a)). It was (about 3 mm) closer to the muscles than that crushed on sciatic nerve (about 10 mm), which led to the result that the disconnected muscle after tibial nerve crush could be reinnervated in shorter time than that in sciatic nerve crush. After the crush, care was taken to preserve the epineurium, to facilitate regeneration of the nerves along their endoneural sheaths. This was done by visual control under a dissecting microscope. The skin was then sutured. When the animals recovered from the anesthetic, the baby rats were returned to their mother. Following nerve crush, rats were allowed to recover for at least 7 weeks and reinnervation of muscles was allowed to proceed unhindered.

Sham or injured rats were then randomly divided into groups as follows: Sham operated 5-day-old rats (Sham), 5-day-old sciatic nerve crush rats with 7-week reinnervation (5SC7), 5-day-old sciatic nerve crush rats with 30-week reinnervation (5SC30), and 5-day-old tibial nerve crush rats with 14-week reinnervation (5TC14).

2.3. Electrophysiological Experiment in Reinnervated Adult Rats. Rats recovered from the nerve crush at 5 days old at 7, 14, or 30 weeks were reanesthetized with α-chlorose (400 mg/kg, i.p.). The absence of a withdrawal reflex was used to judge the anesthesia level during the whole experimental period, and additional anesthetic (α-chlorose, 100 mg/kg, i.p.) was administered when necessary. During the experiment, body temperature was maintained at 37.0 ± 0.5°C with a heating blanket (Harvard Apparatus Limited, Edenbridge, UK) similar to previously reported [22].

Left ventral aspect hind leg was operated and the lateral gastrocnemius-soleus (LG-S) nerve and medial gastrocnemius (MG) nerve were separated from sciatic nerve and its branch then cut off the remote end in order to recording or stimulated. The back closed side of the fifth lumbar (L5) dorsal nerve root was cut off then stimulated for evoking monosynaptic reflexes (MSRs). Rat was then moved to stereotaxic instrument. The exposed vertebra and leg tissue and skin were fixed on both sides of stereotaxic frame to form a cube-pool filled with 37°C paraffin. Three pairs of silver bipolar electrode (0.5 mm silver, WPI) was used to either stimulate or record. Stimulation testing electrode (E1): it is put into spinal petrolin cube-pool and fixed with dissociated point of L5 dorsal nerve root to activate MSRs; MSRs recording electrode (E2): it is put into hind leg petrolin cube-pool and fixed with incomplete branch of near point of MG nerve or G-S nerve to record MSRs; adverse conditions stimulation electrode (E3): it is put into hind leg petrolin cube-pool and fixed with incomplete branch of near point of MG nerve or G-S nerve to produce reverse impulse (see Figure 1(a)).

2.4. Electrophysiology Data Acquisition and Analysis. Dorsal root of L5 was stimulated at a frequency of 1 Hz and intensity of 2–5 V to evoke MSRs, and the stimulus strength related to input/output relation was first studied to explore the threshold for MSR generation and the maximal response of the MSR (Figure 1(b)). The maximal MSR response was later used for all the experiments with the stimulus strength at 5x-threshold. Recorded MSRs were amplified (×1000) (Neurology System, Digitimer, UK) and input to a computer via CED1401 and processed by Spike2 (Cambridge Electronics, UK). Condition stimulus was delivered 0–50 ms before testing stimulus, and the interval was set at 0, 2, 3, 4, 5, 8, 15, 30, 40, and 50 ms. RI was expressed as the percentage reduction of the MSR amplitude.

2.5. Horseradish Peroxidase (HRP) Retrograde Marked G-S Motoneuron Pool. In some of the 5SC7 group animals,

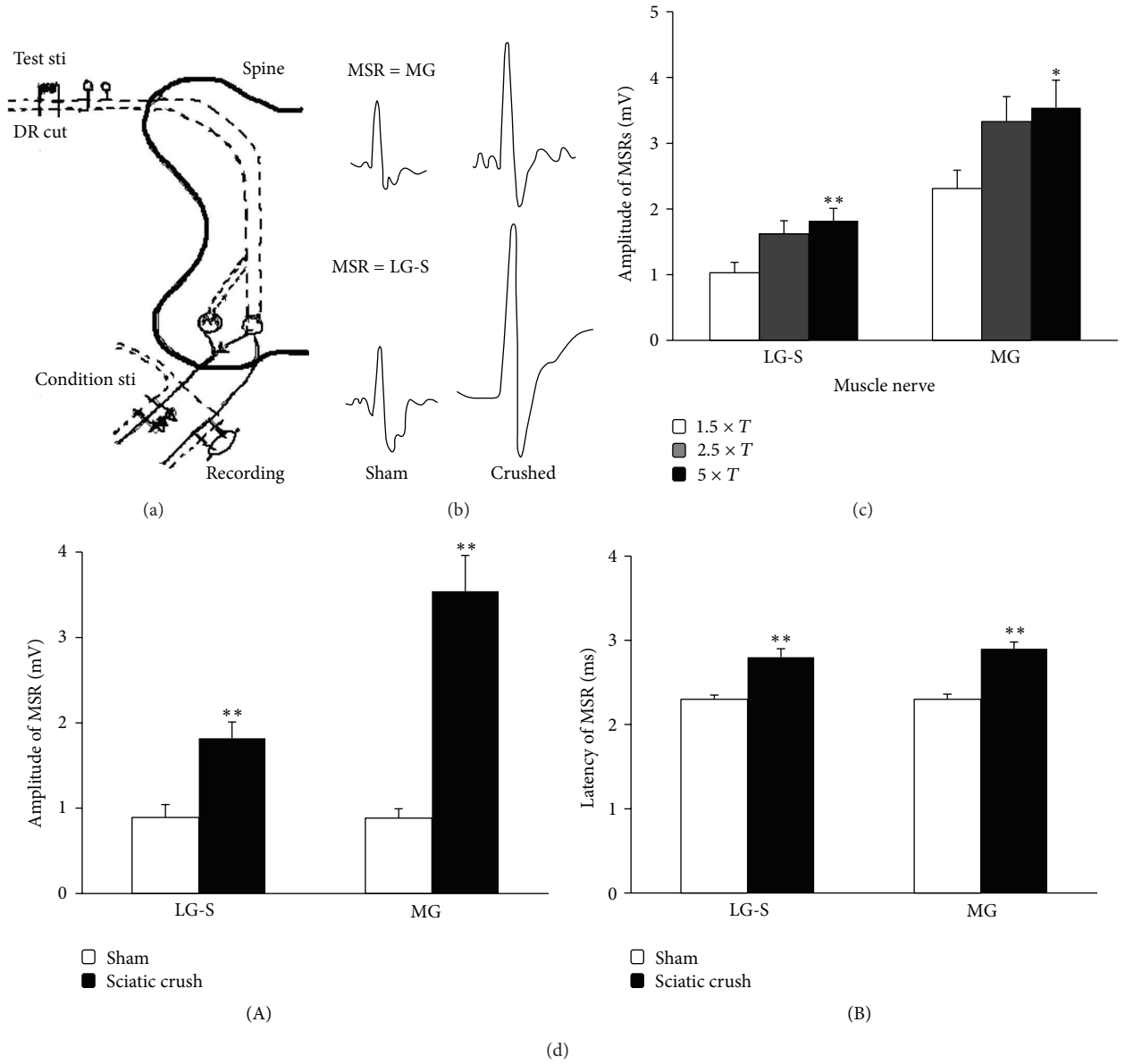

Figure 1: Characterization of the monosynaptic reflexes (MSR) in sham and sciatic nerve crush rats. (a) Illustration to show the test, condition stimulation, and recording arrangement during the experiment; (b) examples of the recorded MSR in sham and sciatic nerve crush rat; (c) Bar histogram showing the relationship between monosynaptic reflexes amplitude and the stimulus intensity; (d-e) bar histogram showing the monosynaptic reflexes amplitude (b) and latency (d) recorded from LG-S and MG nerves in sham (open) and sciatic nerve crushed adult rats. ($^{**}P < 0.01$ in comparison with the sham control rats.)

the exposed left G-S muscle was injected with 20% (1 uL) HRP into both inner and outer sides of the muscle. 48 h after HRP injection, animals were perfused and postfixed for 4 hours, before the spinal section of L4–L6 was dissected out. Frozen section was cut for immunohistochemistry by using Hanker-Yates solution (Hanker-Yates reagent 150 mg, dimethyl arsenic acid salt buffer 100 mL, 1% H_2O_2 1 mL). The spinal sections were then stained for 15–25 min with gallocyanin (heating 10 g chrome alum dissolved into 100 mL ultrapure water, added 0.3 g cyanin) and mounted on coverslips and dried 24 h at room temperature.

2.6. Muscular Tissue Staining. At the end of each acute experiment (7 weeks after the initial nerve crush on day 5 of the age), the gastrocnemius and soleus muscles on both sides were dissected out and weighted separately. Gastrocnemius muscles were then quickly stored in liquid nitrogen for later SDH staining. Frozen sections (10 μm) were cut, mounted on coverslips, and then dried at room temperature. After stained with hematoxylin, sections were stained again with succinic dehydrogenase (SDH) by Nicholas method (0.1 mol/L phosphate buffer 32.8 mL, 1 mol/L succinic acid sodium solution 2 mL, 15 mmol/L nitrogen blue four thiazole solution

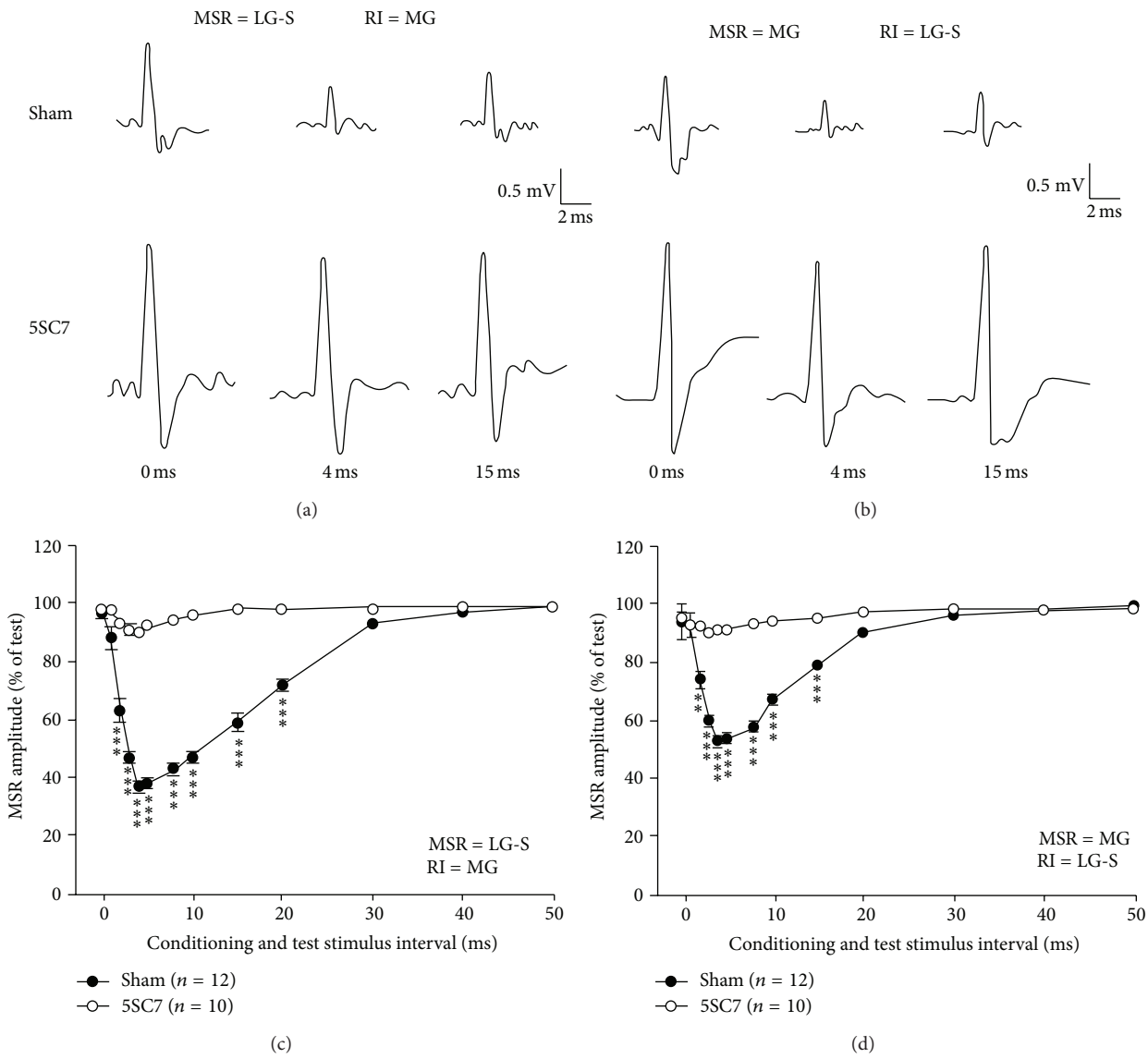

Figure 2: Recurrent inhibition in 5-day-old sciatic nerve crush rats—(1) 7 weeks recovery time. Recurrent inhibitory curves illustrate the amount (mean ± SEM) of recurrent inhibition (RI) of monosynaptic reflexes (MSR) in the 5-day-old sciatic nerve crush rats 7 weeks after nerve crush. The RI/MSR combinations tested were MG/LG-S (a, c) and LG-S/MG (b, d). (a-b) Raw traces of the recorded MSR from either LG-S (a) or MG (b) in different condition-test stimulus interval of 0, 4, and 15 ms from either sham control rat (upper traces) or sciatic nerve crush rat (lower traces). (c-d) recurrent inhibitory curves showing the time course of the RI in different condition-test stimulus interval. ($^{**}P < 0.01$ and $^{***}P < 0.001$ in comparison with the sham control rats.)

4 mL, 0.1 mol/L KCN 0.4 mL and 10 mmol/L phenazine-N-metilsulfate solution 0.8 mL).

2.7. Data Analyses and Statistics. Data were presented as mean ± SEM. Student's t-test and One-way ANOVA with post hoc Newman-Keuls test were used to detect statistical differences. $P < 0.05$ was considered as statistically significant.

3. Results

3.1. Effect of Sciatic Nerve Crush in 5-Day-Old Rats on the MSR in Adulthood after Reinnervation. MSRs were recorded in the two branches of the sciatic nerve, LG-S and MG nerve, respectively, by stimulating the peripheral sectioned spinal root L5 (Figures 1(a) and 5(a)). The evoked MSR was stimulus strength dependent; the higher the stimulation current is, the larger the MSR responses are (Figure 1(c)). The maximal response of the MSR was chosen for late experiments. Seven weeks after sciatic nerve crush performed at day 5 after birth, the evoked MSR in crushed animals showed longer latency and larger responses. The averaged amplitude for recording from LG-S was 0.89 ± 0.15 mV ($n = 12$) in sham control rats and 1.82 ± 0.19 mV ($n = 10$) in sciatic nerve crushed rats ($P < 0.01$) and the averaged amplitude for recording from MG was 0.87 ± 0.11 mV ($n = 12$) in sham control rats and 3.54 ± 0.42 mV ($n = 10$) in sciatic nerve crushed rats

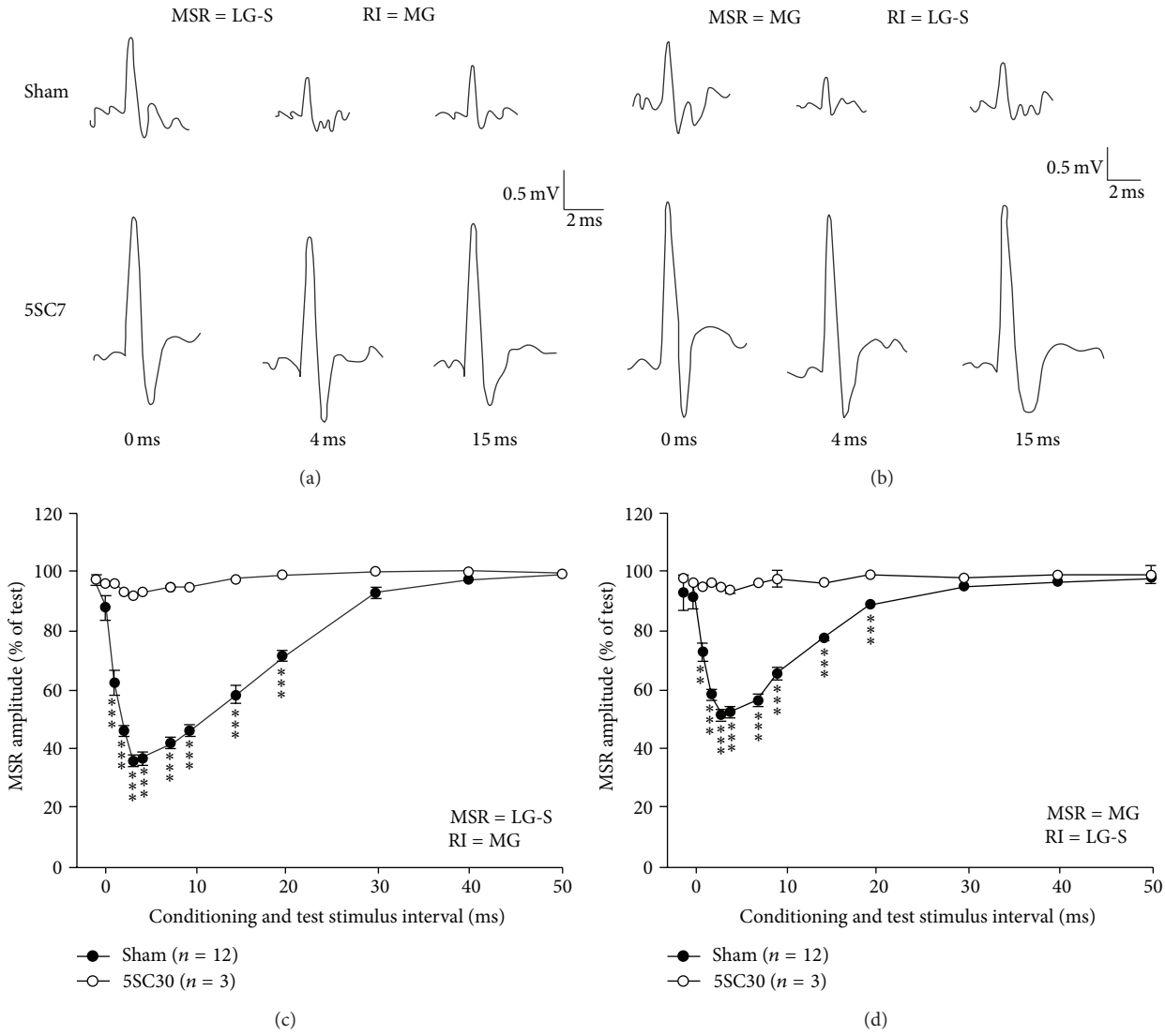

Figure 3: Recurrent inhibition in 5-day-old sciatic nerve crush rats—(2) 30 weeks recovery time. Recurrent inhibitory curves illustrate the amount (mean ± SEM) of recurrent inhibition (RI) of monosynaptic reflexes (MSR) in the 5-day-old sciatic nerve crush rats 30 weeks after nerve crush. The RI/MSR combinations tested were MG/LG-S (a, c) and LG-S/MG (b, d). (a-b) Raw traces of the recorded MSR from either LG-S (a) or MG (b) in different condition-test stimulus interval of 0, 4 and, 15 ms from either sham control rat (upper traces) or sciatic nerve crush rat (lower traces). (c-d) Recurrent inhibitory curves showing the time course of the RI in different condition-test stimulus interval. ($^{**}P < 0.01$ and $^{***}P < 0.001$ in comparison with the sham control rats.)

($P < 0.01$) (Figure 1(d)(A)). The mean latency of MSRs of LG-S was 2.30 ± 0.05 ms ($n = 12$) in sham control rats and 2.80±0.10 ms ($n = 10$) in sciatic nerve crushed rats ($P < 0.01$) and the mean latency of MSRs of MG was 2.30 ± 0.06 ms ($n = 12$) in sham control rats and 2.90 ± 0.08 ms ($n = 10$) in sciatic nerve crushed rats ($P < 0.01$) (Figure 1(d)(B)).

3.2. Effect of Sciatic Nerve Crush at 5-Day-Old Rats on the RI of MSRs after 7-Week Recovery. RI was measured by applying conditioning stimulus on one sciatic nerve branch with an interstimulus interval before the test stimulus on the sectioned L5 root while recording was on the other sciatic branch.The MSR amplitude decrease indications of the RI [1]. Our results showed that, in normal condition in sham operated animals, the MSR amplitude was interstimulus interval related suppressed, with the maximal change (RI_{Max}) occurring at interstimulus interval of 4 ms (Figure 2), and the duration of the RI in this preparations was about 15–20 ms, similar to previously reported [20]. However, the RI was severely impaired by the sciatic nerve crush performed when the rats were only 5 days old after birth. Compared with the RI obtained from sham control rats in the same RI/MSR combinations, the mean values of the RI between regenerated LG-S and MG motoneurons were all significantly ($P < 0.001$, One-way ANOVA) smaller than those from the sham control group (Figures 2(c) and 2(d)). Measured at 7 weeks after the nerve crush, the maximal RI (RI_{Max}) from MG to LG-S was significantly reduced from a sham control

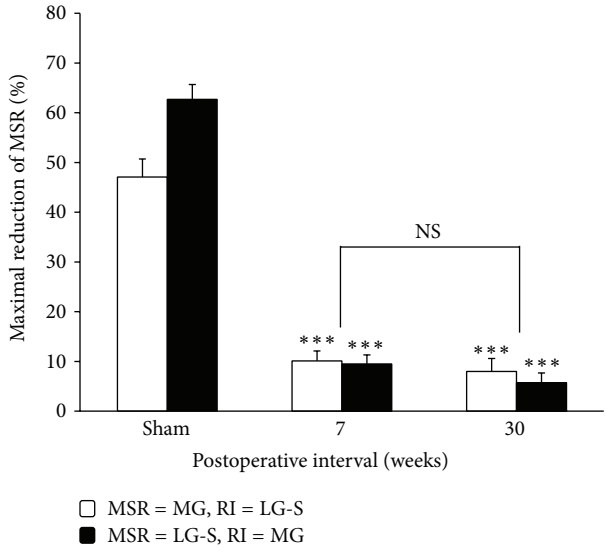

Figure 4: Recovery time course of the recurrent inhibition after sciatic nerve crush at age of 5 days. Bar diagram showing the recovery time course of the maximal recurrent inhibition, expressed as MSR amplitude reduction, 7 and 30 weeks after sciatic nerve crush at age of 5 days. The RI/MSR combinations tested were MG/LG-S and LG-S/MG. $^{***}P < 0.001$, two-tailed student's t-test.

value from 62.7 ± 3.6% ($n = 12$) to 10.1 ± 2.0% ($n = 10$) in sciatic nerve crushed rats ($P < 0.001$) and the RI_{Max} from LG-S to MG was reduced from 47.1 ± 3.0% ($n = 12$) in sham control rats to 9.5 ± 1.8% ($n = 10$) in sciatic nerve crushed rats ($P < 0.001$) (Figures 2(c), and 2(d)). The duration of RI in this preparation was also much smaller than that in control animals. The test-conditioning stimuli interval time to get to maximal MSR depression, however, had the same value as that in sham control rats. These results indicated that when the nerve crush was applied to sciatic nerve at its early postnatal life, the RI could be depressed dramatically even when the regeneration has completed, which is different from the adult sciatic nerve crush preparation [20].

3.3. Effect of Sciatic Nerve Crush on 5-Day-Old Rats on the RI of the MSRs after 30-Week Recovery. A group of rats with sciatic nerve crush at age of 5 days were tested to check the RI change between MG and LG-S motoneuron pools 30 weeks after the nerve crush. In this preparation, a successive reduction in the amount of RI has been observed in which RI from MG to LG-S and from LG-S to MG was only capable of reducing the amplitude of MSRs to about 92.0 ± 2.6% ($n = 3$) and 94.3 ± 2.0% ($n = 3$) of the size of unconditioned MSR (Figure 3). In other words, the maximal RIs were only 8.0 ± 2.6% and 5.7 ± 2.0%, which were 12.8% (MG/LG-S) and 12.0% (LG-S/MG) of the corresponding value of the RI in sham control rats, respectively (Figure 4). The amounts of RI from this preparation were all significantly smaller than those from sham control rats ($P < 0.001$, One-way ANOVA).

In addition, comparing the group data of 7-week and 30-week postoperative nerve crush rats, the RI was not different statistically ($P > 0.5$ in MG/LG-S, $P > 0.1$ in LG-S/MG, t-test) (Figure 4). These results indicated that the depressive effect of the nerve injury on the spinals RI could not recover following regeneration or, in other words, this impairment seems permanent.

3.4. Effect of Tibial Nerve Crush at 5-Day-Old Rats on the RI of MSRs after 14-Week Recovery. In another group of the rats, tibial nerve, instead of the sciatic nerve, was crush injured at age of 5 days and the RI was examined 14 weeks later. The RIs of MSRs between regenerated MG and LG-S motoneurons 14 weeks after tibial nerve crush were all significantly reduced ($P < 0.05$, One-way ANOVA) (Figure 5(b)). The maximal RI reduction occurring in either combination was at 4 ms of interstimulus interval (Figures 5(d) and 5(e)). The RI from MG motoneurons to LG-S motoneurons maximally reduced the amplitude of the MSRs to 62.0 ± 9.2% ($n = 4$) of the size of the unconditioned reflexes, which is indication of a RI_{Max} value of 38.0 ± 9.2% (Figure 5(d)). The corresponding value of the MSR reduction from LG-S to MG was 68.4 ± 5.3% ($n = 4$) and a RI_{Max} of 31.6 ± 5.3% (Figure 5(e)). Comparing these results in neonatal tibial nerve crush rats with those from the sham control rats (Figures 5(d) and 5(e)), the RI_{Max} was significantly reduced either LG-S to MG or MG to LG-S combinations ($P < 0.05$, t-test) (Figures 5(d) and 5(e)).

3.5. Effect of Sciatic Nerve Crush at 5-Day-Old Rats on the Spinal Motoneurons and the Hindlimb Muscles after 7-Week Recovery. Our previous results indicate that, after sciatic nerve crush in adult, either the spinal motorneurons or the relative muscles were fully recovered from the initial insult after at least 6-week reinnervation [20]. Here we further examined whether sciatic nerve crush performed during early development at age of 5 days would affect the number of the spinal motorneurons and the property of the muscles after reinnervation. Our results showed that, 7 weeks after sciatic nerve crush performed at 5-day-old rats, the number of the spinal motorneurons located in the ventral side of the spinal cord was not different between the sham control group and the nerve crushed group (Figure 6(a)). There was similar number of the spinal G-S neuron among crushed group (166 ± 10, $n = 4$) and the sham control group (174 ± 12, $n = 4$) ($P > 0.05$) (Figure 6(c)). Although there was no motoneurone loss after nerve crush in 5-day-old rats, in contrast, compared to the uninjured side, the muscle weight for both gastrocnemius-soleus and tibial muscles was significantly reduced 7 weeks after sciatic nerve crush at age of 5 days ($P < 0.05$, Figure 6(d)). The gastrocllemius muscles had the weight at 58.0 ± 3.1% ($n = 8$) of the contralateral control value, and the soleus muscles were 52.4 ± 5.0% ($n = 8$) of the control value. Loss of muscle weight after peripheral nerve crush in 5-day-old sciatic nerve crush rats observed in this study is in agreement with the other results [23, 24]. In addition, the muscles, which were stained with succinic dehydrogenase (SDH) to show its oxidative capacity, showed that the denervated/regenerated muscle of gastrocnelnius muscle virtually stained darkly, in comparison with control muscle having mixture of fibers which have either a low (pale staining) or high (dark staining) oxidative capacity (Figure 6(b)). The result of muscle fiber type change is in good agreement with previous reports [23–25].

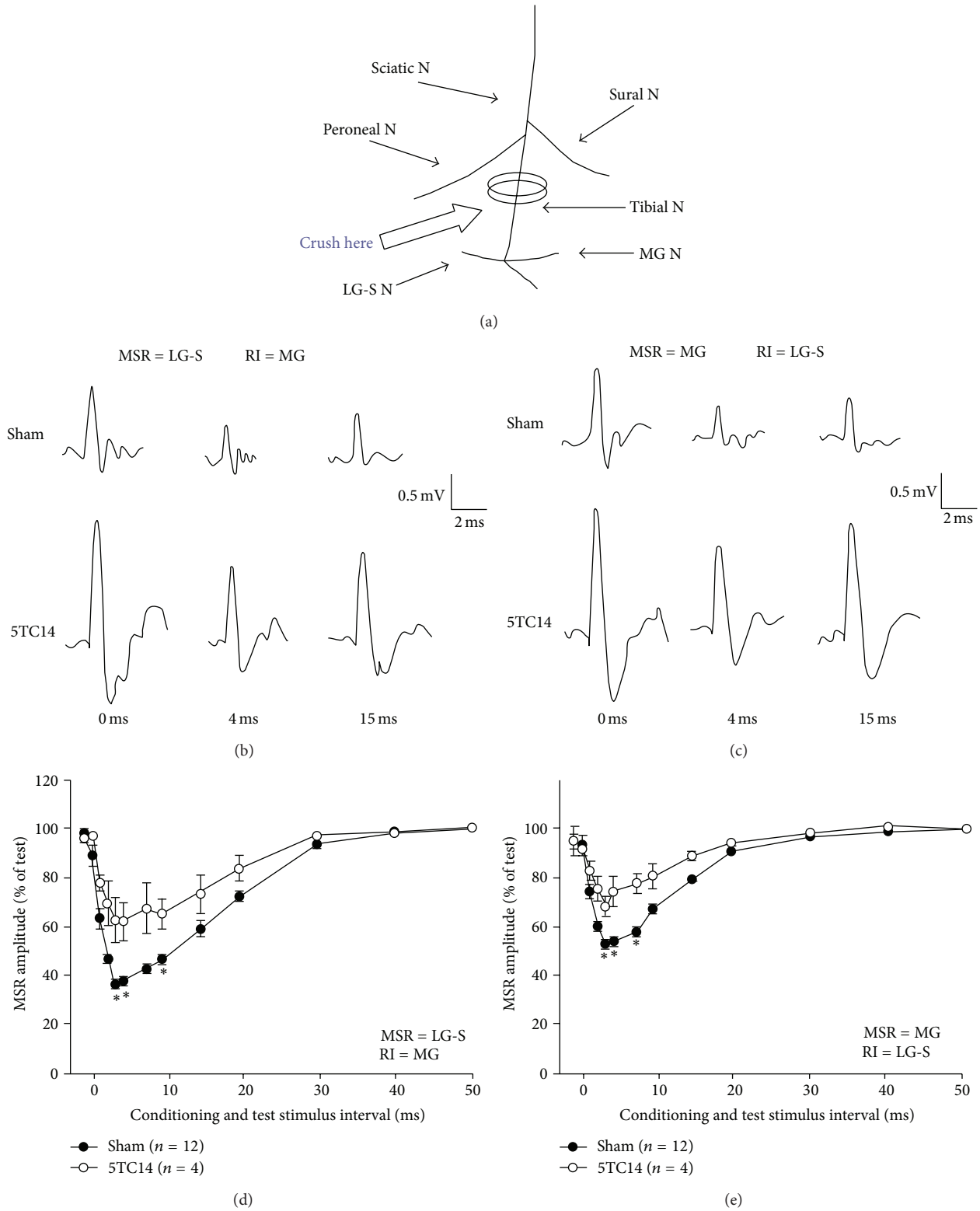

Figure 5: Recurrent inhibition in 5-day-old tibial nerve crush rats. (a) Illustration of the tibial nerve crush site and the relation to the recording and testing nerves. (b-c) Raw traces of the recorded MSR from either LG-S (a) or MG (b) in different condition-test stimulus interval of 0, 4, and 15 ms from either sham control rat (upper traces) or sciatic nerve crush rat (lower traces). (d-e) Recurrent inhibitory curves illustrate the amount (mean ± SEM) of recurrent inhibition (RI) of monosynaptic reflexes (MSR) in different condition-test stimulus interval. $^{**}P < 0.01$ and $^{***}P < 0.001$ in comparison with the sham control rats.

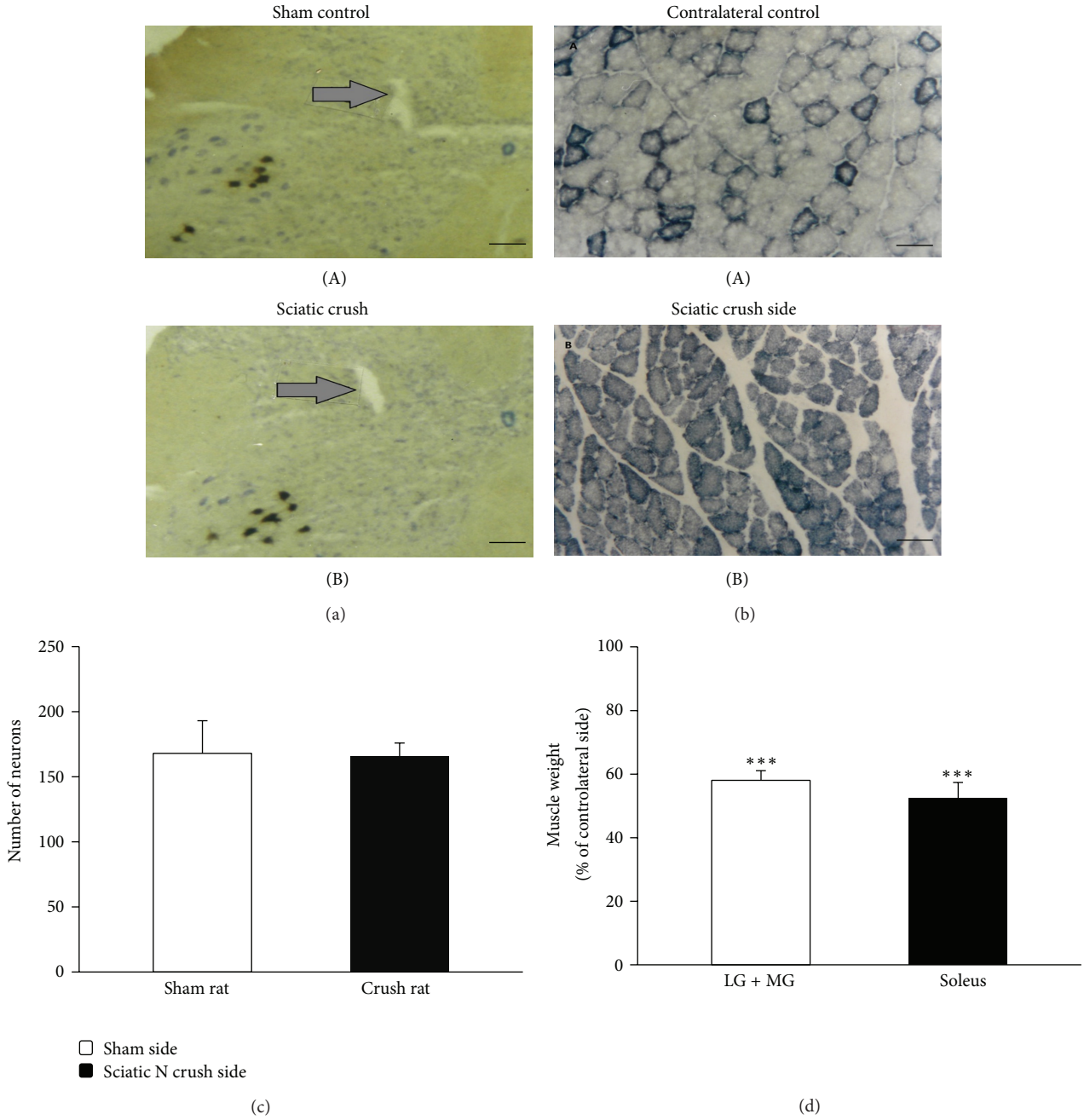

Figure 6: Spinal motoneuron and peripheral muscle change 7 weeks after the 5-day-old sciatic nerve crush. (a) Photograph taken under low magnification (4x) showing nerve crush side of the spinal cord with the HRP labeled cells is located on dorsolateral part of the anterior horn. The hole pointed by the arrow indicates the HRP injected side. (b) Examples of cross-sections from reinnervated (B) and contralateral control (A) gastrocnemius muscles from a 5-day-old sciatic nerve crush rat stained for SDH 7 weeks after nerve crush. (c-d) Bar diagrams showing the motoneuron number of the gastrocnemius pool (c) and gastrocnemius and soleus muscle weights (d) in 5-day-old sciatic nerve crush rats 7 weeks after reinnervation. The scale bar in ((a)(A) and (a)(B)) is 500 μm and in ((b)(A) and (b)(B)) is 80 μm. $^{***}P < 0.001$ in comparison with the sham control.

4. Discussion

The current research is the first to report the change of the Renshaw recurrent inhibition (RI) of spinal MSRs in rats after reinnervation following the sciatic nerve crush injury during neonatal period. The following results were obtained. (1) In 5-day-old sciatic nerve crush preparation, the monosynaptic reflexes evoked from the regenerated motoneurons not only had a longer latency but also had larger amplitude. (2) The amounts of RI between regenerated motor pools were significantly suppressed, and they were virtually lost compared with the normal RI size (15–20% of the normal RI value) even

after a long recovery period (10–15% of the sham control at up to 30 weeks after nerve crush). (3) In contrast to the huge reduction in sciatic nerve crush preparation, the amounts of RI following tibial nerve crush, which was more close to their target muscles, at age of 5 days were only reduced to about 60–70% of the normal RI size. This may suggest that shortening the disconnection time between motoneurons and their target muscles would lead to less impairment in the RI pathway after nerve crush. (4) Despite being without motoneuron loss, the muscles innervated by those injured nerves were changed particularly with changed composition of the muscle fibers.

In the 1940s Renshaw discovered RI of motoneuron axon collateral inhibited spinal MSR induced by activating a group of interneurons located in the spinal motoneuron area via reverse stimulation of the axon of the motoneurons [1], thus the interneuron named Renshaw cell and the inhibition named Renshaw recurrent inhibition [2, 8]. It was reported that the Renshaw cell to motoneuron ratio is estimated to be 1 : 5 [26]. The findings from current study showing that the MSR latency was prolonged after nerve crush may attribute to decreased rate of axon transmission. The mechanism of decreased RI of neuron axon because of injury may be long term or permanent which agrees with the result of peripheral nervous regeneration after cutoff. Havton and Kellerth [27] and Kellerth et al. [28] found that motoneuron axon collateral disappeared after never injury associated with the change of RI in cats, which indicated the possibility of less axon collaterals leading to subdued RI intensity. Whether or not the axon collaterals die out in rats after sciatic nerve crush was not studied in current experiment, and further studies are certainly needed. Moreover, the lower activity of Renshaw cells was thought to relate to the decreased RI, especially in the early period of injury. Although it is unclear how Renshaw cell changes after sciatic nerve injury, Sanna and her colleagues [29] found that activity of Renshaw cells weakened upon sciatic nerve crush 1 week after injury that was likely to be a result of disappearance of axon collaterals and abnormal function of motoneurons.

Monosynaptic reflexes generated from adult injury and regenerated motoneurons and recorded in a peripheral nerve crush rat had a similar strength as in normal [20]. In contrast, monosynaptic reflexes recorded from regenerated motoneurons in 5-day-old sciatic nerve crush rats are much different from those in sham control rats not only by their latency, but also by their amplitude. However, the latencies of MSRs in regenerated motoneurons (either from adult or 5-day-old sciatic nerve crush rats) were significantly longer than those in sham control rats. This may be due to the observed reduction of axon conduction velocity in injured motoneurons [30–32]. The largely increased amplitude of MSRs seen in 5-day-old sciatic nerve crush rats was not seen in adult crush rats. This MSR amplitude increase is in agreement with the early report that after temporary loss of contact with the target in young animals, the surviving motoneurons became more active than normal; however, in animals which had their nerve crushed as adults the motoneuron activity was as normal [33]. It is possible that nerve injury in neonatal animals disrupted the normal developmental process and prevented the usual elimination of synapse from the surface of the motoneurones, which would result in enhancement of the monosynaptic EPSPs [14, 33, 34]. The enhanced monosynaptic EPSPs evoked from crushed nerve were reported only in a period of 8 to 12 weeks after nerve crush [34, 35]. Since the sciatic nerve crush carried out on 5-day-old rats in this study led to both deafferentation and denervation of the sciatic motor pool, albeit briefly, these changes of motoneuron synaptic input may result in the enhancement of MSRs.

Compared to our previous study on the adult sciatic nerve crush rats [28], it is clear that peripheral nerve injury in young animals affects the RI pathway more than that in adult. This result may relate to the findings in muscles and motoneurones [23, 24, 33, 36–40]. For example, immature motoneurones are more likely to die as a result of axonal damage than mature ones [23, 36] and even the surviving motoneurones are unable to recover the original size of their peripheral field [41]. Adult mammalian muscles recover virtually completely from nerve injury if the reinnervation is allowed to proceed unhindered [20, 36, 37]. However, the reinnervated muscles in neonatal nerve injury animals are affected to a much greater extent than after similar injury in adult animals, seen in both current neonatal nerve crush study and our previous adult sciatic nerve crush study [20]. The effects include gross loss of weight, loss of muscle tension, and muscle fiber grouping [23–25, 36, 37]. The reason why the nerve injury applied in adult and young animals induces such a different impairment to motor units has been explained as a consequence of the development of the muscle fibers being arrested while the motoneurons continue to develop after nerve injury [36]. Upon reinnervation the still immature muscle fibers may not be able to match the functional demands imposed upon them by the now mature nervous system. In the RI pathway in spinal cord, it has been found that after nerve injury the Renshaw cells in adult rat appear to be inactive during reinnervation [29] and motor axon collaterals are eliminated [16, 17]. There is also evidence showing that postnatal elimination of a large number of terminal arborization and synaptic buttons of recurrent motor axon collaterals occur during the first two weeks of postnatal life [42, 43]. This elimination of terminal axon collaterals appears to be coincident with the elimination of polyneuronal innervation which is known to occur at the neuromuscular junction [44]. That may be the factor, that during the period of inactivity of Renshaw cells following the neonatal sciatic nerve crush, the elimination of axon collaterals process underwent. Without interaction with the target (Renshaw cells), more axon collaterals of the motoneurons may be eliminated than those in the normal developmental process, since the activity of the target plays a very important role in the development of motor units. In addition, at the Renshaw cell level, after Renshaw cells restored the ability to respond synaptic input, which in adult is about 6–8 weeks after nerve injury, the postnatal recurrent axon collaterals elimination process has already finished [42, 43] and the immature Renshaw cells thus could not undergo the developing process to match their mature function. If the denervation time is long enough, it may cause the permanent change in Renshaw cell firing properties that never recover to match the mature state. In contrast, in adult animals, both motoneurons and Renshaw interneurons are mature

type at the time of nerve injury and after recovery from temporary "arrest," Renshaw cells recover to active as normal [29]. Thus, the large reduction of recurrent inhibition seen in this study in 5-day-old nerve crush rats may be accounted for by (1) the elimination of recurrent axon collaterals, (2) loss of synaptic contact with regenerated motoneurons by Renshaw cells as those in adult nerve crush rats, and (3) the abnormal excitability of Renshaw cells themselves.

In addition, in this study the length of time during which muscles were separated from their neurons was varied using three different nerve crush sites either on the sciatic nerve or moving along the nerve to the tibial branch in 5-day-old rats. Results showed that shortening the period of denervation improved recovery of the recurrent inhibitory effect. Taken together these experiments show that the degree of permanent impairment of recurrent inhibitory pathway following temporary denervation during the neonatal period is related to the length of time during which the motoneurons and muscles are disconnected. The longer the period of separation is, the more severe the impairment is. These results are supported by the other findings. Lowrie et al. [24] reported that crushing of the peroneal nerves at 3 mm away from the EDL muscle at age of 5 days was followed by a better recovery in EDL muscle than that crushing site at 9 mm away from the muscle. Brown et al. [45] demonstrated a similar result in soleus muscle in 2-day-old rat in which soleus muscle was nearly in complete recovery after a crush on soleus nerve at its point of entry into the muscle. Thus, it could be concluded that nerve crush inducing RI impairment is likely related to the time length of disruption of the motoneuron-muscle interaction.

5. Conclusion

The result presented in this work from the neonatal sciatic nerve crush rats, and adding our previous findings from the adult sciatic nerve crush rats, indicates that regenerated motoneurons in general showed reduced RI with the most dramatic effect being on motoneurons injured in early postnatal life and the decreased RI had a special significance in making up motoneuron's function enhance for the alteration of the muscle power.

Conflict of Interests

The authors declare that there is no conflict of interests regarding to the publication of this paper.

Authors' Contribution

Liang Shu and Jingjing Su have equal contribution.

Acknowledgments

This work was supported by the grants from the Shanghai 9th People's Hospital (JY2011A18) to Liang Shu and from Shanghai Municipal Health Bureau (20114218) to Lichao Peng.

References

[1] B. Renshaw, "Central effects of centripetal impulses in axons of spinal ventral roots," *Journal of Neurophysiology*, vol. 9, pp. 191–204, 1946.

[2] J. C. Eccles, R. M. Eccles, A. Iggo, and M. Ito, "Distribution of recurrent inhibition among motoneurones," *The Journal of Physiology*, vol. 159, pp. 479–499, 1961.

[3] F. J. Alvarez, A. Benito-Gonzalez, and V. C. Siembab, "Principles of interneuron development learned from Renshaw cells and the motoneuron recurrent inhibitory circuit," *Annals of the New York Academy of Sciences*, vol. 1279, pp. 22–31, 2013.

[4] Q. Chang and L. J. Martin, "Glycinergic innervation of motoneurons is deficient in amyotrophic lateral sclerosis mice: a quantitative confocal analysis," *The American Journal of Pathology*, vol. 174, no. 2, pp. 574–585, 2009.

[5] F. J. Alvarez and R. E. W. Fyffe, "The continuing case for the Renshaw cell," *Journal of Physiology*, vol. 584, no. 1, pp. 31–45, 2007.

[6] S. P. Schneider and R. E. W. Fyffe, "Involvement of GABA and glycine in recurrent inhibition of spinal motoneurons," *Journal of Neurophysiology*, vol. 68, no. 2, pp. 397–406, 1992.

[7] A. J. Todd and A. C. Sullivan, "Light microscope study of the coexistence of GABA-like and glycine-like immunoreactivities in the spinal cord of the rat," *Journal of Comparative Neurology*, vol. 296, no. 3, pp. 496–505, 1990.

[8] U. N. Ramirez-Jarquin, R. Lazo-Gomez, L. B. Tovar-y-Romo, and R. Tapia, "Spinal inhibitory circuits and their role in motor neuron degeneration," *Neuropharmacology*, 2013.

[9] F. Fornai, P. Longone, L. Cafaro et al., "Lithium delays progression of amyotrophic lateral sclerosis," *Proceedings of the National Academy of Sciences of the USA*, vol. 105, no. 6, pp. 2052–2057, 2008.

[10] L. Pasquali, P. Longone, C. Isidoro, S. Ruggieri, A. Paparelli, and F. Fornai, "Autophagy, lithium, and amyotrophic lateral sclerosis," *Muscle and Nerve*, vol. 40, no. 2, pp. 173–194, 2009.

[11] D. Gigo-Benato, T. L. Russo, S. Geuna, N. R. S. R. Domingues, T. F. Salvini, and N. A. Parizotto, "Electrical stimulation impairs early functional recovery and accentuates skeletal muscle atrophy after sciatic nerve crush injury in rats," *Muscle and Nerve*, vol. 41, no. 5, pp. 685–693, 2010.

[12] H. Hultborn, E. Pierrot-Deseilligny, and H. Wigstrom, "Recurrent inhibition and afterhyperpolarization following motoneuronal discharge in the cat," *Journal of Physiology*, vol. 297, pp. 253–266, 1979.

[13] J. C. Eccles, B. Libet, and R. R. Young, "The behaviour of chromatolysed motoneurones studied by intracellular recording," *The Journal of Physiology*, vol. 143, no. 1, pp. 11–40, 1958.

[14] M. Kuno and R. Llinás, "Alterations of synaptic action in chromatolysed motoneurones of the cat," *Journal of Physiology*, vol. 210, no. 4, pp. 823–838, 1970.

[15] L. M. Mendell, "Modifiability of spinal synapses," *Physiological Reviews*, vol. 64, no. 1, pp. 260–324, 1984.

[16] L. Havton and J.-O. Kellerth, "Retrograde effects of axotomy on the intramedullary axon collateral systems and recurrent inhibitory reflexes of cat spinal motoneurones," *Neuroscience Letters*, vol. 52, no. 1-2, pp. 13–17, 1984.

[17] L. Havton and J.-O. Kellerth, "Elimination of intramedullary axon collaterals of cat spinal α-motoneurons following peripheral nerve injury," *Experimental Brain Research*, vol. 79, no. 1, pp. 65–74, 1990.

[18] R. C. Foehring, G. W. Sypert, and J. B. Munson, "Motor-unit properties following cross-reinnervation of cat lateral gastrocnemius and soleus muscles with medial gastrocnemius nerve. I. Influence of motoneurons on muscle," *Journal of Neurophysiology*, vol. 57, no. 4, pp. 1210–1226, 1987.

[19] C. M. Bowe, N. H. Evans, and V. Vlacha, "Progressive morphological abnormalities observed in rat spinal motor neurons at extended intervals after axonal regeneration," *Journal of Comparative Neurology*, vol. 321, no. 4, pp. 576–590, 1992.

[20] L. Shu, Y. R. Dong, W. H. Yan, Y. Zhai, Y. Wang, and W. Li, "Long term depression of the recurrent inhibition of monosynaptic spinal reflexes after sciatic nerve crush in adult rats," *Sheng Li Xue Bao*, vol. 63, no. 4, pp. 291–299, 2011.

[21] D. H. Lee and J. K. Lee, "Animal models of axon regeneration after spinal cord injury," *Neuroscience Bulletin*, vol. 29, no. 4, pp. 436–444, 2013.

[22] Y. Wang, J.-S. Qi, S. Kong et al., "BDNF-TrkB signaling pathway mediates the induction of epileptiform activity induced by a convulsant drug cyclothiazide," *Neuropharmacology*, vol. 57, no. 1, pp. 49–59, 2009.

[23] M. B. Lowrie, S. Krishnan, and G. Vrbova, "Permanent changes in muscle and motoneurones induced by nerve injury during a critical period of development of the rat," *Developmental Brain Research*, vol. 31, no. 1, pp. 91–101, 1987.

[24] M. B. Lowrie, U. Shahani, and G. Vrbova, "Impairment of developing fast muscles after nerve injury in the rat depends upon the period of denervation," *Journal of the Neurological Sciences*, vol. 99, no. 2-3, pp. 249–258, 1990.

[25] M. B. Lowrie and G. Vrbova, "Different pattern of recovery of fast and slow muscles following nerve injury in the rat," *Journal of Physiology*, vol. 349, pp. 397–410, 1984.

[26] G. Z. Mentis, V. C. Siembab, R. Zerda, M. J. O'Donovan, and F. J. Alvarez, "Primary afferent synapses on developing and adult Renshaw cells," *Journal of Neuroscience*, vol. 26, no. 51, pp. 13297–13310, 2006.

[27] L. Havton and J.-O. Kellerth, "Plasticity of recurrent inhibitory reflexes in cat spinal motoneurons following peripheral nerve injury," *Experimental Brain Research*, vol. 79, no. 1, pp. 75–82, 1990.

[28] J. O. Kellerth, A. Mellström, and S. Skoglund, "Postnatal excitability changes of kitten motoneurones," *Acta Physiologica Scandinavica*, vol. 83, no. 1, pp. 31–41, 1971.

[29] P. P. Sanna, M. R. Celio, F. E. Bloom, and M. Rende, "Presumptive Renshaw cells contain decreased calbindin during recovery from sciatic nerve lesions," *Proceedings of the National Academy of Sciences of the USA*, vol. 90, no. 7, pp. 3048–3052, 1993.

[30] M. Kuno, Y. Miyata, and E. J. Munoz Martinez, "Properties of fast and slow alpha motoneurones following motor reinnervation," *Journal of Physiology*, vol. 242, no. 1, pp. 273–288, 1974.

[31] R. C. Foehring, G. W. Sypert, and J. B. Munson, "Properties of self-reinnervated motor units of medial gastrocnemius of cat. II. Axotomized motoneurons and time course of recovery," *Journal of neurophysiology*, vol. 55, no. 5, pp. 947–965, 1986.

[32] R. C. Foehring, G. W. Sypert, and J. B. Munson, "Properties of self-reinnervated motor units of medial gastrocnemius of cat. I. Long-term reinnervation," *Journal of neurophysiology*, vol. 55, no. 5, pp. 931–946, 1986.

[33] R. Navarrete and G. Vrbova, "Differential effect of nerve injury at birth on the activity patterns of reinnervated slow and fast muscles of the rat," *Journal of Physiology*, vol. 351, pp. 675–685, 1984.

[34] R. Gallego, M. Kuno, R. Nunez, and W. D. Snider, "Enhancement of synaptic function in cat motoneurones during peripheral sensory regeneration," *Journal of Physiology*, vol. 306, pp. 205–218, 1980.

[35] J. Hellgren and J.-O. Kellerth, "A physiological study of the monosynaptic reflex responses of cat spinal α-motoneurons after partial lumbosacral deafferentation," *Brain Research*, vol. 488, no. 1-2, pp. 149–162, 1989.

[36] M. B. Lowrie, S. Krishnan, and G. Vrbova, "Recovery of slow and fast muscles following nerve injury during early post-natal development in the rat," *Journal of Physiology*, vol. 331, pp. 51–66, 1982.

[37] M. Albani, M. B. Lowrie, and G. Vrbova, "Reorganization of motor units in reinnervated muscles of the rat," *Journal of the Neurological Sciences*, vol. 88, no. 1–3, pp. 195–206, 1988.

[38] R. Navarrete, U. Shahani, and G. Vrbova, "Long-lasting modification of reflexes after neonatal nerve injury in the rat," *Journal of the Neurological Sciences*, vol. 96, no. 2-3, pp. 257–267, 1990.

[39] H. Schmalbruch, "Growth and denervation response of skeletal muscle fibers of newborn rats," *Muscle and Nerve*, vol. 13, no. 5, pp. 421–432, 1990.

[40] J. Dekkers and R. Navarrete, "Persistence of somatic and dendritic growth associated processes and induction of dendritic sprouting in motoneurones after neonatal axotomy in the rat," *NeuroReport*, vol. 9, no. 7, pp. 1523–1527, 1998.

[41] J. Zelena and P. Hnik, "Motor and receptor units in the soleus muscle after nerve regeneration in very young rats," *Physiologia Bohemoslovenica*, vol. 12, pp. 277–290, 1963.

[42] S. Cullheim and M. Risling, "Observations on the morphology and the axon conduction velocity of axotomized and regenerating sciatic motoneurons in the kitten," *Experimental Brain Research*, vol. 45, no. 3, pp. 428–432, 1982.

[43] S. Cullheim and B. Ulfhak, "Postnatal changes in the termination pattern of recurrent axon collaterals of triceps surae alpha-motoneurons in the cat," *Brain Research*, vol. 349, no. 1-2, pp. 63–73, 1985.

[44] J. Bagust, D. M. Lewis, and R. A. Westerman, "Polyneuronal innervation of kitten skeletal muscle," *Journal of Physiology*, vol. 229, no. 1, pp. 241–255, 1973.

[45] M. C. Brown, J. K. S. Jansen, and D. van Essen, "Polyneuronal innervation of skeletal muscle in newborn rats and its elimination during maturation," *Journal of Physiology*, vol. 261, no. 2, pp. 387–422, 1976.

Hindawi Publishing Corporation
Neural Plasticity
Volume 2014, Article ID 675128, 15 pages
http://dx.doi.org/10.1155/2014/675128

Research Article

Involvement of Thalamus in Initiation of Epileptic Seizures Induced by Pilocarpine in Mice

Yong-Hua Li,[1] Jia-Jia Li,[2] Qin-Chi Lu,[2] Hai-Qing Gong,[1] Pei-Ji Liang,[1] and Pu-Ming Zhang[1]

[1] *School of Biomedical Engineering, Shanghai Jiao Tong University, 800 Dong-Chuan Road, Shanghai 200240, China*
[2] *Department of Neurology, Ren Ji Hospital, School of Medicine, Shanghai Jiao Tong University, Shanghai 200127, China*

Correspondence should be addressed to Pu-Ming Zhang; pmzhang@sjtu.edu.cn

Received 30 November 2013; Accepted 5 February 2014; Published 20 March 2014

Academic Editor: Yun Wang

Studies have suggested that thalamus is involved in temporal lobe epilepsy, but the role of thalamus is still unclear. We obtained local filed potentials (LFPs) and single-unit activities from CA1 of hippocampus and parafascicular nucleus of thalamus during the development of epileptic seizures induced by pilocarpine in mice. Two measures, redundancy and directionality index, were used to analyze the electrophysiological characters of neuronal activities and the information flow between thalamus and hippocampus. We found that LFPs became more regular during the seizure in both hippocampus and thalamus, and in some cases LFPs showed a transient disorder at seizure onset. The variation tendency of the peak values of cross-correlation function between neurons matched the variation tendency of the redundancy of LFPs. The information tended to flow from thalamus to hippocampus during seizure initiation period no matter what the information flow direction was before the seizure. In some cases the information flow was symmetrically bidirectional, but none was found in which the information flowed from hippocampus to thalamus during the seizure initiation period. In addition, inactivation of thalamus by tetrodotoxin (TTX) resulted in a suppression of seizures. These results suggest that thalamus may play an important role in the initiation of epileptic seizures.

1. Introduction

Temporal lobe epilepsy (TLE) has been associated with hippocampal sclerosis and pathological changes in the closed neighboring structures, including entorhinal cortex, amygdala and dentate gyrus [1–3]. Scalp electroencephalogram (EEG) recordings from patients with TLE usually demonstrate interictal and ictal epileptiform abnormalities over the mid/anterior temporal region [4]. Studies using depth electrodes further confirmed the electrographic origin of these seizures in the hippocampal formation [5]. However, recent studies have shown that the pathological substrate of TLE is not confined to the temporal lobe. Structural and metabolic imaging studies, such as magnetic resonance imaging (MRI), functional MRI, diffusion tensor imaging, and positron emission tomography, demonstrated abnormalities extending from hippocampus to subcortical structures and bilateral cortical regions in the precentral gyrus in patients with TLE [6, 7]. In clinical practice, resection of epileptic focus within the temporal lobe might still fail to control the seizures in some patients with TLE. The main factor contributing to these failures is probably the incomplete resection of the epileptogenic zone or that the patients might suffer from a complex epileptogenic network, which may involve the subcortical structures [8, 9]. In brief, more and more studies have shown that the hippocampal formation, although very important, may be not the only epileptogenic zone of TLE. So we should extend investigations outside the temporal lobe and focus on the neuronal circuits that may support the seizures [10, 11].

Thalamus is one of the potential critical components in the neuronal circuits that may take part in the initiation and spread of seizures in TLE. It has rich and reciprocal connections with cerebral cortex and limbic system [12, 13]. These connections participate in relaying sensory and motor signals, along with regulation of consciousness, sleep, and

alertness in the normal physiological condition and also could be involved in the genesis or propagation or both of focal and generalized seizures in the pathological state [14].

The role of thalamus has been well demonstrated in animal models of absence seizures which are the most pure form of generalized epilepsy [15]. The epileptic network was defined as a reciprocal circuit involving the neocortex and thalamic relay nuclei, and the thalamic reticular nucleus served as a key modulator. In this network, the cortex provided the excitatory drive, and the thalamic relay nuclei organized the drive into the epileptic spike wave pattern [16].

However, the role of thalamus in TLE is still less understood. Recently, some clinical trials targeted various thalamic nuclei as therapeutic electrical stimulation zones in attempt to control the intractable epilepsy, mostly TLE, with varying degrees of seizure reduction in more than half of the patients [17]. Moreover, there were evidences of thalamic involvement in seizures of TLE in patients, although the role of the thalamus was not well defined [9]. In animal models of TLE, studies have provided the histopathologic evidence for cell loss in the medial subdivisions of thalamus that coupled with synaptic alterations, which could enhance the excitability of thalamic seizure circuits [18]. Enhancement of GABA activity in the medial dorsal nucleus (MD) of thalamus resulted in a significant reduction of seizure duration [18, 19]. Further investigations proposed that thalamus could act as an excitatory amplifier through divergent-convergent circuits in the seizures [10, 20]. Besides MD, other nuclei of thalamus may also participate in seizures. Electrical stimulation of the reticular nucleus suppressed the limbic motor seizures in a hippocampal kindling model [21]. Electrical stimulation of the anterior nucleus (ANT) showed an improvement in seizure control in the status epilepticus (SE) model of TLE [22], and the possible mechanism was that the stimulation of ANT caused decreases in concentrations of glutamate and increases in GABA in hippocampus [23]. In the kainic acid model of TLE, high-frequency electrical stimulation of the parafascicular nucleus (PF) interrupted the ongoing hippocampal paroxysmal discharges, and the administration of NMDA antagonist and $GABA_A$ agonist suppressed the hippocampal discharges, whereas NMDA agonist and $GABA_A$ antagonist increased the hippocampal discharges [24]. These findings indicated that several nuclei of thalamus had close relation with the hippocampus in the neuronal circuits of seizures. However, in the study of absence seizures, enhancement of glutamate activity of PF significantly suppressed the spike-and-wave discharges [25]. It is interesting that activating PF had the opposite effects on epileptic discharges in the temporal lobe epileptic seizures and the absence seizures, calling for more investigations on the role of PF in seizures.

Studies mentioned above mainly investigated the role of thalamus by pharmaceutically modulating or electrical stimulating the thalamus nuclei. In the present study we investigated the role of thalamus in the development of seizures by computational methods. We used multichannel microelectrode techniques to obtain the local field potentials (LFPs) and single-unit discharges from CA1 of hippocampus and PF of thalamus during the development of epileptic seizures induced by pilocarpine in mice. Computational methods from symbolic dynamics and information theory were used to analyze the electrophysiological characters of neuronal activities and the information flow between thalamus and hippocampus. We found that LFPs became more regular during the seizure in both hippocampus and thalamus, and in some cases LFPs showed a transient disorder state at the seizure onset. The information tended to flow from thalamus to hippocampus during seizure initiation period, and inactivation of thalamus by tetrodotoxin (TTX) resulted in a suppression of seizures. These findings indicated that thalamus may play an important role in the initiation of epileptic seizures.

2. Materials and Methods

2.1. Animals. Experiments were performed on 4- to 6-month-old male C57BL/6 mice. The mice were housed in individual cages with food and water *ad libitum*, and kept in a 12 h light/dark cycle. All animal experimentations were approved by the Ethic Committee, School of Biomedical Engineering, Shanghai Jiao Tong University. All efforts were made to minimize the animal suffering and reduce the number of animals used in the experiments.

2.2. Recording Electrodes. The 16-channel electrodes, consisting of two independently movable bundles of 2 tetrodes, were secured to a recording microdrive (Figure 1(a)). The microdrive was constructed as described [26]. Each tetrode was formed of four twisted polyester insulated nickel-chrome alloy wires (diameter, 13 μm; STABLOHM 675, California Fine Wire Co, USA) with an impedance of 0.5–1 MΩ.

2.3. Surgery. Mice were handled for about one week prior to surgery to minimize the potential stress of human interaction. During the surgery, mice were anesthetized by pentobarbital sodium (100 mg/kg) intraperitoneally and mounted in a stereotaxic frame (51600, Stoelting Co, USA). The skin covering the skull was opened and the skull was exposed. The skull was perforated using a high speed dental drill (K.1070 High Speed Rotary Micromotor Kit, Foredom Co, USA) with 1.2 mm diameter drill tips. Seven small holes were drilled: five for the positioning of anchor screws and two for the placement of electrodes. Two cortical screws placed in the bilateral frontal bone were used as the reference and ground. Two bundles of electrodes were implanted into the target regions. The recording microdrive was then fixed to the skull using zinc phosphate cement (Hoffmann Dental Manufaktur GmbH, Germany). Throughout the experiments, body temperature was maintained at 37.5°C using a closed-loop animal blanket system (SS20-2, Huaibei Zhenghua Biologic Apparatus Facilities LTD Co, China). Animals were allowed at least one week for recovery before seizure induction.

2.4. Seizure Induction. Mice were injected intraperitoneally with atropine sulfate (1 mg/kg) and 30 minutes later with a single dose of pilocarpine (300 mg/kg). Their behavior was scored according to the Racine scale [27], and status

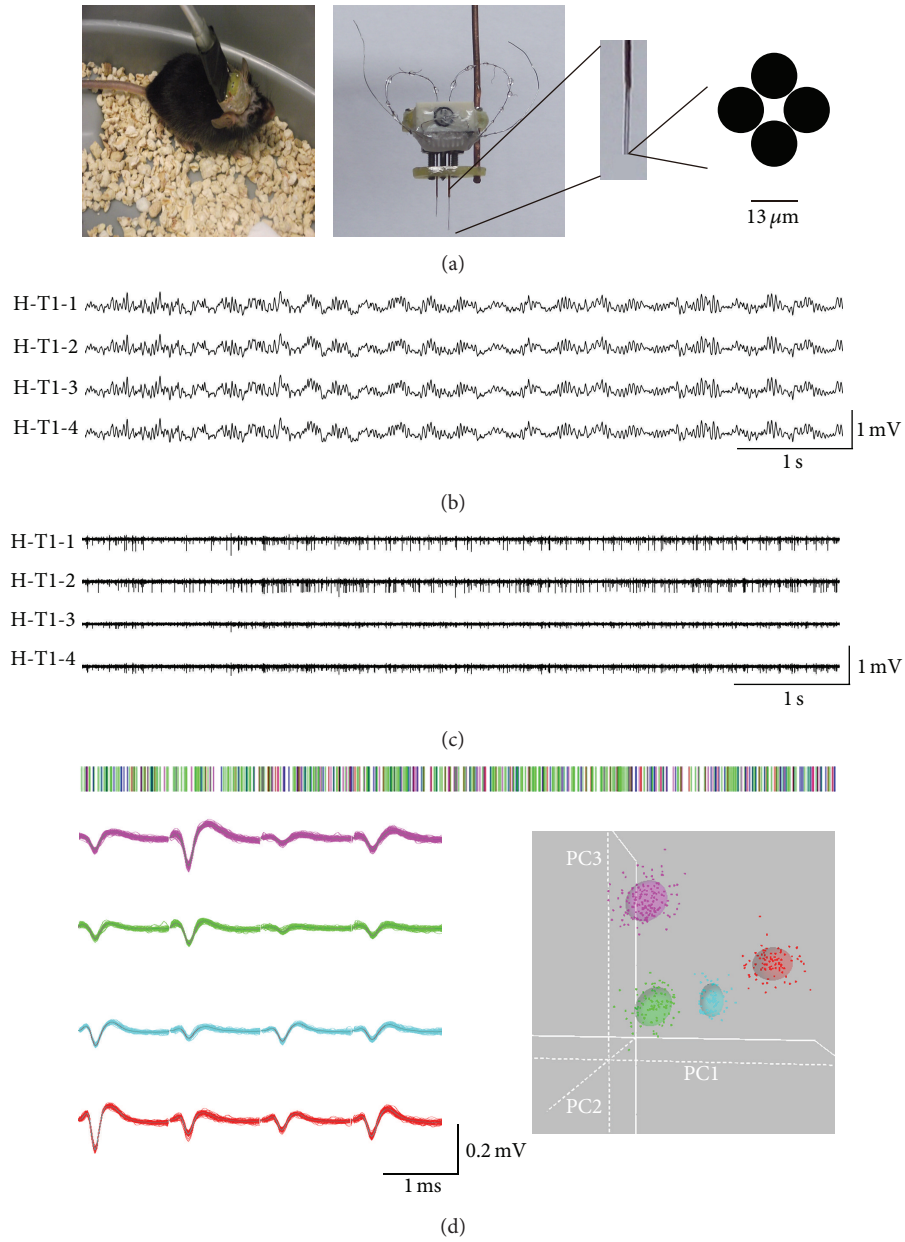

Figure 1: Multichannel microelectrode recordings. Two bundles of electrodes were inserted into the CA1 region of the left hippocampus and PF region of the left thalamus, respectively. Each bundle consists of two tetrodes and each tetrode is formed of four insulated nickel-chrome alloy electrodes (diameter of 13 μm, impedance of 0.5–1.0 MΩ). For each electrode, we extracted single-unit activities and LFPs. Single-unit activities were obtained by filtering the recording at 300–6000 Hz and sorting the filtered data using OfflineSorter software (Plexon Co, USA). To obtain the LFPs, we filtered the data at 0.5–100 Hz. (a) Multichannel microelectrode. The enlarged view shows one bundle of electrodes consisted of two tetrodes and the cross-section through a tetrode. (b) LFPs from a tetrode in the normal hippocampus. (c) Multiunit activity (MUA) of the same tetrode. (d) Example of single-unit activity. The upper trace is the spike train sorted from the MUA in (c). The spikes were from four neurons denoted by four colors. The left bottom traces show the superimposed single waveforms of spikes of four neurons. The right bottom figure shows the four clusters in the feature space, which were projected by the spikes of the four neurons, by using the principal component analysis (PCA) method. H, hippocampus; T, thalamus; T1&T2, Tetrode 1 and Tetrode 2 in a bundle. For example, H-T1-2 means the second channel of Tetrode 1 in hippocampus.

epilepticus (SE) was defined as continuous Stage 3 or more serious seizures. SE was terminated after 1 h by injection of diazepam (10 mg/kg).

2.5. Electrophysiological Recordings. A bundle of electrodes was inserted in CA1 of the left hippocampus (with bregma as the reference, anteroposterior (AP), −2.3 mm; mediolateral (ML), −2.1 mm; dorsoventral (DV), −1.0 to −1.4 mm) [28]. The other bundle of electrodes was implanted into the left PF (AP, −2.3 mm; ML, −0.5 mm; DV, −3.0 to −3.4 mm). Each bundle of electrodes can be independently regulated in the depth direction. The depth of the CA1 region was determined

electrophysiologically. The initial depth was 1.0 mm below the dura. Then the electrodes were lowered slowly. When the electrode reached the pyramidal cell layer of the CA1 region, single-unit activities were recorded. Similarly, the electrodes in the PF region were adjusted between the depth of 3.0 mm and 3.4 mm until single-unit activities were recorded. The electrodes were lowered to the target areas at least one day before the seizure induction.

The data were amplified (×500), filtered (0.5–6,000 Hz), and stored in a computer (16 bits AD converter, 40 kHz sampling rate) using OmniPlex D Neural Data Acquisition System (Plexon Co, USA).

2.6. Histological Experiments. At the end of the electrophysiological recordings, mice were deeply anesthetized with pentobarbital sodium (120 mg/kg) and perfused transcardially with 20 mL of 0.9% saline solution followed by 50 mL of fixative (4% paraformaldehyde in 0.1 M sodium phosphate buffer (PBS), pH 7.4). The brains were then removed and postfixed in 4% paraformaldehyde 0.1 M PBS solution at 4°C for 24 h, equilibrated in 30% sucrose in 0.1 M PBS at least overnight. The whole brain was frozen and sectioned coronally on a cryostat microtome set at 70 μm. Electrodes outside the target regions were excluded in the analysis.

2.7. Data Analysis. The data were replayed and filtered with two different band-pass filters: 0.5–100 Hz to obtain LFPs and 300–6,000 Hz to obtain spikes as illustrated in Figures 1(b) and 1(c), respectively. The spike data were later sorted into single-unit activities using the Offline Sorter software (Plexon Co, USA). Single-unit activities were sorted according to a threshold and shape detector using principal component analysis method (Figure 1(d)). LFP signals were resampled by the frequency of 500 Hz. In addition, LFPs recorded from 4 channels of a tetrode were highly similar since the distance between wires in a tetrode was only about 15–25 μm. Therefore we used the mean of LFP signals recorded from the four channels in a tetrode to represent the LFP signal of the tetrode. The term of LFP below refers to the mean value.

2.7.1. Cross-Correlation of Single-Unit Activities. We analyzed the synchronization of firing activities between the recorded neurons by calculating the cross-correlation function (CCF). CCF is one of the most commonly used methods to evaluate the synchronization of firing activities between neurons. In order to calculate CCF, each neuron's spike train is symbolized into "0" and "1" within a time bin (time bin = 2 ms, to ensure there is only up to one spike in one time bin), where "1" means that neuron i fires in the tth time bin and "0" means no firing. CCF is calculated as

$$\mathrm{CCF}(\Delta t) = \frac{N \sum_{t=1+|\Delta t|}^{N-|\Delta t|} r_1(t)\, r_2(t+\Delta t)}{(N-2|\Delta t|)\sqrt{\sum_{t=1}^{N} r_1(t)^2 \sum_{t=1}^{N} r_2(t)^2}}, \quad (1)$$

where $r_i(t)$ for $i = 1, 2$, denotes the spike train generated by the ith neuron at the moment t and N indicates the length of spike train [29]. The maximum of CCF reflects a maximal synchronization of two sequences when the $r_1(t)$ was postponed for lag Δt. In order to examine the dynamics of neuron population activities, we used a moving window with length of 5 seconds and shifted in 1-second steps to calculate CCF. In each window, Δt ranges from −200 ms to 200 ms.

2.7.2. Redundancy of LFP. Various methods have been used to analyze the temporal evolution of brain activities from EEG or LFP recordings, ranging from traditional linear methods to nonlinear methods [30]. To some extent, the nonlinear methods are superior to the traditional linear methods in extracting information from EEG or LFP data [31]. However, these nonlinear methods assume that the signal is stationary and originates from a low dimensional nonlinear system. Without doubt, EEG or LFP is nonstationary signal. Recently, Bandt and Pompe proposed an ordinal time series analysis method, that is, permutation entropy, which measures the irregularity of nonstationary time series [32]. This method concentrates on the order relations between the values of a time series but not the values themselves. The advantages of this method are its simplicity and low complexity in computation without further model assumptions [32, 33]. Furthermore, the Bandt-Pompe method is robust in the presence of observational and dynamical noise [34]. Over the last few years, the permutation entropy and related metrics have emerged as particularly appropriate complexity measures in the study of time series from biological systems, such as the brain or the heart. It is mainly used in researches on epilepsy, anesthesiology, and cognitive neuroscience [33].

Redundancy is equal to one minus normalized permutation entropy; thus, it is also an index to measures the irregularity of nonstationary time series, with the opposite trend to the permutation entropy. Here, the redundancy of LFPs was analyzed to deduce the signals' irregularity changing during the development of epileptic seizures.

Given a time series of length L, $\{x_1, x_2, \ldots, x_L\}$, a vector is generated by an embedding procedure: $S_t = [x_t, x_{t+\tau}, \ldots, x_{t+(m-1)\tau}]$, where m and τ are the embedding dimension and the lag, respectively. S_t is rearranged in an ascending order, $x_{t+(j_1-1)\tau} \le x_{t+(j_2-1)\tau} \le \cdots \le x_{t+(j_m-1)\tau}$. We set $j_{r-1} < j_r$ in the case of $x_{t+(j_{r-1}-1)\tau} = x_{t+(j_r-1)\tau}$. For m different numbers, there are $N = m! = (1\times2\times\cdots\times m)$ possible ordinal patterns π_i, $i = 1, \ldots, N$, also called permutations. Then we count the occurrences of the ordinal pattern π_i, which is denoted as $C(\pi_i)$, and the relative frequency is calculated by $p(\pi_i) = C(\pi_i)/[L-(m-1)\tau], i = 1, 2, \ldots, N$ [35].

Using the empirical probabilities $p(\pi_i)$, we compute the permutation entropy [32] of the time series, which is defined as

$$H = -\sum_{i=1}^{N} p(\pi_i) \cdot \log_2 p(\pi_i). \quad (2)$$

The index i runs over all possible ordinal patterns. $H_{\max} = \log_2 N$. If H is divided by $H_{\max}$, one obtains the normalized permutation entropy, which takes values from 0 to 1.

Here we used a moving window of length 2,500 sample points corresponding to 5 s duration, which was shifted forward in 1 s steps. Bandt and Pompe recommended that the length of the ordinal patterns should be set as $m = 3, \ldots, 7$

[32]. When m was set as 3, 4, or 5, the results were similar in our analysis (data not shown). For longer patterns, the duration of the moving window would have to be increased in order to reliably estimate these relative frequencies, and then the temporal resolution would become too low to track the dynamics of electrical activities during the epileptic seizures. So m was set to 3, yielding $3! = 6$ possible different patterns. The lag $\tau = 1$. Each moving window contains $2{,}500 - 3 + 1 = 2498$ patterns of length $m = 3$ and thus is large enough to estimate the relative frequencies of single patterns.

The redundancy is defined as follows [36]:

$$R = 1 - \frac{-\sum_{i=1}^{N} p(\pi_i) \cdot \log_2 p(\pi_i)}{\log_2 N} = 1 - \frac{H}{H_{\max}}. \tag{3}$$

The redundancy (R) takes values in the range [0, 1]. When only a single ordinal pattern occurs, R reaches its maximal value of one. If all ordinal patterns occur with equal probability, R becomes zero. In other words, "monomorphic" LFP signals map to high redundant ordinal time series consisting of very few ordinal pattern, while "pleomorphic" LFP signals will map to less redundant ordinal time series consisting of many ordinal patterns [36].

2.7.3. Directionality Index between Hippocampus and Thalamus. Various methods have been proposed to analyze the coupling direction between neuronal signals from different brain areas, such as Granger causality method [37] and state-pace and phase-dynamic approaches [38]. The Granger causality methods can be successfully applied to linear models but cannot be directly applied to nonlinear time series. The state-space approach requires optimal embedding parameters and the phase-dynamics approach requires strong oscillations in signals. The methods based on information theory are also proposed to estimate the coupling direction between neuronal signals, including transfer entropy [39] and conditional mutual information [40]. Recently, the permutation analysis and conditional mutual information were integrated, which was called permutation conditional mutual information (PCMI), to estimate the coupling direction between neuronal signals from different neuronal populations [41]. The stimulation results show that this method is superior to the conditional mutual information method and the Granger causality method for identifying the coupling direction between unidirectional or bidirectional neuronal populations [41].

For these reasons above, PCMI between LFPs recorded from hippocampus and thalamus was computed to assess the coupling direction between the two brain areas.

The LFPs are denoted as $X = \{x_t\}$ and $Y = \{y_t\}$. X and Y are converted to ordinal time series. The marginal probability distribution functions of X and Y are denoted as $p(\pi_i)$ and $p(\pi_j)$, respectively. The joint probability functions of X and Y is denoted as $p(\pi_i, \pi_j)$. The conditional probability function of X given Y is denoted as $p(\pi_i \mid \pi_j)$.

The joint permutation entropy between X and Y is defined as

$$H(X,Y) = -\sum_{i=1}^{N}\sum_{j=1}^{N} p(\pi_i, \pi_j) \log p(\pi_i, \pi_j). \tag{4}$$

Then, the conditional permutation entropy of X given Y is defined as

$$H(X \mid Y) = -\sum_{i=1}^{N}\sum_{j=1}^{N} p(\pi_i, \pi_j) \log p(\pi_i \mid \pi_j). \tag{5}$$

The PCMI is calculated by the following equations [41]:

$$\begin{aligned} I^{\delta}_{X\to Y} &= H(X \mid Y) + H(Y_\delta \mid Y) - H(X, Y_\delta \mid Y), \\ I^{\delta}_{Y\to X} &= H(Y \mid X) + H(X_\delta \mid X) - H(Y, X_\delta \mid X), \end{aligned} \tag{6}$$

where X_δ or Y_δ is an observation derived from the state of the process X or Y δ steps in the future. The information that is transferred from the process X (or Y) to the process Y (or X) is defined as

$$\begin{aligned} I_{X\to Y} &= \frac{\sum_{\delta=\delta_1}^{\delta_2} I^{\delta}_{X\to Y}}{\delta_2 - \delta_1 + 1}, \\ I_{Y\to X} &= \frac{\sum_{\delta=\delta_1}^{\delta_2} I^{\delta}_{Y\to X}}{\delta_2 - \delta_1 + 1}, \end{aligned} \tag{7}$$

where δ_1 and δ_2 are the minimal and maximal steps, respectively. To decrease fluctuations of the estimated directionality index, $I_{X\to Y}$ and $I_{Y\to X}$ were averaged over a short range of steps. Based on the conditional mutual information, the directionality index between X and Y is defined by

$$D_{XY} = \left(\frac{I_{X\to Y} - I_{Y\to X}}{I_{X\to Y} + I_{Y\to X}}\right). \tag{8}$$

The value of D_{XY} ranges from -1 to 1. $D_{XY} > 0$ means that the information flows from the process X to Y. $D_{XY} < 0$ means that the information flows from the process Y to X, and $D_{XY} = 0$ means that the interactions between X and Y are symmetrical [41].

Here the length m of the patterns was set to 3. To reliably estimate these relative frequencies of each pattern, the length of moving window was set to 2,500 sample points corresponding to 5 s duration and shifted forward in 1-s steps. The lag $\tau = 1$. δ_1 and δ_2 were set to 1 and 10, respectively.

2.8. Thalamic Inactivation. In order to confirm the results of the data analysis above, we performed the pharmacological experiments. We used the sodium channel blocker tetrodotoxin (TTX) to inactivate the thalamus and examined its effect on the seizure development. These experiments were performed on anesthetic mice because of the limitation of our present experiment conditions. Mice were anesthetized by pentobarbital sodium (100 mg/kg) intraperitoneally and mounted in a stereotaxic frame. Prior to injection of TTX,

animals had a baseline seizure induced by the intraperitoneal injection of pilocarpine (300 mg/kg). To deliver drugs to the thalamus, a 1-μL syringe was loaded with either 0.1 mM TTX or 0.9% saline solution for control. The tip of the syringe was placed into PF (AP, −2.3 mm; ML, −0.5 mm; DV, −3.0 mm). The standard TTX injection was 0.8 μL (0.1 mM), released slowly over several minutes. LFPs from CA1 (AP, −2.3 mm; ML, −2.1 mm; DV, −1.4 mm) and PF (AP, −2.3 mm; ML, −0.5 mm; DV, −3.4 mm) were simultaneously recorded with the drug delivery. Electrodes or syringe needles outside the target regions were excluded in the analysis.

3. Results

Neural electrical activities were simultaneously recorded from CA1 of hippocampus and PF of thalamus during the development of seizures from 9 mice. Typically, seizures initiated 12–65 min after pilocarpine was injected (31.7 ± 17.8 min, mean ± S.D., $n = 9$) and manifested both behaviorally and electrographically. The seizure onset time of seizures was determined by visual inspection based on LFP recordings and confirmed by at least three authors. Clear seizure activities with high-voltage discharges were firstly identified, which usually exceeded the threshold of three times the standard deviation of the baseline. Meanwhile the behavioral severity should be over Stage 4 based on Racine's scale [27]. Then we looked back on the signals with the clear seizure activity to find out the earliest appearance of ictal discharges by eye. In this study, seizures usually started with the hypersynchronous-onset type. Occasionally, seizures started with a period of low-amplitude, high-frequency oscillations, which would develop into high-amplitude, low-frequency oscillations in a few seconds. These two kinds of seizure onset types were very similar as described previously [42]. Generally, the seizures started almost simultaneously from the hippocampus and the thalamus (Figure 2(a)), and the power of LFPs raised immediately over a wide frequency band, including theta, alpha, beta, and gamma activity (Figure 2(b)). Because we used a 50 Hz notch filter when collecting the data, the power density spectral showed a low-power frequency band around 50 Hz. The seizures lasted 20 s up to 73 s (41.3 ± 21.3 s, mean ± S.D., $n = 9$) and then were terminated. Figure 2(c) shows the tonic phase and clonic phase of the seizure shown in Figure 2(a). After the first seizure, recurrent seizures were followed with intervals of 10 to 30 min. In order to obtain comparable results, only the first seizure in each mouse was included in the analysis below.

3.1. Redundancy of LFP and Cross-Correlation of Single-Unit Activities. Redundancy of LFP reflects the irregularity of LFP signals. More "monomorphic" LFP yields higher redundancy, while more "pleomorphic" LFP yields lower redundancy. The cross-correlation of single-unit activities reflects the synchronization of firing between neurons. We used these two measures to qualify the dynamic changes of neuronal activities in hippocampus or thalamus during the development of epileptic seizures in different spatial scales.

The redundancy (R) of LFP for each tetrode was computed. The results for two example mice (Mouse #2 and #6) are displayed in Figure 3. R increased shortly after the seizure onset and then followed by a fluctuating time course with an overall tendency to decrease toward the seizure termination and into the post-seizure time period (Figure 3(b)). R maintained at high level throughout the seizure for Mouse #2, while R reached its maximum value at the beginning half of seizure and then slowly decreased to the end for Mouse #6. The trends of R corresponding to the evolution of the two seizures were consistent, though the details were different.

The statistics analysis results across all of the 9 seizures from 9 mice are illustrated in Figure 4. The pre-seizure time period (PreSz) contains 120 s before the seizure onset, and the post-seizure time period (PostSz) contains 30 s immediately after the seizure termination. Here we chose the time course of PostSz shorter than that of PreSz. Because the mouse would soon come out of the depressed pos-tseizure state and began preparing for the next seizure about 30 s after the seizure termination based on our experiences. The time period between the seizure onset and termination is denoted as "Sz," whose period varies from seizure to seizure, lasting 20 s to 73 s. The control period contains 120 s before the pilocarpine injection (Figure 4(a)). As shown in Figure 4(b), in both hippocampus and thalamus, R of Sz was significantly larger than control (pair-wised t-test, $P < 0.05$, $n = 9$), and R of PostSz was significantly smaller than control (pair-wised t-test, $P < 0.05$, $n = 9$). There was no significant difference between control and PreSz period (Figure 4(b)). This indicated that the LFPs during the seizure are more "monomorphic" and rhythmic. In addition, R of Sz and PostSz in hippocampus were significantly larger than that in thalamus, but there was no significant difference during the control and PreSz periods. This indicated that during the Sz and PostSz periods LFPs in hippocampus were more rhythmic than those in thalamus.

In some cases, R showed a transient decrease at the seizure onset, which may last 6 to 12 s (9.1 ± 2.3 s, mean ± S.D., $n = 4$) (Figure 3(b)). 4 of 9 seizures showed this phenomenon. It reflected that the patterns of LFPs become more random at the seizure onset, but the random state would not last long and it would be soon replaced by the rhythmic state.

We further analyzed the single-unit activities recorded from tetrode H-T2 in Mouse #2 and tetrode T-T1 in Mouse #6. Two neurons were sorted from each tetrode (Figure 3(d)). It is difficult to reliably identify the single units during the seizure when the LFP showed sharp ictal discharges. So only the first few seconds after the seizure onset were included in the analysis. We computed the CCF of spike trains. It showed a transient desynchronization of neuronal activities at the seizure onset and a resynchronization phase in the flowing period in Mouse #2, while it did not show the desynchronization phase in Mouse #6 (Figures 3(c) and 3(d)).

As shown in Figures 3(b) and 3(c), the variation tendency of the peak values of CCF between neurons matched the variation tendency of R of LFP. As we know, LFP is a summation of synaptic activities of many of neurons around the recording electrode. It reminds us that the rhythmic LFP might reflect the synchronization of neurons to some extent. In some way, the dynamic of LFP could reflect the interactions between neurons, including the synchrony

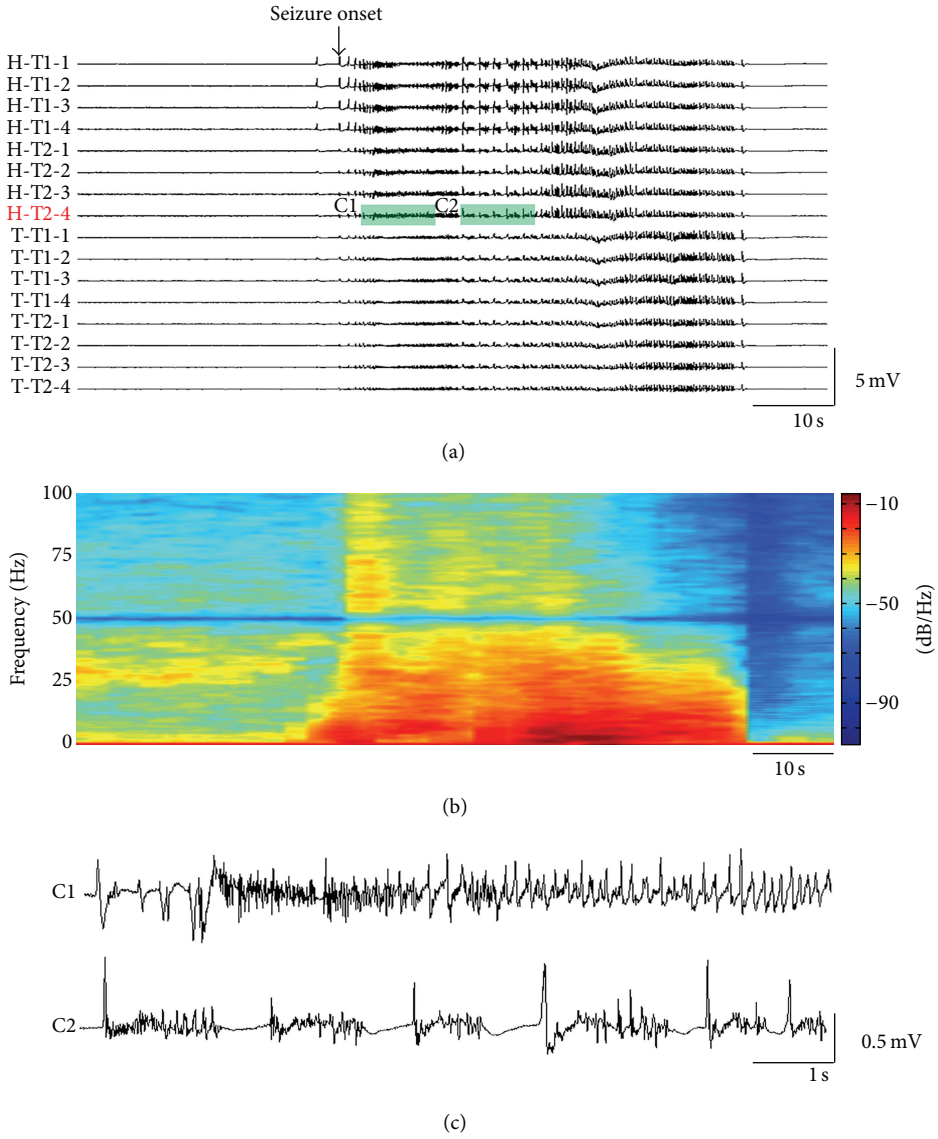

Figure 2: LFPs during the first seizure of an example mouse. (a) Single seizure recorded by four tetrodes. All data were filtered at 0.5–100 Hz. The seizure onset time is marked by an arrow. (b) Power spectral of LFP from Channel H-T2-4. (c) The details of the recordings shown in the shadow in (a). (C1) shows the tonic phase of epileptic seizure and (C2) shows the clonic phase of epileptic seizure. H, hippocampus; T, thalamus; T1&T2, Tetrode 1 and Tetrode 2 in a bundle.

characteristics. Unfortunately, we could not get the statistical analysis results of the cross-correlation of single neurons, since we could only get the recordings from a few of single neurons steadily during the induction of seizures at the present experiment conditions.

3.2. Directionality Index between Hippocampus and Thalamus. To assess the interaction between two neuronal populations recorded from hippocampus and thalamus, we computed directionality index (D_{XY}) between LFP signals of the two areas. Figure 5(a) shows the LFPs recorded by four tetrodes during the first seizure from Mouse #2. The red line indicates the seizure onset time. D_{XY} between LFP signals of the two areas are displayed in Figure 5(b) and the averaged D_{XY} is displayed in Figure 5(c). The results showed that the information flowed from hippocampus to thalamus before seizure, and inversely, the information flowed from thalamus to hippocampus at the seizure onset. After about 30 s, the direction of information flows recovered. After the seizure termination, D_{XY} was very small, which means the interaction between hippocampus and thalamus were almost symmetrical.

We inspected D_{XY} between hippocampus and thalamus of all seizures (Figure 6(a)). The results show that the information flowed from thalamus to hippocampus at the seizure onset or shortly after the seizure onset in most cases, no matter what the direction was before the seizure onset or after the early part of the seizure. For the statistics analysis, we further divided the Sz period into three parts. The first part is the initiation period of the seizure (IS), containing one-fifth

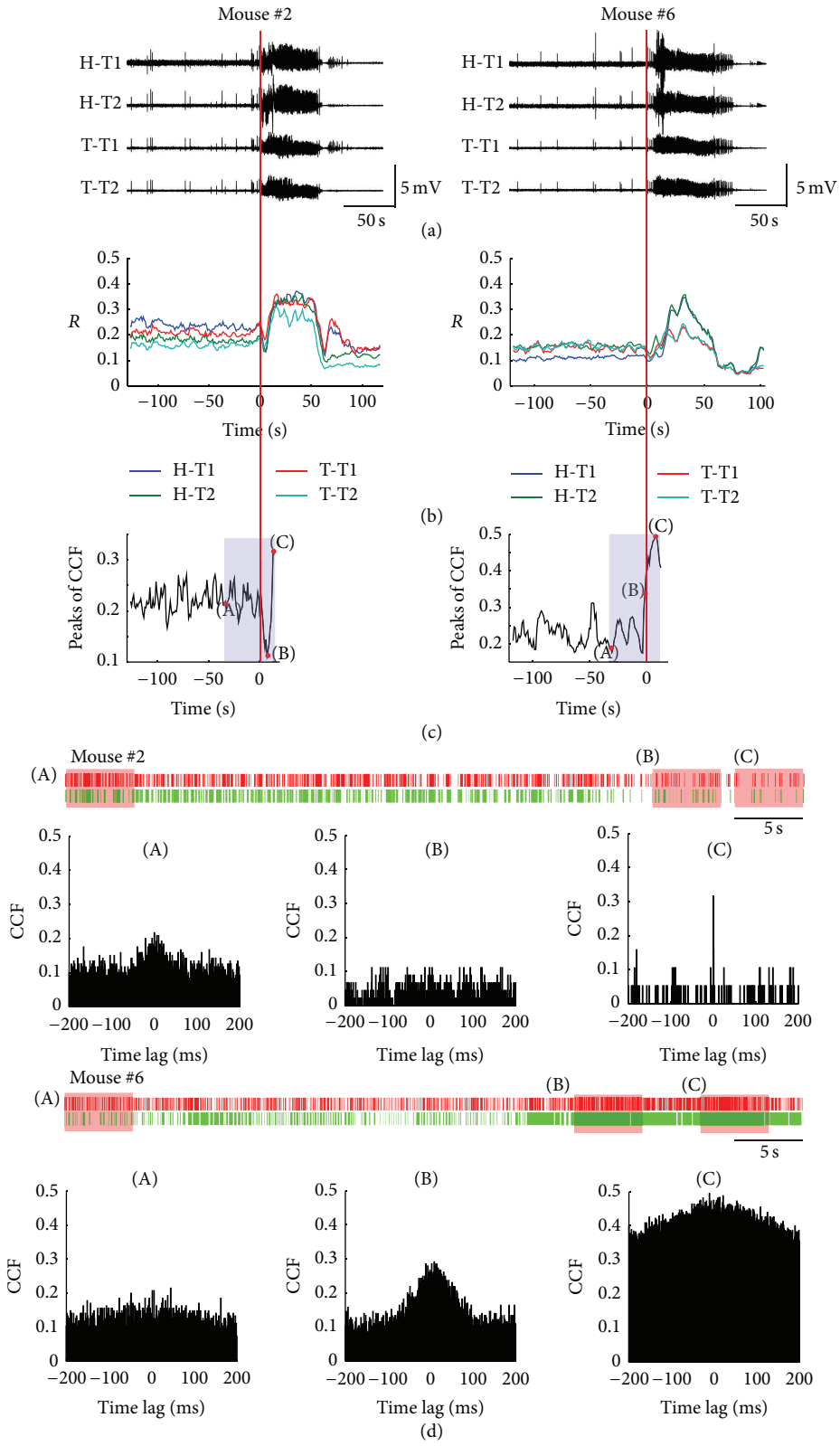

FIGURE 3: Peri-ictal changes of electrical brain activities as assessed by redundancy (R) of LFP and cross-correlation function (CCF) of single-unit activities. (a) LFPs of two sample seizures from Mouse #2 and Mouse #6. Seizure onset is marked by red line. (b) Peri-ictal changes of R of LFPs during the seizures shown in (a). (c) Dynamic changing of peak values of CCF of two neuronal spike trains sorted from tetrode H-T2 in Mouse #2 and tetrode T-T1 in Mouse #6. (d) Raster of the spikes from two neurons sorted from the two tetrodes above (shadows in (c)) and CCF in the periods of 5 s marked by (A), (B), and (C) in (c). H, hippocampus; T, thalamus; T1&T2, Tetrode 1 and Tetrode 2 in a bundle.

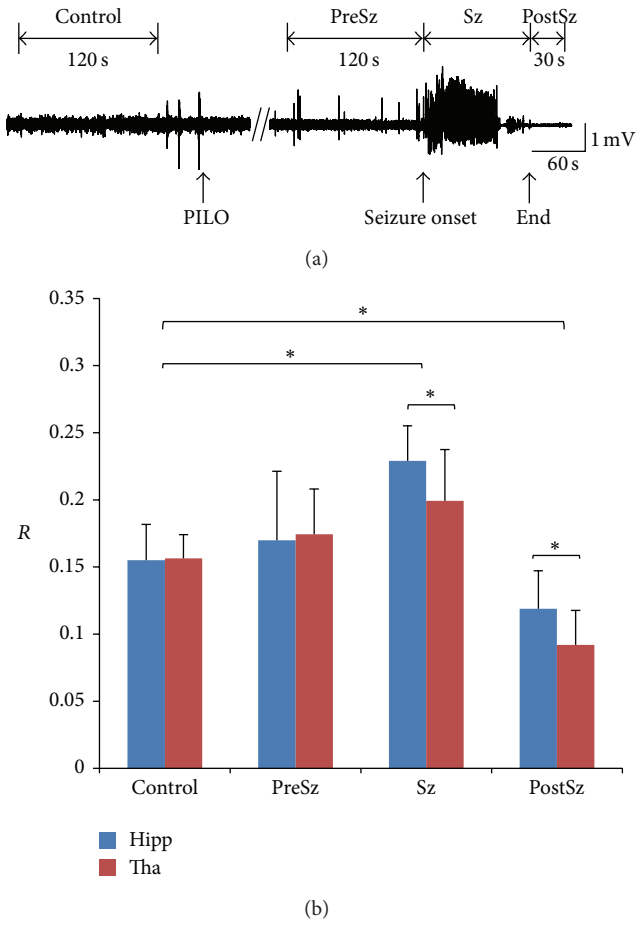

FIGURE 4: Statistics analysis result of signal redundancy for all 9 mice. (a) Time periods' definition. Control period contains 120 s before the pilocarpine injection. Pre-seizure (PreSz) time period is before the seizure onset with 120-s long. Post-seizure (PostSz) time period is immediately after seizure termination with 30 s long. Time period between seizure onset and termination is denoted as "Sz." (b) Statistical analysis results of redundancy (R). Error bar means standard deviation. Stars ($*$) indicate statistically significant differences between the distributions for control period and the following three time periods (pair-wised t-tests, significance level $P < 0.05$). Hipp, hippocampus; Tha, thalamus; PILO, pilocarpine.

of the time course of the seizure from the seizure onset. The third part is the end of the seizure (ES), containing one-fifth of the time course of the seizure immediately before the seizure termination. The second part is the middle part of the seizure (MS) between the first and the third part (Figure 6(b)). We then calculated the percentages of the two directions of information flow during the three periods of the seizure for each mouse. We obtained D_{XY} in each moving window during the three periods. For a certain period and for each mouse, we defined the percentage of $D_{XY} > 0$ as the percentage of information flow from hippocampus to thalamus and the percentage of $D_{XY} < 0$ as the percentage of information flow from thalamus to hippocampus, respectively. For each mouse, the summation of percentages of the two directions is 100% during each specific period. For the IS period, the information flowed from thalamus to hippocampus in most cases (7 of 9 seizures, including Mouse #2, #4, #5, #6, #7, #8, and #9). In the other two seizures, the information flow was symmetrically bidirectional, but none was found in which the information flowed from hippocampus to thalamus during the IS period (Figure 6(c)). In the other two periods, we did not find consistent results (data not shown). These results suggest that the thalamus may play an important role in the initiation of seizure.

3.3. Inactivation of Thalamus. To further confirm the role of thalamus, we used the pharmacological method to inactivate thalamus to examine its effect on the seizure. After the animals had a baseline seizure induced by pilocarpine, TTX was injected into the thalamus ($n = 2$). The inactivation of thalamus caused a reduction of seizure activities (Figures 7(a) and 7(c)), and there was a power reduction as shown in Figure 7(b), though the power was larger than the baseline. But the injections of normal saline ($n = 1$) had little effect on the development of seizure activities and the power spectral (Figures 7(d)–7(f)). In both cases, the directionality index (D_{XY}) did not show obvious change after the injection of TTX or normal saline (Figures 7(a) and 7(d)). These results indicated that PF did not play the leading role after seizure initiation, but it still had an effect on the seizure activities.

4. Discussion

In this study, we used 16-channel microelectrode to record the LFPs and single-unit activities from hippocampus and thalamus of mice. The computational methods from symbolic dynamics and information theory were used to investigate the dynamic changes of neural activities from each brain area and the direction of information flow between the two brain areas. These methods mapped the raw LFP signals into ordinal time series, which reflected the relational aspects between consecutive values of the original LFP signals but not the values themselves. Our findings, mainly based on analysis of LFPs, reveal two important points about the epileptic seizures induced by pilocarpine.

First, we found a global increase of redundancy of ictal LFPs, either in hippocampus or in thalamus (Figures 3 and 4). However, in some cases, the redundancy of LFP (R) shows a transient decrease shortly after the seizure onset, which may last 6 to 12 s (9.1 ± 2.3 s, mean ± S.D., $n = 4$) (Figure 3(b)). The increase of R suggests more rhythmic LFPs occurred during the ictal state, while the transient decrease of R suggests that the LFPs are transiently disordered at the seizure onset. In a traditional view, epileptic seizures are commonly considered to be the result of monolithic, hypersynchronous activities arising from an imbalance between the excitation and inhibition in neuronal network. However, our results indicate that the epileptic seizure is not a monolithic state. In recent years, several studies have demonstrated the heterogeneity of epileptic seizure in different spatial scales. Schindler and his colleagues find that the correlation of multichannel EEG either remains approximately unchanged or decreases during the first half of the seizures in patients with pharmacoresistant focal epilepsy [43]. In a smaller

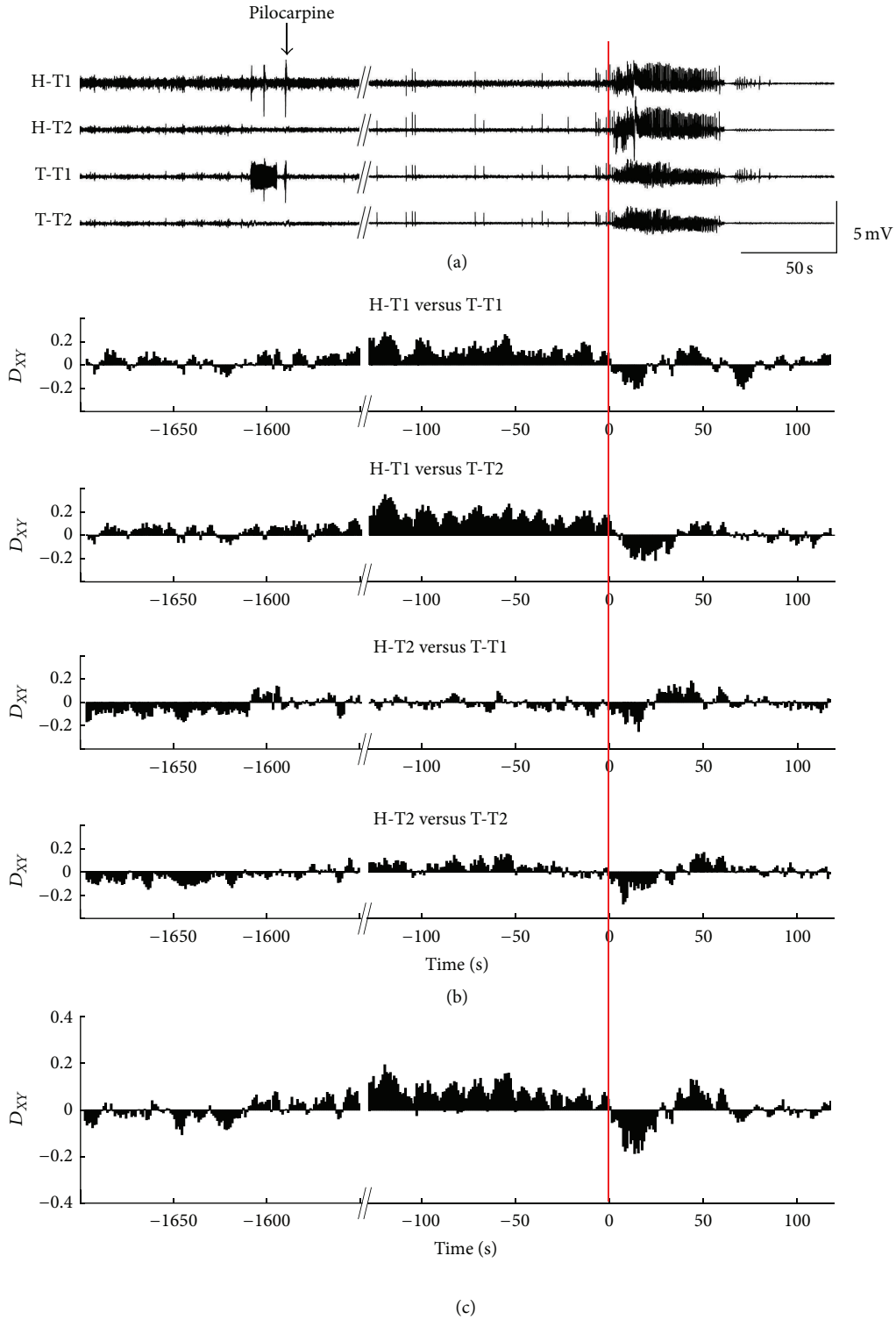

Figure 5: One example of peri-ictal coupling dynamics between hippocampus and thalamus. (a) Mean values of LFPs recorded from four channels of each tetrode. (b) The directionality index (D_{XY}) between hippocampus and thalamus. We calculated D_{XY} between each tetrode's recording from hippocampus and thalamus of the example mouse, getting four combinations. (c) The averaged directionality index (D_{XY}). The red line indicates the seizure onset time. H, hippocampus; T, thalamus; T1&T2, Tetrode 1 and Tetrode 2 in a bundle.

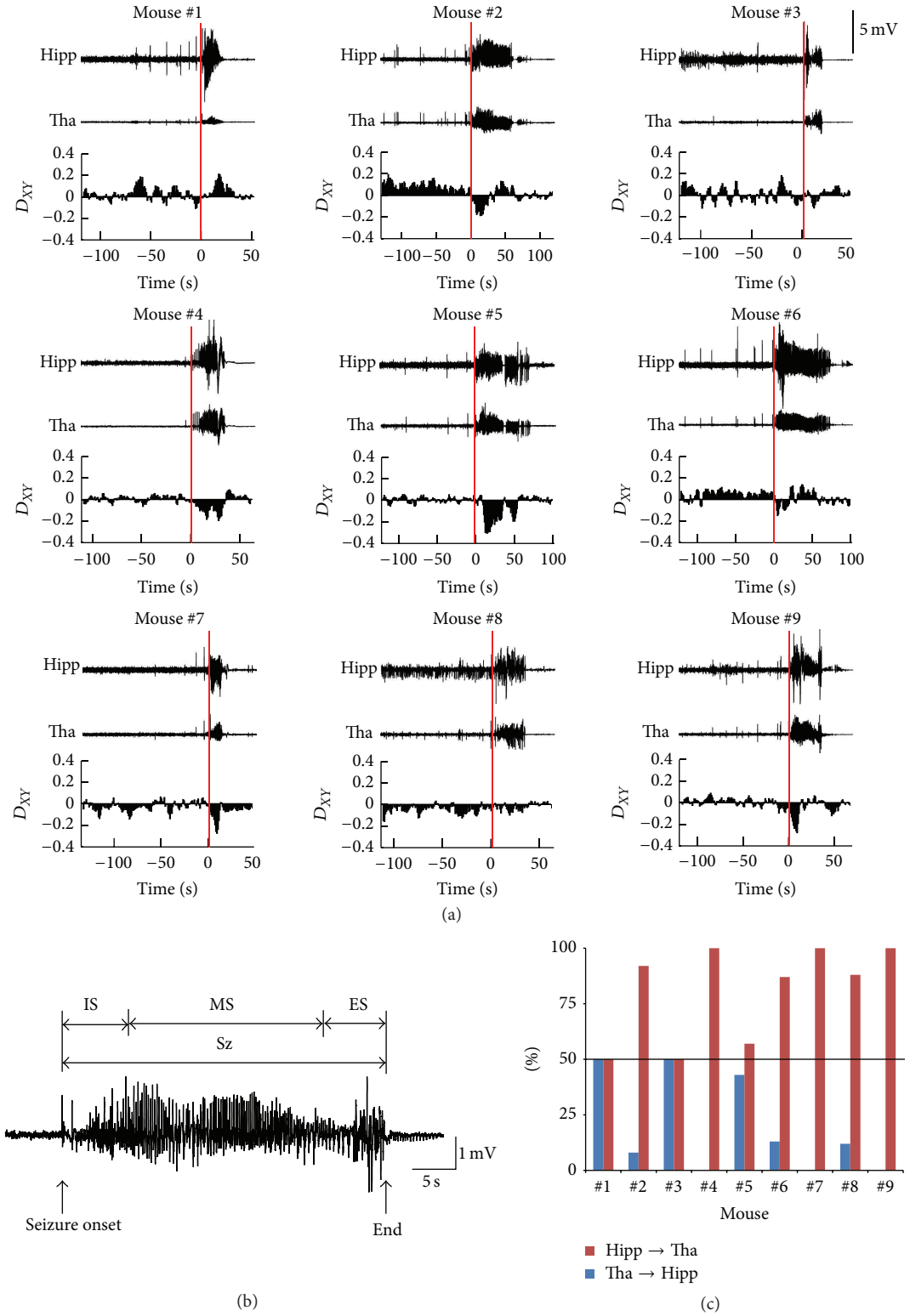

FIGURE 6: Peri-ictal coupling dynamics between hippocampus and thalamus. (a) Time course of directionality index (D_{XY}) between hippocampus and thalamus during the epileptic seizures in 9 mice. The upper two traces show the averaged LFPs from hippocampus and thalamus. The lower trace shows the averaged D_{XY}. The red line indicates the seizure onset time. (b) Time periods' definition. We divided the Sz period into three parts. The first part is the initiation period of seizure (IS), containing one-fifth of the time course of seizure from the seizure onset. The third part is the end of seizure (ES), containing one-fifth of the time course of seizure immediately before the termination of seizure. The second part is the middle part of the seizure (MS) between the first and the third part. (c) Percentages of coupling direction "hippocampus → thalamus" and "thalamus → hippocampus" during the initiation period of seizure (IS). The black solid line marks the threshold of 50%. Hipp, hippocampus; Tha, thalamus.

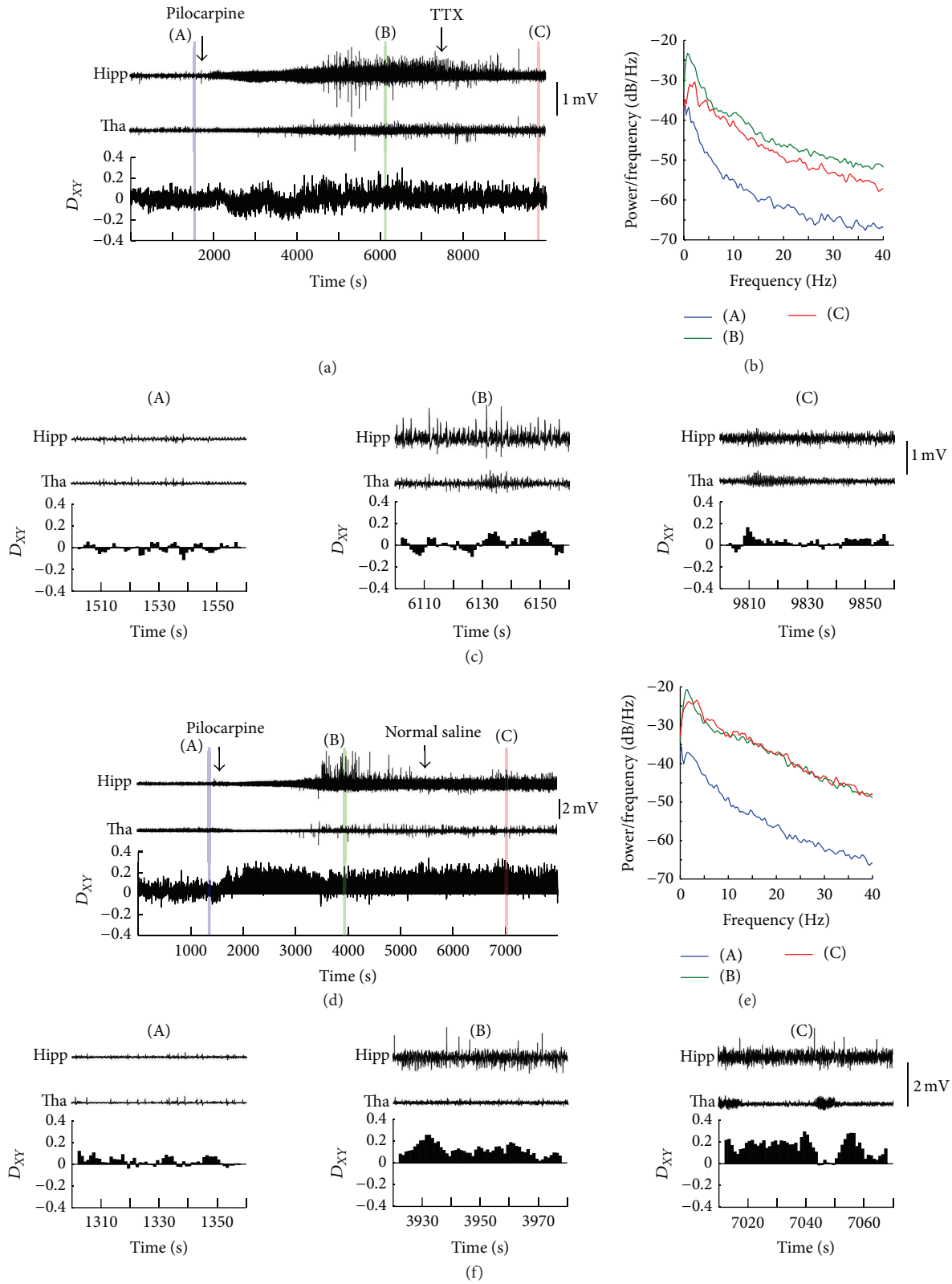

Figure 7: Seizures affected by the TTX injection in thalamus. (a) LFPs from hippocampus and thalamus and the averaged directionality index (D_{XY}) between the two brain areas before and after the injection of TTX into thalamus. (b) The power spectral density of the LFPs in hippocampus (shadowed areas in (a)). (c) 60-second samples from each trace in (a) (the shadowed areas). (d) LFPs from hippocampus and thalamus and averaged directionality index (D_{XY}) between the two brain areas before and after the injection of normal saline into thalamus in a control mouse. (e) The power spectral density of the LFPs in hippocampus (shadowed areas in (d)). (f) 60-second samples from each trace in (d) (the shadowed areas). Hipp, hippocampus; Tha, thalamus.

spatial scale, studies indicate that the LFP synchrony between the seizure generating brain and the other brain regions is lower in epilepsy patients than in control patients [44]. Another study shows that fractured microdomains exist in the epileptic brain, which can be observed by isolated microelectrodes rather than clinical macroelectrodes [45]. In a much smaller scale, it was shown that neuronal spiking activity during the initiation and spreading of seizures in humans was highly heterogeneous, suggesting complex and variable interactions between different neuronal groups [46].

Since LFPs are a summation of the synaptic activities of many of neurons around the recording electrode, we then examined how the single neurons acted during the peri-ictal period. The variation tendency of the peak values of CCF between neurons matches the variation tendency of R of LFP recorded from the same electrode very well, even in the period of transient decrease of R. As shown in Figures 3(b) and 3(c), when the CCF peak value gets larger, R gets larger as well. CCF of single neurons pair is a measure of the synchronization of neuronal activities. So we speculate that the lager R may reflect higher level of the synchronization of single neurons to some extent. The global increase of R during the seizures may reflect the global synchronization of neurons around the electrode to some extent, while the transient decrease of R may reflect the transient desynchronization of neurons around the electrode to some extent. Interestingly, Cymerblit-Sabba and Schiller find the similar biphasic network dynamics, which composed of an early desynchronization phase and a late resynchronization phase, in the pre-ictal state of pharmacologically induced seizures in rats [47]. The biphasic network dynamics may reveal a specific network mechanism underlying the development of epileptic seizure. But unfortunately, we do not have enough evidence to confirm this now. We cannot record lager amount of single-unit activities during the development of seizure in the present experiment conditions. We will try to improve the recording techniques to collect much more single-unit firing activities to confirm our conclusion.

Second, we found that the information tended to flow from thalamus to hippocampus during the initiation period of seizure (Figures 5 and 6). This indicates that the thalamus led the hippocampus during the initiation period to some extent. In clinical study, it shows the similar coupling direction between hippocampus and thalamus during the seizure initiation period in some of patients with TLE [9]. In animal models of TLE, studies have shown that thalamus indeed plays an important role in the initiation and spread of seizures, though the exact role is less understood [18, 19, 21–25]. Bertram put forward a framework to explain the neuronal circuits that support the different stages of seizures. It contains four parts, seizure focus, initiating circuits, paths of spread and neuromodulatory centers. In this framework, thalamus is served as part of the initiating circuit, which is the separate neuronal populations that are necessary to support the start of a seizure [10]. Although the framework need to be confirmed using a larger amount of data in the future, it provides a new view point to consider the role of brain structures out of the temporal lobe in TLE at the level of neuronal circuits. Our results are consistent with this framework, suggesting thalamus may play an important role in the initiation of epileptic seizures induced by pilocarpine. On the contrary, studies by Toyoda and colleagues have demonstrated that dorsomedial thalamus has consistently late seizure onsets and is unlikely involved in the seizure initiation in pilocarpine-treated rat model [48]. The controversial conclusion may be due to the different recording sites or different animal species. In addition, they drew the conclusion by simply comparing the seizure onset time across different brain regions. Without detectable epileptiform discharges in thalamus at the first moment of seizure onset does not mean that there is no information exchange between thalamus and the brain areas where the seizure starts, and thalamus may be involved in the seizure initiation circuits. Applying computational methods, such as PCMI, to analysis LFPs may reveal the characteristics of epileptic network which might not be accessible by the examination of the waveforms of neuronal signals. Of course, we cannot draw a strong conclusion only by the mathematical results. But we provide a new perspective to understand the seizure generation induced by pilocarpine in mice.

The pharmacological experiments show a suppression effect on the seizure activities by injection of TTX into thalamus but not completely. The power of LFPs in hippocampus after TTX injection is smaller than that before TTX injection but is higher than the baseline (Figure 7). Since the injection site was located at PF of thalamus, this result reminds us that the PF of thalamus may be not the only structure which has effect on the development of seizure, but it does have effect partially.

The TTX delivery experiment was done at the anesthetic state because of the limitation of our experiment conditions. TTX was injected into PF after the mouse had a baseline seizure. It is difficult to induce epileptic seizure by pilocarpine under anesthetic state. If TTX was injected before the seizure induction, we cannot determine whether the TTX injection had effect on the seizure or the seizure was not induced at all. So we cannot observe the effect of TTX on the initiation of epileptic seizures. In our experiments, D_{XY} did not change after TTX injection, suggesting that PF did not play the leading role after seizure initiation. This result does not conflict with our results in freely moving state, nor can confirm the results before. So we will keep working on it in freely moving state in the future.

From a therapeutic perspective, researches on the role of thalamus in TLE may provide a potential target to the clinical resection and the deep brain stimulation. They may also further the understanding of the nature of seizure initiation and spread. Our data analysis brought new insight into the dynamic changes of single brain area and the interaction between brain areas during the development of seizures, and we still have many jobs to improve and further confirm our results.

Conflict of Interests

The authors declare that there is no conflict of interests regarding the publication of this paper.

Acknowledgments

This work was supported by the Key Basic Research Project of Science and Technology Commission of Shanghai (13DJ1400303), the Natural Science Foundation of Shanghai (12ZR1413800), the Shanghai Jiao Tong University Fund for Interdisciplinary Research for Medical Applications (YG2012ZD08), and the Seed Fund of Ren Ji Hospital (RJZZ13-005). The authors thank Dr. Sheng-Tian Li for comments on the paper.

References

[1] R. Kuruba, B. Hattiangady, and A. K. Shetty, "Hippocampal neurogenesis and neural stem cells in temporal lobe epilepsy," *Epilepsy and Behavior*, vol. 14, no. 1, pp. 65–73, 2009.

[2] J. Pilli, S. Abbasi, M. Richardson, and S. S. Kumar, "Diversity and excitability of deep-layer entorhinal cortical neurons in a model of temporal lobe epilepsy," *Journal of Neurophysiology*, vol. 108, no. 6, pp. 1724–1738, 2012.

[3] V. Aroniadou-Anderjaska, B. Fritsch, F. Qashu, and M. F. M. Braga, "Pathology and pathophysiology of the amygdala in epileptogenesis and epilepsy," *Epilepsy Research*, vol. 78, no. 2-3, pp. 102–116, 2008.

[4] P. D. Williamson, J. A. French, V. M. Thadani et al., "Characteristics of medial temporal lobe epilepsy: II. Interictal and ictal scalp electroencephalography, neuropsychological testing, neuroimaging, surgical results, and pathology," *Annals of Neurology*, vol. 34, no. 6, pp. 781–787, 1993.

[5] D. King and S. S. Spencer, "Invasive electroencephalography in mesial temporal lobe epilepsy," *Journal of Clinical Neurophysiology*, vol. 12, no. 1, pp. 32–45, 1995.

[6] B. C. Bernhardt, S. Hong, A. Bernasconi, and N. Bernasconi, "Imaging structural and functional brain networks in temporal lobe epilepsy," *Frontiers in Human Neuroscience*, vol. 7, article 624, 2013.

[7] C. la Fougère, A. Rominger, S. Förster, J. Geisler, and P. Bartenstein, "PET and SPECT in epilepsy: a critical review," *Epilepsy and Behavior*, vol. 15, no. 1, pp. 50–55, 2009.

[8] M. J. Hennessy, R. D. C. Elwes, C. D. Binnie, and C. E. Polkey, "Failed surgery for epilepsy: a study of persistence and recurrence of seizures following temporal resection," *Brain*, vol. 123, no. 12, pp. 2445–2466, 2000.

[9] M. Guye, J. Régis, M. Tamura et al., "The role of corticothalamic coupling in human temporal lobe epilepsy," *Brain*, vol. 129, no. 7, pp. 1917–1928, 2006.

[10] E. H. Bertram, "Neuronal circuits in epilepsy: do they matter?" *Experimental Neurology*, vol. 244, pp. 67–74, 2013.

[11] L. E. Jehi, "Cortico-thalamic connections and temporal lobe epilepsy: an evolving story," *Epilepsy Currents*, vol. 12, no. 5, pp. 203–204, 2012.

[12] S. Çavdar, F. Y. Onat, Y. Ö. Çakmak, H. R. Yananli, M. Gülçebi, and R. Aker, "The pathways connecting the hippocampal formation, the thalamic reuniens nucleus and the thalamic reticular nucleus in the rat," *Journal of Anatomy*, vol. 212, no. 3, pp. 249–256, 2008.

[13] Y. D. van der Werf, M. P. Witter, and H. J. Groenewegen, "The intralaminar and midline nuclei of the thalamus. Anatomical and functional evidence for participation in processes of arousal and awareness," *Brain Research Reviews*, vol. 39, no. 2-3, pp. 107–140, 2002.

[14] S. M. Sherman and R. W. Guillery, *Exploring the Thalamus and Its Role in Cortical Function*, MIT Press, Cambridge, Mass, USA, 2006.

[15] D. A. McCormick and D. Contreras, "On the cellular and network bases of epileptic seizures," *Annual Review of Physiology*, vol. 63, pp. 815–846, 2001.

[16] H. K. M. Meeren, J. P. M. Pijn, E. L. J. M. van Luijtelaar, A. M. L. Coenen, and F. H. L. da Silva, "Cortical focus drives widespread corticothalamic networks during spontaneous absence seizures in rats," *Journal of Neuroscience*, vol. 22, no. 4, pp. 1480–1495, 2002.

[17] D. M. Andrade, D. Zumsteg, C. Hamani et al., "Long-term follow-up of patients with thalamic deep brain stimulation for epilepsy," *Neurology*, vol. 66, no. 10, pp. 1571–1573, 2006.

[18] E. H. Bertram, P. S. Mangan, D. Zhang, C. A. Scott, and J. M. Williamson, "The midline thalamus: alterations and a potential role in limbic epilepsy," *Epilepsia*, vol. 42, no. 8, pp. 967–978, 2001.

[19] E. H. Bertram, D. Zhang, and J. M. Williamson, "Multiple roles of midline dorsal thalamic nuclei in induction and spread of limbic seizures," *Epilepsia*, vol. 49, no. 2, pp. 256–268, 2008.

[20] D. M. Sloan, D. Zhang, and E. H. Bertram, "Excitatory amplification through divergent-convergent circuits: the role of the midline thalamus in limbic seizures," *Neurobiology of Disease*, vol. 43, no. 2, pp. 435–445, 2011.

[21] Z. Nanobashvili, T. Chachua, A. Nanobashvili, I. Bilanishvili, O. Lindvall, and Z. Kokaia, "Suppression of limbic motor seizures by electrical stimulation in thalamic reticular nucleus," *Experimental Neurology*, vol. 181, no. 2, pp. 224–230, 2003.

[22] C. Hamani, M. Hodaie, J. Chiang et al., "Deep brain stimulation of the anterior nucleus of the thalamus: effects of electrical stimulation on pilocarpine-induced seizures and status epilepticus," *Epilepsy Research*, vol. 78, no. 2-3, pp. 117–123, 2008.

[23] H. G. Liu, A. C. Yang, D. W. Meng, N. Chen, and J. G. Zhang, "Stimulation of the anterior nucleus of the thalamus induces changes in amino acids in the hippocampi of epileptic rats," *Brain Research*, vol. 1477, pp. 37–44, 2012.

[24] M. Langlois, P. Polack, H. Bernard et al., "Involvement of the thalamic parafascicular nucleus in mesial temporal lobe epilepsy," *Journal of Neuroscience*, vol. 30, no. 49, pp. 16523–16535, 2010.

[25] K. Nail-Boucherie, B. Lê-Pham, S. Gobaille, M. Maitre, D. Aunis, and A. Depaulis, "Evidence for a role of the parafascicular nucleus of the thalamus in the control of epileptic seizures by the superior colliculus," *Epilepsia*, vol. 46, no. 1, pp. 141–145, 2005.

[26] L. Lin, G. Chen, K. Xie, K. A. Zaia, S. Zhang, and J. Z. Tsien, "Large-scale neural ensemble recording in the brains of freely behaving mice," *Journal of Neuroscience Methods*, vol. 155, no. 1, pp. 28–38, 2006.

[27] R. J. Racine, "Modification of seizure activity by electrical stimulation: II. Motor seizure," *Electroencephalography and Clinical Neurophysiology*, vol. 32, no. 3, pp. 281–294, 1972.

[28] K. Fraklin and G. Paxinos, *The Mouse Brain in Stereotaxic Coordinates*, Elsevier, London, UK, 3rd edition, 2007.

[29] L. Xiao, D. K. Zhang, Y. Q. Li, P. J. Liang, and S. Wu, "Adaptive neural information processing with dynamical electrical synapses," *Frontiers in Computational Neuroscience*, vol. 7, article 36, 2013.

[30] C. J. Stam, "Nonlinear dynamical analysis of EEG and MEG: review of an emerging field," *Clinical Neurophysiology*, vol. 116, no. 10, pp. 2266–2301, 2005.

[31] M. I. Rabinovich, P. Varona, A. I. Selverston, and H. D. I. Abarbanel, "Dynamical principles in neuroscience," *Reviews of Modern Physics*, vol. 78, no. 4, pp. 1213–1265, 2006.

[32] C. Bandt and B. Pompe, "Permutation entropy: a natural complexity measure for time series," *Physical Review Letters*, vol. 88, no. 17, Article ID 174102, 4 pages, 2002.

[33] M. Zanin, L. Zunino, O. A. Rosso, and D. Papo, "Permutation entropy and its main biomedical and econophysics applications: a review," *Entropy*, vol. 14, no. 8, pp. 1553–1577, 2012.

[34] O. A. Rosso, H. A. Larrondo, M. T. Martin, A. Plastino, and M. A. Fuentes, "Distinguishing noise from chaos," *Physical Review Letters*, vol. 99, no. 15, Article ID 154102, 4 pages, 2007.

[35] G. Ouyang, X. Li, C. Dang, and D. A. Richards, "Deterministic dynamics of neural activity during absence seizures in rats," *Physical Review E*, vol. 79, no. 4, Article ID 041146, 8 pages, 2009.

[36] K. Schindler, H. Gast, M. Goodfellow, and C. Rummel, "On seeing the trees and the forest: single-signal and multisignal analysis of periictal intracranial EEG," *Epilepsia*, vol. 53, no. 9, pp. 1658–1668, 2012.

[37] M. Lungarella and O. Sporns, "Mapping information flow in sensorimotor networks," *PLoS Computational Biology*, vol. 2, no. 10, article e144, 2006.

[38] D. A. Smirnov and R. G. Andrzejak, "Detection of weak directional coupling: phase-dynamics approach versus state-space approach," *Physical Review E*, vol. 71, no. 3, Article ID 036207, 13 pages, 2005.

[39] C. Ma, X. Pan, R. Wang, and M. Sakagami, "Estimating causal interaction between prefrontal cortex and striatum by transfer entropy," *Cognitive Neurodynamics*, vol. 7, no. 3, pp. 253–261, 2013.

[40] M. Vejmelka and M. Paluš, "Inferring the directionality of coupling with conditional mutual information," *Physical Review E*, vol. 77, no. 2, Article ID 026214, 12 pages, 2008.

[41] X. Li and G. Ouyang, "Estimating coupling direction between neuronal populations with permutation conditional mutual information," *NeuroImage*, vol. 52, no. 2, pp. 497–507, 2010.

[42] M. Levesque, P. Salami, J. Gotman, and M. Avoli, "Two seizure-onset types reveal specific patterns of high-frequency oscillations in a model of temporal lobe epilepsy," *Journal of Neuroscience*, vol. 32, no. 38, pp. 13264–13272, 2012.

[43] K. Schindler, H. Leung, C. E. Elger, and K. Lehnertz, "Assessing seizure dynamics by analysing the correlation structure of multichannel intracranial EEG," *Brain*, vol. 130, no. 1, pp. 65–77, 2007.

[44] C. P. Warren, S. Hu, M. Stead, B. H. Brinkmann, M. R. Bower, and G. A. Worrell, "Synchrony in normal and focal epileptic brain: the seizure onset zone is functionally disconnected," *Journal of Neurophysiology*, vol. 104, no. 6, pp. 3530–3539, 2010.

[45] M. Stead, M. Bower, B. H. Brinkmann et al., "Microseizures and the spatiotemporal scales of human partial epilepsy," *Brain*, vol. 133, no. 9, pp. 2789–2797, 2010.

[46] W. Truccolo, J. A. Donoghue, L. R. Hochberg et al., "Single-neuron dynamics in human focal epilepsy," *Nature Neuroscience*, vol. 14, no. 5, pp. 635–641, 2011.

[47] A. Cymerblit-Sabba and Y. Schiller, "Network dynamics during development of pharmacologically induced epileptic seizures in rats in vivo," *Journal of Neuroscience*, vol. 30, no. 5, pp. 1619–1630, 2010.

[48] I. Toyoda, M. R. Bower, F. Leyva, and P. S. Buckmaster, "Early activation of ventral hippocampus and subiculum during spontaneous seizures in a rat model of temporal lobe epilepsy," *Journal of Neuroscience*, vol. 33, no. 27, pp. 11100–11115, 2013.

Hindawi Publishing Corporation
Neural Plasticity
Volume 2014, Article ID 310146, 11 pages
http://dx.doi.org/10.1155/2014/310146

Research Article

Downregulated GABA and BDNF-TrkB Pathway in Chronic Cyclothiazide Seizure Model

Shuzhen Kong,[1,2] Zhihua Cheng,[3] Jianhui Liu,[2] and Yun Wang[1]

[1] *Institutes of Brain Science and State Key Laboratory of Medical Neurobiology, Fudan University, Shanghai 200032, China*
[2] *Chongqing Key Laboratory of Catalysis and Functional Organic Molecules and Chongqing Key Laboratory of Nature Medicine Research, Chongqing Technology and Business University, Chongqing 400067, China*
[3] *Department of Neurosurgery, Shanghai Ninth People's Hospital, School of Medicine, Shanghai Jiao Tong University, Shanghai 200011, China*

Correspondence should be addressed to Yun Wang; yunwang@fudan.edu.cn

Received 12 December 2013; Accepted 28 January 2014; Published 13 March 2014

Academic Editor: Sheng Tian Li

Cyclothiazide (CTZ) has been reported to simultaneously enhance glutamate receptor excitation and inhibit GABAA receptor inhibition, and in turn it evokes epileptiform activities in hippocampal neurons. It has also been shown to acutely induce epileptic seizure behavior in freely moving rats. However, whether CTZ induced seizure rats could develop to have recurrent seizure still remains unknown. In the current study, we demonstrated that 46% of the CTZ induced seizure rats developed to have recurrent seizure behavior as well as epileptic EEG with a starting latency between 2 weeks and several months. In those chronic seizure rats 6 months after the seizure induction by the CTZ, our immunohistochemistry results showed that both GAD and GAT-1 were significantly decreased across CA1, CA3, and dentate gyrus area of the hippocampus studied. In addition, both BDNF and its receptor TrkB were also decreased in hippocampus of the chronic CTZ seizure rats. Our results indicate that CTZ induced seizure is capable of developing to have recurrent seizure, and the decreased GABA synthesis and transport as well as the impaired BDNF-TrkB signaling pathway may contribute to the development of the recurrent seizure. Thus, CTZ seizure rats may provide a novel animal model for epilepsy study and anticonvulsant drug testing in the future.

1. Introduction

Gamma-aminobutyric acid (GABA) is the primary inhibitory neurotransmitter and exists widely in central nervous system of mammal animals. GABA receptors mediate inhibitory neurotransmission to prevent neurons from being overexcited in adult brain [1]. GABA is synthesized from glutamate by glutamate decarboxylase (GAD), which is a rate-limiting enzyme in GABA synthesis. Then GABA is released from neurons to synaptic cleft and exerts inhibitory effect. The major cortical GABA transporters (GAT), which uptake the GABA to neurons or glia from synaptic cleft, primarily localized to the presynaptic terminals and to glial processes adjacent to the synaptic cleft. Meanwhile, GAT also has been reported to participate in GABA releasing to adjust GABA concentration in synaptic cleft [2].

Brain-derived neurotrophic factor (BDNF) is a member of the neurotrophin family and mainly exists in hippocampus, amygdale, cortex, and cerebellum. It is synthesized by both neurons and glia and involved in survival, differentiation, and regeneration of neurons by binding its high affinity receptor, TrkB [3, 4]. BDNF is found in hippocampus which is highly sensitive for epileptiform insults [5–7]. However, there are still many controversial viewpoints about the role of BDNF in epileptogenesis.

Cyclothiazide (CTZ) not only blocks AMPA receptor desensitization, but also inhibits GABAA receptors [8], which leads to induction of epileptiform activities in hippocampal neurons in both in vitro and in vivo preparations [7, 9–11]. CTZ has also been demonstrated to acutely induce seizure behavior and epileptic EEG in freely moving rats [12], which involves extrasynaptic GABAA receptor participation [13].

Thus, CTZ is thought to be a useful convulsant for seizure animal model generation. However, whether CTZ could induce chronic seizure and the property of CTZ induced chronic seizure have still not been fully investigated. Here, we firstly reported the observation of a high proportion of the acutely CTZ induced seizure rats having recurrent seizure behavior during the period of up to 6 months after CTZ injection. We also demonstrated that the recurrent seizure induced by CTZ was associated with the typical epileptic EEG. The immunohistochemistry results further showed that the occurrence of the recurrent seizure was likely mediated by the impaired GABA inhibitory transmitter system and BDNF-TrkB pathway.

2. Methods

2.1. Animals. Adult male Sprague-Dawley rats (250–280 g; supplied by the Research Institute of Surgery, Chinese Third Military Medical University, Chongqing, China) were used for seizure induction and behavioral observation. All animal experiments were approved by the local committee of Laboratory Animals Usage of Chongqing Business and Technology University and carried out in accordance with Chinese National Science Foundation animal research regulation.

2.2. Behavioral Test and EEG Recording. Acute seizure induced by i.c.v. injection of CTZ was described in detail preciously [12]. 13 kindled seizure rats induced by CTZ (0.25 μmol in 5 μL, i.c.v.) injection, with behavioral seizure of grade IV and V, and 8 control rats treated with DMSO (5 μL, i.c.v.) were recorded for both behavior and EEG for 2 hours every other day until the 6th month. In two cases, the behavioral observation was carried out for continuous 6 months; both rats showed multiple recurrent seizure episodes. Behavioral seizures were scored using 5-graded Racine score system as previously defined [14]: briefly, Racine score I, facial clonus; score II, head nodding; score III, unilateral forelimb clonus; score IV, rearing with bilateral forelimb clonus; score V, rearing and falling (loss of postural control). The recurrent seizure assessment was based on the latency for spontaneous seizure behavior, the seizure score, and the seizure number. The seizure score in an animal was calculated based on the maximal behavioral seizure grade observed [15, 16].

For EEG recordings, electrophysiological signals were amplified (×1000) and filtered (0–50 Hz) using NeuroLog system (Digitimer Ltd, Hertfordshire, UK), digitized with CED Micro 1401 (Cambridge Electronic Design, Cambridge, UK), and recorded in a personal computer using Spike 2 software (version 6.0, Cambridge Electronic Design, Cambridge, UK). The presence of high-amplitude EEG seizure activity was used as a seizure marker. In some cases, the EEG recordings were unable to continue for the whole 6-month recording period due to their loss of the implanted skull electrodes.

2.3. Tissue Preparation. At the end of the 6-month recording, all rats, except those which died earlier, were perfused through the ascending aorta with 0.9% NaCl rapidly followed by 200 mL 4% paraformaldehyde in phosphates buffer. The brains were postfixed in the same fixative overnight at 4°C and were embedded in paraffin after dehydration with alcohol of different concentration. 6 mm thick sections were cut in a microtome and mounted on poly-L-lysine coated slides. The CTZ rats exhibited grade IV or V recurrent seizure behavior and the DMSO rats were selected for immunohistochemistry staining.

2.4. Nissl Staining. Four to six slides for every rat were deparaffinated with xylene and alcohol of different concentration, rinsed in tap water and then in distilled water, stained in 0.1% thionine solution for 10 minutes, rinsed quickly in distilled water, differentiated in 95% HCl-alcohol for 2–10 minutes, dehydrated in alcohol of different concentration for 5 minutes every time, cleared in xylene for 5 minutes, and mounted with neutral balsam solution.

2.5. Immunohistochemistry. SP immunohistochemistry assay for different receptor subunits was performed. Four to six slides from each rat were deparaffinated with xylene and alcohol of different concentration and incubated with 3% H_2O_2. Antigens of sections were retrieved with 0.125% trypsin solution. Sections were rinsed in Tris-HCl-buffered saline and preincubated with normal goat serum (SP-9001, ZSGB-BIO, China), followed by incubation with the primary antibodies, anti-GAD65 + GAD67 (Abcam), anti-GAT1 (Abcam), anti-BDNF (Abcam), and anti-TrkB (Abcam), at 4°C overnight. Subsequently, they were incubated with horseradish peroxidase-coupled goat anti-rabbit secondary antibodies (SP-9001, ZSGB-BIO, China) for 60 min at 37°C temperature. Finally, the sections were reacted with 0.4 mM 3,30-diaminobenzidine (ZSGB-BIO, China) and 0.01% H_2O_2 for 10–15 min. After each incubation step, except the preincubation, three 5 min washes with Tris-HCl-buffered saline were performed.

2.6. Image Acquisition and Analysis. Bright field images were acquired digitally on a Nikon 80i microscope with an NIS-elements 3.0 software (Nikon, Japan). Quantitative analysis of number of neurons in Nissl staining was performed manually and the numbers of GAD, GAT1, BDNF, and TrkB positive cells were quantitatively analyzed with NIS-elements 3.0 software.

2.7. Data Analysis. All data were expressed as mean ± SEM. Comparison between the CTZ group and the DMSO group was executed with independent-sample t-test. Results were considered significant at $P < 0.05$.

3. Results

3.1. Recurrent Seizure Behavior and Epileptic EEG of Chronic CTZ Seizure Model Rats. Previously we have reported that intracerebroventricular administration of CTZ acutely induced robust epileptic seizure [12]. Here we further studied the seizure behavior in 13 CTZ induced seizure rats for their chronic seizure activities for a period up to 6 months

Table 1: Recurrent seizure behavior (Racine score IV-V behavior) occurrence in the chronic phase in CTZ induced seizure rats.

Group	n	Mortality rate	Racine III recurrent seizure rate	Racine IV-V recurrent seizure rate	Seizure IV-V latency (days)	Acute seizure score	Recurrent seizure score
CTZ	13	30.8% ($n = 4/13$)	46.2% ($n = 6/13$)	46.2% ($n = 6/13$)	76.3 ± 24.8 ($n = 6$)	$4.75 \pm 0.16^{***}$ ($n = 10$)	$2.60 \pm 0.72^{*}$ ($n = 10$)
DMSO	8	0% ($n = 0/8$)	12.5% ($n = 1/8$)	0% ($n = 0/8$)	—	0 ($n = 8$)	0.38 ± 0.38 ($n = 8$)

$^{*}P < 0.05$, $^{***}P < 0.001$, in comparison with the DMSO control.

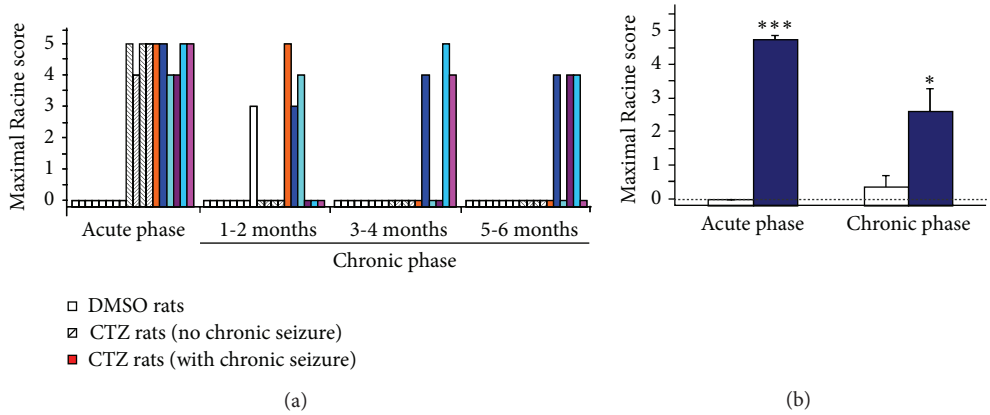

Figure 1: Recurrent seizure behavior occurrence in the chronic phase after CTZ induced seizure rats. (a) Bar chart showing the seizure behavior occurrence within 6-month period after CTZ induced acute seizure in individual rats studied. DMSO control rats ($n = 8$) were represented with white bar and CTZ rats ($n = 10$) were represented with either black strip bars ($n = 4$) or color bars ($n = 6$) for rats without or with recurrent seizure observed, respectively. (b) Bar chart showing the group maximal seizure scores obtained from the DMSO control rats ($n = 8$) and CTZ rats ($n = 10$) recorded for 6 months after CTZ induction of the seizure ($^{*}P < 0.05$, $^{***}P < 0.001$, in comparison with the DMSO control).

after CTZ administration in a noncontinuous monitoring experimental paradigm (see Section 2). In these 13 rats, they all had Racine score 4 and score 5 seizure behavior during the acute seizure induction phase (Figure 1). Among them, 6 (46.2%) had been observed to have recurrent seizure behavior with the shortest latency of 15 days (mean latency of 76.3 ± 24.8 days) after CTZ injection; 4 of them were without recurrent seizure being observed (Figure 1(a)); and 4 other rats were dead at days 6, 9, 15, and 99 after the CTZ injection (including 1 that had generalized seizure one day before its death at day 15). Recurrent seizure behavior showed as blinking, salivating, facial or automatisms, forelimb clonus, and even rearing and falling, similar to those behaviors showed during the acute phase [12]. Among those 6 rats observed to have recurrent seizure behavior, we found 2 rats having multiple seizure episodes (4 and 3, resp.) within 6-month recording period (Figure 1(a)), and the mean maximal Racine score for those 6 rats having recurrent seizures was 4.33 ± 0.16 ($n = 6$, Figure 1(b)), similar to the acutely induced seizure behavior (4.75 ± 0.16, $n = 6$) in these 6 rats. In contrast, 8 DMSO (i.c.v.) administered rats during acute seizure induction phase were not observed to have any seizure behavior, and only 1 rat had a stage 3 behavior at day 14 after injection, but not in the other 7 rats for recording up to 6 months (Table 1). As a group ($n = 10$ including those having and not having recurrent seizure but without 3 dead rats), the mean maximal recurrent seizure score was 2.60 ± 0.72 in those CTZ rats, which significantly differed to the DMSO control group (0.38 ± 0.38, $n = 8$; $P < 0.05$) (Figure 1(b)).

In addition to the seizure behavior observed in the chronic phase, we also successfully recorded the EEG response in 3 out of 6 of the CTZ induced seizure model rats at the certain period within the 6-month observation period. As shown in Figure 2, the epileptiform EEG activities were detected on day 150 after initial seizure induction in one rat. The ictal like high amplitude high frequency bursting activities were usually associated with the typical seizure behaviors with the Racine score III or above (Figure 2(b)). In addition, interictal spikes or sharp waves also appeared before or after the ictal like bursting EEG activities (Figure 2(b)). However, neither interictal spikes nor ictal like bursting EEG activities were observed during the period while the seizure behavior was absent (Figure 2(a)).

Above all, CTZ seizure models exhibited recurrent seizure behaviors associated with epileptic EEG changes in chronic phase 1–6 months after acute seizure induction.

3.2. CTZ Seizure Did Not Affect the Hippocampal Neuronal Fate for up to 6-Month Chronic Recurrent Phase in Rats. Nissl staining was used to investigate the morphological alteration

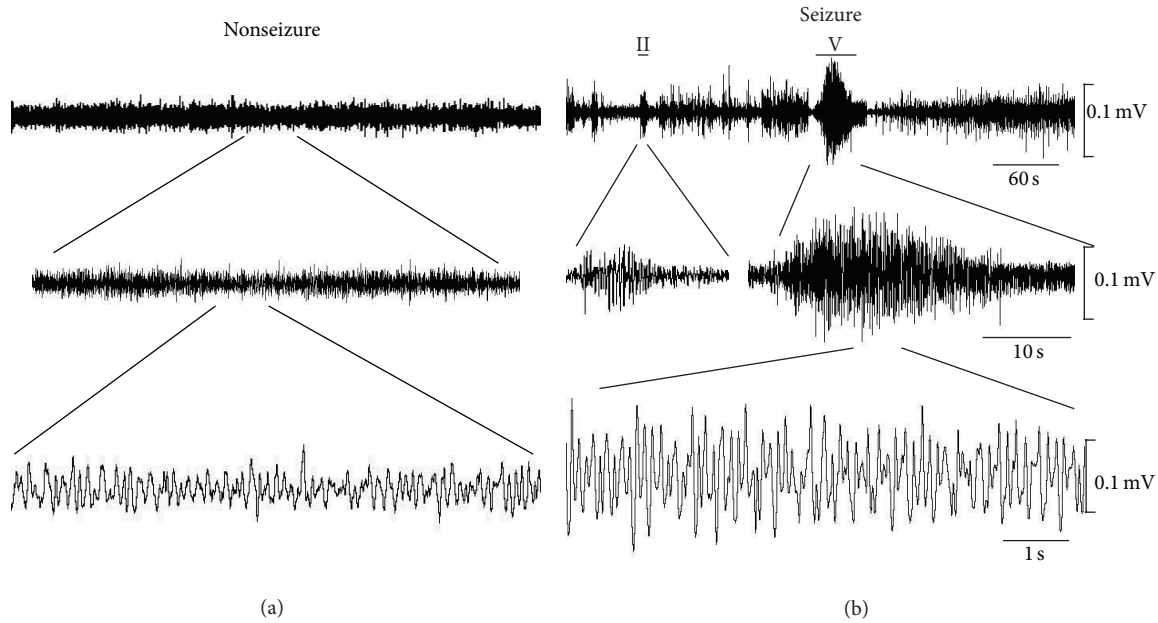

Figure 2: Epileptic EEG recorded in the chronic phase of a CTZ induced seizure rat. Raw EEG recording traces showing (a) normal EEG waveform during nonseizure period and (b) high amplitude high frequency interictal and ictal like epileptic EEG associated with the seizure behavior (marked with bars above the EEG traces) from CTZ induced seizure rats at the time of 6 months after initial seizure induction by CTZ.

and neuron loss [17]. In our current study, Nissl staining was performed in the hippocampal slices taken from 3 CTZ rats with chronic seizure score of grade VI or V and also 3 DMSO rats without chronic seizures 6 months after either DMSO or CTZ injection. It showed that undamaged Nissl positive neurons in both CA1 and CA3 of either left or right hippocampus had similar number count (Figure 3). There were also some damaged neurons, but with the minority in count, in all the areas including CA1, CA3, and DG, which showed incomplete forms, cell swelling or shrinkage, vague outlines, and confused boundaries with Nissl staining. The Nissl positive neurons in left CA1 and CA3 in DMSO control rats were 333 ± 54 and 158 ± 8 (per section of the area counted) and in CTZ treated rats were 322 ± 64 and 161 ± 27, respectively. The corresponding number counts for the right CA1 and CA3 were 320 ± 27 and 171 ± 9 for DMSO control and 321 ± 111 and 161 ± 42 for CTZ rats, respectively.

This result demonstrated that CTZ itself did not have profound effect on the cell death seen in the other major convulsant induced seizure animal models, which was consistent with the previous notion suggested according to the in vitro work [9].

3.3. Decreased GAD Staining in Hippocampus in Chronic CTZ Seizure Model Rats. GABA deficiency is one of the reasons for imbalance between excitation and inhibition associated with the seizure induction. Previous studies have indicated that CTZ induced seizure is likely generated from hippocampus [7, 9, 10]. In this aspect, we investigated whether GABAergic neurons in the hippocampus were also affected during epileptogenesis in its chronic phase, by immunostaining of GAD, a rate-limiting enzyme in GABA synthesis, and GAT-1, a cell membrane localized GABA transporter [18–20]. GAD positive immunohistochemistry staining brown particles were observed to exist in cytoplasm of the cells. GAD positive neurons distributed densely adjacent to pyramidal cell layer of CA1 and CA3 subregion and adjacent to granule cell layer of DG subregion of hippocampus in DMSO treated rats, and there are also some diffused GAD positive neurons in molecular layer and oriens layer of the hippocampus (Figures 4(a) and 4(b)). In comparison with the DMSO control rats, GAD positive particle containing neurons were also observed to localize in CA1, CA3, and DG area of CTZ induced seizure rats, but with significantly less amount. The number of GAD positive neurons in CA1, CA3, and DG was significantly decreased from 75.2 ± 13.0 in CA1, 79.7 ± 9.7 in CA3, and 251.5 ± 4.3 in DG, respectively, in the time matched DMSO control rats ($n = 3$) (mean ± SEM in counted area per section, see above Method) to 3.0 ± 0.5 in CA1, 3.6 ± 0.9 in CA3, and 5.3 ± 1.8 in DG in left hippocampus of 3 CTZ rats with recurrent seizure 6 months after CTZ injection ($P < 0.05$, $P < 0.01$) (Figures 4(a) and 4(c)). Further, the reduction of the GAD positive particles in either left or right brain had no obvious preference (Figures 4(c) and 4(d)), despite the fact that CTZ was injected in the left cerebral ventricle during acute seizure induction phase [12].

GAD represents the ability of GABA synthesis and GAD positive neurons are regarded as GABAergic neurons [21]. Thus, the above results suggest that GABA in hippocampus became reduced in chronic phase of the CTZ induced epileptic seizure, which may lead to a deficiency of GABA inhibition. The decline in DG of the GAD positive neurons in CTZ seizure models was most obvious, which suggest that

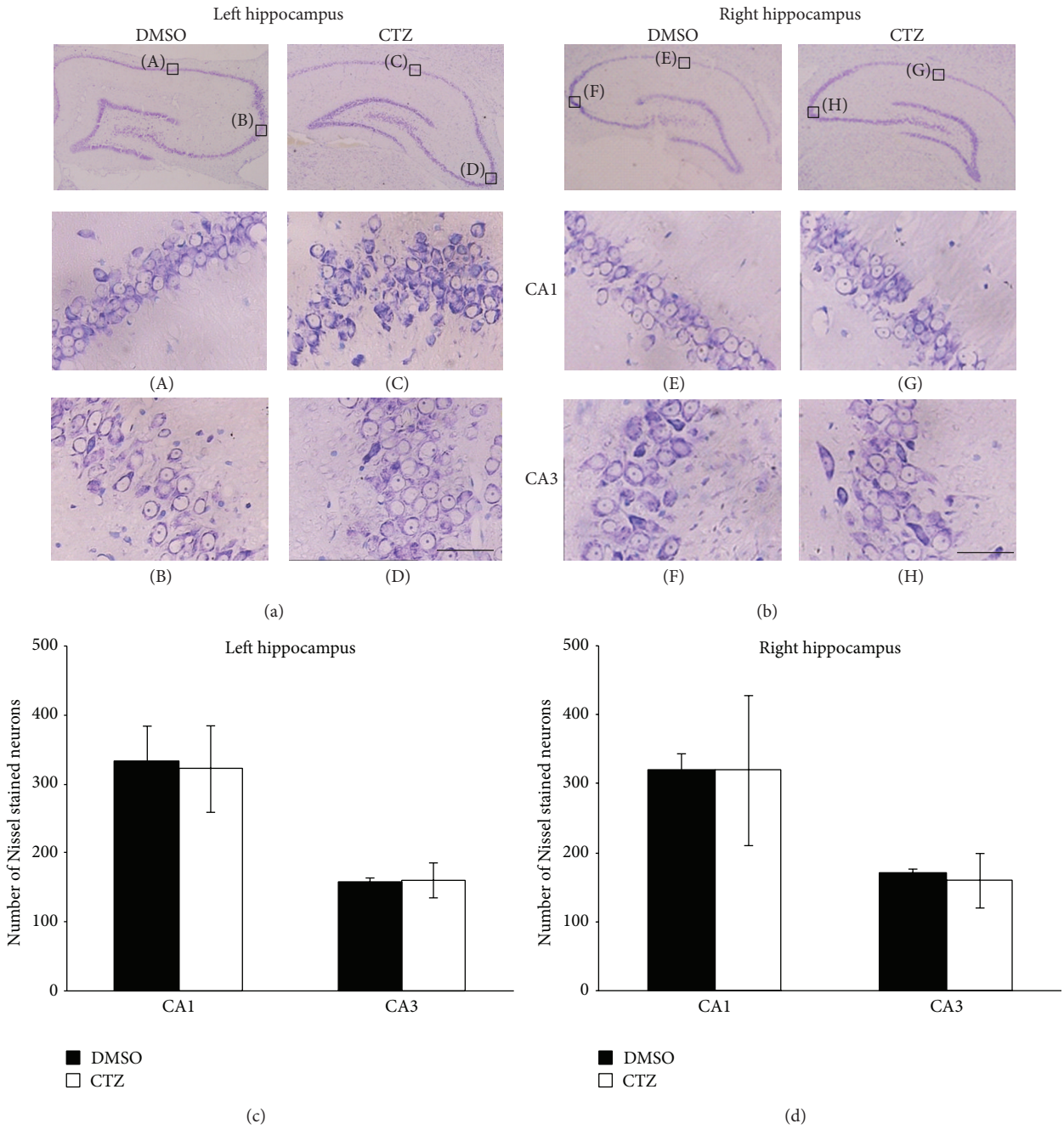

Figure 3: Nissl staining of the hippocampal neurons in chronic CTZ seizure rats 6 months after seizure induction. (a-b) Pictures showing the Nissl staining of the left (a) and right (b) hippocampus of either DMSO or CTZ treated rats. The expanded pictures (A–H) showing the detail of the Nissl stained hippocampal CA1 and CA3 neurons. (c-d) Group data of the counted Nissl stained hippocampal neurons in left (c) and right (d) hippocampus of either DMSO or CTZ chronic seizure rats. Scale bar = 50 μm.

the GABAergic neurons in this region was likely damaged most seriously.

3.4. Decreased GAT in Neurons of Hippocampus in CTZ Seizure Rats in Chronic Recurrent Phase. In addition, GAT-1 stained positive particles were also seen in the cytoplasm of the cells located adjacent to the pyramidal cell layer of CA1 and CA3 subregion and the granule cell layer of DG subregion of the hippocampus in DMSO control rats. Similar to the GAD staining, GAT-1 positive neurons were also significantly reduced in CA1, CA3, and DG regions in the CTZ seizure rats (Figures 5(a) and 5(b)). The number of the GAT-1 positive neurons were counted as 20.7 ± 8.6 in CA1, 24.3 ± 3.4 in CA3, and 24.7 ± 13.3 in DG (mean ± SEM in counted area per section, see above Method) in left hippocampus of 3 CTZ rats with recurrent seizure 6 months after CTZ injection, which

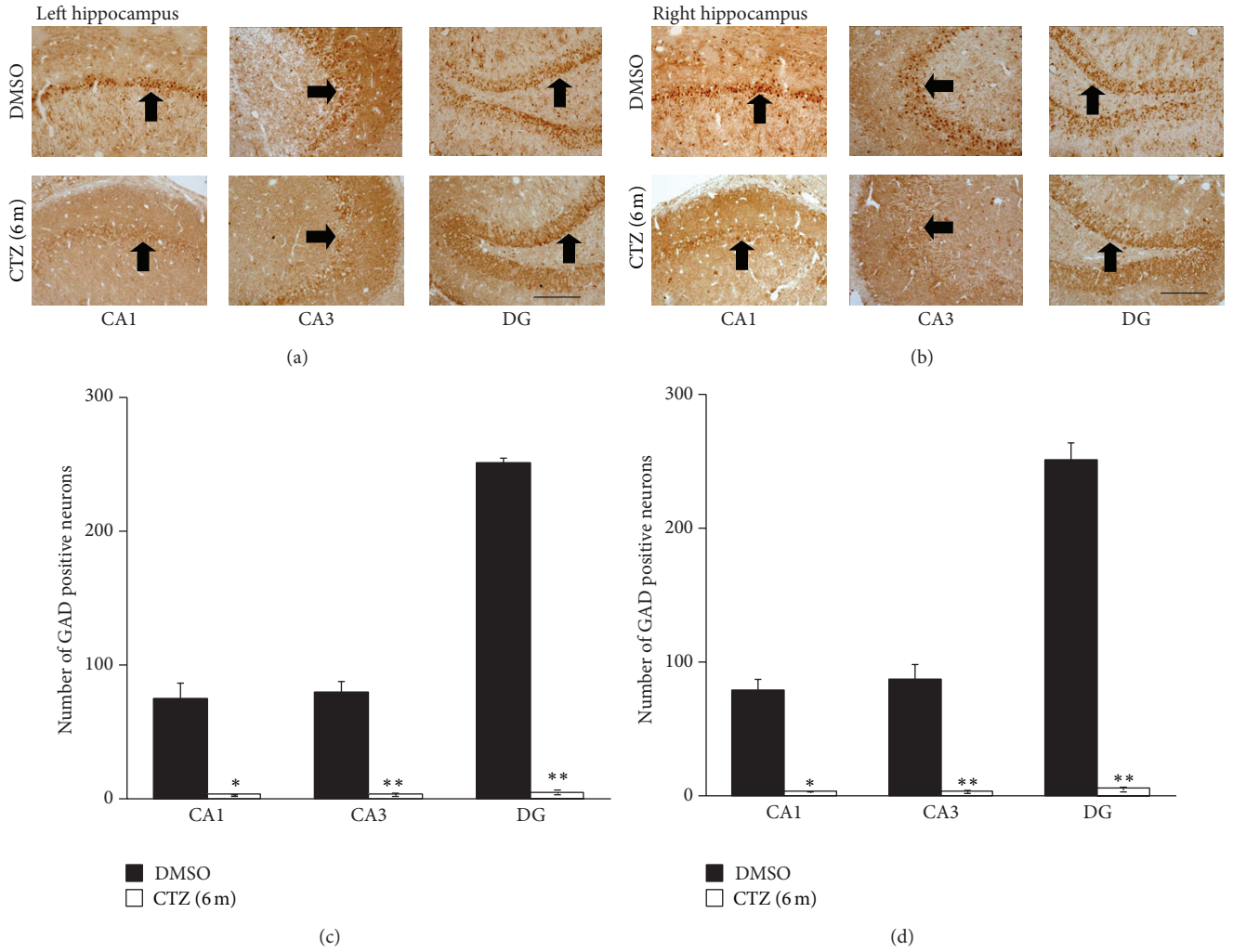

Figure 4: Decreased GAD staining in hippocampus of recurrent seizure rats 6 months after seizure induction by CTZ. (a-b) Pictures showing GAD positive cells (arrow indicated) in left (a) and right (b) hippocampus from rats 6 months after either DMSO (top) or CTZ (bottom) treatment. (c-d) Group data showing significant decreases of the GAD staining cells in CA1, CA3, and DG area of the hippocampus from rats 6 months after either DMSO ($n = 3$) or CTZ ($n = 3$) treatment. $^{*}P < 0.05$, $^{**}P < 0.01$ compared to the DMSO control group. Scale bar in (a) and (b) = 200 μm.

was significantly less than those of time matched DMSO control rats (60.7 ± 3.0 in CA1, 55.7 ± 9.1 in CA3, and 212.3 ± 11.3 in DG, resp.; $n = 3$) ($P < 0.05$, $P < 0.001$) (Figures 5(a) and 5(c)). Similar to the result of GAD staining, the proportion of the decreased GAT-1 positive neuron had no obvious difference between left and right brain of the CTZ rats (Figures 5(c) and 5(d)). The result showed that GAT significantly reduced in all the hippocampal subregions, similar to the GAD, in the chronic phase of the CTZ seizure model.

3.5. Downregulated BDNF-TrkB Signaling Pathway in Chronic Recurrent Phase in Hippocampus of CTZ Seizure Rats. We have previously demonstrated that BDNF-TrkB signaling pathway is involved in the induction of the epileptiform activities induced by CTZ in hippocampus [7]. In the current study, we further investigated whether BDNF-TrkB signaling pathway was remaining affected in the chronic recurrent phase in CTZ seizure rats. Immunohistochemistry study showed that the BDNF positive particles existed in the cytoplasm of cells which localized in CA1, CA3, and DG regions close to the pyramidal neuron and granule cells layer, as well as in the molecular and oriens layer of the hippocampus (Figures 6(a) and 6(b)) in DMSO control rats. However, BDNF positive particle containing cells significantly decreased in CA1, CA3, and DG region in CTZ seizure rat hippocampus 6 months after CTZ injection. The number of the BDNF positive neurons was 4.1 ± 1.0 in CA1, 2.9 ± 0.1 in CA3, and 21.2 ± 16.2 in DG in counted area per left hippocampal slice in 3 CTZ rats with recurrent seizure 6 months after CTZ injection, which was significantly reduced in comparison with the time matched DMSO control rats (70.7 ± 9.0 in CA1, 72.2 ± 3,7 in CA3, and 138.3 ± 15.9 in DG ($n = 3$), resp.; $P < 0.01$, $P < 0.001$) (Figure 6(c)). There

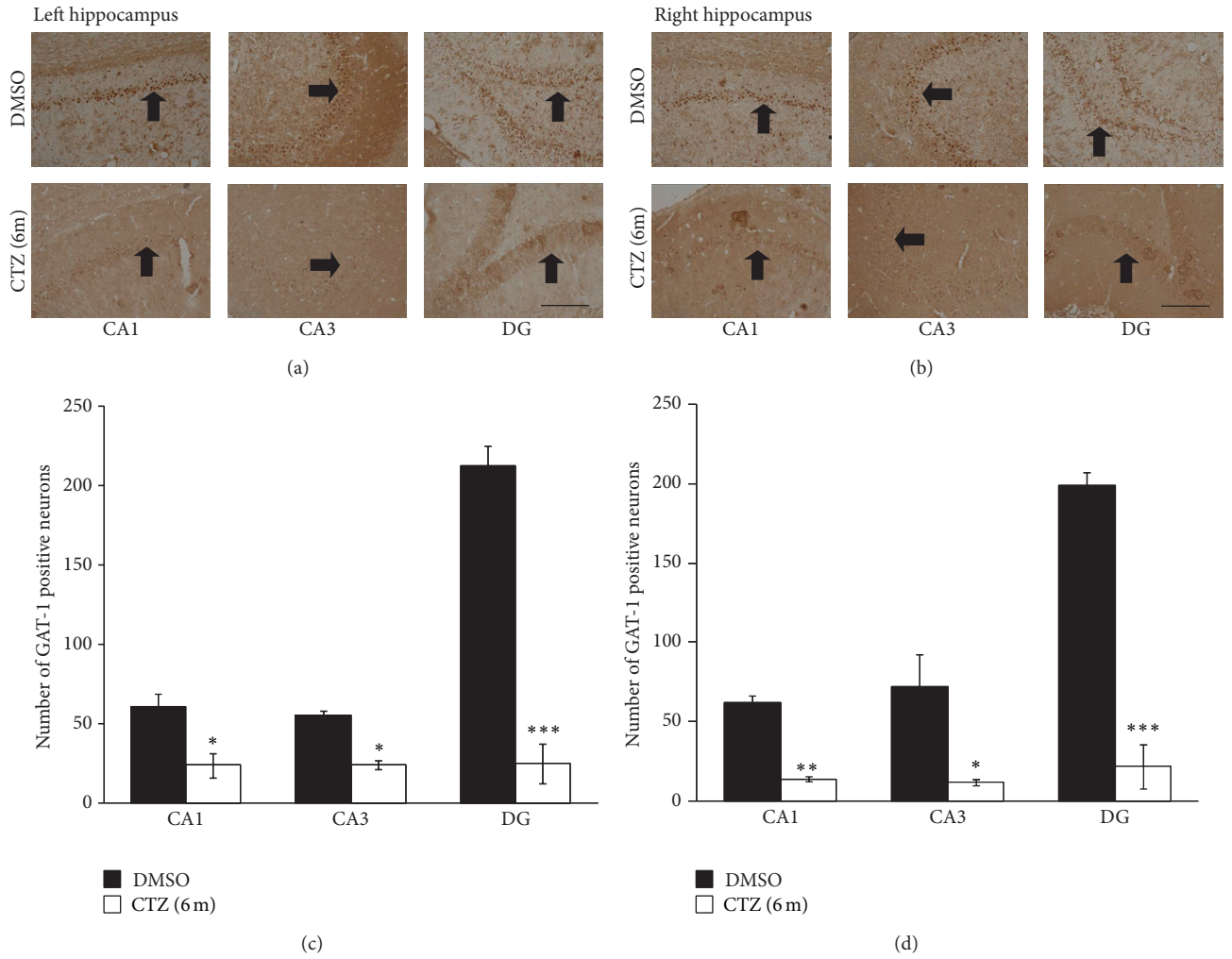

Figure 5: Decreased GAT-1 staining in hippocampus of recurrent seizure rats 6 months after seizure induction by CTZ. (a-b) Pictures showing GAT-1 positive cells (arrow indicated) in left (a) and right (b) hippocampus from rats 6 months after either DMSO (top) or CTZ (bottom) treatment. (c-d) Group data showing significant decreases of the GAT-1 staining cells in CA1, CA3, and DG area of the hippocampus from rats 6 months after either DMSO ($n = 3$) or CTZ ($n = 3$) treatment. $^{*}P < 0.05$, $^{**}P < 0.01$, and $^{***}P < 0.001$ compared to the DMSO control group. Scale bar in (a) and (b): 200 μm.

was also no left right difference in CTZ rats (Figures 6(c) and 6(d)).

In addition, the expression of TrkB in hippocampus of the CTZ rats was also studied as TrkB is known to mediate BDNF effect for epileptogenesis in various seizure models [6, 22, 23], including CTZ induced acute seizure behavior [7]. TrkB positive particles were found to be distributed in the same area as the BDNF in hippocampal subregions of both DMSO and CTZ treated seizure rats (Figures 7(a) and 7(b)). The number of TrkB positive neurons was 64.7 ± 16.2 in CA1, 158.3 ± 41.7 in CA3, and 250.3 ± 46.8 in DG in the counted area per slice of left hippocampus in 3 CTZ rats with recurrent seizure behavior, which was significantly less than those in DMSO control rats ($n = 3$) with the count of 126.7 ± 7.2 in CA1, 275.7 ± 56.3 in CA3, and 399.2 ± 22.4 in DG ($P < 0.05$, $P < 0.01$, except CA1 region) (Figure 7(c)). There was also no left right preference of the TrkB staining change observed in this study (Figures 7(c) and 7(d)).

These data indicate that the BDNF-TrkB signaling pathway possibly has been damaged in long term in the chronic phase of the CTZ seizure models.

4. Discussions

In this study, we demonstrated that, in chronic recurrent seizure phase, a large proportion of the rats with acute seizure induced by CTZ exhibited spontaneous seizure behaviour accompanied with epileptic EEG. The immunohistochemistry results, in addition, showed that the number of GABAergic neurons expression of both GAD and GAT was substantially decreased in hippocampus, which would lead to weak GABA inhibitory function in those rats. In addition, a proepileptic signaling pathway, BDNF-TrkB signaling pathway, in acute seizure induction phase [7] was also seen to be

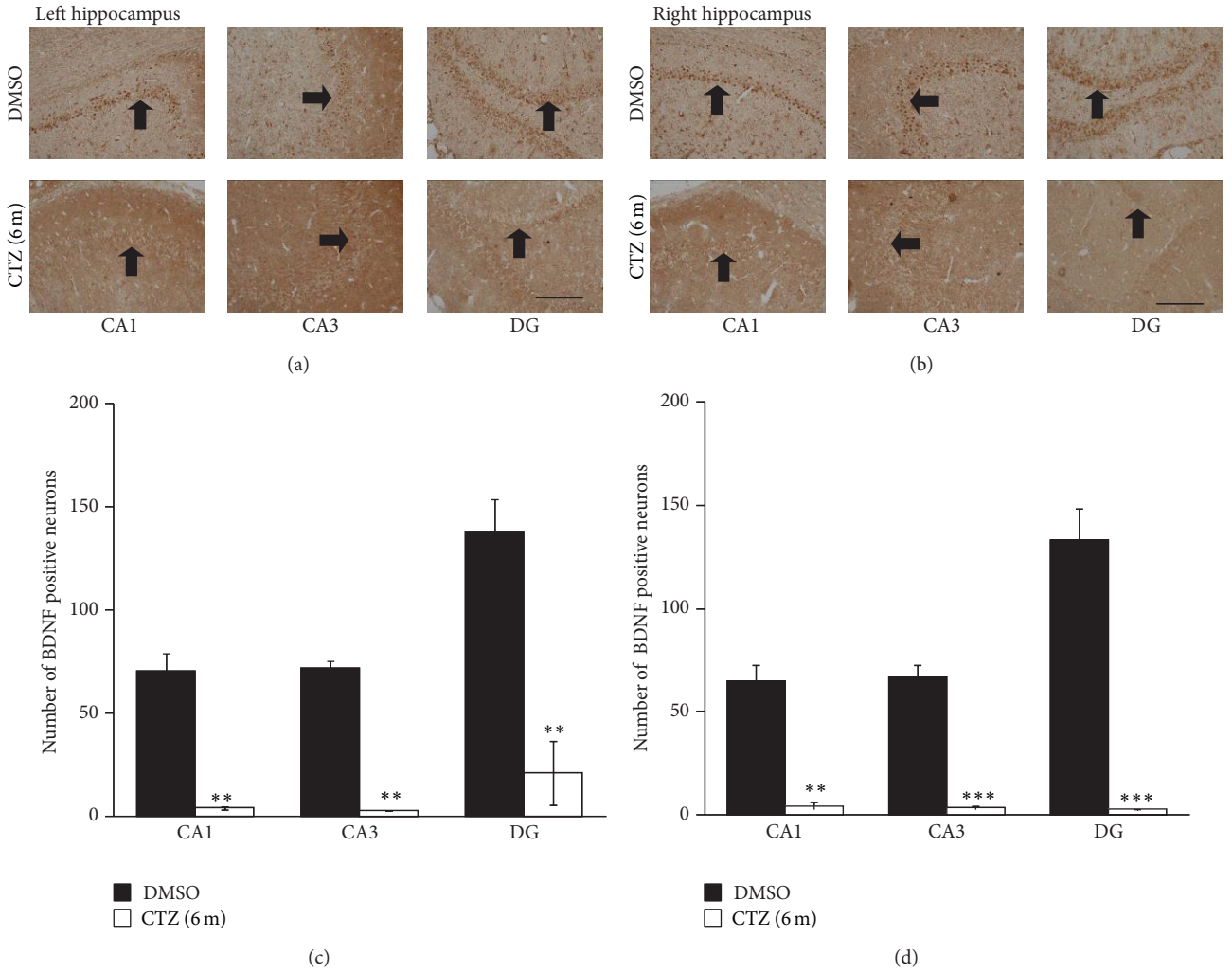

Figure 6: Decreased BDNF staining in hippocampus of recurrent seizure rats 6 months after seizure induction by CTZ. (a-b) Pictures showing BDNF positive cells (arrow indicated) in left (a) and right (b) hippocampus from rats 6 months after either DMSO (top) or CTZ (bottom) treatment. (c-d) Group data showing significant decreases of the BDNF staining cells in CA1, CA3, and DG area of the hippocampus from rats 6 months after either DMSO ($n = 3$) or CTZ ($n = 3$) treatment. $^{**}P < 0.01$, $^{***}P < 0.001$, compared to the DMSO control group. Scale bar in (a) and (b): 200 μm.

downregulated in the chronic phase in comparison with the DMSO control rats.

4.1. Characterization of the CTZ Induced Chronic Seizure Animal Model. Previously we have studied the probability of the CTZ as a convulsant with the advantage of its dual action property of simultaneous acting on both glutamate excitatory receptors and GABAA inhibitor receptors [8] to induce epileptiform activities in hippocampal neurons [9, 10, 13]. Although we have demonstrated that CTZ induced seizure in freely moving rats [12], a successful seizure animal model requires the animals to develop recurrent seizure and also have a high proportion to have recurrent seizure [24]. In this aspect we carried out the current study to investigate whether the acutely induced seizure rats by CTZ could develop to have recurrent seizure. Indeed, we found that over 46% of the CTZ rats (6 out of 13) had recurrent seizure with the latency between 2 weeks to 6 months. The silent period between acute seizure induction and the occurrence of the recurrent seizure in this CTZ seizure rat model seems well in agreement with the other classic seizure animal model, at around two-week time of latency, such as pilocarpine and Kainic acid induced seizure models [24, 25]. However, the rate of the animal to have recurrent seizure seems lower than other seizure models. We believe this is due to the underestimating of the rats having recurrent seizure in our current study by using the experimental paradigm of recording 2 hours a day of the seizure behavior during the whole 6-month observation period. Indeed, in 2 rats which were video recorded day and night continuously for 6 months, the recurrent seizure was captured in both of them and also showed multiple recurrent seizure episodes (3 and 4 episodes, resp.) in the 6-month period. In this aspect, we cannot fully rule out that the 4 animals without recurrent seizure behavior observed were

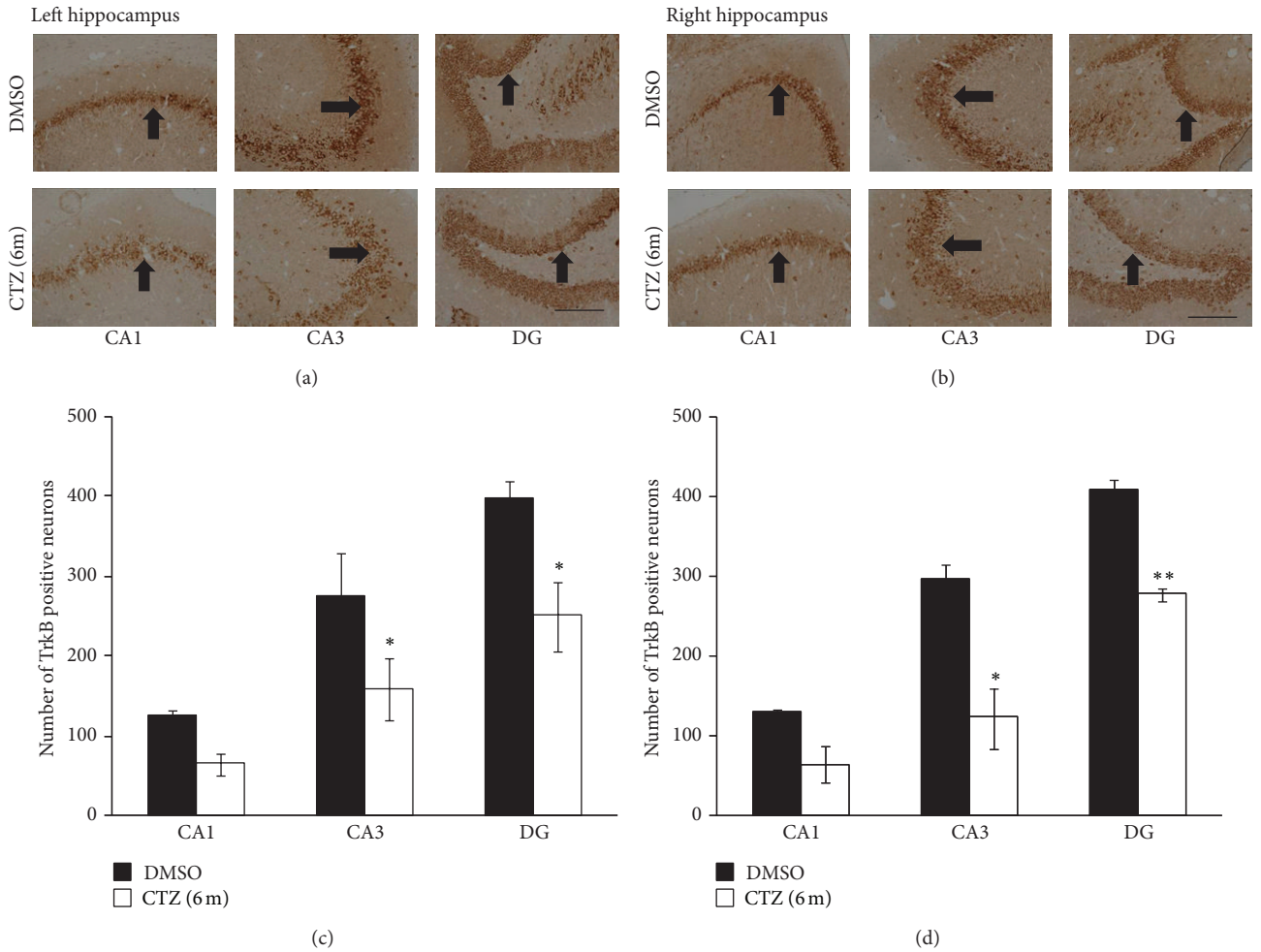

Figure 7: Decreased TrkB staining in hippocampus of recurrent seizure rats induced by CTZ. (a-b) Pictures showing TrkB positive cells (arrow indicated) in left (a) and right (b) hippocampus from rats 6 months after either DMSO (top) or CTZ (bottom) treatment. (c-d) Group data showing significant decreases of the TrkB staining cells in CA1, CA3, and DG area of the hippocampus from rats 6 months after either DMSO ($n = 3$) or CTZ ($n = 3$) treatment. $^{*}P < 0.05$, $^{**}P < 0.01$, compared to the DMSO control group. Scale bar in (a) and (b): 200 μm.

"nonchronic seizure" rats. In addition, among 4 out of the 13 rats that died between 15 and 99 days after initial CTZ seizure induction, one of the rats, by chance, was observed to have generalised seizure (Racine score V behavior) and died at the next day. In this aspect, we hypothesise that the other 3 dead rats possibly had also seizure episode(s) which was the cause for their death, since none of the DMSO control rats ($n = 8$) died during our 6-month experimental period. Taking these together, we believe that the CTZ induced seizure rats would have much higher recurrent seizure occurrence rate. However, this needs to be studied in the future in more careful design of the experiment protocol.

4.2. Decreased GABAergic Transmission in Chronic Phase of the CTZ Seizure Rats. CTZ not only blocks AMPA receptor desensitization, but also inhibits GABAA receptors [8], and GABAA receptors were involved in the CTZ induced epileptiform activities in hippocampal neurons [9–11, 13]. In this study, we reported further that, at the chronic phase of the CTZ seizure rat, there was a significant reduction of the GAD and GAT containing neurons in the hippocampus. Lack of GAD may lead to the weakened GABA inhibition and increased probability of the seizure occurrence. Indeed, our preliminary result on determination of the amount of GABA in the hippocampus in the chronic CTZ seizure rats with GABA antibody showed that the optical density for GABA staining was lower in neurons of CA1, CA3, and DG of CTZ seizure models than those of DMSO rats (data not supplied). Decreased GABA may cause the imbalance of excitation and inhibition, which could be one of the reasons to cause the recurrent spontaneous seizure.

GABA is the primary inhibitory neurotransmitter in the adult brain, and its effects at receptors are primarily terminated by diffusion and transportation by GABA transporters, GAT-1 and GAT-3. They are primarily localized to presynaptic terminals and to glial processes adjacent to the synaptic cleft [18–20]. There are controversial opinions about expression and mechanism of GAT-1 in hippocampus after seizure. Although the exact mechanism for a decrease in

transporter is unknown, it is interesting to note that the expression of this protein is dependent on the extracellular GABA level [26]. In this study, we observed that GAT-1 became reduced in hippocampus in chronic phase of the CTZ rats, which had a similar pattern as the loss of the GABA synthesis protein (GAD) reduction in the hippocampus in chronic CTZ rats. Thus, reduced GAT-1 may serve as a compensatory mechanism for reduced GABA release, which would partly reverse the GABA inhibitory function in the recurrent spontaneous seizure phase.

4.3. Downregulated BDNF-TrkB Signaling Pathway Induced Recurrent Spontaneous Seizure in CTZ Model Rats. Epileptogenic insults increase BDNF synthesis and TrkB receptor activation [5, 27]. Many studies convincingly support the notion that these phenomena have a proepileptogenic role [6, 27]. The previous in vitro and in vivo study also showed that, during CTZ induced acute seizure, BDNF-TrkB signaling pathway is activated to promote the epileptiform activities in hippocampal neurons [7]. However, our current results demonstrated that BDNF decreased significantly in CA1, CA3, and DG and its receptor, TrkB, also decreased with less extent in chronic seizure phase in CTZ rats. It has recently been demonstrated that epileptogenic seizures promote accumulation of selected BDNF splice variants into the distal dendritic compartment whereas others remain restricted to the cell soma [28, 29]. BDNF in soma may favor survival or regeneration (or both) of hippocampal neurons damaged by seizure [30]. BDNF also can amplify GABA currents in oocytes expressing GABAA receptors transplanted from surgically removed specimens of human epileptic brains [31]. In this study, decreased BDNF occurred in soma of neurons in hippocampus, and neurotrophic action was impaired and could not amplify GABA currents. Thus, the downregulated BDNF-TrkB signaling pathway may suggest involving in inducing recurrent spontaneous seizure in CTZ model rats.

5. Conclusion

In the current study, we investigated in detail the occurrence of the recurrent seizure behavior for up to 6 months in CTZ induced seizure rats. Results demonstrated that high proportion of the acute seizure animals induced by CTZ could develop to chronic seizure, which was associated with the damaged GABA inhibitory system and BDNF-TrkB signaling pathway. This study provides further evidence for using CTZ as a convulsant for epilepsy study and CTZ rats may serve as an animal model for anticonvulsant drug test.

Conflict of Interests

The authors declare that there is no conflict of interests regarding the publication of this paper.

Authors' Contribution

Shuzhen Kong and Zhihua Cheng have equally contributed to this paper.

Acknowledgments

This work was supported by Grants from the Nature Science Foundation of China (31129003, 81171224), the Science and Technology Commission of Shanghai Municipality (13DJ1400302), and Chongqing Science and Technology Commission (CHTC2007BA5025) to Yun Wang, Chongqing Educational Ministry (KJ090719, KJ0707021) to Shuzhen Kong, and the Innovative Research Team Development Program in University of Chongqing (KJTD201314).

References

[1] P. D. Suzdak and J. A. Jansen, "A review of the preclinical pharmacology of tiagabine: a potent and selective anticonvulsant GABA uptake inhibitor," *Epilepsia*, vol. 36, no. 6, pp. 612–626, 1995.

[2] P. R. Patrylo, D. D. Spencer, and A. Williamson, "GABA uptake and heterotransport are impaired in the dentate gyrus of epileptic rats and humans with temporal lobe sclerosis," *Journal of Neurophysiology*, vol. 85, no. 4, pp. 1533–1542, 2001.

[3] J. J. Mitchell, M. Paiva, D. W. Walker, and M. B. Heaton, "BDNF and NGF afford in vitro neuroprotection against ethanol combined with acute ischemia and chronic hypoglycemia," *Developmental Neuroscience*, vol. 21, no. 1, pp. 68–75, 1999.

[4] H. E. Scharfman, "Brain-derived neurotrophic factor and epilepsy—a missing link?" *Epilepsy Currents*, vol. 5, no. 3, pp. 83–88, 2005.

[5] D. K. Binder, S. D. Croll, C. M. Gall, and H. E. Scharfman, "BDNF and epilepsy: too much of a good thing?" *Trends in Neurosciences*, vol. 24, no. 1, pp. 47–53, 2001.

[6] X. Liu, J. Liu, X. L. Liu et al., "BDNF-TrkB signaling pathway is involved in pentylenetetrazole-evoked progression of epileptiform activity in hippocampal neurons in anesthetized rats," *Neuroscience Bulletin*, vol. 29, no. 5, pp. 565–575, 2013.

[7] Y. Wang, J.-S. Qi, S. Kong et al., "BDNF-TrkB signaling pathway mediates the induction of epileptiform activity induced by a convulsant drug cyclothiazide," *Neuropharmacology*, vol. 57, no. 1, pp. 49–59, 2009.

[8] L. Deng and G. Chen, "Cyclothiazide potently inhibits γ-aminobutyric acid type A receptors in addition to enhancing glutamate responses," *Proceedings of the National Academy of Sciences of the United States of America*, vol. 100, no. 22, pp. 13025–13029, 2003.

[9] J. Qi, Y. Wang, M. Jiang, P. Warren, and G. Chen, "Cyclothiazide induces robust epileptiform activity in rat hippocampal neurons both in vitro and in vivo," *Journal of Physiology*, vol. 571, no. 3, pp. 605–618, 2006.

[10] B. Qian, Y. Sun, Z. Wu et al., "Epileptiform response of CA1 neurones to convulsant stimulation by cyclothiazide, kainic acid and pentylenetetrazol in anaesthetized rats," *Seizure*, vol. 20, no. 4, pp. 312–319, 2011.

[11] L. Wan, X. Liu, W. Ren et al., "Activation of extrasynaptic GABAA receptors inhibits cyclothiazide induced epileptiform activity in hippocampal CA1 neurons," *Neuroscience Bulletin*. In press.

[12] S. Kong, B. Qian, J. Liu, M. Fan, G. Chen, and Y. Wang, "Cyclothiazide induces seizure behavior in freely moving rats," *Brain Research*, vol. 1355, pp. 207–213, 2010.

[13] Y. Sun, Z. Wu, S. Kong et al., "Regulation of epileptiform activity by two distinct subtypes of extrasynaptic GABAA receptors," *Molecular Brain*, vol. 6, article 21, 2013.

[14] R. J. Racine, "Modification of seizure activity by electrical stimulation: II. Motor seizure," *Electroencephalography and Clinical Neurophysiology*, vol. 32, no. 3, pp. 281–294, 1972.

[15] Z.-T. Bai, R. Zhao, X.-Y. Zhang, J. Chen, T. Liu, and Y.-H. Ji, "The epileptic seizures induced by BmK I, a modulator of sodium channels," *Experimental Neurology*, vol. 197, no. 1, pp. 167–176, 2006.

[16] R. Zhao, C.-C. Weng, Q. Feng et al., "Anticonvulsant activity of BmK AS, a sodium channel site 4-specific modulator," *Epilepsy and Behavior*, vol. 20, no. 2, pp. 267–276, 2011.

[17] Q. Chen, S. He, X.-L. Hu et al., "Differential roles of NR2A- and NR2B-containing NMDA receptors in activity-dependent brain-derived neurotrophic factor gene regulation and limbic epileptogenesis," *The Journal of Neuroscience*, vol. 27, no. 3, pp. 542–552, 2007.

[18] J. N. Cammack, S. V. Rakhilin, and E. A. Schwartz, "A GABA transporter operates asymmetrically and with variable stoichiometry," *Neuron*, vol. 13, no. 4, pp. 949–960, 1994.

[19] S. Mager, N. Kleinberger-Doron, G. I. Keshet, N. Davidson, B. I. Kanner, and H. A. Lester, "Ion binding and permeation at the GABA transporter GAT1," *Journal of Neuroscience*, vol. 16, no. 17, pp. 5405–5414, 1996.

[20] C. E. Ribak, W. M. Tong, and N. C. Brecha, "GABA plasma membrane transporters, GAT-1 and GAT-3, display different distributions in the rat hippocampus," *Journal of Comparative Neurology*, vol. 367, no. 4, pp. 595–606, 1996.

[21] C. R. Houser and M. Esclapez, "Downregulation of the α5 subunit of the GABA(A) receptor in the pilocarpine model of temporal lobe epilepsy," *Hippocampus*, vol. 13, no. 5, pp. 633–645, 2003.

[22] R. Kotloski and J. O. McNamara, "Reduction of TrkB expression de novo in the adult mouse impairs epileptogenesis in the kindling model," *Hippocampus*, vol. 20, no. 6, pp. 713–723, 2010.

[23] F. Papaleo, J. L. Silverman, J. Aney et al., "Working memory deficits, increased anxiety-like traits, and seizure susceptibility in BDNF overexpressing mice," *Learning and Memory*, vol. 18, no. 8, pp. 534–544, 2011.

[24] F. A. Scorza, R. M. Arida, M. Priel, L. Calderazzo, and E. A. Cavalheiro, "The contribution of the lateral posterior and anteroventral thalamic nuclei on spontaneous recurrent seizures in the pilocarpine model of epilepsy," *Arquivos de Neuro-Psiquiatria*, vol. 60, no. 3A, pp. 572–575, 2002.

[25] A. Bragin, A. Azizyan, J. Almajano, C. L. Wilson, and J. Engel Jr., "Analysis of chronic seizure onsets after intrahippocampal kainic acid injection in freely moving rats," *Epilepsia*, vol. 46, no. 10, pp. 1592–1598, 2005.

[26] E. M. Bernstein and M. W. Quick, "Regulation of γ-aminobutyric acid (GABA) transporters by extracellular GABA," *Journal of Biological Chemistry*, vol. 274, no. 2, pp. 889–895, 1999.

[27] S. Reibel, A. Depaulis, Y. Larmet et al., "BDNF and epilepsy—the bad could turn out to be good," *Trends in Neurosciences*, vol. 24, no. 6, pp. 318–319, 2001.

[28] E. Tongiorgi, M. Armellin, P. G. Giulianini et al., "Brain-derived neurotrophic factor mRNA and protein are targeted to discrete dendritic laminas by events that trigger epileptogenesis," *Journal of Neuroscience*, vol. 24, no. 30, pp. 6842–6852, 2004.

[29] P. P. Pattabiraman, D. Tropea, C. Chiaruttini, E. Tongiorgi, A. Cattaneo, and L. Domenici, "Neuronal activity regulates the developmental expression and subcellular localization of cortical BDNF mRNA isoforms in vivo," *Molecular and Cellular Neuroscience*, vol. 28, no. 3, pp. 556–570, 2005.

[30] M. Simonato, E. Tongiorgi, and M. Kokaia, "Angels and demons: neurotrophic factors and epilepsy," *Trends in Pharmacological Sciences*, vol. 27, no. 12, pp. 631–638, 2006.

[31] E. Palma, G. Torchia, C. Limatola et al., "BDNF modulates GABAA receptors microtransplanted from the human epileptic brain to Xenopus oocytes," *Proceedings of the National Academy of Sciences of the United States of America*, vol. 102, no. 5, pp. 1667–1672, 2005.

Hindawi Publishing Corporation
Neural Plasticity
Volume 2014, Article ID 827161, 10 pages
http://dx.doi.org/10.1155/2014/827161

Research Article

Active Calcium/Calmodulin-Dependent Protein Kinase II (CaMKII) Regulates NMDA Receptor Mediated Postischemic Long-Term Potentiation (i-LTP) by Promoting the Interaction between CaMKII and NMDA Receptors in Ischemia

Ning Wang,[1] Linlin Chen,[1] Nan Cheng,[1] Jingyun Zhang,[2] Tian Tian,[1] and Wei Lu[1,2]

[1] *Department of Neurobiology, Nanjing Medical University, Nanjing, China*
[2] *Key Laboratory of Developmental Genes and Human Disease, Institute of Life Sciences, Southeast University, Nanjing, China*

Correspondence should be addressed to Wei Lu; luwei@seu.edu.cn

Received 23 December 2013; Accepted 27 January 2014; Published 10 March 2014

Academic Editor: Sheng Tian Li

Active calcium/calmodulin-dependent protein kinase II (CaMKII) has been reported to take a critical role in the induction of long-term potentiation (LTP). Changes in CaMKII activity were detected in various ischemia models. It is tempting to know whether and how CaMKII takes a role in NMDA receptor (NMDAR)-mediated postischemic long-term potentiation (NMDA i-LTP). Here, we monitored changes in NMDAR-mediated field excitatory postsynaptic potentials (NMDA fEPSPs) at different time points following ischemia onset *in vitro* oxygen and glucose deprivation (OGD) ischemia model. We found that 10 min OGD treatment induced significant i-LTP in NMDA fEPSPs, whereas shorter (3 min) or longer (25 min) OGD treatment failed to induce prominent NMDA i-LTP. CaMKII activity or CaMKII autophosphorylation displays a similar bifurcated trend at different time points following onset of ischemia both *in vitro* OGD or *in vivo* photothrombotic lesion (PT) models, suggesting a correlation of increased CaMKII activity or CaMKII autophosphorylation with NMDA i-LTP. Disturbing the association between CaMKII and GluN2B subunit of NMDARs with short cell-permeable peptides Tat-GluN2B reversed NMDA i-LTP induced by OGD treatment. The results provide support to a notion that increased interaction between NMDAR and CaMKII following ischemia-induced increased CaMKII activity and autophosphorylation is essential for induction of NMDA i-LTP.

1. Introduction

Ischemic stroke, a brain attack induced by the reduction of blood flow, is one of the leading causes of death and disability worldwide [1]. Unfortunately, the mechanisms underlying stroke processing are less understood, and there are no effective treatments targeting it. Following stroke, a pathological neural plasticity termed postischemic long-term potentiation (i-LTP) often occurs over time [2, 3]. And emerging evidences from animal models suggest that such i-LTP plays important roles in both injury and recovery. Thus, it is necessary to improve the comprehension of the mechanisms mediating i-LTP after stroke.

It is generally accepted that the pathological plasticity initiated by excessive calcium influx follows the activation of NMDAR after stroke [4]. Over the past two decades, though there are many published papers reporting the phenomenon termed NMDAR-mediated i-LTP, most researchers focused on the detailed mechanisms and significant implication in NMDAR dependent postischemic plasticity while NMDAR-mediated response got less attention [5, 6]. In previous articles, NMDAR fEPSPs were isolated in low-magnesium ACSF perfusion medium in presence of $GABA_AR$ antagonist BMI (10 μM) and AMPAR antagonist NBQX (10 μM). NMDAR antagonist D-APV was selected to identify whether NMDAR mediated i-LTP by recording this in ACSF perfusion medium [7, 8]. It has been favored that there was cascade response followed by calcium influx in i-LTP [9]; the conspicuous response is CaMKII activation and autophosphorylation which is involved in i-LTP after ischemia [9, 10].

In addition, it has been reported that the component of postsynaptic NMDARs changes in i-LTP and some researchers have proved the GluN2B-containing NMDAR plays an important role in i-LTP [11, 12]. The specific GluN2B antagonist ifenprodil exhibits a dose dependent inhibition of i-LTP, as well as the lower infarction volume. In the early studies, CaMKII activation and autophosphorylation initiated the succedent association between NMDAR and CaMKII and the sites of their interaction have been reported clearly in activity-dependent forms of synaptic plasticity, long-term potentiation (LTP), and long-term depression (LTD), proposed as the mechanism of learning and memory [13–15]. CaMKII has been widely studied as GluN2B binding protein in promoting the translocation of GluN2B to postsynaptic sites [16–18]. And it was clarified that both NMDAR antagonist and CaMKII inhibitor reduced the targeting of CaMKII to GluN2B, as well as the NMDAR translocation to postsynaptic membrane [11]. In summary, we emphasized on the most important question that whether this mechanism is involved in pathological neural plasticity or not.

On the other hand, the time points play an important role in ischemia injury and recovery. However, it still fails to form a consensus that multiple time points bring about different NMDAR-mediated i-LTP. After the induction, the mechanisms of the NMDAR-mediated i-LTP are not clear. The ability of recovery from ischemia is proposed to depend on the duration of the injury [19]. OGD treatment for 9 min and 14 min exhibited different phenomena. The shorter the OGD lasted, the easier the function could recover. Otherwise, after occlusion for 90 sec and 90 min, there were distinctions between the levels of αCaMKII phosphorylation at T286 site. The phosphorylation of Thr286-αCaMKII was significantly improved by 90 sec occlusion, while the phosphorylation of Thr286-αCaMKII was apparently decreased by 90 min occlusion [20].

In this study, the NMDAR-mediated i-LTP induced by OGD was demonstrated by employing electrophysiological recordings in hippocampal slices. An apparent increase of NMDAR in postsynaptic membrane caused by photothrombotic lesion (PT) was observed through Western blotting. The activity and autophosphorylation levels of CaMKII at different time points after ischemia were determined on OGD and PT models. Furthermore, using short disturbing peptides, it was found that the active CaMKII promotes the interaction between CaMKII and NMDARs and regulates NMDAR-mediated i-LTP in ischemia. Our data deepens the comprehension of the pathological plasticity after cerebral ischemia and provides useful experimental results for stroke therapeutics.

2. Materials and Methods

2.1. Hippocampal Slice. All animals and experimental protocols were carried out by the guidance of the National Institutes of Health (NIH) for the Care and Use of Laboratory Animals. Adult C57BL/6 mice were anesthetized with 1% pelltobarbitalum natricum and decapitated. The entire brain was quickly removed. Brain slices (350 μm thickness) were cut on a vibratome (VT1000S, Leica, Germany) in ice-cold artificial cerebrospinal fluid (ACSF) containing (in mM) 126 NaCl, 2.5 KCl, 1 $MgCl_2$, 1 $CaCl_2$, 1.25 KH_2PO_4, 26 $NaHCO_3$, and 20 glucose, pH 7.4, which was gassed with 95% O_2 and 5% CO_2. The fresh slices were incubated in a chamber with oxygenated ACSF and were recovered at 34°C. The slices were stored homogenized in cold 0.32 M sucrose containing 1 mM HEPES, 1 mM $MgCl_2$, 1 mM $NaHCO_3$, 20 mM sodium pyrophosphate, 20 mM β-phosphoglycerol, 0.2 mM dithiothreitol, 1 mM EDTA, 1 mM EGTA, 50 mM NaF, 1 mM Na_3VO_4, and 1 mM p-nitrophenyl phosphate, pH 7.4, in the presence of the following protease inhibitors and phosphatase inhibitors: 1 mM phenylmethylsulfonyl fluoride (PMSF), 5 g/mL aprotinin, 5 g/mL leupeptin, 5 g/mL pepstatin A, and 16 g/mL benzamidine. The homogenate was centrifuged at 1,000 ×g for 10 min and the supernatant was collected. The content of protein was measured using a BCA protein assay (Pierce, USA) [21].

2.2. Western Blotting and Coimmunoprecipitation. Slices used for coimmunoprecipitation analyses were preincubated with Tat-GluN2B (ChinaPeptides). Total protein was incubated with antibody against CaMKII (2 μg) overnight at 4°C in immunoprecipitation buffer (0.05 M HEPES, pH 7.4, containing 10% glycerol, 0.15 M NaCl, 1% TritonX-100, 0.5% Nonidet P-40, and 1 mM concentration of each of EDTA, EGTA, PMSF, and Na_3VO_4). Then protein A/G-agarose beads were added, mildly vortexed, and incubated for 2 h at 4°C. The beads were recovered by centrifugation at 12,000 ×g and gently washed three times with immunoprecipitation buffer. The left beads were treated the same as Western blot. For Western blot, total protein (20 μg) was boiled and was separated with 7.5% SDS-PAGE and transferred onto a PVDF membrane. Membranes were blocked in 3% (w/v) BSA (fraction V) in TBST (0.1% Tween 20) for 1 hr at room temperature (RT). Detection antibodies for Western blot analysis were from Biotime (β-Tubulin, 1 : 3000), Santa Cruz (p-CaMKII, 1 : 800), and Santa Cruz (GluN1, 1 : 800). Conjugated antibodies were from GE Healthcare (anti-mouse IgG-HRP, 1 : 4000) and Santa Cruz (rabbit anti-goat IgG-HRP, 1 : 8000). Signals were visualized with ECL kit (Amersham Biosciences). Band intensities were quantified by ImageJ (NIH, USA).

2.3. Electrophysiological Recordings in Acute Slices. Field excitatory postsynaptic potentials (fEPSPs) recordings were made as previous researches described [22]. Briefly, a stimulating electrode was located in Schaffer collateral; a recording pipette filled with 3 mM NaCl was put in stratum radiatum of CA1. Bicuculline methiodide (BMI, 10 μM) was from Tocris; 1,2,3,4-tetrahydro-6-nitro-2,3-dioxobenzo[f]-quinoxaline-7-sulfonamide (NBQX, 10 μM) was from Sigma; Tat-GluN2B was from ChinaPeptides.

2.4. Oxygen-Glucose-Deprivation-Induced Ischemia Model. The slices were deprived of anoxia/hypoglycemia by replacing 95% O_2/5% CO_2 with 95% N_2/5% CO_2 and switching to an

ACSF solution containing 20 mM sucrose instead of glucose for 5 to 10 minutes.

2.5. Photothrombotic Lesion. The female C57BL/6 mice (8–12 weeks) weighing 20–25 g were anesthetized using 1% pelltobarbitalum natricum with the body dose of 50 mg/kg. The scalps of anesthetized animals were exposed through shaving the mice hair. Before illumination, 1% Rose Bengal (Sigma) dissolved in 0.9% saline was intraperitoneally infused via the body dose of 100 mg/kg. Subsequently, focal illumination of the brain continued for 15 minutes with a strong cold light source through the intact skull leading to focal infarcts ranging from cortical to hippocampal area.

2.6. TTC Staining. The infarct size, location, and geometry of mice were measured 24 h after photothrombotic lesion. After anesthetization and execution, brains were removed directly and frozen at −20°C for 5 min. The whole brains of mice were incised to corresponding slices at 2 mm and sections were immersed in 1% 2,3,5-triphenyltetrazolium chloride (TTC; Sigma) at 37°C for 20 min in light-blocking environment. The presence or absence of infarction was distinctly visible by examining TTC-stained sections, and the pale region represented the focal infarcts.

2.7. Neuron Culture and Live-Cell Microscopy. Primary hippocampal neurons were disassociated from embryonic day 18 (E18), plated onto poly-D-lysine (Sigma-Aldrich, USA) coated coverglasses, and cultured in neurobasal medium supplemented with 2% B27 and 1% Glutamax (Life Technology, USA). At 11–14 days *in vitro* (DIV), cells were transfected with adenovirus expressing superecliptic pHluorin (SEP) tagged GluN1 and 48 hr later with adenovirus expressing GluN2A. The sequences encoding GluN1 and GluN2A were obtained from the plasmid pCI-SEP-NR1 (plasmid 23999, Addgene, USA) and pCI-SEP-NR2A (plasmid 23997, Addgene) contributed by Kopec et al. [23].

A Ti-E inverted fluorescence microscope with a Perfect Focus System (Nikon, Japan) was employed. Images were collected through a 100x oil-immersion objective (Plan Apo, NA. = 1.45, Nikon) and recorded by a cooled CCD (Orca-ER, Hamamatsu, Japan). 48 hr after GluN2A transfection (DIV15-18), coverglasses with hippocampal neurons were placed in an imaging chamber (AC-PI, Live Cell Instrument, South Korea) and perfused with the extracellular solution (ECS) containing (in mM) 140 NaCl, 5 KCl, 1.3 $CaCl_2$, 25 HEPES, 33 glucose, and 1 $MgCl_2$ (pH 7.4) at 37°C. During OGD treatment, neurons were perfused with the medium containing sucrose instead of glucose, which had been saturated with 95% N_2/5% CO_2. Cells were incubated with Tat-GluN2B for 15 min or not. Subsequently, live-cell imaging was performed on 5 min before and 10 min after ECS (as control) or OGD treatment. The images were processed and analyzed by NIS-element AR software (Nikon) or Fiji software (National Institutes of Health, USA).

2.8. Data Analysis. All population data were expressed as mean ± SEM. Paired-Samples t-test was used to assess statistical significance and Independent-Samples t-test and analysis of variance (ANOVA) were performed to compare between multiple groups. $P < 0.05$ values were accounted for statistical significance, and the significance for homogeneity of variance test was set at 0.1.

3. Results

3.1. Synaptic Plasticity in NMDAR-Mediated Responses Depends on Duration of OGD and PT Treatment in Hippocampal Slices. To examine whether plasticity in NMDAR-mediated synaptic responses was affected by duration of OGD treatment, we recorded i-LTP in NMDAR-mediated fEPSPs (NMDA fEPSPs) in acute hippocampal slices [24–27]. NMDA fEPSPs were isolated in the presence of $GABA_A$ antagonist BMI (10 μM) and AMPAR antagonist NBQX (10 μM) in low-magnesium ACSF. We found that OGD treatment for different time periods indeed exerted differential effects on inducing NMDAR-mediated i-LTP (NMDA i-LTP). OGD treatment for 3 min only elicited a slight but persistent increase of fEPSP amplitude (Figure 1(a), 1.18 ± 0.03, $n = 6$, $P < 0.05$). When the OGD duration went up to 10 min, a significant potentiation of fEPSP amplitude was observed, which kept stable at least for 30 min in our recordings (Figure 1(b), 1.37 ± 0.07, $n = 5$, $P < 0.05$). When OGD duration went up to 25 min, however, no potentiation in NMDA fEPSPs was detected (Figure 1(c), 1.03 ± 0.04, $n = 5$, $P > 0.05$). These results indicate that the magnitude of NMDA i-LTP differs with OGD duration; 10 min OGD treatment tends to elicit NMDA i-LTP more easily. Shorter or longer OGD treatment seems relatively inefficient to induce NMDA i-LTP.

Then we established ischemia model with photothrombotic lesion. We employed sequential brain T2-w MRI and TTC staining method to confirm the infarct region after ischemia modeling (Figure 2(b)). We also employed Western blotting to analyze possible alterations in postsynaptic NMDAR expression. Triton X-100-insoluble fraction (TIF) was used to roughly represent the postsynaptic fraction [21]. Different exposure times were selected, and here 1 hr after PT was showed (Figure 2(c), 0 hr after PT, 1.22 ± 0.08, $n = 5$, $^*P < 0.05$; 1 hr after PT, 1.39 ± 0.07, $n = 6$, $^*P < 0.05$; 12 hr after PT, 1.05 ± 0.07, $n = 5$, $P > 0.05$). A dramatic elevation of postsynaptic expression of GluN1, the obligatory component of NMDAR, was found 1 hr after PT. These data suggest that increased NMDAR number may contribute to NMDA i-LTP.

3.2. CaMKII Activity and Autophosphorylation Changed Accompanying NMDAR-Mediated i-LTP in Ischemia. NMDAR activation and Ca^{2+} influx increase intracellular calcium level. This increased Ca^{2+} binds with calmodulin to form a calcium/calmodulin complex, which in turn activates αCaMKII and promotes αCaMKII autophosphorylation at T286 site. Increased CaMKII activity and CaMKII autophosphorylation have been reported in OGD and middle cerebral artery occlusion (MCAO) in brain tissue. Here, we examined CaMKII activity in OGD model at different time points following OGD treatment by using

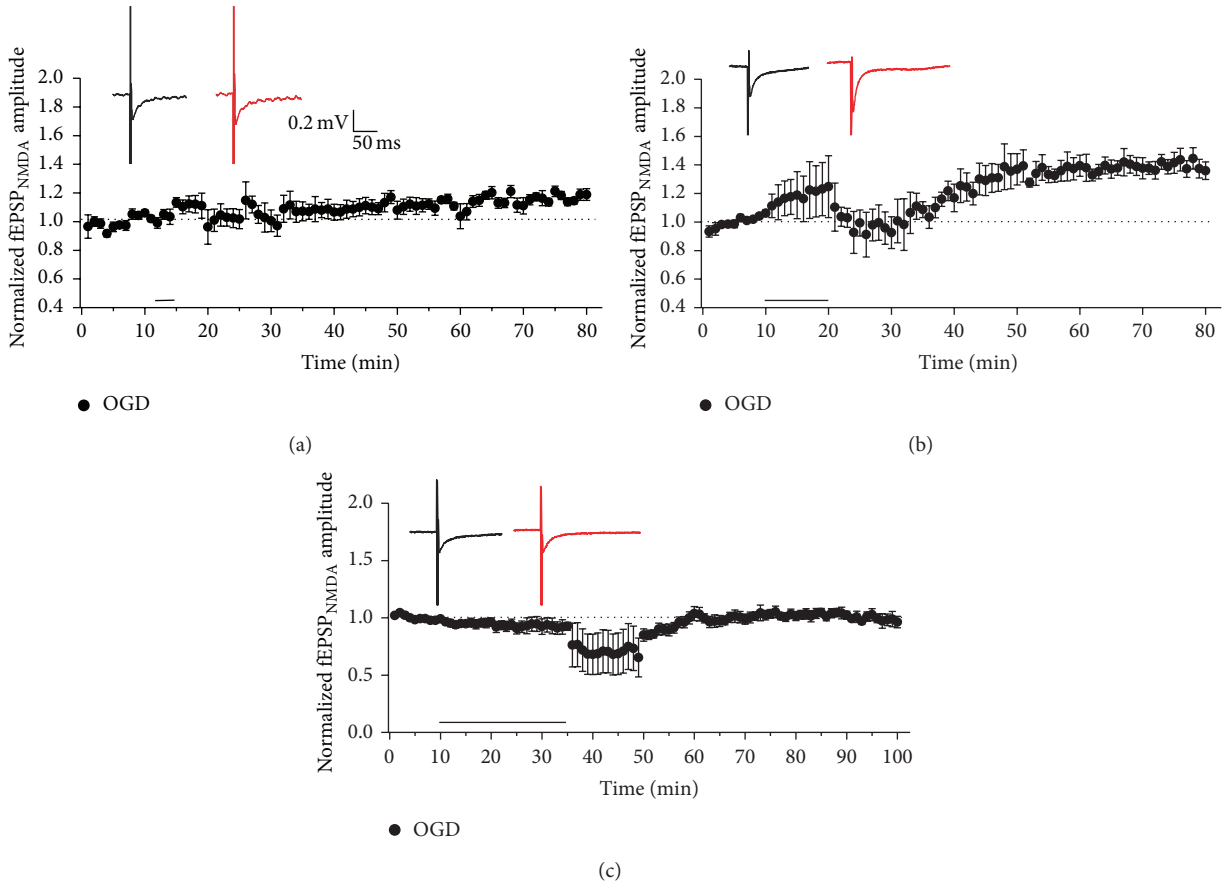

Figure 1: NMDAR-mediated plasticity recorded by fEPSPs is induced using OGD treatment with different time periods. Exposure to 3 min (a), 10 min (b), and 25 min (c) of OGD showed a slight but persistent increase of fEPSP amplitude (1.18 ± 0.03, compared with baseline, $n = 6$, $P < 0.05$), significant potentiation of fEPSP amplitude (1.37 ± 0.07, compared with baseline, $n = 5$, $P < 0.05$), and no obvious effects (1.03 ± 0.04, $n = 5$, $P > 0.05$) on fEPSP amplitude, respectively. Inset: sample traces were from average of the first 10 sweeps in baseline and average of the last 10 sweeps of the whole recordings.

Cyclex CaMKII assay kit (following the instructions) to test whether the alteration in CaMKII activity was correlated with duration of OGD treatment. We found that exposure to OGD for 10 min caused a significant increase in CaMKII activity (Figure 3(a), 1.43 ± 0.13, $n = 4$, $P < 0.05$). In contrast, OGD treatment for 25 min led to inhibition of CaMKII activity (Figure 3(b), 0.65 ± 0.07, $n = 3$, $P < 0.05$). In addition, we also test CaMKII activity change at different time points in PT ischemia model. One hour after PT, CaMKII activity displayed an upward trend (Figure 3(c), 1.38 ± 0.07, $n = 3$, $P < 0.05$). In contrast, CaMKII activity decreased markedly 12 hr after PT (Figure 3(d), 0.41 ± 0.19, $n = 3$, $P < 0.05$). Accordingly, we observed an increase in autophosphorylation of CaMKII following either 3 min or 10 min OGD treatment, but detected a decrease in CaMKII autophosphorylation 25 min after OGD treatment, determined by Western blotting assay (Figures 4(a)–4(c), 3 min OGD, 1.12 ± 0.07, $n = 5$, $P > 0.05$; 10 min OGD, 1.16 ± 0.03, $n = 3$, $^{*}P < 0.05$; 25 min OGD, 0.84 ± 0.03, $n = 5$, $^{*}P < 0.05$). Similar bidirectional changes in CaMKII autophosphorylation were also observed in PT ischemia model. An increase in CaMKII autophosphorylation was observed immediately (0 hr) or 1 hr after PT, while reduction in CaMKII autophosphorylation was detected 12 hr after PT (Figures 4(d)-4(e), 0 hr after PT, 1.28 ± 0.03, $n = 4$, $^{*}P < 0.05$; 1 hr after PT, 1.41 ± 0.06, $n = 5$, $^{*}P < 0.05$; 12 hr after PT, 0.75 ± 0.08, $n = 5$, $^{*}P < 0.05$).

3.3. Active CaMKII Targeting at NMDA Was Involved in Inducing NMDAR-Mediated i-LTP. CaMKII activation and subsequent binding of CaMKII with GluN2B subunit of NMDARs are critical to LTP. We employed coimmunoprecipitation (Co-IP) assay to determine the association between CaMKII and NMDAR at the time points in which we observed significant changes in NMDA fEPSPs and CaMKII phosphorylation in OGD or PT ischemia models. As we expected, an increase in association between CaMKII and NMDAR was observed after 10 min of OGD treatment in OGD model or after 1 hr PT in PT model (Figures 5(a)-5(b)).

To further elucidate whether formation of CaMKII and NMDAR complex is required for the induction of pathological plasticity, we utilized short cell-permeable peptides Tat-GluN2B derived from GluN2B binding sequence (1295–1309) with CaMKII to specially interfere the association between

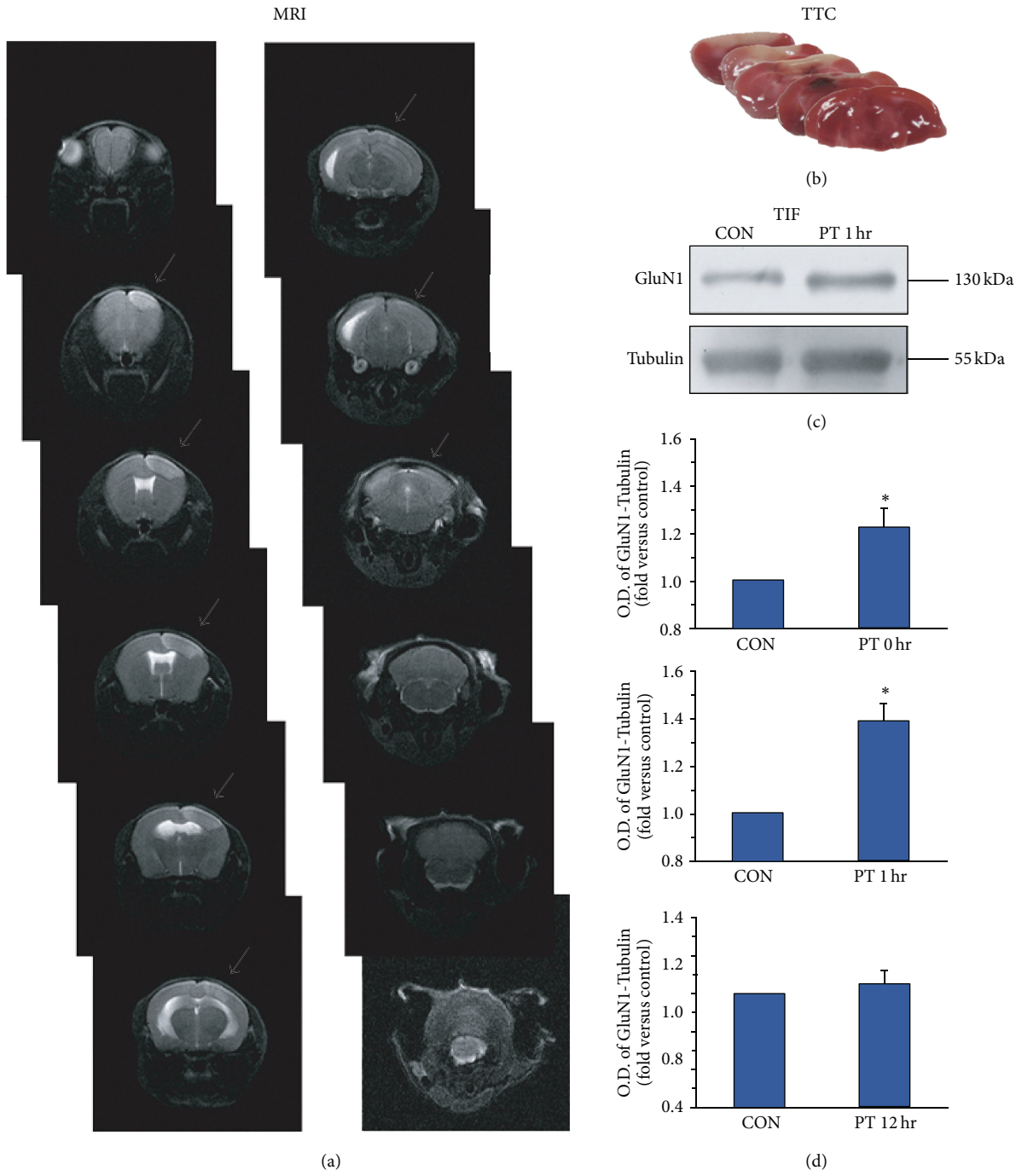

Figure 2: (a) Sequential brain T2-w MRI in an individual mouse with photothrombotic lesion. White arrows indicate infarct region. (b) A series of representative brains stained with TTC after photothrombotic lesion. Pale staining indicates infarct region. (c) Detected by Western blotting, a potentiation of NMDAR in TIF caused by the photothrombotic lesion 1 hr after modeling was shown. (d) Statistical plots of data showing the effects of photothrombotic lesion (0 hr after PT, 1.22 ± 0.08, $n = 5$, $^{*}P < 0.05$; 1 hr after PT, 1.39 ± 0.07, $n = 6$, $^{*}P < 0.05$; 12 hr after PT, 1.05 ± 0.07, $n = 5$, $P > 0.05$).

CaMKII and NMDARs. Tat protein (Tyr-Gly-Arg-Lys-Lys-Arg-Arg-Gln-Arg-Arg-Arg), which was obtained originally from the cell-membrane transduction domain of the human immunodeficiency virus-type 1 (HIV-1), was fused to the constructed peptides and resulted in fusion of Tat-GluN2B peptides. This manipulation allowed the constructed peptides to easily cross the membrane and exert their effects intracellularly [28]. As expected, disturbing the CaMKII-NMDAR interaction with the Tat-GluN2B peptide decreased the association between CaMKII and NMDAR, while

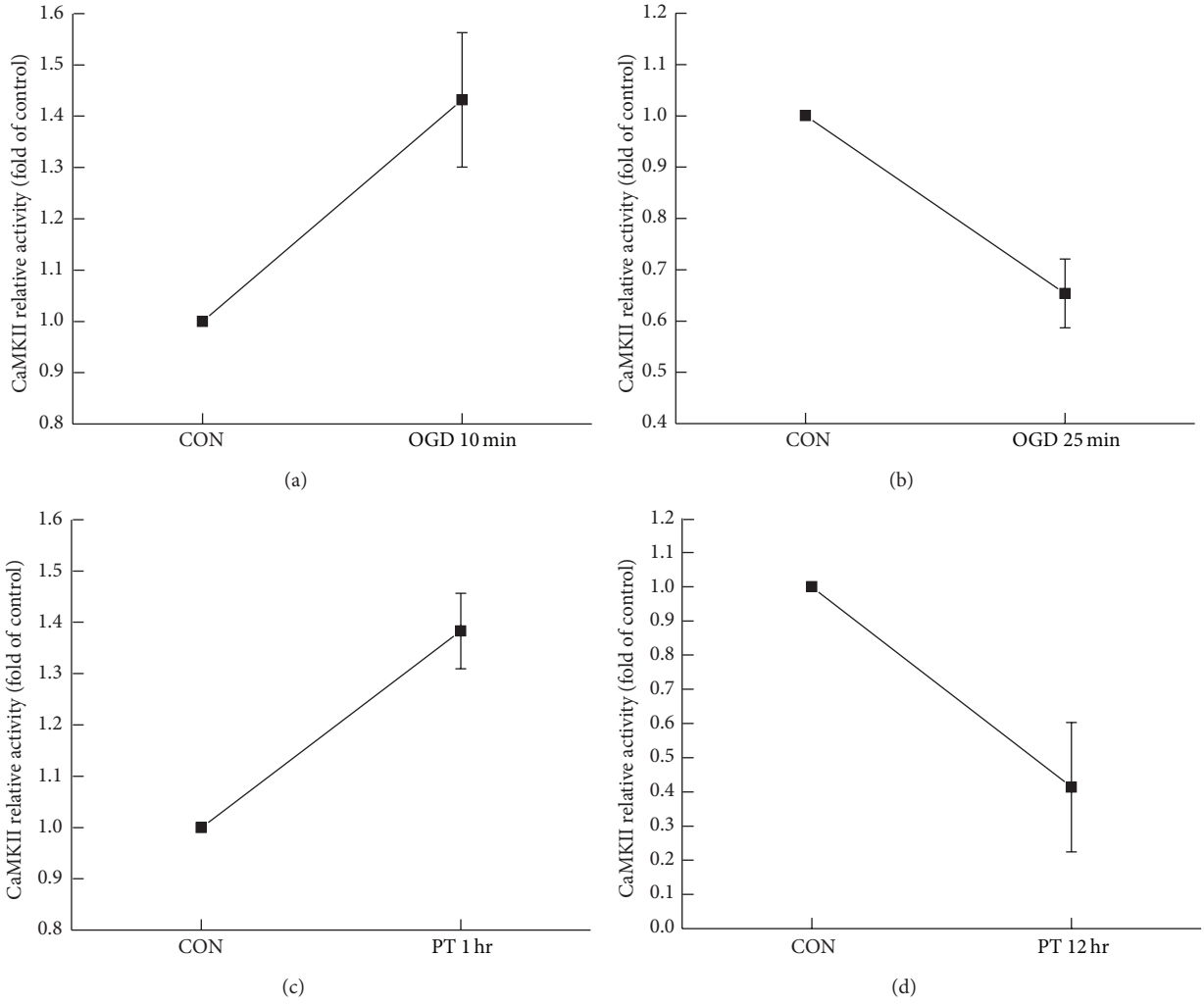

Figure 3: (a) OGD for 10 min caused a significant increase in CaMKII activity (1.43 ± 0.13, $n = 4$, $P < 0.05$). (b) OGD treatment for 25 min led to inhibition of CaMKII activity (0.65 ± 0.07, $n = 3$, $P < 0.05$). (c) 1 hr after PT, CaMKII activity displayed an upward trend (1.38 ± 0.07, $n = 3$, $P < 0.05$). (d) 12 hr after PT, CaMKII activity was inhibited (0.41 ± 0.19, $n = 3$, $P < 0.05$).

scramble peptides failed to display any effect on the association (Figure 5(a)). Interestingly, Tat-GluN2B application also decreased the CaMKII autophosphorylation to baseline level, while scramble peptides failed to exert any effect (Figures 5(c)-5(d), 1.01 ± 0.04, $n = 4$, $P > 0.05$; 1.11 ± 0.03, $n = 4$, $^{*}P < 0.05$), and the CaMKII activity was reduced to the level of control group when Tat-GluN2B was applied, but scramble peptides failed to exert any effect (Figure 5(e), 0.97 ± 0.04, $n = 4$, $P > 0.05$; 1.66 ± 0.18, $n = 4$, $^{*}P < 0.05$). It was observed that there was a decrease in the amplitude of NMDAR-mediated i-LTP after disturbing the connection between CaMKII and NMDAR with peptides Tat-GluN2B (Figure 5(f), $n = 5$, compared with OGD, 0.73 ± 0.02, $P < 0.05$). But scramble peptides failed to exert any effect when the hippocampal slice was exposed to OGD for 10 min (Figure 5(f), $n = 5$, compared with OGD, 1.02 ± 0.03, $P > 0.05$). In line with the changes in CaMKII activity and autophosphorylation, we found that NMDA i-LTP induced by 10 min OGD treatment was also reversed by Tat-GluN2B incubation throughout the recording.

We next examined whether OGD-induced NMDA i-LTP was caused by NMDAR insertion into postsynaptic membrane. We transfected cultured hippocampal cells with GluN1 that is tagged by a pH-sensitive fluorescent protein SEP and employed live-cell imaging to monitor possible changes in fluorescent intensity on surface of spines, where usually excitatory glutamate synapses are located. As shown in Figure 6, the fluorescent intensity at spines increased 10 min after OGD treatment for 2 min, indicating transportation of GluN1 from intracellular vesicles to the plasma membrane of spine. This GluN1 trafficking and subsequent increase in postsynaptic NMDAR number may underlie NMDAR-mediated i-LTP. In addition, disturbing the association between CaMKII and GluN2B with Tat-GluN2B reversed the increase in SEP-GluN1 fluorescent intensity. These results suggest that OGD treatment induced new NMDAR trafficking to spine

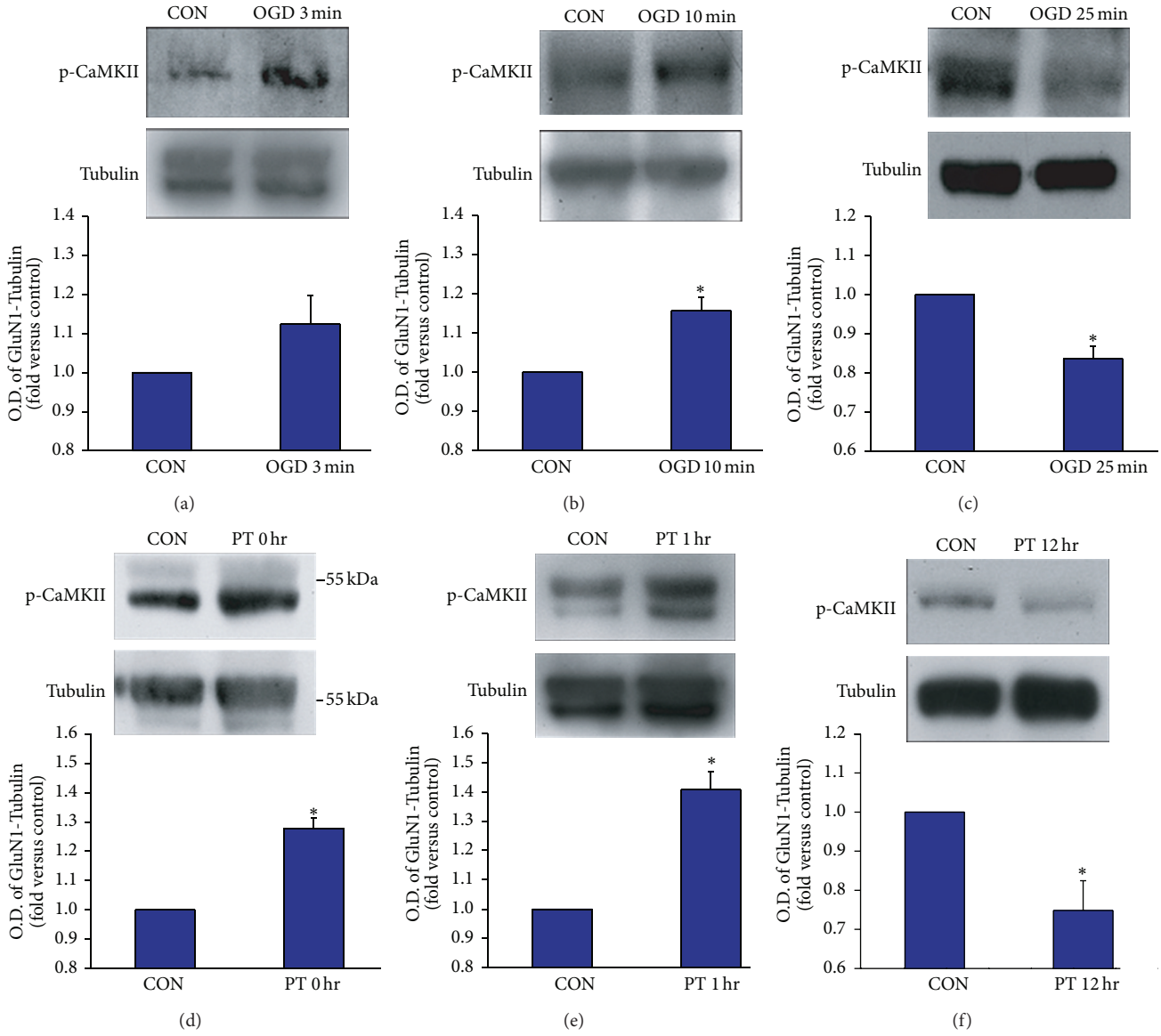

Figure 4: ((a)–(c)) The influence of OGD treatment on autophosphorylation of CaMKII (3 min OGD, 1.12 ± 0.07, $n = 5$, $P > 0.05$; 10 min OGD, 1.16 ± 0.03, $n = 3$, $^{*}P < 0.05$; 25 min OGD, 0.84 ± 0.03, $n = 5$, $^{*}P < 0.05$). ((d)–(f)) The influence of OGD treatment on autophosphorylation of CaMKII (0 hr after PT, 1.28 ± 0.03, $n = 4$, $^{*}P < 0.05$; 1 hr after PT, 1.41 ± 0.06, $n = 5$, $^{*}P < 0.05$; 12 hr after PT, 0.75 ± 0.08, $n = 5$, $^{*}P < 0.05$).

membrane, and CaMKII-GluN2B association is required for this NMDAR trafficking.

4. Discussion

In this study, we used OGD modeling *in vitro* ischemia on the mouse hippocampal slices and photothrombotic lesion modeling *in vivo* ischemia in the mouse hippocampus. As we know, OGD had effects on brain regions including hippocampus to induce NMDAR-mediated i-LTP. But in mounting studies, PT was usually used to research cortical lesion [29, 30]. Therefore it is critical to determine whether hippocampus really suffered from ischemia induced by PT in our experiment. To solve this problem, focal illumination was set to the maximum to widen and deepen the volume of injury to make sure hippocampus suffered from this lesion, but the intensity was set within the extent mice could endure. To examine the lesions of PT, T2-w MRI and TTC staining were conducted after the treatment and the infract region was directly viewed from the photographs.

This study exhibited that NMDAR-mediated i-LTP depends on duration of OGD and PT treatment. Exposure to OGD for 3 min induced a mild increase in i-LTP, while the activity and autophosphorylation level of CaMKII did not display the same trend likewise. Through analysis, it may include two possibilities: one is that the CaMKII assay kit and Western blotting were less sensitive than electrophysiology;

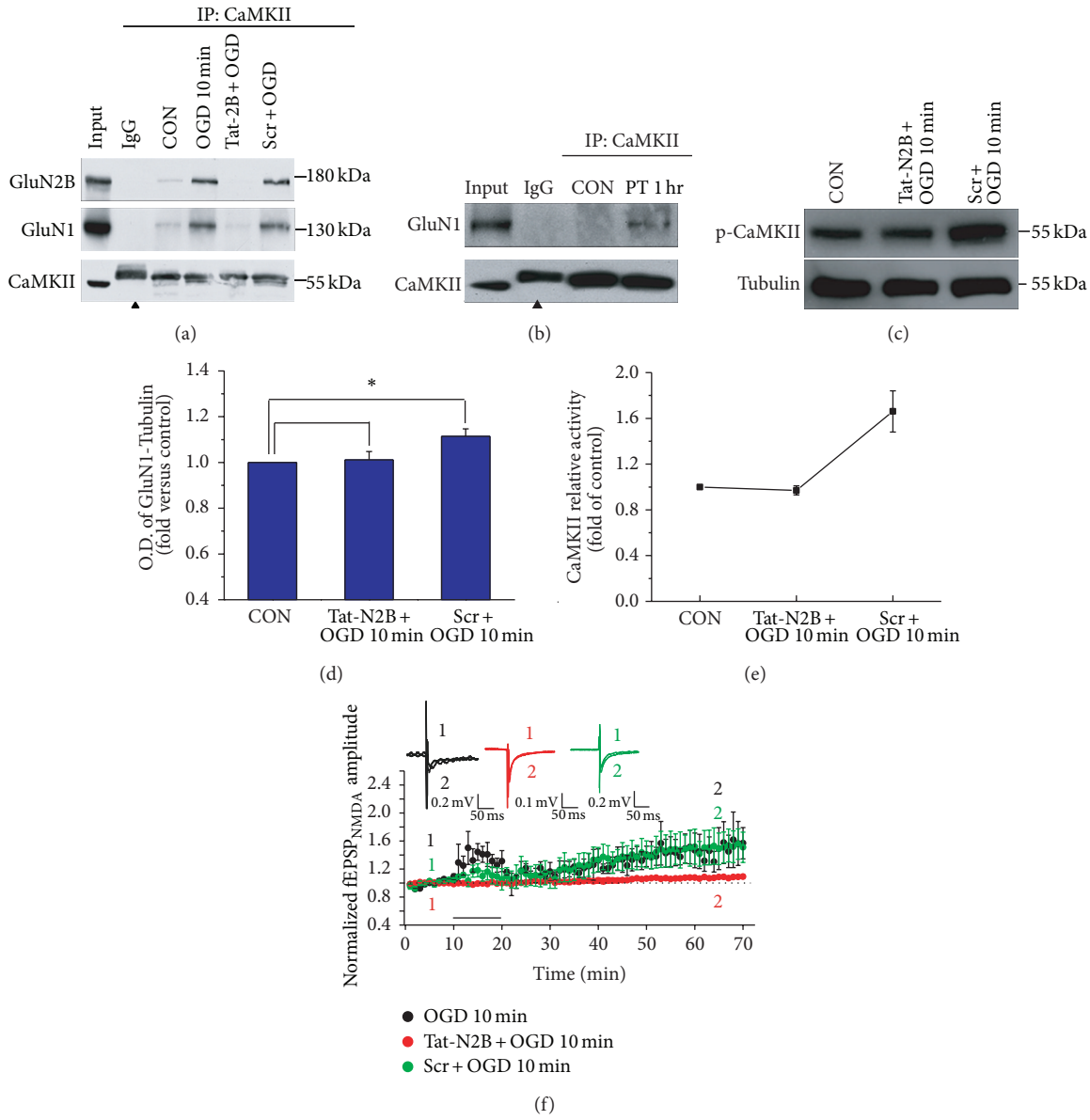

Figure 5: (a) Co-IP assay with anti-CaMKII antibody revealed the association of CaMKII and NMDAR. Peptides occluded the increase of CaMKII and NDMAR by OGD treatment while scramble peptides showed no effect. Arrowhead indicates the nonimmune IgG heavy chain. (b) One hour after photothrombosis caused an increase in the interaction between CaMKII and NMDAR. Arrowhead indicates the nonimmune IgG heavy chain. ((c)-(d)) Peptides Tat-GluN2B suppressed the autophosphorylation of CaMKII in OGD model, compared with control, 1.01 ± 0.04, $n = 4$, $P > 0.05$, while scramble peptides failed to exert any effect on OGD model, compared with control, 1.11 ± 0.03, $n = 4$, $^{*}P < 0.05$. (e) Peptides Tat-GluN2B decreased the CaMKII relative activity when 10 min OGD was applied, compared with control, 0.97 ± 0.04, $n = 4$, $P > 0.05$, while scramble peptides failed to exert any effect when 10 min OGD was used, compared with control, 1.66 ± 0.18, $n = 4$, $^{*}P < 0.05$. (f) Peptides Tat-GluN2B led to impaired i-LTP when the hippocampal slice was exposed to OGD for 10 min, $n = 5$, compared with OGD, $n = 3$, 0.73 ± 0.02, $P < 0.05$. Scramble peptides were used when the hippocampal slice was exposed to OGD for 10 min, $n = 5$, compared with OGD, 1.02 ± 0.03, $P > 0.05$. As a control, OGD treatment for 10 min exhibited normal i-LTP. Overlaid traces above the graph showed changes in amplitude of fEPSPs chosen at the times indicated on the graph.

the other one is, together with active CaMKII, other mechanisms participated in the NMDAR-mediated i-LTP in 3 min exposure to ischemia.

Multiple evidences reported that the downstream reaction triggered by active CaMKII was involved in synaptic plasticity, LTP, and LTD. And CaMKII was observed to be activated in ischemia exposure. It was consistent with our experiment that targeting of active CaMKII to NMDAR has been proved to be important in i-LTP. Tat-GluN2B was to disturb the interaction of CaMKII and NMDAR, and this result has been shown in coimmunoprecipitation. Moreover, 10 min OGD duration with peptides Tat-GluN2B irrigation

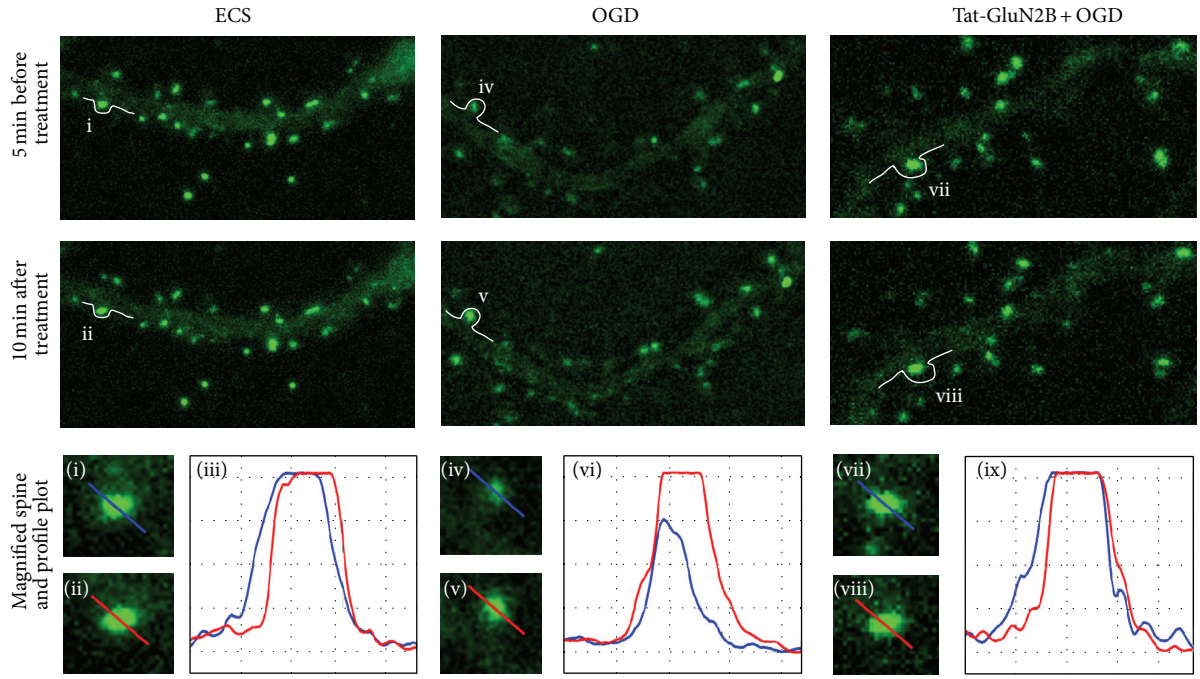

Figure 6: The expression of NMDAR at spine was induced by OGD 2 min treatment and suppressed by Tat-GluN2B incubation. SEP-GluN1 transfected neurons were incubated with Tat-GluN2B for 15 min or not. Subsequently, imaging was performed on 5 min before (first row) and 10 min after (second row) ECS (as control) or OGD 2 min treatment. Magnified images were corresponding to the spines denoted by lowercase Roman numerals ((i), (ii), (iv), (v), (vii), and (viii)). Profile plots were corresponding to the blue and red lines in their left two magnified images ((iii), (vi), and (ix)).

exhibited no increase in the amplitude of fEPSPs; we can concluded that the Tat-GluN2B puts its effects on CaMKII activity, autophosphorylation levels, and NMDAR-mediated i-LTP. But the decreased activity of CaMKII by Tat-GluN2B is always lower than the untreated one. There is connection between CaMKII and NMDAR in normal situation, while the interaction may be more compact or the quantity may be even more after the hippocampus was injured. Before exposure to OGD, Tat-GluN2B was preincubated and then may block the new forming of the complex as well as block the original complex; both cooperate to cause the suppressed activity of CaMKII.

In conclusion, it was determined that NMDAR-mediated i-LTP was induced by different durations of OGD and PT. Meanwhile, CaMKII was activated and autophosphorylated. And our data found the interaction between CaMKII and NMDARs to be promoted by active CaMKII, which was disturbed by Tat-GluN2B after OGD. A similar mechanism was suggested in PT modeling. In earlier studies, as a traditional induction method, OGD was applied to research on hippocampal ischemia widely, but few researchers integrate the corporate results in OGD and PT, a modeling *in vivo*. Hence, our results will provide a novel sight into ischemic research.

Conflict of Interests

The authors declare that there is no conflict of interests regarding the publication of this paper.

Authors' Contribution

Ning Wang and Linlin Chen contributed equally to this work.

Acknowledgments

This work was supported by Grants to Wei Lu from the National Natural Science Foundation of China (NFSC, no. 31025011), the Major State Basic Research Program (973) of China (2013CB733801), and the Open Research Fund of State Key Laboratory of Bioelectronics, Southeast University. The authors acknowledge Professor Robert Malinow who contributed the plasmids pCI-SEP-NR1 and pCI-SEP-NR2A and the Key Laboratory of Molecular Imaging and Functional Imaging of Jiangsu Province in Southeast University for the photothrombotic lesion.

References

[1] L. Li, W. Qu, L. Zhou et al., "Activation of transient receptor potential vanilloid 4 increases nmda-activated current in hippocampal pyramidal neurons," *Frontiers in Cellular Neuroscience*, vol. 7, article 17, 2013.

[2] P. Calabresi, D. Centonze, A. Pisani, L. M. Cupini, and G. Bernardi, "Synaptic plasticity in the ischaemic brain," *The Lancet Neurology*, vol. 2, no. 10, pp. 622–629, 2003.

[3] K.-S. Hsu and C.-C. Huang, "Characterization of the anoxia-induced long-term synaptic potentiation in area CA1 of the rat hippocampus," *British Journal of Pharmacology*, vol. 122, no. 4, pp. 671–681, 1997.

[4] M. P. Mattson, B. Cheng, A. R. Culwell, F. S. Esch, I. Lieberburg, and R. E. Rydel, "Evidence for excitoprotective and intraneuronal calcium-regulating roles for secreted forms of the β-amyloid precursor protein," *Neuron*, vol. 10, no. 2, pp. 243–254, 1993.

[5] K. U. Bayer, É. LeBel, G. L. McDonald, H. O'Leary, H. Schulman, and P. De Koninck, "Transition from reversible to persistent binding of CaMKII to postsynaptic sites and NR2B," *Journal of Neuroscience*, vol. 26, no. 4, pp. 1164–1174, 2006.

[6] R. M. Dixon, J. R. Mellor, and J. G. Hanley, "PICK1-mediated glutamate receptor subunit 2 (GluR2) trafficking contributes to cell death in oxygen/glucose-deprivedhippocampal neurons," *Journal of Biological Chemistry*, vol. 284, no. 21, pp. 14230–14235, 2009.

[7] V. Crepel, C. Hammond, P. Chinestra, D. Diabira, and Y. Ben-Ari, "A selective LTP of NMDA receptor-mediated currents induced by anoxia in CA1 hippocampal neurons," *Journal of Neurophysiology*, vol. 70, no. 5, pp. 2045–2055, 1993.

[8] V. Crepel, C. Hammond, K. Krnjevic, P. Chinestra, and Y. Ben-Ari, "Anoxia-induced LTP of isolated NMDA receptor-mediated synaptic responses," *Journal of Neurophysiology*, vol. 69, no. 5, pp. 1774–1778, 1993.

[9] K. Szydlowska and M. Tymianski, "Calcium, ischemia and excitotoxicity," *Cell Calcium*, vol. 47, no. 2, pp. 122–129, 2010.

[10] P. Jourdain, K. Fukunaga, and D. Muller, "Calcium/calmodulin-dependent protein kinase II contributes to activity-dependent filopodia growth and spine formation," *Journal of Neuroscience*, vol. 23, no. 33, pp. 10645–10649, 2003.

[11] B. Picconi, A. Tortiglione, I. Barone et al., "NR2B subunit exerts a critical role in postischemic synaptic plasticity," *Stroke*, vol. 37, no. 7, pp. 1895–1901, 2006.

[12] W. Yao, F. Ji, Z. Chen et al., "Glycine exerts dual roles in ischemic injury through distinct mechanisms," *Stroke*, vol. 43, no. 8, pp. 2212–2220, 2012.

[13] A. Barria and R. Malinow, "NMDA receptor subunit composition controls synaptic plasticity by regulating binding to CaMKII," *Neuron*, vol. 48, no. 2, pp. 289–301, 2005.

[14] F. Meng, J. Guo, Q. Zhang, B. Song, and G. Zhang, "Autophosphorylated calcium/calmodulin-dependent protein kinase IIα (CaMKIIα) reversibly targets to and phosphorylates N-methyl-D-aspartate receptor subunit 2B (NR2B) in cerebral ischemia and reperfusion in hippocampus of rats," *Brain Research*, vol. 967, no. 1-2, pp. 161–169, 2003.

[15] F. Meng and G. Zhang, "Autophosphorylated calcium/calmodulin-dependent protein kinase II α induced by cerebral ischemia immediately targets and phosphorylates N-methyl-D-aspartate receptor subunit 2B (NR2B) in hippocampus of rats," *Neuroscience Letters*, vol. 333, no. 1, pp. 59–63, 2002.

[16] R. J. Colbran and A. M. Brown, "Calcium/calmodulin-dependent protein kinase II and synaptic plasticity," *Current Opinion in Neurobiology*, vol. 14, no. 3, pp. 318–327, 2004.

[17] A. S. Leonard, K. U. Bayer, M. A. Merrill et al., "Regulation of calcium/calmodulin-dependent protein kinase II docking to N-methyl-D-aspartate receptors by calcium/calmodulin and α-actinin," *Journal of Biological Chemistry*, vol. 277, no. 50, pp. 48441–48448, 2002.

[18] S. Strack and R. J. Colbran, "Autophosphorylation-dependent targeting of calcium/calmodulin-dependent protein kinase II by the NR2B subunit of the N-methyl-D-aspartate receptor," *Journal of Biological Chemistry*, vol. 273, no. 33, pp. 20689–20692, 1998.

[19] R. Nisticò, S. Piccirilli, M. L. Cucchiaroni et al., "Neuroprotective effect of hydrogen peroxide on an in vitro model of brain ischaemia," *British Journal of Pharmacology*, vol. 153, no. 5, pp. 1022–1029, 2008.

[20] K. A. Skelding, N. J. Spratt, L. Fluechter et al., "Alphacamkii is differentially regulated in brain regions that exhibit differing sensitivities to ischemia and excitotoxicity," *Journal of Cerebral Blood Flow and Metabolism*, vol. 32, no. 12, pp. 2181–2192, 2012.

[21] J.-Z. Yan, Z. Xu, S.-Q. Ren et al., "Protein kinase C promotes N-methyl-D-aspartate (NMDA) receptor trafficking by indirectly triggering calcium/calmodulin-dependent protein kinase II (CaMKII) autophosphorylation," *Journal of Biological Chemistry*, vol. 286, no. 28, pp. 25187–25200, 2011.

[22] G. F. Hédou, K. Koshibu, M. Farinelli et al., "Protein phosphatase 1-dependent bidirectional synaptic plasticity controls ischemic recovery in the adult brain," *Journal of Neuroscience*, vol. 28, no. 1, pp. 154–162, 2008.

[23] C. D. Kopec, B. Li, W. Wei, J. Boehm, and R. Malinow, "Glutamate receptor exocytosis and spine enlargement during chemically induced long-term potentiation," *Journal of Neuroscience*, vol. 26, no. 7, pp. 2000–2009, 2006.

[24] M. V. Frantseva, P. L. Carlen, and H. El-Beheiry, "A submersion method to induce hypoxic damage in organotypic hippocampal cultures," *Journal of Neuroscience Methods*, vol. 89, no. 1, pp. 25–31, 1999.

[25] A. M. Pugliese, E. Coppi, G. Spalluto, R. Corradetti, and F. Pedata, "A3 adenosine receptor antagonists delay irreversible synaptic failure caused by oxygen and glucose deprivation in the rat CA1 hippocampus in vitro," *British Journal of Pharmacology*, vol. 147, no. 5, pp. 524–532, 2006.

[26] X. Sun, H. Yao, R. M. Douglas, X. Q. Gu, J. Wang, and G. G. Haddad, "InsulinPI3K signaling protects dentate neurons from oxygen-glucose deprivation in organotypic slice cultures," *Journal of Neurochemistry*, vol. 112, no. 2, pp. 377–388, 2010.

[27] H. Z. Yin, S. L. Sensi, F. Ogoshi, and J. H. Weiss, "Blockade of Ca2+-permeable AMPA/kainate channels decreases oxygen-glucose deprivation-induced Zn2+ accumulation and neuronal loss in hippocampal pyramidal neurons," *Journal of Neuroscience*, vol. 22, no. 4, pp. 1273–1279, 2002.

[28] H. Hashida, M. Miyamoto, Y. Cho et al., "Fusion of HIV-1 Tat protein transduction domain to poly-lysine as a new DNA delivery tool," *British Journal of Cancer*, vol. 90, no. 6, pp. 1252–1258, 2004.

[29] J.-K. Lee, J.-E. Kim, M. Sivula, and S. M. Strittmatter, "Nogo receptor antagonism promotes stroke recovery by enhancing axonal plasticity," *Journal of Neuroscience*, vol. 24, no. 27, pp. 6209–6217, 2004.

[30] A. Lipsanen, S. Flunkert, K. Kuptsova et al., "Non-selective calcium channel blocker bepridil decreases secondary pathology in mice after photothrombotic cortical lesion," *PLoS ONE*, vol. 8, no. 3, Article ID e60235, 2013.

Hindawi Publishing Corporation
Neural Plasticity
Volume 2014, Article ID 205912, 15 pages
http://dx.doi.org/10.1155/2014/205912

Research Article

Effect of the Entorhinal Cortex on Ictal Discharges in Low-Mg^{2+}-Induced Epileptic Hippocampal Slice Models

Ye-Jun Shi,[1] Xin-Wei Gong,[2] Hai-Qing Gong,[2] Pei-Ji Liang,[2] Pu-Ming Zhang,[2] and Qin-Chi Lu[1]

[1] *Department of Neurology, Ren Ji Hospital, School of Medicine, Shanghai Jiao Tong University, 1630 Dong-Fang Road, Shanghai 200127, China*
[2] *School of Biomedical Engineering, Shanghai Jiao Tong University, 800 Dong-Chuan Road, Shanghai 200240, China*

Correspondence should be addressed to Pu-Ming Zhang; pmzhang@sjtu.edu.cn and Qin-Chi Lu; qinchilu@yahoo.com

Received 18 September 2013; Accepted 30 January 2014; Published 3 March 2014

Academic Editor: Masayuki Matsushita

The hippocampus plays an important role in the genesis of mesial temporal lobe epilepsy, and the entorhinal cortex (EC) may affect the hippocampal network activity because of the heavy interconnection between them. However, the mechanism by which the EC affects the discharge patterns and the transmission mode of epileptiform discharges within the hippocampus needs further study. Here, multielectrode recording techniques were used to study the spatiotemporal characteristics of epileptiform discharges in adult mouse hippocampal slices and combined EC-hippocampal slices and determine whether and how the EC affects the hippocampal neuron discharge patterns. The results showed that low-Mg^{2+} artificial cerebrospinal fluid induced interictal discharges in hippocampal slices, whereas, in combined EC-hippocampal slices the discharge pattern was alternated between interictal and ictal discharges, and ictal discharges initiated in the EC and propagated to the hippocampus. The pharmacological effect of the antiepileptic drug valproate (VPA) was tested. VPA reversibly suppressed the frequency of interictal discharges but did not change the initiation site and propagation speed, and it completely blocked ictal discharges. Our results suggested that EC was necessary for the hippocampal ictal discharges, and ictal discharges were more sensitive than interictal discharges in response to VPA.

1. Introduction

Mesial temporal lobe epilepsy (mTLE) is the most common type of intractable epilepsy. It is closely associated with malfunctions of the mesial temporal lobe structures, such as the hippocampus and the entorhinal cortex (EC), which are heavily interconnected [1, 2]. It has been commonly accepted that the hippocampus plays an important role in the genesis of mTLE [3]. Several studies have investigated the cellular and network mechanisms of epileptiform discharges in the hippocampus [4–6]. de Curtis and Avanzini [7] and McCormick and Contreras [8] reported that the mechanisms of epileptiform discharges mainly depend on intrinsic neuronal properties, recurrent synaptic interconnections, and nonsynaptic interactions among closely located neurons, which lead to excessive neuronal synchronization. In addition to the hippocampus, several clinical cases of mTLE showed significant pathologic changes in other limbic structures, such as the EC and the amygdale [9, 10]. Additionally, observations in animal models indicated that the epileptogenic zone was broad, and the substrate for seizure generation was distributed over several limbic structures [11], including the hippocampus, EC, and amygdala.

Epileptiform activities derive from the imbalance between excitatory and inhibitory synaptic transmission in networks [8], which appear as ictal and interictal discharges. Ictal discharges (also termed seizures) typically last for a few tens of seconds to several minutes and represent the primary clinical burden of an active epileptic condition. Interictal discharges exist between seizures and usually last for a couple of hundred milliseconds to a few seconds [12]. Studies have shown that epileptiform activities observed in isolated hippocampal slices obtained from adult animals were mostly interictal discharges, which initiated from CA3a/b regions

and propagated bidirectionally to CA3c and CA1 regions [13], while prolonged ictal discharges that resemble limbic seizures were rarely observed, which was consistent with our previous studies [14, 15]. On the other hand, studies using extracellular field potential recordings have confirmed that ictal discharges originated in the EC and then propagated to the hippocampus in combined EC-hippocampal slices from the adult rats [13]. Compared with the isolated hippocampal slice, the combined slice preserves the EC and its fiber connection with hippocampus. However, the mechanism by which the EC affects the discharge patterns and the transmission mode of interictal and ictal discharges within the hippocampus needs to be studied further.

In the present study, hippocampal slices and combined EC-hippocampal slices of adult male C57BL/6 mice were prepared, and low-Mg^{2+} artificial cerebrospinal fluid (ACSF) was adopted to induce epileptiform discharges in the slices, which results in epileptiform discharges by unblocking the N-methyl-D-aspartate (NMDA) receptors [6]. Microelectrode array (MEA), which has a high resolution and precision in both temporal and spatial domains, was used to record electrical signals in relevant areas simultaneously. Valproate (VPA), one of the major antiepileptic drugs (AEDs) commonly used in clinical practice, was used to examine its pharmacological effects on the different epileptiform discharges in the two slice models.

Our data showed that low-Mg^{2+} ACSF induced interictal discharges in the hippocampal slices while inducing alternating interictal and ictal discharges in the combined EC-hippocampal slices. Interictal discharges initiated in CA3a and propagated bidirectionally to CA3c and CA1 regions, while ictal discharges originated from the EC and propagated to the hippocampus. VPA reversibly suppressed the frequency of interictal discharges, while completely blocking the ictal discharges. The results suggested that EC was necessary for ictal discharges in the low-Mg^{2+}-induced epileptic hippocampal slice models, and ictal discharges were more sensitive than interictal discharges in response to VPA.

2. Materials and Methods

2.1. Combined EC-Hippocampal Slice and Hippocampal Slice Preparation. Adult male C57BL/6 mice aged 12–16 weeks were purchased from the Shanghai Institutes for Biological Sciences. All animal experiments were approved by the Ethic Committee, School of Biomedical Engineering, Shanghai Jiao Tong University. All efforts were made to minimize the number of animals used and their suffering.

All animals were handled and decapitated under deep isoflurane anesthesia. The brain was rapidly removed and placed in oxygenated (95% O_2 and 5% CO_2), ice-cold ACSF for 5 min. The composition of the normal ACSF was as follows (in mM): NaCl 124.0, KCl 3.5, $CaCl_2$ 2.5, NaH_2PO_4 1.2, $MgCl_2{\cdot}6H_2O$ 1.3, $NaHCO_3$ 25.0, and glucose 10.0 (pH 7.4). The cerebellum was removed, and a sagittal cut separated the cerebral hemispheres. The cerebral hemispheres were positioned with the medial surface on a wet cold filter paper. The dorsal cortex of each hemisphere was cut parallel to the rostral/caudal axis and removed (<2 mm thick). The rostral two-thirds of the brain were removed from the caudal third, and all diencephalic and midbrain structures were subsequently removed from the caudal third. The dorsal side of the trimmed tissue was glued down to the base plate of the vibratome (Series 1000, Tissue Sectioning System, Vibratome, Natural Genetic Ltd., USA), with the caudal end towards the blade that was secured at an angle of 10°. Next, combined EC-hippocampal slices (400 μm) were incubated in oxygenated ACSF at 28°C for at least 2 hours before use. In our experiments, only one slice was adopted from each mouse, with the slices obtained from similar positions in the trimmed tissue. The combined slice contained the hippocampus, dentate gyrus (DG), subiculum (Sub), EC, and part of the perirhinal cortex (PRh) (Figure 1(d)). To prepare hippocampal slices (Figure 1(a)), the EC and PRh regions were removed from the combined slices. Epileptiform activities were induced by low-Mg^{2+} ACSF, in which $MgCl_2{\cdot}6H_2O$ was omitted from the normal ACSF without substitution.

2.2. Electrophysiological Recordings. Multichannel recording system (MEA60, Multichannel Systems GmbH, Germany) was used to record electrical activities, and the microelectrode array (MEA) consists of 60 electrodes (electrode diameter is 30 μm and the tip-to-tip interelectrode space is 200 μm) (Figure 1(a)).

The slice was quickly transferred to the MEA recording chamber. A nylon mesh was used to immobilize the slice. The hippocampal area of the slice was placed in the recording area (Figures 1(a) and 1(d)), to record the electrical activities in the hippocampus. In other experiments, we placed the EC with parts of CA1 in the recording area (Figure 4(a)) to analyze the relationship of epileptiform discharges in the EC and the hippocampus. The slice was perfused continuously with oxygenated ACSF which was maintained at 35-36°C with a temperature control unit (Thermostat HC-X, Multichannel Systems GmbH, Germany) and at a flow rate of 2 mL/min with a peristaltic pump (Ismatec SA, USA). An Olympus microscope (Olympus, Japan) and camera (Olympus, Japan) were used to observe the relative position of the slice on the MEA and capture images. All data were recorded with a 60-channel amplifier (single-ended amplifier, bandwidth 1 Hz–3.4 kHz, amplification 1200x, amplifier input impedance $>10^{10}$ Ω, and output impedance 330 Ω) and sampled at 20 kHz. The data were displayed on the computer screen (Figures 1(b) and 1(e)) and stored simultaneously for off-line analysis.

2.3. Chemicals and Drugs. VPA was purchased from Sigma-Aldrich (USA), and the other chemicals were acquired from Sinopharm Chemical Reagent Co., Ltd (SCRC, China). During the experiments, the drugs were dissolved in the low-Mg^{2+} ACSF.

2.4. Data Analysis. Epileptiform activities appear as interictal discharges, as well as tonic-clonic ictal discharges [8]. Interictal discharges usually terminate within a couple of hundred milliseconds to a few seconds. Ictal discharges typically last for a few tens of seconds to several minutes [12]. In the present study, the epileptiform discharges were defined as interictal if they lasted for less than 1 s (usually between 100 and 300 ms)

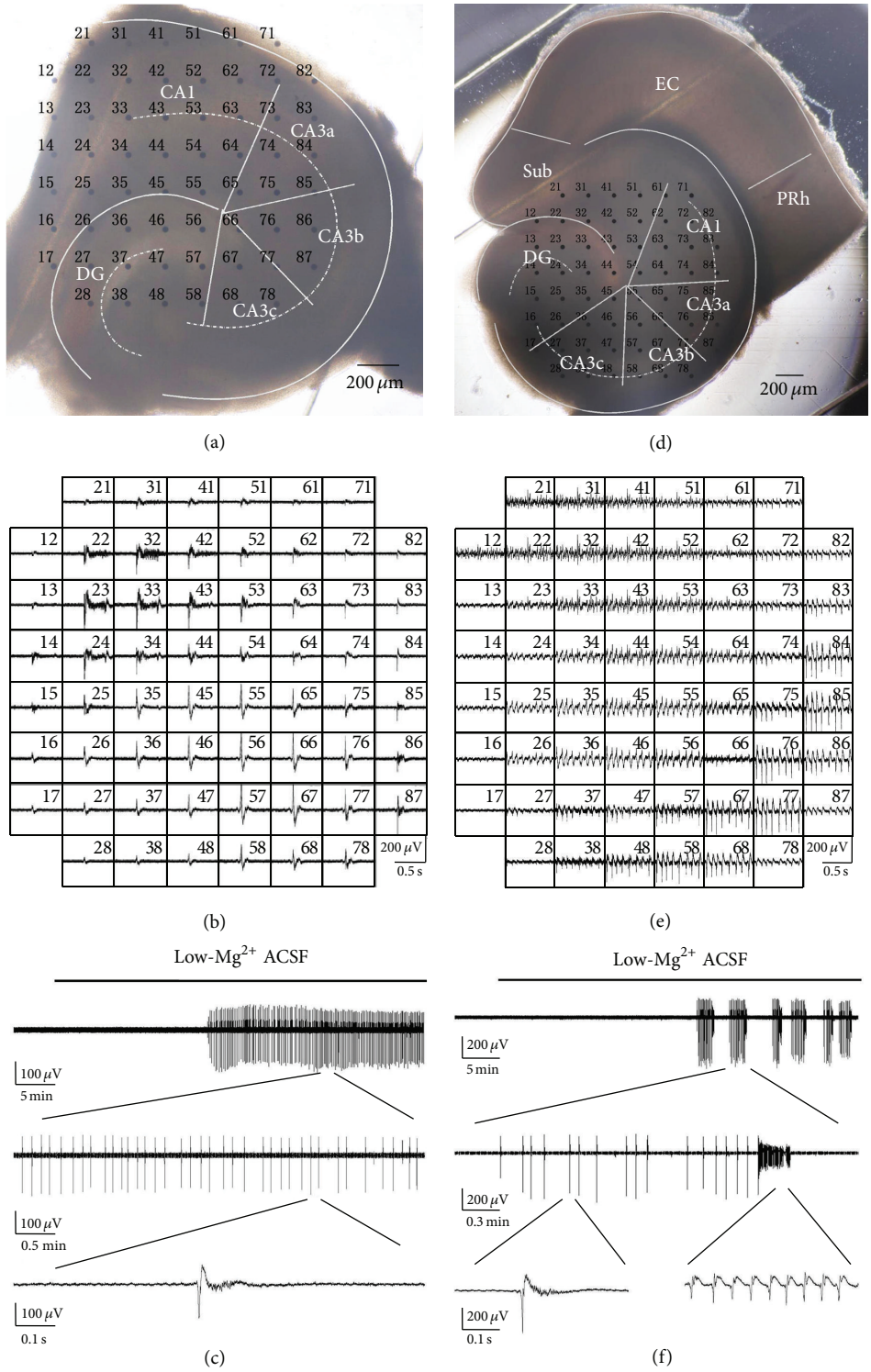

Figure 1: Slices mounted on MEA and low-Mg^{2+}-induced epileptiform discharges. (a) An image of an example of a hippocampal slice mounted on MEA. The black dots indicate the electrodes (60 channels) of the MEA, with each electrode number labeled at its top left corner. (b) Low-Mg^{2+}-induced epileptiform discharges recorded by the MEA. Each data window represented the recording from one electrode, with each electrode number labeled at its top right corner. (c) A portion of raw data recorded by one electrode (number 87), which showed epileptiform discharges in the CA3b region, with epileptiform activities presented using different time scales. (d) An image of an example of combined EC-hippocampal slice mounted on MEA. (e) Low-Mg^{2+}-induced ictal discharges recorded by the MEA. (f) A portion of raw data recorded by one electrode (number 67), which showed epileptiform discharges in the CA3b region of the combined slice. There were two types of epileptiform discharges recorded in the hippocampal area: interictal and ictal discharges. Each discharge cycle consisted of several minutes of interictal discharges and tens of seconds of ictal discharge. After a resting period, this alternating interictal and ictal discharge pattern repeated.

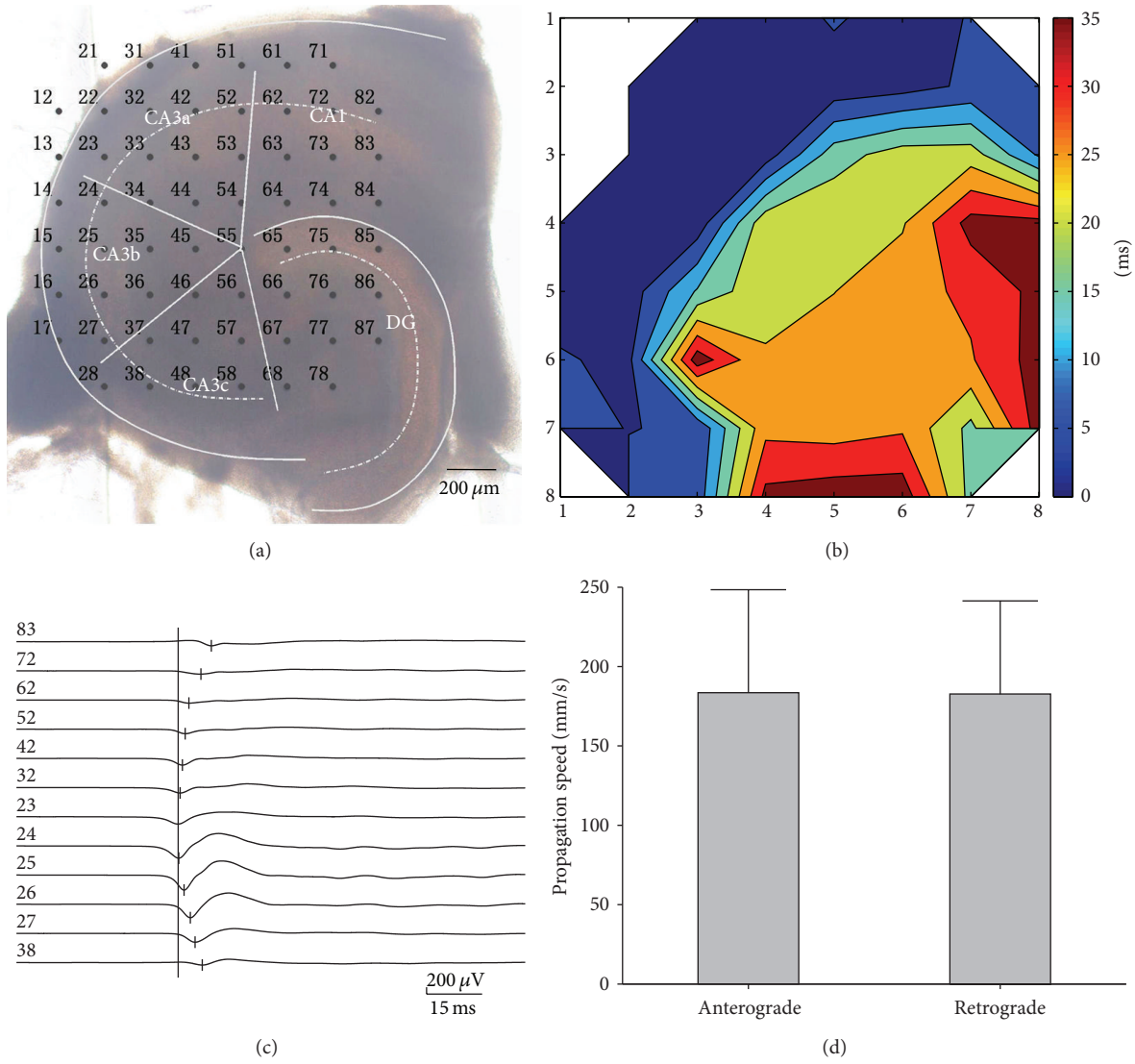

Figure 2: Initiation and propagation of interictal discharges in hippocampal slices. (a) An image of a hippocampal slice mounted on MEA. (b) Contour plot of averaged time delays of the FP relative to signals recorded by electrode number 23. The X and Y coordinates denote the positions of electrodes. (c) The relative time delay of first negative peak of FP recorded along the stratum pyramidale. The interictal discharges initiated from the CA3a region and propagated bidirectionally to the CA1 region (anterograde) and the CA3c region (retrograde). (d) Averaged propagation speeds of interictal discharges in hippocampal slices ($P > 0.05$, paired t-test, $n = 5$).

and occurred at frequency of 0.1~0.3 Hz. Ictal discharges were defined as prolonged events which lasted for 10~30 s and occurred at a frequency of 0.003~0.006 Hz.

Off-line data analysis was performed with MC_Rack 4.1.1 (Multichannel Systems GmbH, Germany), Matlab 7.10.0 (Mathworks, USA), and SPSS Statistics 17.0 (IBM, USA). Raw data were separated into field potential (FP) and multiunit activity (MUA) by 1–100 Hz band-pass and 200 Hz high-pass filtering, respectively. MUA (data not shown) was not obvious in some slices; therefore, FP was used for further analysis. The epileptiform FP was determined when the negative-positive peak of signal exceeded four times the standard deviations from the mean value of 500-ms baseline (no obvious epileptiform discharges). The FPs of the interictal discharges in the hippocampal stratum pyramidale exhibited negative-positive waveforms [14]; thus, in the present study, the initiation and propagation of the interictal discharges were determined by comparing the timing of the first negative peaks of the FP recorded along the stratum pyramidale, and the earliest site of the negative peak of the FP was defined as the initiation site. The propagation speed of the interictal discharges was measured according to the tip-to-tip distance between the adjacent electrodes and the relative time delay of the first negative peak of the FP along the stratum pyramidale. While in the propagation route of the ictal discharges, epileptic waveforms could exhibit negative-positive (stratum pyramidale) as well as positive-negative (stratum radiatum and stratum lacunosum-moleculare) characteristics; therefore, the initiation and propagation of the ictal discharges were determined by comparing the timing of the first negative-positive peaks of the FP recorded by all electrodes in the combined slice. The data are expressed as the means ± SEM.

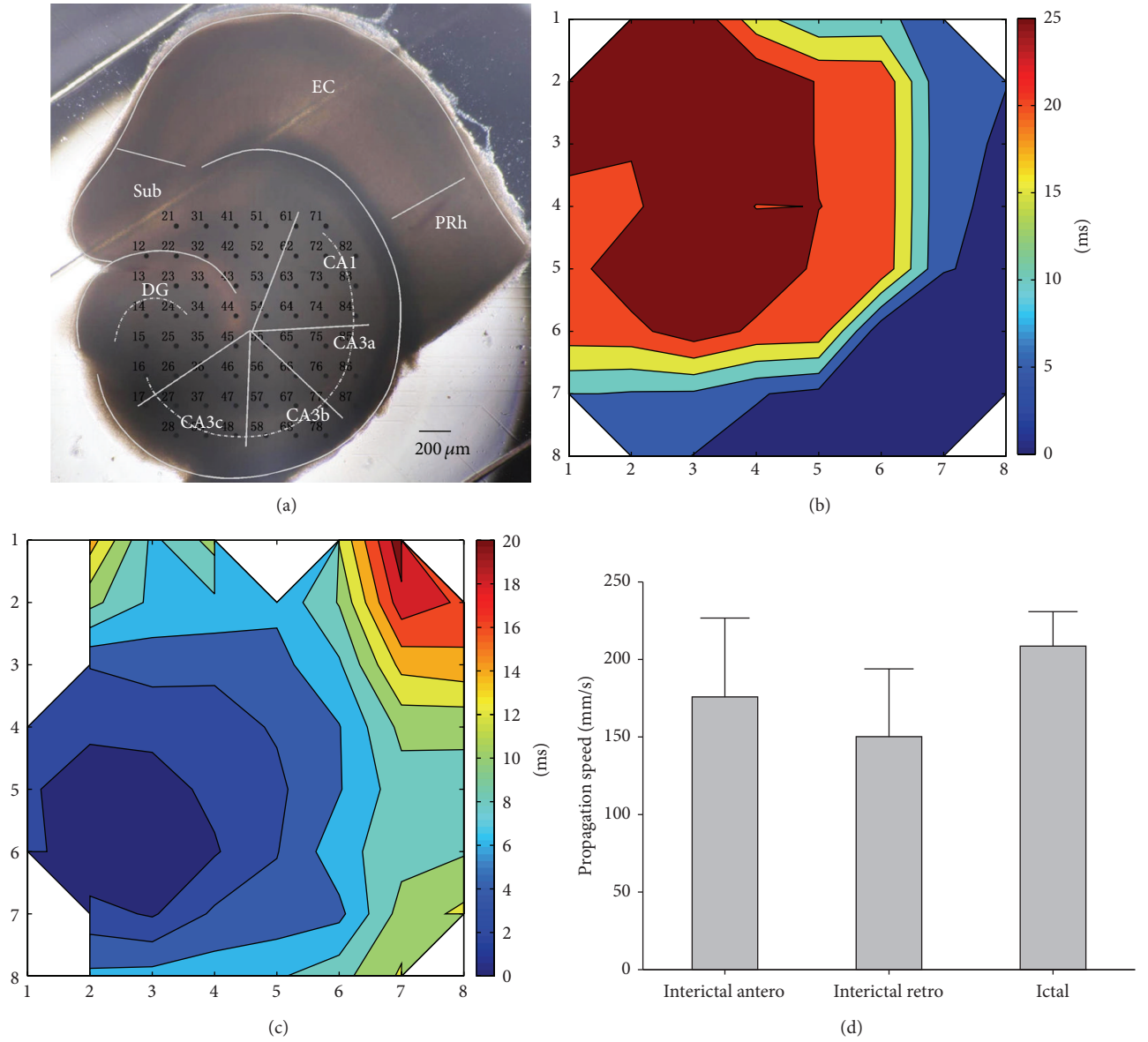

Figure 3: Initiation and propagation of interictal and ictal discharges in the hippocampal area of the combined EC-hippocampal slices. (a) An image of an example of a combined slice mounted on MEA. (b) Contour plot of averaged time delays of the FP relative to signals of electrode number 85. The X and Y coordinates denote the positions of electrodes. (c) Contour plot of averaged time delays of the FP relative to signals of electrode number 25. (d) Averaged propagation speeds of interictal discharges and ictal discharges in the combined slices. antero: anterograde propagation speed; retro: retrograde propagation speed ($P > 0.05$, ANOVA, $n = 5$).

Statistical comparisons were made using paired t-test or one-way ANOVA test. The level of significance was set at $P < 0.05$.

3. Results

3.1. Low-Mg^{2+}-Induced Epileptiform Discharges. In our experiments, the application of low-Mg^{2+} ACSF consistently induced interictal discharges in hippocampal slices. Figures 1(a)–1(c) show an example of a hippocampal slice mounted on MEA and low-Mg^{2+}-induced interictal discharges. The onset of the interictal discharges in different hippocampal slices appeared with different time delays, ranging between 10 and 20 min (16.7 ± 2.5 min, $n = 5$) after the low-Mg^{2+} ACSF perfusion began. The frequency of the interictal discharges was 0.23 ± 0.05 Hz ($n = 5$). The durations of the interictal discharges in different subregions were 184.9 ± 51.2 (CA3a), 191.0 ± 41.2 (CA3b), 176.7 ± 32.3 (CA3c), 175.0 ± 37.7 (CA1), and 151.3 ± 29.1 (DG) ms. There was no significant difference between the durations of interictal discharges in these subregions in hippocampal slices ($P > 0.05$, ANOVA, $n = 5$, Table 1).

Low-Mg^{2+} ACSF only induced interictal discharges in the isolated hippocampal slices; in that case, what was the discharge pattern in the combined slices? To compare the

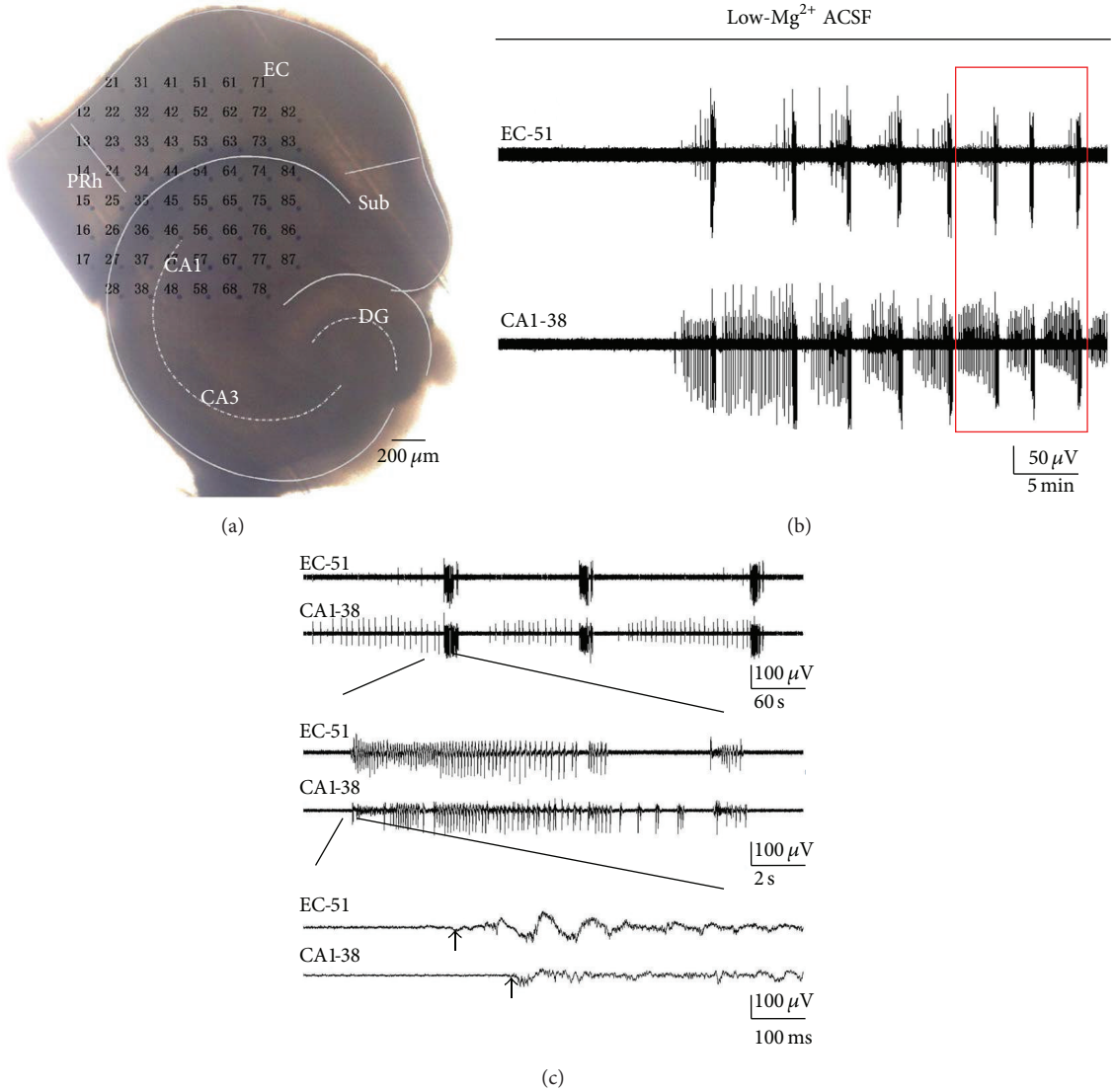

Figure 4: Epileptiform discharges in the EC and CA1 regions of the combined EC-hippocampal slice. (a) An example of a combined slice mounted on MEA. (b) Low-Mg^{2+}-induced epileptiform discharges in the EC and CA1 regions. The FP recorded by two electrodes (numbers 51 and 38 in (a)), which presented epileptiform activities in the EC and CA1 areas. (c) Time delays of ictal discharges with expanded time scales (red box in (b)).

Table 1: Frequency and duration of low-Mg^{2+}-induced epileptiform discharges in two slice models (mean ± SEM, $n = 5$).

	Frequency (Hz)	Duration (interictal: ms/Ictal: s)				
		CA3a	CA3b	CA3c	CA1	DG
HP (interictal)	0.23 ± 0.05	184.9 ± 51.2	191.0 ± 41.2	176.7 ± 32.3	175.0 ± 37.7	151.3 ± 29.1
EC-HP (interictal)	0.24 ± 0.04	218.1 ± 20.6	222.4 ± 16.6	222.6 ± 11.3	211.4 ± 63.5	184.4 ± 18.8
EC-HP (ictal)	0.004 ± 0.001	14.6 ± 1.7	14.6 ± 1.3	14.5 ± 1.5	14.5 ± 1.4	14.6 ± 1.3

HP: hippocampal slices; EC-HP: combined EC-hippocampal slices.

epileptiform discharge patterns in the isolated hippocampal slices and combined EC-hippocampal slices, the hippocampus of the combined slices was placed in the recording area. Figures 1(d)–1(f) show an example of a combined EC-hippocampal slice mounted on MEA and low-Mg^{2+}-induced epileptiform discharges. The onset of the epileptiform activity in different slices was 10~25 min (17.6 ± 6.5 min, $n = 5$) after low-Mg^{2+} ACSF perfusion began. There were two types of epileptiform discharges recorded in the hippocampal area: interictal and ictal discharges. Each discharge cycle consisted of several minutes of interictal discharges (4.7 ± 2.7 min, $n = 5$) and tens of seconds of ictal discharge (14.5 ± 1.3 s,

$n = 5$) (Figure 1(f)). After a resting period (1.3 ± 0.7 min, $n = 5$), this alternating interictal and ictal discharge pattern repeated. The frequency of these interictal discharges was 0.24 ± 0.04 Hz ($n = 5$), and the discharge durations in different subregions were 218.1 ± 20.6 (CA3a), 222.4 ± 16.6 (CA3b), 222.6 ± 11.3 (CA3c), 211.4 ± 63.5 (CA1), and 184.4 ± 18.8 (DG) ms. There was no significant difference between these durations ($P > 0.05$, ANOVA, $n = 5$, Table 1). The ictal discharges were usually prolonged activities, which occurred at the frequency of 0.004 ± 0.001 Hz ($n = 5$) and were characterized by rhythmic oscillations of 7.17 ± 2.75 Hz ($n = 5$). The durations of the ictal discharges in different subregions were 14.6 ± 1.7 (CA3a), 14.6 ± 1.3 (CA3b), 14.5 ± 1.5 (CA3c), 14.5 ± 1.4 (CA1), and 14.6 ± 1.3 (DG) s. There was no significant difference between these durations of ictal discharges ($P > 0.05$, ANOVA, $n = 5$, Table 1).

3.2. Initiation and Propagation of Interictal Discharges in Hippocampal Slices. From the above results, we found that ictal discharges were only observed in the combined slices, which was closely related to the presence of the EC. How will the EC affect the epileptiform discharge pattern in the hippocampus? In the following study, the exact propagation modes of different types of discharges within the hippocampal network in the two slice models were analyzed.

Figure 2(b) shows the contour plot of the averaged time delays of the FP relative to signals recorded by electrode number 23 on the representative hippocampal slice shown in Figure 2(a). The interictal discharge was first observed in the CA3 region and propagated to the other hippocampal regions. The time delays of the first negative peaks of FP recorded along the stratum pyramidale were compared, and the earliest site of the negative peak of FP was defined as the initiation site. As shown in Figure 2(c), the interictal discharges initiated in CA3a (electrode number 23) and propagated bidirectionally to the CA1 (anterograde) and CA3c (retrograde). The data obtained from the other 4 slices showed that the interictal discharges presented similar initiation and propagation patterns. Statistical analysis showed that the propagation speeds of the interictal discharges in the hippocampal slices were 183.5 ± 64.9 mm/s (anterograde, from CA3a to CA1) and 182.7 ± 58.7 mm/s (retrograde, from CA3a to CA3c). There was no significant difference between these two speeds (Figure 2(d), $P > 0.05$, paired t-test, $n = 5$).

3.3. Initiation and Propagation of Interictal and Ictal Discharges in Combined EC-Hippocampal Slices. The initiation and propagation of the two types of discharges in the combined EC-hippocampal slices were analyzed. Figure 3(b) shows the contour plot of averaged time delays of the FP (interictal discharge) relative to the signals of electrode number 85 on the representative combined slice in Figure 3(a). The interictal discharges initiated in CA3a and propagated bidirectionally to the CA1 (anterograde) and CA3c (retrograde). Figure 3(c) shows the contour plot of the averaged time delays of the FP (ictal discharge) relative to the signals of electrode number 25 on the representative combined slice in Figure 3(a). The ictal discharge was first observed in DG and propagated to CA3c, CA3b, CA3a, and CA1 along the stratum pyramidale. The data obtained from the other 4 slices showed similar discharge patterns.

From the above results, we found that the initiation site and propagation direction of the interictal and ictal discharges within the hippocampus were different. The interictal discharges initiated in CA3a and propagated bidirectionally to CA1 and CA3c, whereas the ictal discharge was first observed in the DG and propagated from the CA3c to CA1 along the stratum pyramidale. Furthermore, the propagation speeds of the interictal and ictal discharges in the hippocampal area of combined slices were analyzed. Statistical analysis showed that the propagation speeds of the interictal discharges were 175.8 ± 50.9 mm/s (anterograde, from CA3a to CA1) and 150.2 ± 43.7 mm/s (retrograde, from CA3a to CA3c), and the propagation speed of the ictal discharge was 208.6 ± 22.2 mm/s. There were no significant differences between the above three speeds (Figure 3(d), $P > 0.05$, ANOVA, $n = 5$).

3.4. Interactions between EC and CA1. To explore the characteristics of epileptiform discharges in EC, as well as the relationship between the epileptiform discharges in the EC and hippocampus, the EC, along with parts of CA1, was placed in the recording area in the following experiments (Figure 4(a)).

As shown in Figure 4(b), the continuous application of low-Mg^{2+} ACSF for 14.4 ± 2.1 min ($n = 5$) resulted in epileptiform discharges in EC, and the ictal and interictal discharges were recorded. The interictal discharges in EC occurred irregularly. They generally appeared before an ictal discharge, but, in some cases, they did not appear. Therefore, we did not analyze these interictal discharges in EC in the present study. The duration of the ictal discharges in the EC was 14.4 ± 4.9 s, which occurred at frequency of 0.006 ± 0.001 Hz ($n = 5$). The ictal discharges consisted of rhythmic oscillations of 7.35 ± 0.65 Hz ($n = 5$).

In the CA1 area of combined slices, the interictal and ictal discharges were recorded with the consistent application of low-Mg^{2+} ACSF, and the epileptiform discharge pattern was consistent with that of the combined slices, the hippocampal areas of which were placed in the recording area, as mentioned in Section 3.1. Statistical analysis showed that the interictal discharges appeared with a frequency of 0.21 ± 0.05 Hz, and the duration was 199.9 ± 37.1 ms ($n = 5$). The ictal discharges in the CA1 appeared with the frequency of 0.006 ± 0.001 Hz, which was characterized by rhythmic oscillations of 7.08 ± 2.01 Hz ($n = 5$). The duration of the ictal discharges was 15.5 ± 3.7 s ($n = 5$).

In the combined slices, the ictal discharges occurred in both EC and CA1. As shown in Figure 5(a), both EC and CA1 regions were covered by a few electrodes. We calculated the mean onset time of the electrodes within the two regions and then analyzed the time delay between the EC and CA1 (80.4 ± 18.0 ms, $n = 5$), which inferred that the ictal discharges in the combined slices were observed earlier in EC than in CA1 (Figure 5(b)).

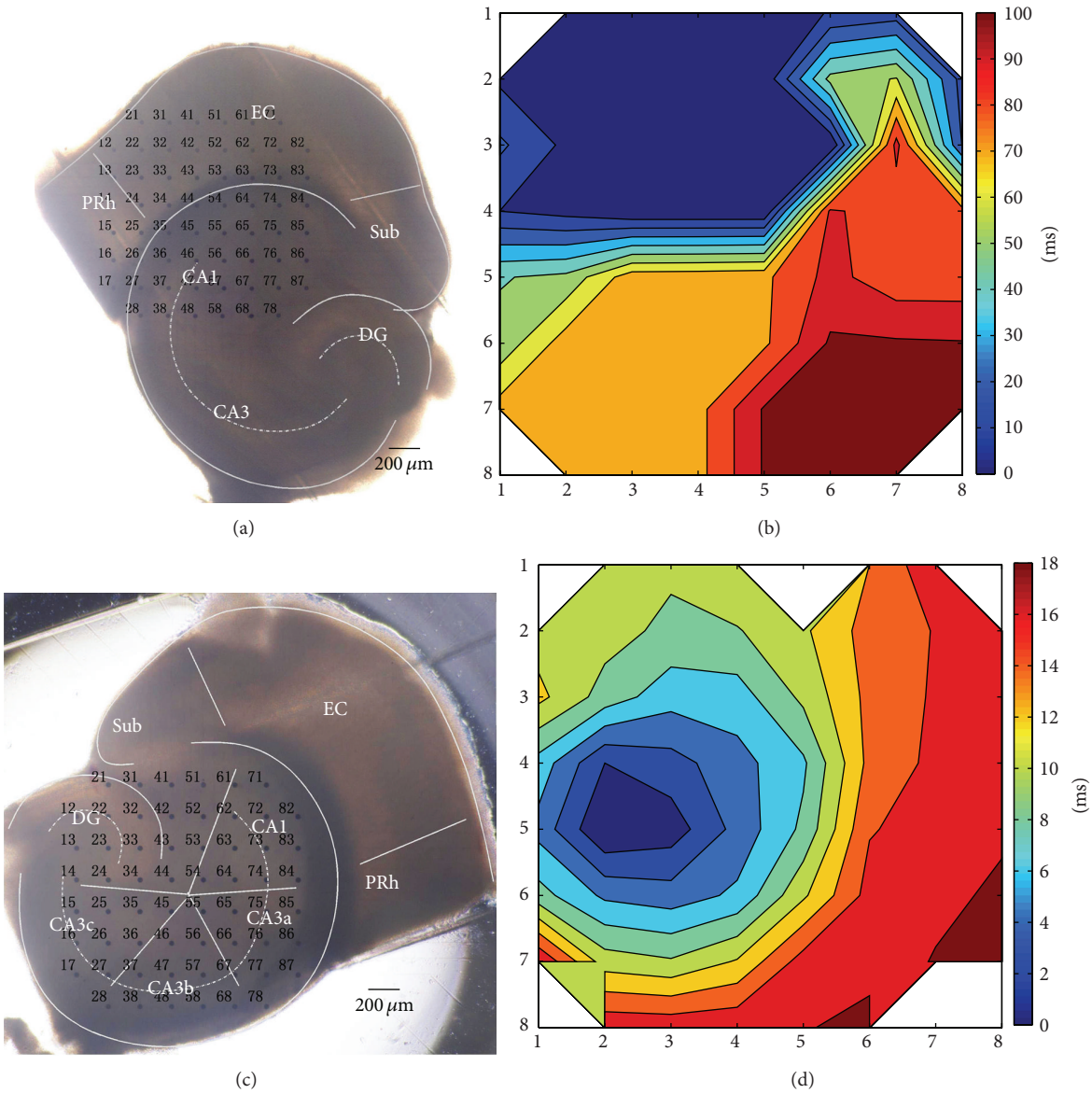

Figure 5: Propagation of ictal discharges in the combined EC-hippocampal slice. (a) An example of a combined slice mounted on MEA. (b) Contour plot of the ictal discharge time delays of the FP relative to signals of electrode number 51 in (a). (c) An example of a combined slice mounted on MEA. (d) Contour plot of the ictal discharge time delays of the FP relative to signals of electrode number 24 in (c).

Then, what was the exact propagation pathway of the ictal discharges in the hippocampus? We placed the hippocampal area of the slice in the recording area, to record the electrical activities in the hippocampus (Figure 5(c)). As shown in Figure 5(d), ictal discharge was first observed in the DG and then propagated to the CA3c, CA3b, CA3a, and CA1 areas along the stratum pyramidale. Therefore, we inferred that the EC produced ictal discharges, and the ictal discharges propagated via the DG, CA3c, CA3b, and CA3a to the CA1 area in the hippocampus.

3.5. Effects of VPA on the Interictal Discharges in Hippocampal Slices. VPA is one of the major antiepileptic drugs commonly used in clinical practice [16]. The pharmacological effects of VPA on epileptiform discharges were examined on the hippocampal slices. Application of 3 mM VPA reversibly suppressed the frequency of the interictal discharges (Figure 6(b)). The frequencies of the interictal discharges measured before, during, and after the application of VPA were 0.23 ± 0.05, 0.15 ± 0.03, and 0.26 ± 0.03 Hz, respectively. There were significant differences between the VPA group and the Control/Wash ($^{*}P < 0.05$, ANOVA, $n = 5$). Figure 6(c) shows the duration of the interictal discharges in different regions (CA3a, CA3b, CA3c, CA1, and DG) of the hippocampal slice before (Control), during (VPA), and after (Wash) the application of VPA. There were no significant differences between the duration of VPA group and the Control/Wash ($P > 0.05$, ANOVA, $n = 5$, Table 3).

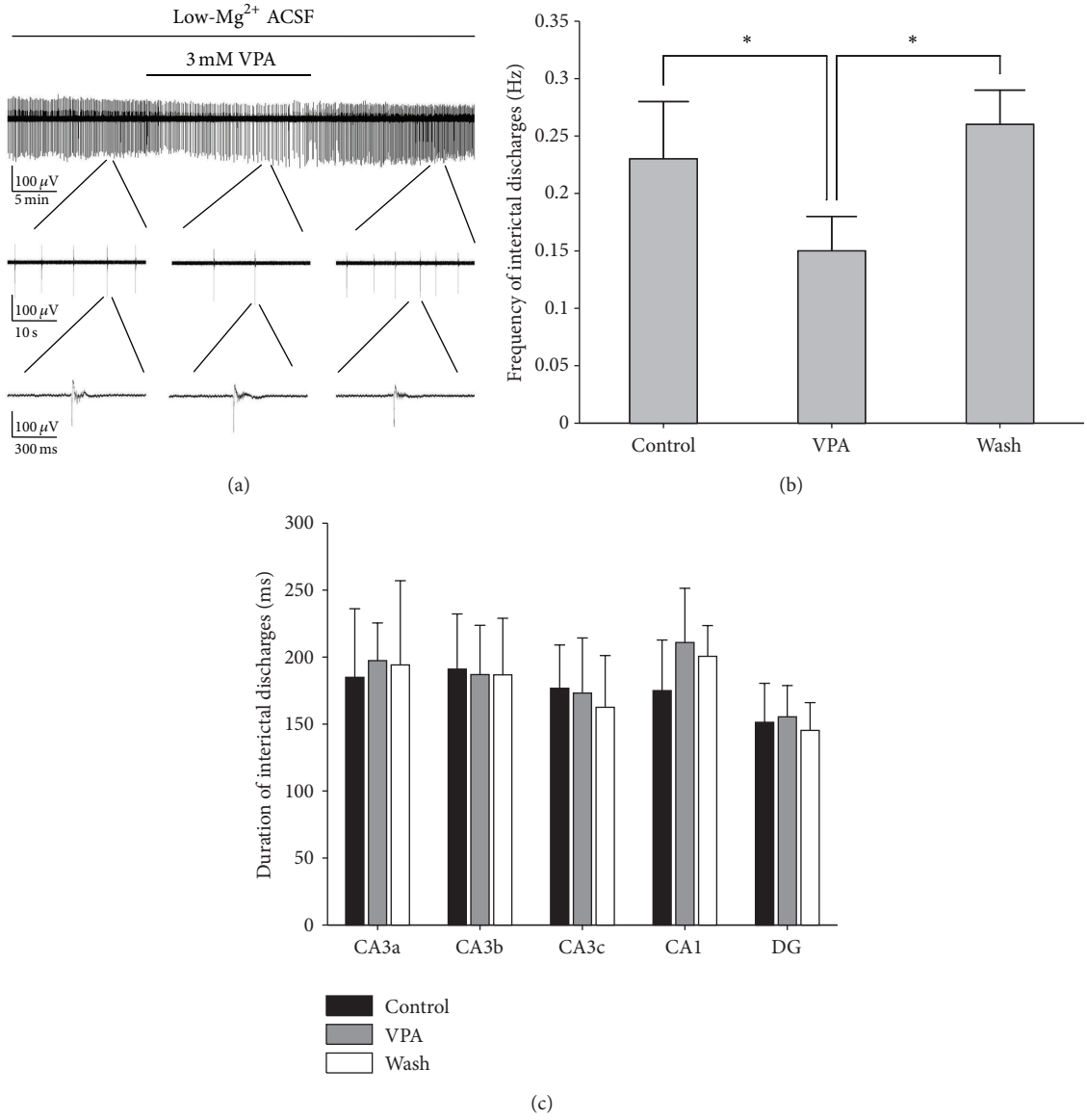

Figure 6: Effects of VPA on low-Mg^{2+}-induced interictal discharges in hippocampal slices. (a) Long-term display of the epileptiform discharges before, during, and after 3 mM VPA application, which represented the recordings of electrode number 87 in the CA3b region (Figure 1(a)). (b) Effects of VPA on interictal discharge frequency. There were significant differences between the VPA group and the Control/Wash ($^{*}P < 0.05$, ANOVA, $n = 5$). (c) Effects of VPA on interictal discharge duration. There were no significant differences between the VPA group and the Control/Wash ($P > 0.05$, ANOVA, $n = 5$).

Table 2: Statistical analysis results of VPA effects on the propagation speed of epileptiform discharges in the two slice models (mean ± SEM, $n = 5$).

Speed (mm/s)	HP (interictal)		EC-HP (interictal)		EC-HP (ictal)
	Anterograde	Retrograde	Anterograde	Retrograde	
Control	183.5 ± 64.9	182.7 ± 58.7	175.8 ± 50.9	150.2 ± 43.7	208.6 ± 22.2
VPA	150.1 ± 48.3	170.1 ± 37.6	159.4 ± 54.9	168.7 ± 54.6	/
Wash	158.3 ± 54.7	174.9 ± 49.1	172.4 ± 71.6	168.9 ± 22.5	196.0 ± 25.2

HP: hippocampal slice; EC-HP: combined EC-hippocampal slice.

Table 3: Statistical analysis results of VPA effects on the duration of interictal discharges in the two slice models (mean ± SEM, $n = 5$).

		Duration (ms)				
		CA3a	CA3b	CA3c	CA1	DG
HP	Control	184.9 ± 51.2	191.0 ± 41.2	176.7 ± 32.3	175.0 ± 37.7	151.3 ± 29.1
	VPA	197.4 ± 28.1	186.9 ± 36.8	173.1 ± 41.2	210.9 ± 40.5	155.4 ± 23.4
	Wash	194.1 ± 62.9	186.7 ± 42.3	162.5 ± 38.7	200.6 ± 22.9	145.3 ± 20.7
EC-HP	Control	218.1 ± 20.6	222.4 ± 16.6	222.6 ± 11.3	211.4 ± 63.5	184.4 ± 18.8
	VPA	215.6 ± 50.4	241.7 ± 32.0	210.5 ± 22.7	221.5 ± 67.6	185.2 ± 17.1
	Wash	222.8 ± 38.6	240.2 ± 14.8	200.7 ± 17.6	229.5 ± 57.3	168.5 ± 14.9

HP: hippocampal slice; EC-HP: combined EC-hippocampal slice.

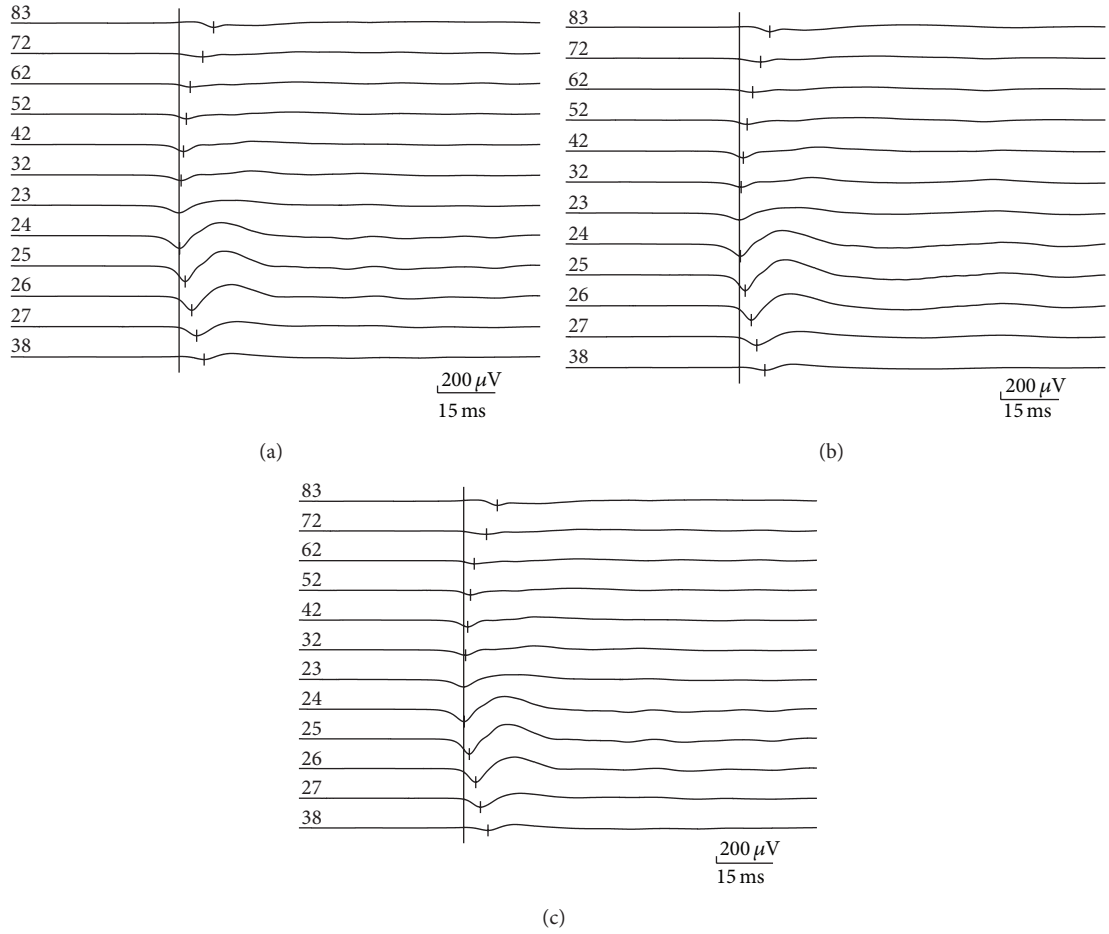

Figure 7: Effects of VPA on the initiation and propagation of the interictal discharges. The initiation and propagation of interictal discharge in an example of a hippocampal slice (Figure 2(a)) before (a), during (b), and after (c) application of 3 mM VPA.

We further investigated whether VPA changed the initiation and propagation of the interictal discharges in the hippocampal slices. Figure 7 shows the relative times of the first negative peak of FP before, during, and after application of 3 mM VPA. Before dosing, the interictal discharges initiated from CA3a and propagated bidirectionally to the CA1 (anterograde) and CA3c (retrograde) ($n = 5$). VPA did not significantly change the initiation site and the propagation direction. The statistical analysis of the results obtained from 5 slices showed that the anterograde speeds (from CA3a to CA1) and retrograde speeds (from CA3a to CA3c) in the hippocampal slices were not affected significantly during the VPA perfusion (Table 2).

Therefore, the inhibitory effect of VPA was mainly reducing the interictal discharge frequency, while the discharge duration, as well as the initiation site and propagation speed, was not affected significantly.

3.6. Effects of VPA on the Interictal and Ictal Discharges in Combined EC-Hippocampal Slices. Figure 8(a) shows the long-term display of low-Mg^{2+}-induced epileptiform discharges before, during, and after 3 mM VPA application,

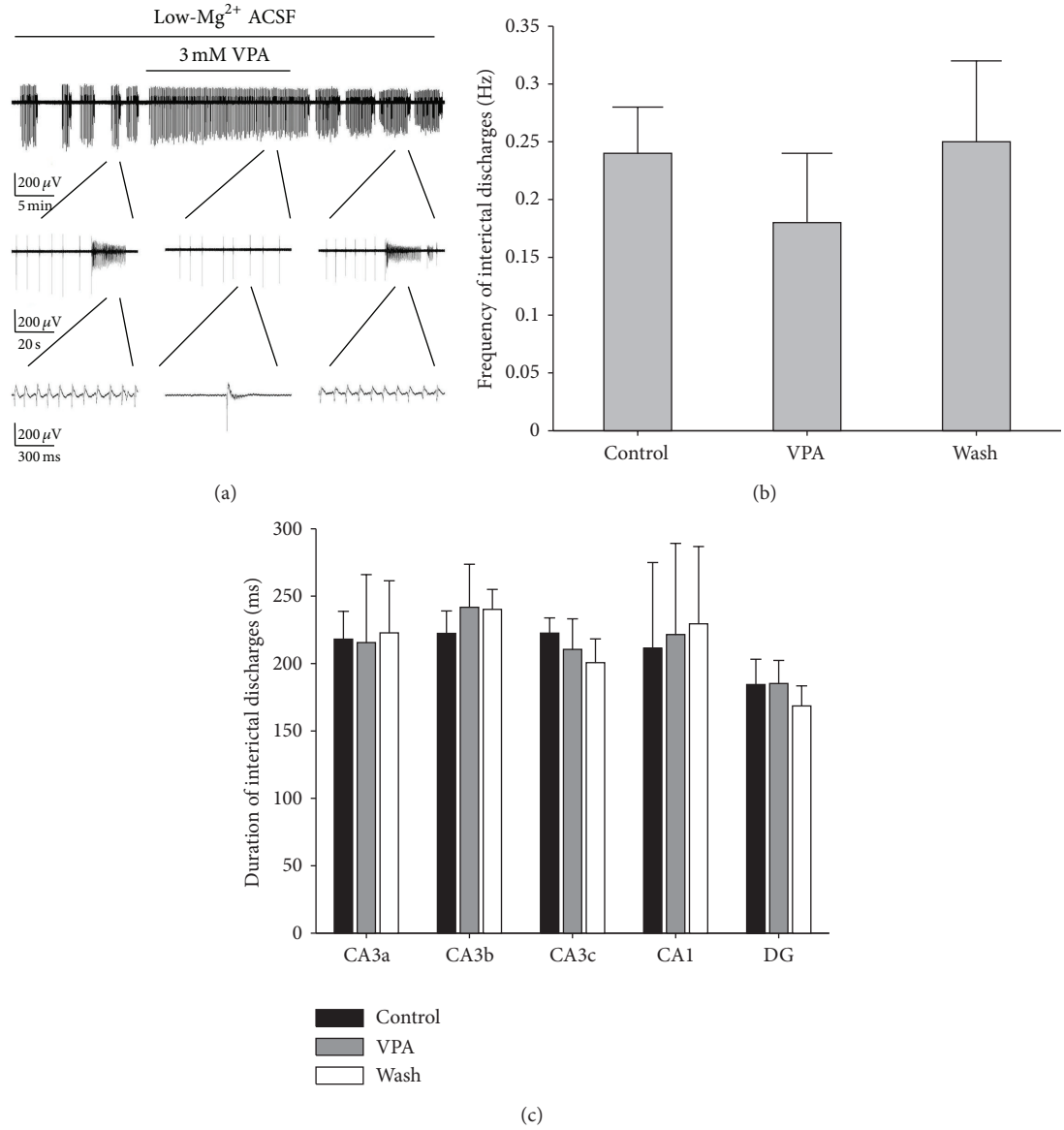

Figure 8: Effects of 3 mM VPA on low-Mg^{2+}-induced epileptiform discharges in the hippocampal area of combined slices. (a) Long-term display of low-Mg^{2+}-induced epileptiform discharges before, during, and after VPA application, which represents the recordings of electrode number 67 in the CA3b region (Figure 1(d)). (b) Effects of 3 mM VPA on interictal discharge frequency. There are no significant differences between the VPA group and the Control/Wash ($P > 0.05$, ANOVA, $n = 5$). (c) Effects of 3 mM VPA on interictal discharge duration. There are no significant differences between the VPA group and the Control/Wash ($P > 0.05$, ANOVA, $n = 5$).

which represents the recordings of one electrode (number 67) in CA3b region (Figure 1(d)) of one combined slice. The other 4 slices showed similar results. VPA reversibly changed the discharge pattern in the combined slices. The ictal discharges were completely blocked by VPA, whereas the interictal discharges were still preserved. The ictal discharges appeared again after the washout of VPA, with a frequency of 0.005 ± 0.002 Hz and consisted of a train of rhythmic oscillations of 7.72 ± 2.33 Hz ($n = 5$). The durations of the ictal discharges in different regions of the hippocampal area were 17.0 ± 7.2 (CA3a), 17.1 ± 7.3 (CA3b), 16.9 ± 7.2 (CA3c), 17.2 ± 7.3 (CA1), and 16.9 ± 7.3 (DG) s ($P > 0.05$, ANOVA, $n = 5$). The frequencies of interictal discharges measured before, during, and after application of VPA were 0.24 ± 0.04, 0.18 ± 0.06, and 0.25 ± 0.07 Hz, respectively. There were no significant differences between the VPA group and the Control/Wash ($P > 0.05$, ANOVA, $n = 5$, Figure 8(b)). Figure 8(c) shows the duration of the interictal discharges in different regions (CA3a, CA3b, CA3c, CA1, and the DG) of the combined slice before (Control), during (VPA), and after (Wash) application of VPA. There were no significant differences between the duration of VPA group and the Control/Wash ($P > 0.05$, ANOVA, $n = 5$, Table 3).

We further investigated the effects of VPA on the initiation and propagation of the interictal and ictal discharges in the combined slices. Before dosing (Control), the interictal

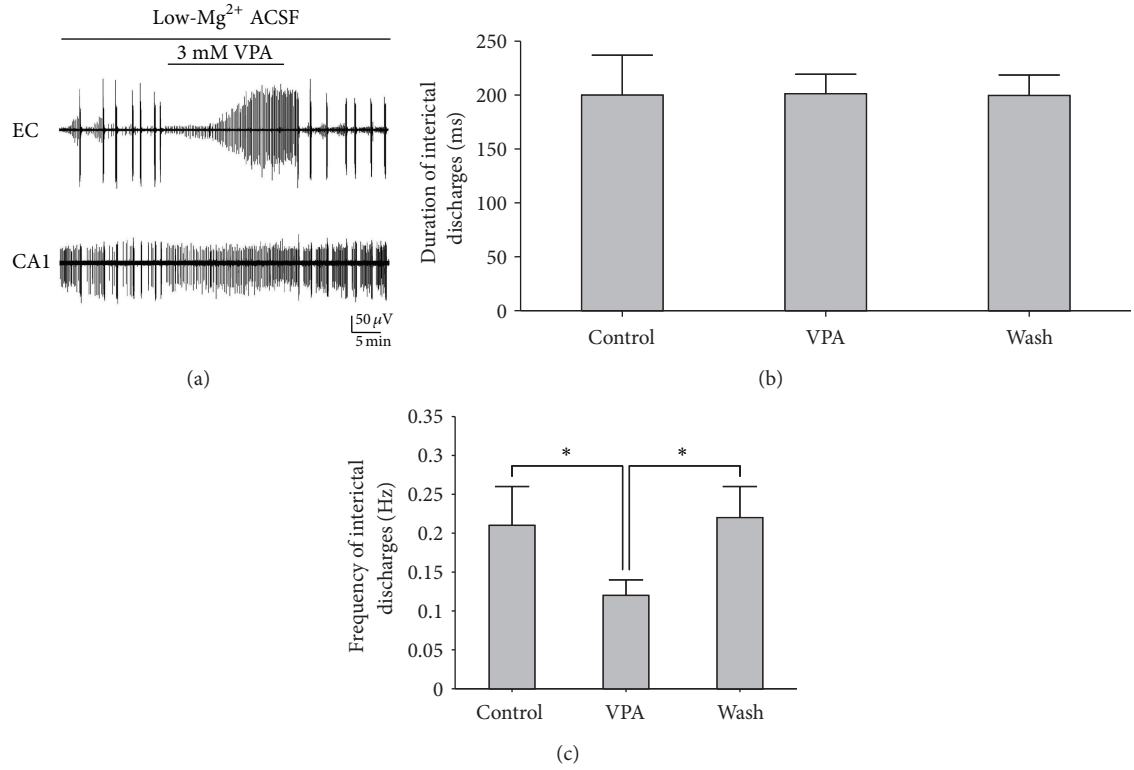

Figure 9: Effects of VPA on the epileptiform discharges in the EC and CA1 areas of the combined slices. (a) Long-term display of the effects of VPA (before, during, and after VPA application) on the discharge patterns in the EC and CA1 areas of an example of a combined slice. (b) The statistical analysis of VPA effects on duration of interictal discharges in CA1. There were no significant differences between the VPA group and the Control/Wash ($P > 0.05$, ANOVA, $n = 5$). (c) The statistical analysis of VPA effects on frequency of interictal discharges in the CA1. There were significant differences between the VPA group and the Control/Wash ($^*P < 0.05$, ANOVA, $n = 5$).

discharges initiated from the CA3a region and propagated bidirectionally to the CA1 (anterograde) region and the CA3c region (retrograde) ($n = 5$). VPA did not significantly change the initiation site and propagation direction. The anterograde (from CA3a to CA1) and retrograde speeds (from CA3a to CA3c) were not significantly affected during the VPA perfusion (Table 2). The ictal discharges were completely blocked by VPA. After the washout of VPA, the ictal discharges appeared again and propagated from the DG to CA3c, CA3b, CA3a, and CA1 ($n = 5$).

From the above results, we found that the inhibitory effect of VPA completely blocked the ictal discharges but had no significant effect on the interictal discharges.

3.7. Effects of VPA on the Epileptiform Discharges of EC/CA1. As an example shown in Figure 9(a), the application of 3 mM VPA reversibly suppressed the ictal discharges in EC, and the neural activity changed into interictal discharges. In CA1, on perfusion with VPA, the ictal discharges disappeared while the interictal discharges still existed; after the washout of VPA, the ictal discharges appeared again (Figure 9(a)). The data obtained from the other 4 slices showed that the discharge pattern in the EC/CA1 presented similar characteristics when perfused with VPA.

The interictal discharges observed in the EC during the perfusion with VPA lasted for 0.18~0.71 s (0.39 ± 0.22 s, $n = 5$), with a frequency of 0.03~0.13 Hz (0.08 ± 0.04 Hz, $n = 5$). Figure 9(b) shows the duration of the interictal discharges in the CA1 region of the combined slices before (Control), during (VPA), and after (Wash) the application of VPA. There were no significant differences between the duration of the VPA group and the Control/Wash ($P > 0.05$, ANOVA, $n = 5$). The interictal discharge frequency measured before, during, and after application of VPA was 0.21 ± 0.05, 0.12 ± 0.02, and 0.22 ± 0.04 Hz, respectively. There were significant differences between the VPA group and the Control/Wash ($^*P < 0.05$, ANOVA, $n = 5$, Figure 9(c)).

4. Discussion

4.1. Interictal and Ictal Discharges in the Hippocampal Slice and Combined EC-Hippocampal Slice. In the present study, the application of low-Mg^{2+} ACSF consistently induced interictal discharges in the hippocampal slices and the hippocampal area of combined slices. Our results showed that the hippocampal network itself could maintain stable interictal discharges with low-Mg^{2+} ACSF perfusion, and these interictal discharges initiated from CA3a and propagated bidirectionally to CA1 and CA3c, which was consistent with other studies [17]. Additionally, in previous studies carried in our laboratory, relevant results indicated that, in the hippocampal network, interictal discharges originated from

CA3a/b regions and propagated bidirectionally to the CA3c and CA1 regions, respectively [14, 15]. Some morphological data support such anterograde and retrograde propagation mechanisms. CA3 pyramidal cells send axons back to the hilar region, in which they excite mossy cells and hilar interneurons [18]. CA3 pyramidal cells also send axons to CA1 via Schaffer collaterals [19], and sectioning of the Schaffer collaterals between CA3 and CA1 abolished interictal discharges in CA1 by preventing their propagation from CA3 [20], which further confirmed that the hippocampal CA3 was sufficient to produce interictal discharges. Studies have shown that CA3 in the hippocampus is particularly prone to be pacemakers of epileptiform discharges owing to the presence of intrinsically burst-generating neurons and strong recurrent excitatory connections [21, 22].

By comparing the different discharge patterns in the hippocampal slices and the combined slices induced by low-Mg^{2+} ACSF, it is inferred that isolated hippocampal slices could only produce interictal discharges. The ictal discharges observed in the combined slices were closely related to the presence of the EC. The combined slice preparation preserved fiber connections between the hippocampus and the EC. In neuroanatomy, neurons in EC project to the DG via the perforant pathway, granule cells of the DG project to CA3 via mossy fiber projections, and pyramidal neurons in CA3 project to CA1 via Schaffer collaterals, which form the classic trisynaptic circuit [23]. A large number of in vitro studies have shown that the EC was the initiation site of ictal discharges, and they propagate from the EC to the hippocampus when the perforant path-DG route was well-preserved [13, 24]. In our experiments, we further analyzed the exact propagation pathways within the combined slices; it was not difficult to find out that ictal discharges initiated in EC, and, within the hippocampus, they first appeared in the DG and then propagated to the CA3c, CA3b, CA3a, and CA1 regions along the stratum pyramidale.

From the above description, it could be inferred that the initiation and propagation characteristics of the two types of epileptiform discharges were different. The interictal discharges initiated in the CA3a region and propagated bidirectionally to the CA1 and CA3c regions, whereas the ictal discharges initiated in the EC and propagated to DG, CA3c, CA3b, CA3a, and CA1 along the stratum pyramidale. The clinical seizure semiology is heavily influenced by the onset and spread of seizure activity, and suppressing the generation and propagation of epileptiform discharges is an effective way to control epilepsy. The role played by the EC as the generator of ictal discharges is in line with clinical evidence that dysfunction of the EC has been documented in patients with mTLE [25], and surgical removal of the EC is essential for achieving control of drug-resistant limbic seizures [26]. Therefore, a better understanding of the epileptiform discharge initiation and propagation mode may effectively guide clinical surgical planning.

4.2. Effects of VPA on the Interictal and Ictal Discharges. VPA is one of the major antiepileptic drugs, which is widely used in both generalized and partial epilepsies, bipolar disorders, and neuropathic pain and as a migraine prophylaxis [27]. Its antiepileptic effects are enhancing GABA-ergic inhibitory functions and reducing NMDA-ergic excitatory functions of the nervous system [16].

In the present study, we tested the inhibitory effects of VPA on different epileptiform discharges in the hippocampal slices and the combined EC-hippocampal slices. The results showed that VPA reversibly suppressed the frequency of the interictal discharges but did not change the initiation site and propagation characteristics, which initiated in the CA3a region and propagated bidirectionally to the CA1 and CA3c regions. VPA completely blocked the ictal discharges, which initiated in EC and propagated to DG, CA3c, CA3b, CA3a, and CA1 within the hippocampus. It could be inferred that ictal discharges were more sensitive than interictal discharges in response to VPA. Our results are in keeping with clinical evidence, which indicated that interictal activity was unaffected by antiepileptic drugs (AEDs) that were effective against seizures [28]. Studies have shown that the ability of AEDs to control in vitro epileptiform activities depended mainly on the characteristics of the epileptiform discharges, such as discharge duration. AEDs could abolish prolonged (>3 s) ictal discharges but failed to block shorter epileptiform events, which were reminiscent of interictal activities [29]. In the present study, ictal discharges (>10 s) were stably suppressed by 3 mM VPA, whereas interictal discharges still existed, even though the frequency was reduced. The intracellular correlate of the interictal discharge is an overt depolarization, which is called the paroxysmal depolarizing shift (PDS), and the transition from the generation of a single PDS during the interictal discharge to prolonged ictal discharge has been associated with the gradual loss of afterhyperpolarization and the progressive appearance of prolonged afterdepolarization [30]. Traub et al. have suggested that afterdepolarization is generated by NMDA receptors, which provides a prolonged depolarization of the dendrites of neuron cells, resulting in regenerative dendritic Na^+/Ca^{2+} spikes at 10–20 Hz, which then drive the repetitive bursts of action potentials at the soma [31]. VPA can suppress the depolarization responses mediated by glutamate receptors (NMDA receptors) [32, 33]; thus, it could block the low-Mg^{2+}-induced ictal discharges in our experiment.

5. Conclusions

In summary, our work analyzed whether the presence of the EC had an impact on the network status, as well as the resulting changes in the epileptiform discharge patterns. Low-Mg^{2+} ACSF induced interictal discharges in the adult mouse hippocampal slices and alternating interictal and ictal discharges in the combined EC-hippocampal slices. The initiation and propagation of the interictal and ictal discharges were different. The interictal discharges initiated in CA3a and propagated bidirectionally to CA1 and CA3c; the ictal discharges initiated in EC and propagated to DG, CA3c, CA3b, CA3a, and CA1 within the hippocampus. The ictal discharges were more sensitive than the interictal discharges in response to antiepileptic drug VPA.

However, in the in vitro experiments, many factors must be regarded with caution when extrapolating the mechanisms

of seizures, such as epileptic models, strain of rat, age of animals, thickness of the brain slices, and the other technical issues which would affect in vitro experiments. Owing to the complexity of the generation and propagation of epileptiform discharges, the network mechanisms of hippocampal slices and combined EC-hippocampal slices need to be studied further.

Conflict of Interests

The authors declare that there is no conflict of interests regarding the publication of this paper.

Acknowledgments

This work was supported by the Natural Science Foundation of Shanghai (11ZR1421800 and 12ZR1413800), the Shanghai Jiao Tong University Fund for Interdisciplinary Research for Medical Applications (YG2012ZD08), the Key Basic Research Project of Science and Technology Commission of Shanghai (13DJ1400303), and the Seed Fund of Ren Ji Hospital (RJZZ13-005).

References

[1] F. H. Lopes da Silva, M. P. Witter, P. H. Boeijinga, and A. H. M. Lohman, "Anatomic organization and physiology of the limbic cortex," *Physiological Reviews*, vol. 70, no. 2, pp. 453–511, 1990.

[2] O. Von Bohlen Und Halbach and D. Albrecht, "Reciprocal connections of the hippocampal area CA1, the lateral nucleus of the amygdala and cortical areas in a combined horizontal slice preparation," *Neuroscience Research*, vol. 44, no. 1, pp. 91–100, 2002.

[3] L. Tassi, A. Meroni, F. Deleo et al., "Temporal lobe epilepsy: neuropathological and clinical correlations in 243 surgically treated patients," *Epileptic Disorders*, vol. 11, no. 4, pp. 281–292, 2009.

[4] R. Miles and R. K. S. Wong, "Excitatory synaptic interactions between CA3 neurones in the guinea-pig hippocampus," *Journal of Physiology*, vol. 373, pp. 397–418, 1986.

[5] R. D. Traub, C. Borck, S. B. Colling, and J. G. R. Jefferys, "On the structure of ictal events in vitro," *Epilepsia*, vol. 37, no. 9, pp. 879–891, 1996.

[6] R. D. Traub, J. G. R. Jefferys, and M. A. Whittington, "Enhanced NMDA conductance can account for epileptiform activity induced by low Mg^{2+} in the rat hippocampal slice," *Journal of Physiology*, vol. 478, no. 3, pp. 379–393, 1994.

[7] M. de Curtis and G. Avanzini, "Interictal spikes in focal epileptogenesis," *Progress in Neurobiology*, vol. 63, no. 5, pp. 541–567, 2001.

[8] D. A. McCormick and D. Contreras, "On the cellular and network bases of epileptic seizures," *Annual Review of Physiology*, vol. 63, pp. 815–846, 2001.

[9] N. Bernasconi, A. Bernasconi, Z. Caramanos, S. B. Antel, F. Andermann, and D. L. Arnold, "Mesial temporal damage in temporal lobe epilepsy: a volumetric MRI study of the hippocampus, amygdala and parahippocampal region," *Brain*, vol. 126, no. 2, pp. 462–469, 2003.

[10] L. Bonilha, E. Kobayashi, C. Rorden, F. Cendes, and L. M. Li, "Medial temporal lobe atrophy in patients with refractory temporal lobe epilepsy," *Journal of Neurology, Neurosurgery and Psychiatry*, vol. 74, no. 12, pp. 1627–1630, 2003.

[11] E. H. Bertram, "Functional anatomy of spontaneous seizures in a rat model of limbic epilepsy," *Epilepsia*, vol. 38, no. 1, pp. 95–105, 1997.

[12] J. G. R. Jefferys, P. Jiruska, M. de Curtis et al., *Limbic Network Synchronization and Temporal Lobe Epilepsy*, 2012.

[13] M. Avoli, M. D'Antuono, J. Louvel et al., "Network and pharmacological mechanisms leading to epileptiform synchronization in the limbic system in vitro," *Progress in Neurobiology*, vol. 68, no. 3, pp. 167–201, 2002.

[14] X. W. Gong, F. Yang, J. S. Liu et al., "Investigation of the initiation site and propagation of epileptiform discharges in hippocampal slices using microelectrode array," *Progress in Biochemistry and Biophysics*, vol. 37, no. 11, pp. 1240–1247, 2010.

[15] J. S. Liu, X. W. Gong, H. Q. Gong et al., "Exploring spatiotemporal patterns of epileptiform discharge in hippocampal slice using multi-electrode arrays," *Sheng Li Xue Bao*, vol. 62, no. 2, pp. 163–170, 2010.

[16] W. Löscher, "Valproate: a reappraisal of its pharmacodynamic properties and mechanisms of action," *Progress in Neurobiology*, vol. 58, no. 1, pp. 31–59, 1999.

[17] V. I. Dzhala and K. J. Staley, "Transition from interictal to ictal activity in limbic networks in vitro," *Journal of Neuroscience*, vol. 23, no. 21, pp. 7873–7880, 2003.

[18] T. B. Kneisler and R. Dingledine, "Synaptic input from CA3 pyramidal cells to dentate basket cells in rat hippocampus," *Journal of Physiology*, vol. 487, part 1, pp. 125–146, 1995.

[19] X. G. Li, P. Somogyi, A. Ylinen, and G. Buzsaki, "The hippocampal CA3 network: an in vivo intracellular labeling study," *Journal of Comparative Neurology*, vol. 339, no. 2, pp. 181–208, 1994.

[20] J. S. Liu, J. B. Li, X. W. Gong et al., "Spatiotemporal dynamics of high-K(+)-induced epileptiform discharges in hippocampal slice and the effects of valproate," *Neuroscience Bulletin*, vol. 29, no. 1, pp. 28–36, 2013.

[21] L. Wittner and R. Miles, "Factors defining a pacemaker region for synchrony in the hippocampus," *Journal of Physiology*, vol. 584, no. 3, pp. 867–883, 2007.

[22] L. M. de la Prida, G. Huberfeld, I. Cohen, and R. Miles, "Threshold behavior in the initiation of hippocampal population bursts," *Neuron*, vol. 49, no. 1, pp. 131–142, 2006.

[23] P. Andersen, R. Morris, D. Amaral, T. Bliss, and J. O'Keefe, *The Hippocampus Book*, Oxford University, Oxford, UK, 2007.

[24] M. Barbarosie and M. Avoli, "CA3-driven hippocampal-entorhinal loop controls rather than sustains in vitro limbic seizures," *Journal of Neuroscience*, vol. 17, no. 23, pp. 9308–9314, 1997.

[25] S. S. Spencer and D. D. Spencer, "Entorhinal-hippocampal interactions in medial temporal lobe epilepsy," *Epilepsia*, vol. 35, no. 4, pp. 721–727, 1994.

[26] S. Goldring, I. Edwards, G. W. Harding, and K. L. Bernardo, "Results of anterior temporal lobectomy that spares the amygdala in patients with complex partial seizures," *Journal of Neurosurgery*, vol. 77, no. 2, pp. 185–193, 1992.

[27] C. U. Johannessen, "Mechanisms of action of valproate: a commentatory," *Neurochemistry International*, vol. 37, no. 2-3, pp. 103–110, 2000.

[28] J. Gotman and M. G. Marciani, "Electroencephalographic spiking activity, drug levels, and seizure occurrence in epileptic patients," *Annals of Neurology*, vol. 17, no. 6, pp. 597–603, 1985.

[29] M. D'Antuono, R. Köhling, S. Ricalzone, J. Gotman, G. Biagini, and M. Avoli, "Antiepileptic drugs abolish ictal but not interictal epileptiform discharges in vitro," *Epilepsia*, vol. 51, no. 3, pp. 423–431, 2010.

[30] G. F. Ayala, H. Matsumoto, and R. J. Gumnit, "Excitability changes and inhibitory mechanisms in neocortical neurons during seizures," *Journal of Neurophysiology*, vol. 33, no. 1, pp. 73–85, 1970.

[31] R. D. Traub, R. Miles, and J. G. R. Jefferys, "Synaptic and intrinsic conductances shape picrotoxin-induced synchronized after-discharges in the guinea-pig hippocampal slice," *Journal of Physiology*, vol. 461, pp. 525–547, 1993.

[32] P. W. Gean, C.-C. Huang, C.-R. Hung, and J.-J. Tsai, "Valproic acid suppresses the synaptic response mediated by the NMDA receptors in rat amygdalar slices," *Brain Research Bulletin*, vol. 33, no. 3, pp. 333–336, 1994.

[33] M. L. Zeise, S. Kasparow, and W. Zieglgansberger, "Valproate suppresses N-methyl-D-aspartate-evoked transient depolarizations in the rat neocortex in vitro," *Brain Research*, vol. 544, no. 2, pp. 345–348, 1991.

Hindawi Publishing Corporation
Neural Plasticity
Volume 2013, Article ID 424651, 6 pages
http://dx.doi.org/10.1155/2013/424651

Review Article

Methylcobalamin: A Potential Vitamin of Pain Killer

Ming Zhang, Wenjuan Han, Sanjue Hu, and Hui Xu

Institute of Neurosciences, The Fourth Military Medical University, Xi'an 710032, China

Correspondence should be addressed to Hui Xu; xubz@fmmu.edu.cn

Received 19 September 2013; Revised 6 November 2013; Accepted 12 November 2013

Academic Editor: Sheng Tian Li

Methylcobalamin (MeCbl), the activated form of vitamin B12, has been used to treat some nutritional diseases and other diseases in clinic, such as Alzheimer's disease and rheumatoid arthritis. As an auxiliary agent, it exerts neuronal protection by promoting regeneration of injured nerves and antagonizing glutamate-induced neurotoxicity. Recently several lines of evidence demonstrated that MeCbl may have potential analgesic effects in experimental and clinical studies. For example, MeCbl alleviated pain behaviors in diabetic neuropathy, low back pain and neuralgia. MeCbl improved nerve conduction, promoted the regeneration of injured nerves, and inhibited ectopic spontaneous discharges of injured primary sensory neurons. This review aims to summarize the analgesic effect and mechanisms of MeCbl at the present.

1. Introduction

Vitamin B12 had been usually treated as sport nutrition, and used to keep old people from getting anemic in past years. Vitamin B12 was regarded as painkilling vitamin in some countries from 1950. Recently studies have shown that vitamin B12 played a key role in the normal functioning of the brain and nervous system and the formation of blood. Vitamin B12 is normally involved in several metabolisms such as DNA synthesis and regulation, fatty acid synthesis, and energy production. Vitamin B12 has some analogs including cyanocobalamin (CNCbl), methylcobalamin (MeCbl), hydroxocobalamin (OHCbl), and adenosylcobalamin (AdoCbl). In mammalian cells, CNCbl and OHCbl are inactive forms and AdoCbl acts as a coenzyme of methylmalonyl Co-A mutase in mitochondria. However, vitamin B12 was not used directly in human body, and it should be translated into activating forms such as MeCbl or AdoCbl. MeCbl differs from vitamin B12 in that the cyanide is replaced by a methyl group (Figure 1) [1]. It is a coenzyme of methionine synthase, which is required for the formation of methionine from homocysteine in the methylation cycle which involves methylation of DNA or proteins [2–5]. Compared with other analogs, MeCbl is the most effective one in being uptaken by subcellular organelles of neurons. Therefore, MeCbl may provide better treatments for nervous disorders through effective systemic or local delivery.

As an auxiliary agent, MeCbl has been always used to treat many diseases, such as B12 deficiency and Alzheimer's disease syndromes [6, 7]. L-methylfolate, MeCbl, and N-acetylcysteine improved memory, emotional functions, and communication with other people among Alzheimer's patients [7, 8]. MeCbl also has neuronal protection including promoting injured nerve and axonal regeneration [9, 10] and confronting against glutamate-induced neurotoxicity [9, 11]. In addition, MeCbl improved nerve conduction in either patients of diabetic neuropathy [12–14] or streptozotocin-diabetic rats [15] and experimental acrylamide neuropathy [16]. MeCbl also improved visual function [17], rheumatoid arthritis [18], Bell's palsy, and sleep-wake rhythm disorder [19, 20]. Recently, MeCbl has been demonstrated to have potential analgesic effects on neuropathic pain in experimental and clinical studies.

2. The Analgesic Effect of MeCbl

MeCbl is one active form of vitamin B12 which can directly participate in homocysteine metabolism. More and more researches showed that MeCbl has beneficial effects on clinical and experimental peripheral neuropathy.

Table 1: The analgesic effect of MeCbl or combined use with other drugs on patients with diabetic neuropathic pain.

Effects of MeCbl	Indices	Measures of intervention	Reference
Alleviation of neuropathic pain symptoms; improved nerve conduction velocity	Pain scale scores of patients; measure of nerve conduction velocity	Oral administration of MeCbl for 3 months	Devathasan et al. [12]
Improved nerve conduction velocity	Measure of nerve conduction velocity	Intravenous administration of MeCbl	Ishihara et al. [14]
Improved the symptoms of paresthesia, burning pains, and heaviness; no effect on nerve conduction velocity	Pain symptoms; measure of nerve conduction velocity	Repeated intrathecal injection of MeCbl at a high dose of 2.5 mg/10 mL	Ide et al. [21]
Relieved spontaneous pain by 73%	Likert-type pain intensity scale; Patients' Global Impression of Change (PGIC) scale	Intramuscular injection of MeCbl for four weeks followed by oral administration of MeCbl for additional eight weeks	Li [22]
Relieved pain and paresthesia; improved motor and sensory nerve conduction velocity	Neurolgical disability score for the grades of pain and paresthesia	Intravenous injection of MeCbl for 6 weeks	Kuwabara et al. [13]
Reduced pain scores and good tolerance	Visual analog scale and chemical safety	Oral administration of immediate-release methylcobalamin and sustained-release pregabalin for 2 weeks.	Dongre and Swami [23]

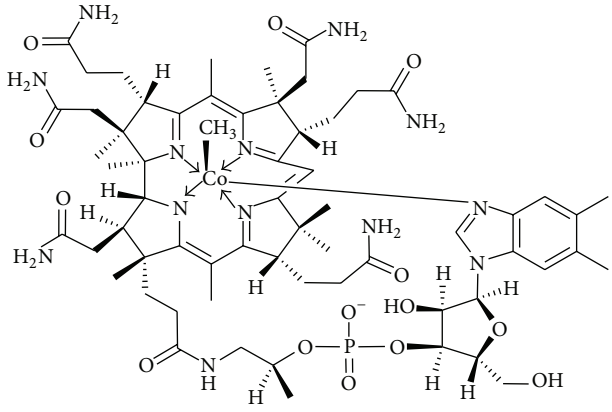

Figure 1: The chemical structure of MeCbl.

2.1. Diabetic Peripheral Neuropathic Pain. Clinical symptoms in legs, such as paresthesia, burning pains, and spontaneous pain, were ameliorated by MeCbl [21, 22] (Table 1). The effects of single use of MeCbl or combined use with other drugs were reviewed in diabetic neuropathy pain [12, 23] (Table 1). Clinical evidence proved that MeCbl had the capacity to inhibit the neuropathic pain associated with diabetic neuropathy.

The intensity of the pain is variable and may be described as a hot, burning, cold, aching, or itching sensation with, at times, increased skin sensitivity. In clinics, it is still a challenge to treat diabetic neuropathic pain. Carbamazepine and dolantin were not able to relieve these symptoms. Similarly, therapeutic effects of aldose reductase inhibitors and nimodipine were not encouraging in clinic as much as basic studies showed. Fortunately, MeCbl may bring a glimmer of hope to treat diabetic neuropathic pain.

2.2. Low Back Pain. Between 70 and 80% adults have experienced low back pain at some times in their life [24]. Back pain is one of the most common health complaints. But the causes are extensive, cancer, infection, inflammatory disorders, structural disorders of the spine itself, and disk herniation, are somewhat more common, and together account for back pain. It is supposed that the MeCbl is becoming a decent choice for the therapy to the chronic low back pain. Neurogenic claudication distance was improved significantly after the application of MeCbl [25] (Table 2). However Waikakul's research demonstrated that MeCbl was not good for pain on lumbar spinal stenosis [25]. In a trial, the analgesic effect of MeCbl has been investigated in nonspecific low back pain patients with intramuscular injection [26] (Table 2). The inconsistent effect of MeCbl might be due to different causes of lumbar spinal stenosis and nonspecific low back pain. Further studies are needed to determine the effect of MeCbl on low back pain.

2.3. Neck Pain. Chronic neck pain is becoming a common problem in the adult population, for the prevalence of 30%–50% in 12 months [27, 28]. It was shown that spontaneous pain, allodynia, and paresthesia of patients with neck pain were improved significantly in the MeCbl group, and with the increase of treatment time of MeCbl, the analgesic effect was more obvious [29] (Table 2).

2.4. Neuralgia

2.4.1. Subacute Herpetic Neuralgia. The treatment of MeCbl significantly reduced continuous pain, paroxysmal pain, and allodynia in the subacute herpetic neuralgia (SHN) patients [30] (Table 3). Thus, MeCbl may be an alternative candidate for treating SHN.

Table 2: The analgesic effects of MeCbl on low back pain and neck pain in clinical trials.

Effects of MeCbl	Indices	Measures of intervention	Reference
Relieved spontaneous pain, allodynia, and paresthesia.	Pain symptoms of patients with neck pain	Oral administration of MeCbl for 4 weeks	Hanai et al. [29]
Amelioration of neurogenic claudication distance; no effect on pain improvement and neurological signs	Pain symptoms; measure the neurogenic claudication distance of patients with degenerative lumbar spinal stenosis	Oral administration of MeCbl as an adjuvant medication for 6 months	W. Waikakul and S. Waikakul [25]
Reduced pain	Oswestry disability index questionnaire (ODI) and visual analogue scale (VAS) pain score of patients with nonspecific low back pain	Intramuscular injection of MeCbl for 2 weeks	Chiu et al. [26]

Table 3: The analgesic effect of MeCbl or combined with other agents on neuralgia.

Effects of MeCbl	Indices	Measures of intervention	Reference
Reduced or eliminated pain symptoms	Pain scales in patients with trigeminal neuralgia	Intravenous injection of MeCbl at a single dose of 0.5 mg	Teramoto [32]
Relieved overall pain, continuous spontaneous pain, paroxysmal pain, and allodynia	Likert-type pain intensity scale; Patients' Global Impression of Change (PGIC) scale	Local subcutaneous injection of MeCbl for 4 weeks	Xu et al. [30]
Lowered pain intensities; improved pain relief; reduced pain interference with quality of life	Numerical pain scale and brief pain inventory of glossopharyngeal neuralgia	Oral administration of gabapentin, tramadol, and MeCbl (0.5 mg)	Singh et al. [31]

2.4.2. Glossopharyngeal Neuralgia. Glossopharyngeal neuralgia (GPN) is a common facial neuralgia in the pain clinics. It was reported that the numerical pain scales were decreased substantially with the treatment of MeCbl combined with gabapentin and tramadol in GPN patients [31] (Table 3). And degree of interference in quality of life including mood, interpersonal relationship, and emotion was improved earlier [31].

2.4.3. Trigeminal Neuralgia. The pain of trigeminal neuralgia (TN) can be described as agonizing, paroxysmal and lancinating which may be activated by small activities such as chewing, speaking, and swallowing. A clinical trial proved that the pain of TN patients was alleviated greatly in the MeCbl group, and no recurrence of TN in pain symptoms was closed to 64% [32] (Table 3).

2.5. Neuropathic Pain of Animal Models. The coapplication of MeCbl and pioglitazone dramatically decreased allodynia and hyperalgesia in diabetic rats [33]. And the combined application of MeCbl and vitamin E alleviated thermal hyperalgesia in sciatic nerve crush injured rats [34]. Our recent work observed that tactile allodynia was markedly alleviated following a chronic treatment of MeCbl injection in chronic compression of dorsal root ganglion (CCD) rats (Figure 2).

3. Mechanisms Underlying the Analgesic of MeCbl

For many years, the B12 group of vitamins had been used to treat pain. In some countries, vitamin B12 was categorised as an analgesic drug. It was suggested that vitamin B12 may increase availability and effectiveness of noradrenaline and 5-hydroxytryptamine in the descending inhibitory nociceptive system [35]. MeCbl exerted therapeutic effects on neuropathic pain in diabetics, possibly through its neurosynthesis and neuroprotective actions [13, 36]. But the analgesic mechanisms of MeCbl remained elusive till now.

3.1. Improving Nerve Conduction Velocity. Previous studies showed that high doses of MeCbl improved nerve conduction in either patients with diabetic neuropathy [12–14], streptozotocin-diabetic rats [15], or experimental acrylamide neuropathy [16]. Morphological and histological evidence confirmed that a long-term administration of MeCbl promoted the synthesis and regeneration of myelin [37]. These morphological and histological recoveries of myelin may result in improving nerve conduction velocity and neuronal function in peripheral neuropathy.

3.2. Promoting the Regeneration of Injured Nerves. MeCbl advanced the incorporation of radioactive leucine into the protein fraction of the crushed sciatic nerve in vivo. As a result, the activity abilities of injured nerve were recovered [38]. In this study, the most terminals were degenerated in the mutant mouse, but the sprouts were more frequently observed in the MeCbl treatment group [39]. MeCbl had the ability to promote the injured nerves regeneration. In the experimental acrylamide neuropathy and sciatic nerve injury models, the number of regenerations of motor fibers showed significant increase with high-dose methylcobalamin [16]. And the combined use of L-methylfolate, MeCbl, and pyridoxal 5′-phosphate improved the calf muscle surface neural density [40].

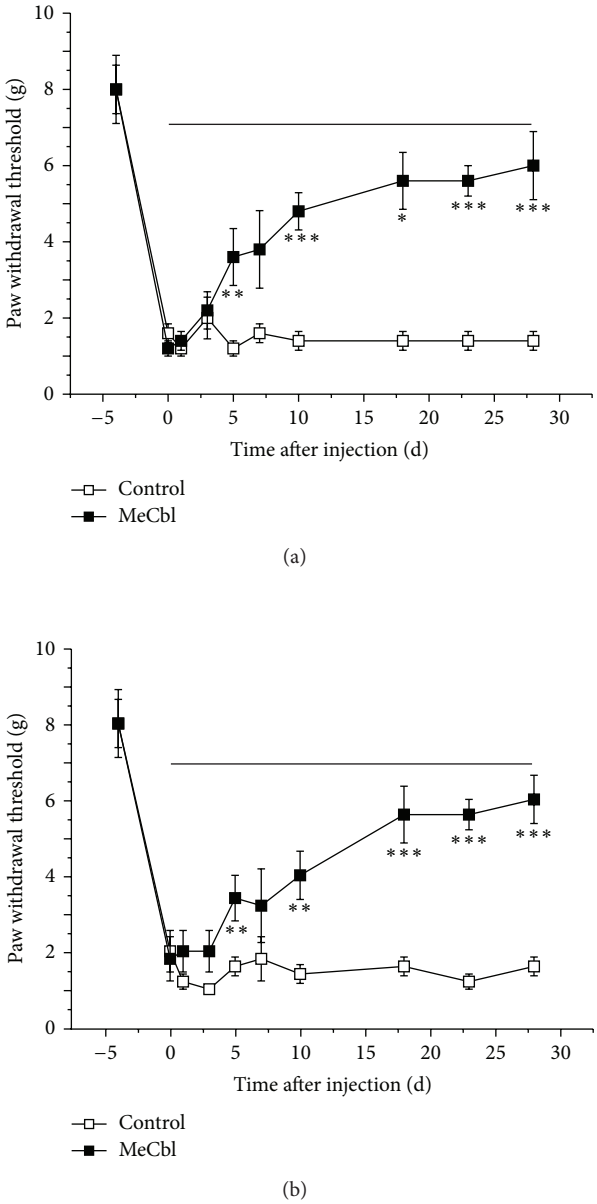

Figure 2: An anti-allodynic effect of MeCbl. MeCbl was successively received by intraperitoneal injections from the 3rd postoperative day (line segment). Bilateral paw withdrawal thresholds to von Frey filaments were decreased following a long-term application of MeCbl. (a) Ipsilateral side and (b) contralateral side. ($^{*}P < 0.05$, $^{**}P < 0.01$, $^{***}P < 0.001$, multivariate analysis of variance).

3.3. Inhibiting Ectopic Spontaneous Discharge. Ectopic spontaneous discharges are likely to initiate spontaneous pain, hyperalgesia, and allodynia [41–45]. It was reported that MeCbl suppressed the ectopic firing induced by chemical materials in the dog dorsal root [46]. Our recent work demonstrated that MeCbl markedly inhibited the ectopic spontaneous discharges of dorsal root ganglion neurons in CCD rats (Figure 3). Our results suggested that MeCbl exhibited its anti-allodynic effect by inhibiting peripheral pain signals.

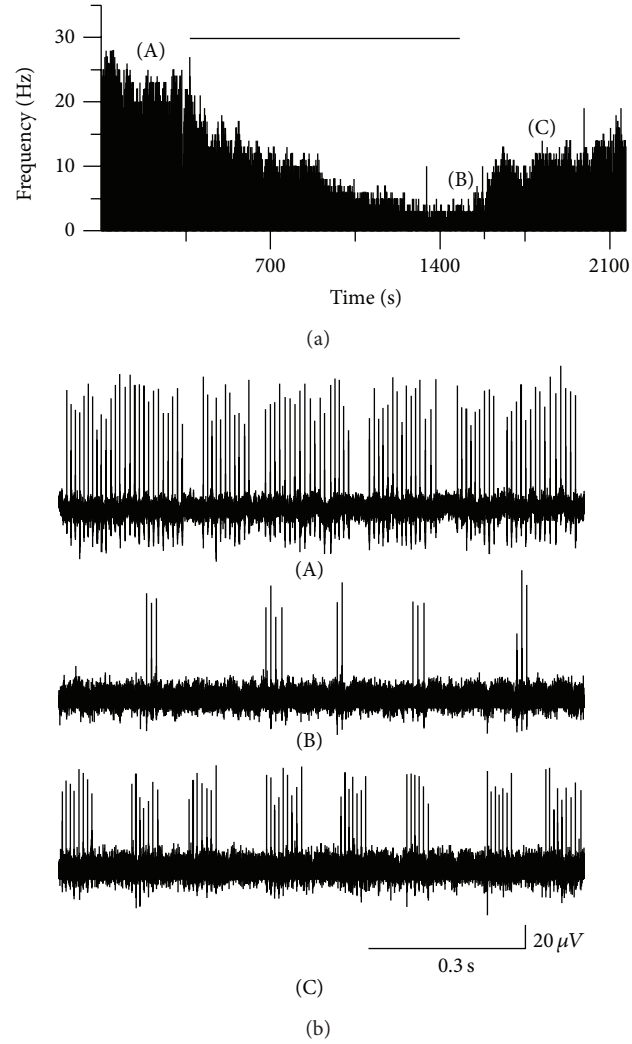

Figure 3: Inhibitory effect of MeCbl on ectopic spontaneous discharges of dorsal root. (a) Time histogram showing that local application of the MeCbl (300 μmol/L) decreased the basal firing rate of dorsal roots. (b) Three traces in right panel show firing patterns before (A), during (B), and wash out (C) the application of MeCbl.

4. Conclusions

MeCbl or its combined use with other agents has the potential analgesic effect in specific patients and animal models, for example, nonspecific low back pain; neck pain; diabetic neuropathic pain, subacute herpetic neuralgia, glossopharyngeal neuralgia, and trigeminal neuralgia. However, its mechanisms underlying the analgesic effect were poorly understood. On the basis of recent work, the possible mechanisms can be considered as follows. (1) MeCbl improved nerve conduction velocity; (2) MeCbl promoted injured nerve regeneration, recovering the neuromuscular functions in peripheral hyperalgesia and allodynia; and (3) MeCbl inhibited the ectopic spontaneous discharges from peripheral primary sensory neurons in neuropathic pain states. As a vitamin, MeCbl may be a potential candidate for treating peripheral neuropathy with good safety.

Acknowledgments

This work was supported by Grants from the National Natural Science Foundation of China (nos. 30870830 and 31371120 to Dr. Hui Xu) and the Ministry of Education Foundation for returned overseas students (HG3503 to Dr. Hui Xu).

References

[1] L. R. McDowell, *Vitamins in Animal and Human Nutrition*, John Wiley & Sons, 2008.

[2] R. Banerjee and S. W. Ragsdale, "The many faces of vitamin B12: catalysis by cobalamin-dependent enzymes," *Annual Review of Biochemistry*, vol. 72, pp. 209–247, 2003.

[3] S. K. Ghosh, N. Rawal, S. K. Syed, W. K. Paik, and S. D. Kim, "Enzymic methylation of myelin basic protein in myelin," *Biochemical Journal*, vol. 275, part 2, pp. 381–387, 1991.

[4] A. Pfohl-Leszkowicz, G. Keith, and G. Dirheimer, "Effect of cobalamin derivatives on in vitro enzymatic DNA methylation: methylcobalamin can act as a methyl donor," *Biochemistry*, vol. 30, no. 32, pp. 8045–8051, 1991.

[5] J. I. Toohey, "Vitamin B12 and methionine synthesis: a critical review. Is nature's most beautiful cofactor misunderstood?" *BioFactors*, vol. 26, no. 1, pp. 45–57, 2006.

[6] Y. Takahashi, S. Usui, and Y. Honda, "Effect of vitamin B12 (mecobalamin) on the circadian rhythm of rat behavior," *Clinical Neuropharmacology*, vol. 15, supplement 1, part A, pp. 46A–47A, 1992.

[7] A. McCaddon and P. R. Hudson, "L-methylfolate, methylcobalamin, and N-acetylcysteine in the treatment of Alzheimer's disease-related cognitive decline," *CNS Spectrums*, vol. 15, supplement 1, no. 1, pp. 2–6, 2010.

[8] T. Ikeda, K. Yamamoto, K. Takahashi et al., "Treatment of Alzheimer-type dementia with intravenous mecobalamin," *Clinical Therapeutics*, vol. 14, no. 3, pp. 426–437, 1992.

[9] M. Kikuchi, S. Kashii, Y. Honda, Y. Tamura, K. Kaneda, and A. Akaike, "Protective effects of methylcobalamin, a vitamin B12 analog, against glutamate-induced neurotoxicity in retinal cell culture," *Investigative Ophthalmology and Visual Science*, vol. 38, no. 5, pp. 848–854, 1997.

[10] X. Kong, X. Sun, and J. Zhang, "The protective role of Mecobalamin following optic nerve crush in adult rats," *Yan Ke Xue Bao*, vol. 20, no. 3, pp. 171–177, 2004.

[11] A. Akaike, Y. Tamura, Y. Sato, and T. Yokota, "Protective effects of a vitamin B12 analog, methylcobalamin, against glutamate cytotoxicity in cultured cortical neurons," *European Journal of Pharmacology*, vol. 241, no. 1, pp. 1–6, 1993.

[12] G. Devathasan, W. L. Teo, and A. Mylvaganam, "Methylcobalamin in chronic diabetic neuropathy. A double-blind clinical and electrophysiological study," *Clinical Trials Journal*, vol. 23, no. 2, pp. 130–140, 1986.

[13] S. Kuwabara, R. Nakazawa, N. Azuma et al., "Intravenous methylcobalamin treatment for uremic and diabetic neuropathy in chronic hemodialysis patients," *Internal Medicine*, vol. 38, no. 6, pp. 472–475, 1999.

[14] H. Ishihara, M. Yoneda, and W. Yamamoto, "Efficacy of intravenous administration of methycobalamin for diabetic peripheral neuropathy," *Med Consult N Remedies*, vol. 29, no. 1, pp. 1720–1725, 1992.

[15] M. Sonobe, H. Yasuda, I. Hatanaka et al., "Methylcobalamin improves nerve conduction in streptozotocin-diabetic rats without affecting sorbitol and myo-inositol contents of sciatic nerve," *Hormone and Metabolic Research*, vol. 20, no. 11, pp. 717–718, 1988.

[16] T. Watanabe, R. Kaji, N. Oka, W. Bara, and J. Kimura, "Ultra-high dose methylcobalamin promotes nerve regeneration in experimental acrylamide neuropathy," *Journal of the Neurological Sciences*, vol. 122, no. 2, pp. 140–143, 1994.

[17] T. Iwasaki and S. Kurimoto, "Effect of methylcobalamin in accommodative dysfunction of eye by visual load," *Journal of UOEH*, vol. 9, no. 2, pp. 127–132, 1987.

[18] M. Yamashiki, A. Nishimura, and Y. Kosaka, "Effects of methylcobalamin (vitamin B12) on in vitro cytokine production of peripheral blood mononuclear cells," *Journal of Clinical and Laboratory Immunology*, vol. 37, no. 4, pp. 173–182, 1992.

[19] M. Ikeda, M. Asai, T. Moriya, M. Sagara, S. Inoué, and S. Shibata, "Methylcobalamin amplifies melatonin-induced circadian phase shifts by facilitation of melatonin synthesis in the rat pineal gland," *Brain Research*, vol. 795, no. 1-2, pp. 98–104, 1998.

[20] K. Takahashi, M. Okawa, M. Matsumoto et al., "Double-blind test on the efficacy of methylcobalamin on sleep-wake rhythm disorders," *Psychiatry and Clinical Neurosciences*, vol. 53, no. 2, pp. 211–213, 1999.

[21] H. Ide, S. Fujiya, Y. Asanuma, M. Tsuji, H. Sakai, and Y. Agishi, "Clinical usefulness of intrathecal injection of methylcobalamin in patients with diabetic neuropathy," *Clinical Therapeutics*, vol. 9, no. 2, pp. 183–192, 1987.

[22] G. Li, "Effect of mecobalamin on diabetic neuropathies. Beijing Methycobal Clinical Trial Collaborative Group," *Zhonghua Nei Ke Za Zhi*, vol. 38, no. 1, pp. 14–17, 1999.

[23] Y. U. Dongre and O. C. Swami, "Sustained-release pregabalin with methylcobalamin in neuropathic pain: an Indian real-life experience," *International Journal of General Medicine*, vol. 6, pp. 413–417, 2013.

[24] J. W. Frymoyer, "Back pain and sciatica," *The New England Journal of Medicine*, vol. 318, no. 5, pp. 291–300, 1988.

[25] W. Waikakul and S. Waikakul, "Methylcobalamin as an adjuvant medication in conservative treatment of lumbar spinal stenosis," *Journal of the Medical Association of Thailand*, vol. 83, no. 8, pp. 825–831, 2000.

[26] C. K. Chiu, T. H. Low, Y. S. Tey, V. A. Singh, and H. K. Shong, "The efficacy and safety of intramuscular injections of methylcobalamin in patients with chronic nonspecific low back pain: a randomised controlled trial," *Singapore Medical Journal*, vol. 52, no. 12, pp. 868–873, 2011.

[27] L. Manchikanti, E. E. Dunbar, B. W. Wargo, R. V. Shah, R. Derby, and S. P. Cohen, "Systematic review of cervical discography as a diagnostic test for chronic spinal pain," *Pain Physician*, vol. 12, no. 2, pp. 305–321, 2009.

[28] L. Manchikanti, S. Abdi, S. Atluri et al., "American Society of Interventional Pain Physicians (ASIPP) guidelines for responsible opioid prescribing in chronic non-cancer pain: part I—evidence assessment," *Pain Physician*, vol. 15, no. 3, pp. S1–S65, 2012.

[29] I. Y. Hanai, M. K'Yatsume et al., "Clinical study of methylcobalamin on cervicales," *Drug Therapy*, vol. 13, no. 4, p. 29, 1980.

[30] G. Xu, Z. W. Lv, Y. Feng, W. Z. Tang, and G. X. Xu, "A single-center randomized controlled trial of local methylcobalamin injection for subacute herpetic neuralgia," *Pain Medicine*, vol. 14, no. 6, pp. 884–894, 2013.

[31] P. M. Singh, M. Dehran, V. K. Mohan, A. Trikha, and M. Kaur, "Analgesic efficacy and safety of medical therapy alone vs combined medical therapy and extraoral glossopharyngeal nerve

block in glossopharyngeal neuralgia," *Pain Medicine*, vol. 14, pp. 93–102, 2013.

[32] J. Teramoto, "Effects of Methylcobalamin on neuralgia," *Neurological Therapeutics*, vol. 1, no. 2, p. 315, 1984.

[33] A. S. Morani and S. L. Bodhankar, "Neuroprotecive effect of early treatment with pioglitasone and methylcobalamin in alloxan induced diabetes in rats," *Pharmacologyonline*, vol. 3, pp. 282–293, 2007.

[34] A. S. Morani and S. L. Bodhankar, "Early co-administration of vitamin E acetate and methylcobalamin improves thermal hyperalgesia and motor nerve conduction velocity following sciatic nerve crush injury in rats," *Pharmacological Reports*, vol. 62, no. 2, pp. 405–409, 2010.

[35] I. Jurna, "Analgesic and analgesia-potentiating action of B vitamins," *Schmerz*, vol. 12, no. 2, pp. 136–141, 1998.

[36] Y. Sun, M. S. Lai, and C. J. Lu, "Effectiveness of vitamin B12 on diabetic neuropathy: systematic review of clinical controlled trials," *Acta Neurologica Taiwanica*, vol. 14, no. 2, pp. 48–54, 2005.

[37] K. Okada, H. Tanaka, K. Temporin et al., "Methylcobalamin increases Erk1/2 and Akt activities through the methylation cycle and promotes nerve regeneration in a rat sciatic nerve injury model," *Experimental Neurology*, vol. 222, no. 2, pp. 191–203, 2010.

[38] K. Yamatsu, Y. Yamanishi, T. Kaneko, and I. Ohkawa, "Pharmacological studies on degeneration and regeneration of peripheral nerves. (II). Effects of methylcobalamin on mitosis of Schwann cells and incorporation of radio active leucine into protein fraction of crushed sciatic nerve in rats," *Folia Pharmacologica Japonica*, vol. 72, no. 2, pp. 269–278, 1976 (Japanese).

[39] K. Yamazaki, K. Oda, C. Endo, T. Kikuchi, and T. Wakabayashi, "Methylcobalamin (methyl-B12) promotes regeneration of motor nerve terminals degenerating in anterior gracile muscle of gracile axonal dystrophy (GAD) mutant mouse," *Neuroscience Letters*, vol. 170, no. 1, pp. 195–197, 1994.

[40] A. M. Jacobs and D. Cheng, "Management of diabetic small-fiber neuropathy with combination L-methylfolate, methylcobalamin, and pyridoxal 5′-phosphate," *Reviews in Neurological Diseases*, vol. 8, no. 1-2, pp. 39–47, 2011.

[41] W.-H. Xiao and G. J. Bennett, "Synthetic ω-conopeptides applied to the site of nerve injury suppress neuropathic pains in rats," *Journal of Pharmacology and Experimental Therapeutics*, vol. 274, no. 2, pp. 666–672, 1995.

[42] Y. W. Yoon, H. S. Na, and J. M. Chung, "Contributions of injured and intact afferents to neuropathic pain in an experimental rat model," *Pain*, vol. 64, no. 1, pp. 27–36, 1996.

[43] Y. S. Lyu, S. K. Park, K. Chung, and J. M. Chung, "Low dose of tetrodotoxin reduces neuropathic pain behaviors in an animal model," *Brain Research*, vol. 871, no. 1, pp. 98–103, 2000.

[44] J. Lai, M. S. Gold, C. S. Kim et al., "Inhibition of neuropathic pain by decreased expression of the tetrodotoxin-resistant sodium channel, NaV1.8," *Pain*, vol. 95, no. 1-2, pp. 143–152, 2002.

[45] S. R. Chaplan, H.-Q. Guo, D. H. Lee et al., "Neuronal hyperpolarization-activated pacemaker channels drive neuropathic pain," *The Journal of Neuroscience*, vol. 23, no. 4, pp. 1169–1178, 2003.

[46] I. T. Atsuta Y, O. Sugawara, T. Muramoto, T. Watakabe, and Y. Takemitsu, "The study of generating and suppressive factors of ectopic firing in the lumbar dorsal root using an in vitro model," *Rinsho Seikei Geka*, vol. 29, pp. 441–446, 1994.

Hindawi Publishing Corporation
Neural Plasticity
Volume 2013, Article ID 130642, 7 pages
http://dx.doi.org/10.1155/2013/130642

Clinical Study

A Simple Spatial Working Memory and Attention Test on Paired Symbols Shows Developmental Deficits in Schizophrenia Patients

Wei Song,[1] Kai Zhang,[2] Jinhua Sun,[3] Lina Ma,[1] Forrest Fabian Jesse,[1] Xiaochun Teng,[4] Ying Zhou,[1] Hechen Bao,[1] Shiqing Chen,[1] Shuai Wang,[1] Beimeng Yang,[1] Xixia Chu,[1] Wenhua Ding,[3] Yasong Du,[3] Zaohuo Cheng,[2] Bin Wu,[5] Shanguang Chen,[5] Guang He,[1] Lin He,[1,2] Xiaoping Chen,[5] and Weidong Li[1,2]

[1] *Bio-X Institutes, Key Laboratory for the Genetics of Developmental and Neuropsychiatric Disorders, Ministry of Education, Shanghai Jiao Tong University, Shanghai 200240, China*
[2] *Wuxi Mental Health Center, Wuxi 214151, China*
[3] *Shanghai Mental Health Center, Shanghai Jiao Tong University School of Medicine, Shanghai 200030, China*
[4] *Department of Endocrinology and Metabolism, The First Affliliated Hospital, China Medical University, Shenyang 110001, China*
[5] *National Key Laboratory of Human Factors Engineering, China Astronaut Research and Training Center, Beijing 100094, China*

Correspondence should be addressed to Xiaoping Chen; xpchen2009@163.com and Weidong Li; liwd@sjtu.edu.cn

Received 20 August 2013; Accepted 12 September 2013

Academic Editor: Yun Wang

People with neuropsychiatric disorders such as schizophrenia often display deficits in spatial working memory and attention. Evaluating working memory and attention in schizophrenia patients is usually based on traditional tasks and the interviewer's judgment. We developed a simple Spatial Working Memory and Attention Test on Paired Symbols (SWAPS). It takes only several minutes to complete, comprising 101 trials for each subject. In this study, we tested 72 schizophrenia patients and 188 healthy volunteers in China. In a healthy control group with ages ranging from 12 to 60, the efficiency score (accuracy divided by reaction time) reached a peak in the 20–27 age range and then declined with increasing age. Importantly, schizophrenia patients failed to display this developmental trend in the same age range and adults had significant deficits compared to the control group. Our data suggests that this simple Spatial Working Memory and Attention Test on Paired Symbols can be a useful tool for studies of spatial working memory and attention in neuropsychiatric disorders.

1. Introduction

Studies have shown working memory [1–3] and attention [4, 5] deficits in individuals with schizophrenia. Working memory is a temporary storage facility that lasts for only seconds, accessible to conscious attention. It is fundamentally important as it underpins capacity for complex thought [6]. The visuospatial sketchpad theory proposes that the visual and spatial impression of a limited number of objects is temporarily stored, manipulated, and allows subselections to be created through the focus of attention [7]. Attention is the cognitive process of selecting some elements, from an environment (real or otherwise) while ignoring other elements and it is a precondition for exercising working memory. It determines what enters into working memory, and shifting attention can disrupt the contents of working memory. When presented with a shorter stimulus, the stimuli's entrance into working memory may be less complete [8].

Currently, tests for working memory include the n-back task [9] which is a continuous performance task commonly used to measure a part of working memory [10], the Sternberg Item Recognition Paradigm [11, 12], the Visual Patterns Test

[13], the Spatial Working Memory task (SPWM) [14], and others [15–18]. Existing tests for attention include the Continuous Performance Test (CPT) [19, 20] and the Sustained Attention Test [21]. Some existing tests require extended periods of time to complete or require verbal knowledge, which may impede the subject's ability to complete the test due to age or education. With the objective of creating a simple test of working memory and attention for use in treatment of neuropsychiatric disorders, we developed a Spatial Working Memory and Attention Test on Paired Symbols (SWAPS).

2. Materials and Methods

2.1. Subjects. The study tested 188 healthy volunteers from 12 to 60 years old. They were divided into 5 groups by age: a 10s age group ranging from 12 to 16 years old (14.2 ± 0.1, $n = 43$ (male = 23, female = 20)); 20s age group ranging from 20 to 27 years old (23.8 ± 0.2, $n = 37$ (male = 18, female = 19)); 30s age group ranging from 30 to 39 years old (33.7 ± 0.5, $n = 41$ (male = 21, female = 20)); 40s age group ranging from 40 to 49 years old, (45.5 ± 0.5, $n = 35$ (male = 17, female = 18)); 50s age group ranging from 50 to 60 years old (53.5 ± 0.5, $n = 32$ (male = 17, female = 15)). All schizophrenia patients were recruited from Shanghai Mental Health Center and Wuxi Mental Health Center. They had been diagnosed with schizophrenia according to the criteria set forth by the DSM-IV-TR publication, with the following exclusion criteria: alcohol or drug abuse or dependence, major medical or neurological illness, or noticeable lower intelligence as determined by at least two professional psychiatrists. A total of 72 schizophrenia patients currently undergoing treatment in these hospitals, ages 13 to 40, were divided into 3 groups according to age: a SZ10s group ranging from 13 to 19 years old (15.8 ± 0.2, $n = 24$ (male = 11, female = 13)); SZ20s group ranging from 20 to 29 years old (25.0 ± 0.5, $n = 24$ (male = 12, female = 12)); SZ30s group ranging from 30 to 40 years old (35.9 ± 0.6, $n = 24$ (male = 12, female = 12)). All subjects participated WITH their own free will and with informed consent. Subjects under age 18 also participated with parental consent. The study was approved by the Bio-Ethics Board of the Bio-X Institutes, Shanghai Jiao Tong University.

2.2. SWAPS Test. The novel Spatial Working Memory and Attention Test on Paired Symbols (SWAPS) was inspired by the Chinese historical *Jiugongtu* (see Supplementary Figure 3 in Supplemetary Materials available online at http://dx.doi.org/10.1155/2013/130642) [22, 23]. *Jiugongtu* is well known in Chinese culture, making it a familiar spatial map for subjects. The SWAPS test uses the nine spaced *Jiugongtu* grid as a background but filled with paired symbols. SWAPS is a computer-administered test developed in the C# programming language. The test is composed of a visual two-dimensional grid plane presented to the subjects on a computer screen (Figure 1). The grid is segmented into nine regular squares, each of which might contain a symbol. There are 4 possible paired symbols that can be displayed in the grid. The subjects have been instructed to use a pointing device to select the grid location of the matching and missing symbol on the screen. The test randomly presents symbol pairs in different locations on the grid, for a learning time duration (Lt) of 0.5 seconds or 2 seconds (Figure 1(a)). The test then presents an empty screen for a duration of time which we call the delay span (D), which is 0.5 seconds or 2 seconds (Figure 1(b)), and then randomly presents only one of the symbols. The participants are expected to select the location of the missing one of the paired symbols (Figure 1(c)) or an "uncertain" button beside the grid. As the learning time Lt and delay span D can be 0.5 seconds or 2 seconds, this allows for 4 possible combinations. We record the reaction time of the participants beginning from when the symbol is presented during the memory recall phase (Figure 1(c)) and ending when the subject makes a choice with the pointing device. The percentage of correct choices (C) divided by reaction time (R) produces a score, calculated as the efficiency score (C/R). We also show the percentage of correct choices and reaction time results separately in Supplementary Figures 4–8 and Supplementary Tables 3–5. There are 4 levels of difficulty, which we call loads (1 to 4), where the load is the quantity of paired symbols presented on one grid. Load one has a single pair of symbols, load two has 2 symbol pairs, load three has 3 and load four has 4 (Figures 1(e)–1(h)).

2.3. The Testing Procedure. Subjects are first given an introduction to the test. An identifying number, their gender and their age are then recorded. The SWAPS test consists of 101 trials with the test lasting 7 minutes on average. The first 5 trials are all load one difficulty and are not used in the result. They exist to provide a short practice exercise for the subject prior to the administration of the real test. The next 96 trials are randomly arranged, consisting of 32 trials of all combinations of Lt (0.5 seconds or 2 seconds) and D (0.5 seconds and 2 seconds) per load, for difficulty loads two through four.

2.4. Statistical Analysis. All data were analyzed with Statview software. Results are expressed as mean ± SEM. All error bars represent standard error of the mean (SEM). ANOVA analyses and Fisher's PLSD [24] were used for statistical comparisons between groups as described in the results section or in figure legends. $P < 0.05$ indicates significant difference between groups.

3. Results

3.1. SWAPS Tests Showed a Developmental Peak of Spatial Working Memory and Attention in the 20–27 Age Range in the Healthy Control Group. We first used SWAPS to test normal healthy people. The control group was composed of 188 healthy volunteers from 12 to 60 years old. Age may be a factor influencing both accuracy and reaction time in completing SWAPS [25, 26], so participants were divided into groups by age as 10s, 20s, 30s, 40s, and 50s. Compared to the 10s age group, the 20s group showed significantly better performance in almost all combinations of load level, learning time and delay span (Figure 2, Supplementary Table 1). SWAPS showed the development of spatial working memory

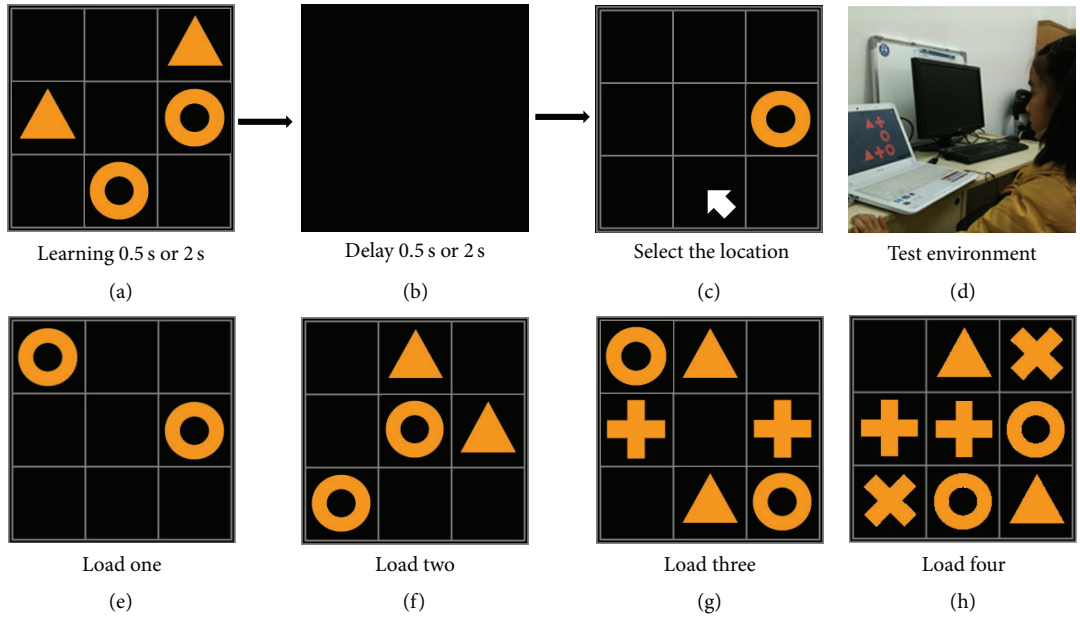

Figure 1: Example of a single trial and examples of 4 loads of difficulty. An example of a single trial ((a), (b), and (c)). The stimulus phase with learning time (Lt) of either 2 seconds or 0.5 seconds (a), the symbols then disappear during delay span (*D*) for either 2 seconds or 0.5 seconds (b). After the delay span, the participant is prompted to select the location of the missing part of the symbol pair with the pointing device (c). (d) shows a participant taking the test. (e)–(h) show examples of the 4 loads of difficulty. Difficulty load 1 is not used in results and exists only to provide a short practice exercise for the subject prior to the administration of the real test. Loads 2 to 4 are used to produce test results, and illustrate the number of paired symbols in each load.

and attention reached a peak in the 20s group and then declined with increasing age. With a shorter learning time of 0.5 seconds which requires closer attention, the result showed significantly better performance in the 20s age group (Figures 2(a) and 2(b)). Detailed statistical results are shown in Supplementary Table 1.

3.2. Schizophrenia Patients Showed No SWAPS Improvement with Age When Comparing SZ10s to SZ20s. Schizophrenia patients were then tested with SWAPS. Seventy-two schizophrenia patients 13 to 40 years old were divided into 3 groups according to age: SZ10s, SZ20s and SZ30s. Interestingly, schizophrenia patients failed to display maturation of spatial working memory and attention capacity in ages 20–29 compared to ages 13–19 (Figures 2(e)–2(h), Supplementary Table 1).

3.3. Schizophrenia Patients Displayed SWAPS Score Deficits in Adults but Not in Adolescents. Compared to the 20s control group, SZ20s schizophrenia patients displayed a significantly lower test score (Figure 3). The SZ30s group in schizophrenia patients also showed significant deficits in test scores under all combinations compared to the 30s control group (Supplementary Figure 2). However, SZ10s schizophrenia patients did not show a difference (under all test conditions) compared to the 10s control group (Supplementary Figure 1). Detailed comparative results of schizophrenia and control groups are shown in Supplementary Tables 1 and 2.

4. Discussion

Difficulty loads of symbols, stimulus duration (learning time), and delay span are important for measuring working memory and attention. In order to guide the development of SWAPS, we conducted a preliminary study in 31 healthy subjects with ages ranging from 18 to 24 years old. The preliminary study had random learning times (0–5 seconds) and delay spans (0–5 seconds) (Supplementary Figure 9). The first versions of the test needed to determine the most appropriate Lt and *D* to show differentiation between loads and we use correct responses to analyze because it is more sensitive within age groups. Supplementary Figure 9(a) shows the variation of correct responses through difficulty loads two, three and four, presenting evidence that the design of the test can discriminate between difficulty loads. We found that *D* of up to 2 seconds had the same results as *D* of up to 5 seconds (Supplementary Figure 9(b)). The added time did not increase accuracy in responses, and so we shortened *D* in our test design to 2 seconds. We found that Lt shows the largest differences between loads when Lt has a value of between 0 and 2 seconds, and when Lt exceeds 2 seconds the test results for all loads of difficulty begin to converge toward a higher percentage of correct response (Supplementary Figure 9(c)). Learning times of 0–2 seconds and delay spans below 2 seconds showed good results and could shorten the testing time. We use values of 0.5 seconds and 2 seconds [27, 28] for both learning time and delay span.

In the SWAPS test, observers focus their attention on the locations (spatial locations) and features (different symbols).

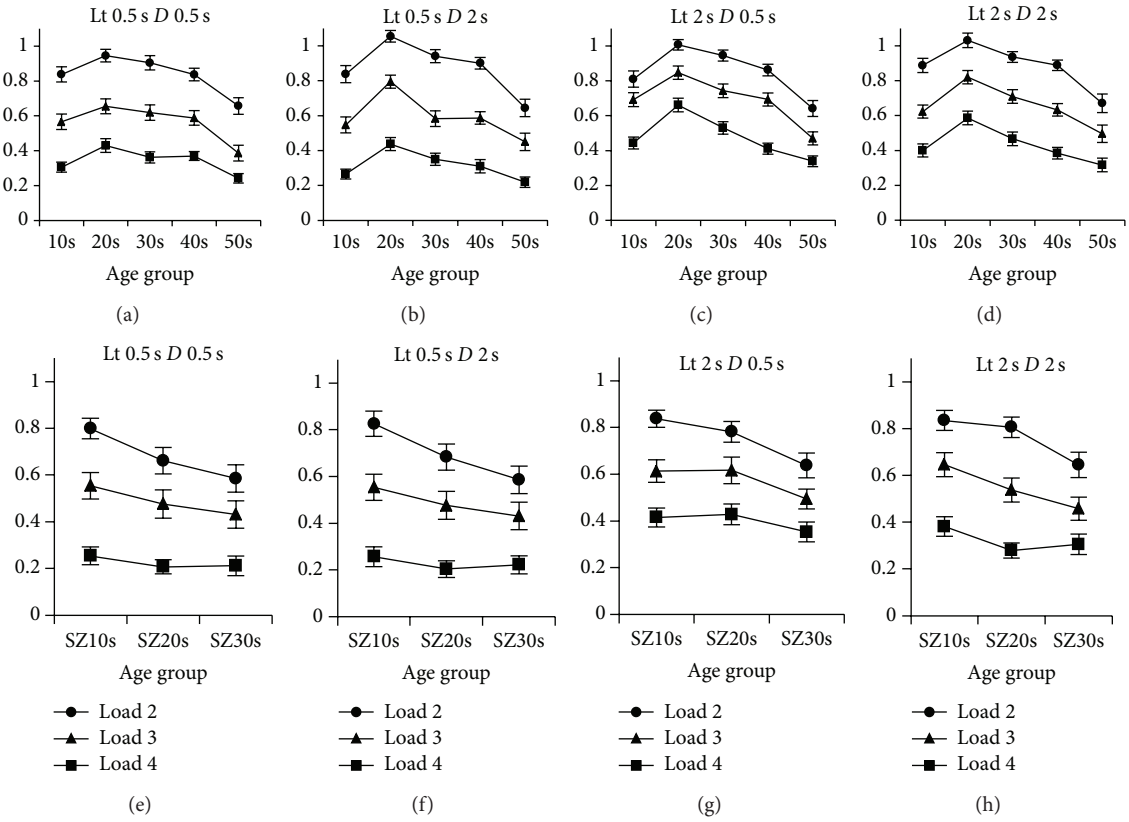

Figure 2: Comparison of schizophrenic and healthy groups. SWAPS showed the highest score in the age 20–27 healthy control group (group 20s) but not in schizophrenia patients ages 20–29 (group SZ20s). (a–d) show the accuracy per second in 5 healthy control age groups (10s, 20s, 30s, 40s, and 50s), at different difficulty loads and with different combinations of learning time and delay span. (e–h) show the accuracy per second for 3 age groups in schizophrenia patients (SZ10s, SZ20s, SZ30s), under the same learning time and delay span conditions as the healthy control groups. Lt: learning time (0.5 seconds or 2 seconds); *D*: delay span (0.5 seconds or 2 seconds).

A shorter learning time Lt of 0.5 seconds requires better attention. A longer delay *D* of 2 seconds requires better working memory, In the most challenging condition of Lt = 0.5 seconds, *D* = 2 seconds and load 4, the healthy control showed the lowest score, and 20 s control group showed peak score compared to other age groups. In contrast, the SZ20s schizophrenia group did not show the peak score when compared to the SZ10s and SZ30s groups.

Both accuracy and reaction time are important variables which reflect the memory and attention capacity of subjects who take the SWAPS test. We used an efficiency score (percentage of correct choice divided by average reaction time) [29] to display a simple result for working memory and attention. The schizophrenia group SZ20s showed more deficits in accuracy than reaction time compared to the 20s twenties age range control group (Supplementary Figure 7), and the SZ30s schizophrenia group showed greater deficits in reaction time than accuracy compared to the 30s thirties age range control group in thirties (Supplementary Figure 8). Using the efficiency score, results revealed clearer deficits in schizophrenia patients compared to their counterparts in the twenties and thirties age range. In other studies an inverse efficiency score is sometimes used [30]; however, because in some circumstances the *Q* score result of the SWAPS test can be 0, we use an efficiency score to quantify results.

Cognitive abilities rise steeply from infancy to young adulthood and then are either maintained or decline to old age [31]. Brain activity studies have shown that healthy young adults develop better neurocognitive ability including working memory and attention [32, 33]. The SWAPS test has shown a plausible developmental pattern in healthy controls especially in difficulty load three and four, which developed well in the 20s group from the 10s group and then decline with increasing age. The more interesting finding in this study is that schizophrenia patients showed no working memory and attention improvement with age when comparing SZ10s to SZ20s. Is it because the developmental process of people with schizophrenia is halted that the spatial working memory and attention of the patients becomes worse in their twenties? To discover the answer to this, we may need to test more finely subdivided age groups both in control and in schizophrenia patients. More importantly, we may need to do a longitudinal study of SWAP tests from childhood to early adulthood for patients [34, 35].

A limitation of this study is that the schizophrenic group was comprised of patients who were diagnosed as

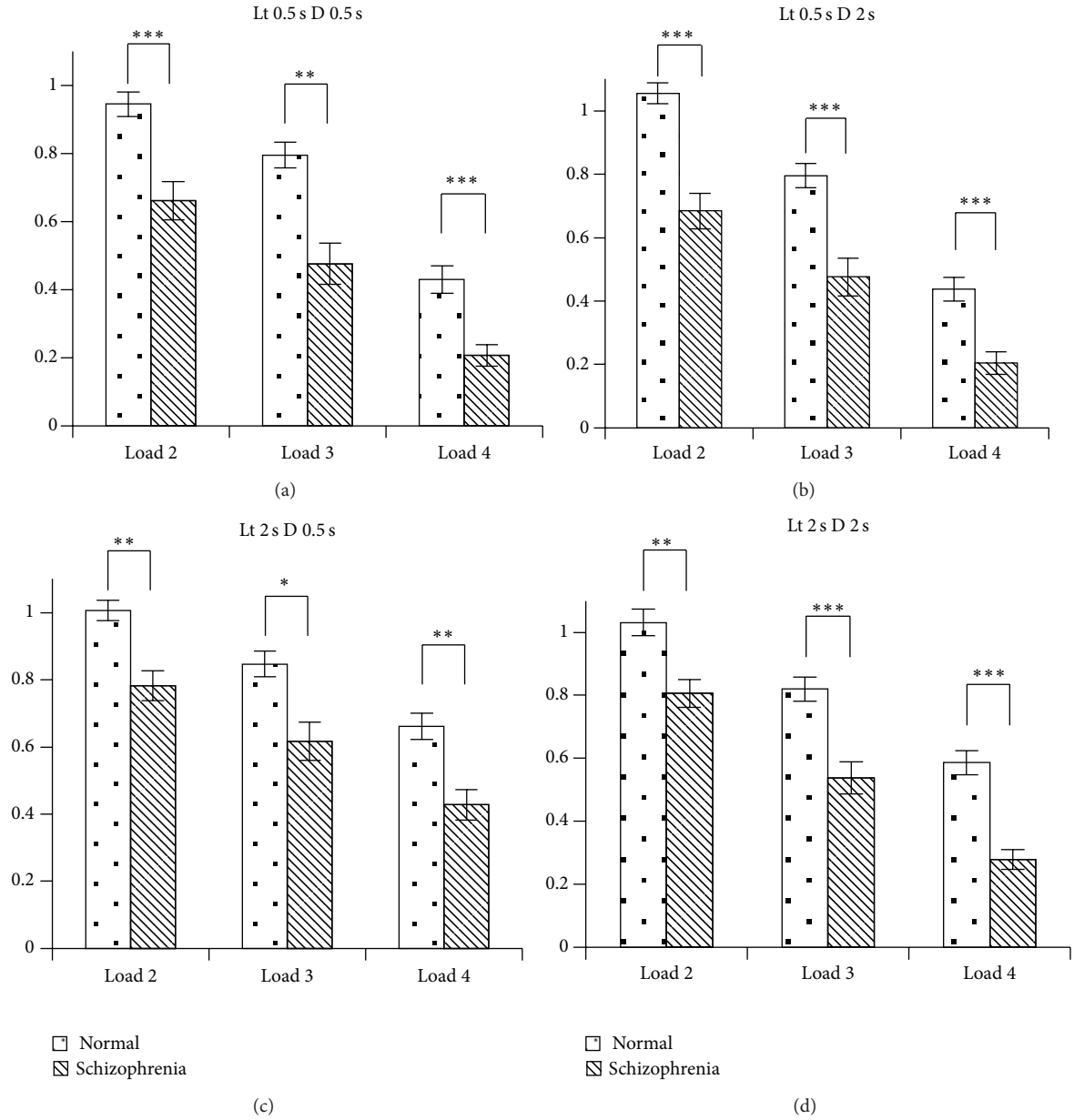

Figure 3: Comparative results of SZ20s and 20 s age groups. a–d show the accuracy per second of SZ20s and 20s age groups, at the different loads of difficulty with combinations of different learning time and delay span. $^{*}P < 0.05$; $^{**}P < 0.01$; $^{***}P < 0.0001$.

schizophrenic and currently undergoing various treatments for schizophrenia. These treatments might influence the performance of spatial working memory and attention in patients. Besides, the age of onset, the course of disease, and education of participants maybe the influence factors, and we made a table (Supplementary Table 6) to show these detailed information. We must treat the conclusion with caution as we cannot exclude the effect of treatment in the current study. Because of these limitations, it is worth testing first-episode schizophrenia patients to confirm SWAPS test results in future studies.

The studies reported the differences in visuospatial processing between males and females [36]. Here, gender was not a dominant factor affecting the score of SWAPS test (Supplementary Table 7).

The test is simple, automatic, and results can be interpreted at the end of the test. Many people can simultaneously take the test. It does not burden the test participant more than requiring a few minutes of time looking at a computer screen. SWAPS was developed with the goal of creating a simple test of working memory and attention for use in clinical studies in China. However, it can be easily adapted by people worldwide as it uses simple symbols. The symbols and duration time also can be easily modified by the investigator for the purposes of their own studies. This short test of attention and spatial working memory may be a useful tool in studying other

mental illness such as attention deficit hyperactivity disorder, major depressive disorders, and bipolar disorder. It may also be used as an objective indicator in determining effects of treatment for neuropsychiatric disorders. Moreover, SWAPS can be combined with fMRI, PET, or EEG methodologies in future studies. As the test is computer-based, it can easily be integrated into many situations and resulting data can be analyzed automatically.

5. Conclusion

SWAPS showed developmental maturation of spatial working memory and attention in ages 20–27 which then declined with increasing age. Schizophrenia patients failed to display a developmental peak of those cognitive abilities in ages 20–29 and had significant deficits compared to control groups in adults. Our data suggests that this simple SWAPS test can be a useful tool for studies of spatial working memory and attention in neuropsychiatric disorders.

Abbreviations

SWAPS: Spatial Working Memory and Attention Test of Paired Symbols
R: Reaction time
C: Percentage of correct choices
Lt: Learning time
D: Delay span.

Acknowledgments

The authors would like to thank all those who participated in the experiment and in the testing process. This work was supported by grants from the National Basic Research Program of China (2010CB529604), National Scientific Foundation of China (81271511), National Science & Technology Pillar Program (2012BAI01B08, 2012BAI01B09), National Key Scientific Research Projects (2013CB967401), Shanghai Pujiang Program (11PJ1405100), "Eastern Scholar," "Shu Guang" project supported by Shanghai Municipal Education Commission and Shanghai Education Development Foundation (10SG14) and "National Major Scientific Instruments Development Project" (2012YQ03026007) to Weidong Li, National Scientific Foundation of China (31171144, 81272177) and National Basic Research Program of China (2011CB711000) to Xiaoping Chen.

References

[1] D. M. Barch and E. Smith, "The cognitive neuroscience of working memory: relevance to CNTRICS and schizophrenia," *Biological Psychiatry*, vol. 64, no. 1, pp. 11–17, 2008.

[2] J. Lee and S. Park, "Working memory impairments in schizophrenia: a meta-analysis," *Journal of Abnormal Psychology*, vol. 114, no. 4, pp. 599–611, 2005.

[3] S. Park and P. S. Holzman, "Schizophrenics show spatial working memory deficits," *Archives of General Psychiatry*, vol. 49, no. 12, pp. 975–982, 1992.

[4] D. L. Braff, "Information processing and attention dysfunctions in schizophrenia," *Schizophrenia Bulletin*, vol. 19, no. 2, pp. 233–259, 1993.

[5] M. I. Posner, T. S. Early, E. Reiman, P. J. Pardo, and M. Dhawan, "Asymmetries in hemispheric control of attention in schizophrenia," *Archives of General Psychiatry*, vol. 45, no. 9, pp. 814–821, 1988.

[6] A. D. Baddeley, *Working Memory, Thought, and Action*, Oxford University Press, UK, Oxford, 2007.

[7] S. Y. Ang and K. Lee, "Central executive involvement in children's spatial memory," *Memory*, vol. 16, no. 8, pp. 918–933, 2008.

[8] R. Lépine, S. Bernardin, and P. Barrouillet, "Attention switching and working memory spans," *European Journal of Cognitive Psychology*, vol. 17, no. 3, pp. 329–345, 2005.

[9] W. K. Kirchner, "Age differences in short-term retention of rapidly changing information," *Journal of Experimental Psychology*, vol. 55, no. 4, pp. 352–358, 1958.

[10] A. Baddeley, "Working memory: looking back and looking forward," *Nature Reviews Neuroscience*, vol. 4, no. 10, pp. 829–839, 2003.

[11] M. R. Johnson, N. A. Morris, R. S. Astur et al., "A functional magnetic resonance imaging study of working memory abnormalities in schizophrenia," *Biological Psychiatry*, vol. 60, no. 1, pp. 11–21, 2006.

[12] S. Sternberg, "High-speed scanning in human memory," *Science*, vol. 153, no. 3736, pp. 652–654, 1966.

[13] S. Della Sala, C. Gray, A. Baddeley, N. Allamano, and L. Wilson, "Pattern span: a tool for unwelding visuo-spatial memory," *Neuropsychologia*, vol. 37, no. 10, pp. 1189–1199, 1999.

[14] S. J. Duff and E. Hampson, "A sex difference on a novel spatial working memory task in humans," *Brain and Cognition*, vol. 47, no. 3, pp. 470–493, 2001.

[15] R. B. Ekstrom and H. H. Harman, *Kit of Factor-Referenced Cognitive Tests*, Educational Testing Service, 1976.

[16] D. Kimura, "Manual activity during speaking—I. Right-handers," *Neuropsychologia*, vol. 11, no. 1, pp. 45–50, 1973.

[17] E. LaBarge, D. Edwards, and J. W. Knesevich, "Performance of normal elderly on the Boston naming test," *Brain and Language*, vol. 27, no. 2, pp. 380–384, 1986.

[18] I. Silverman and M. Eals, "Sex differences in spatial abilities: evolutionary theory and data," in *The Adapted Mind: Evolutionary Psychology and the Generation of Culture*, J. H. Barkow, L. Cosmides, and J. Tooby, Eds., Oxford University Press, New York, NY, USA, 1992.

[19] H. E. Rosvold, A. F. Mirsky, I. Sarason, E. D. Bransome Jr., and L. H. Beck, "A continuous performance test of brain damage," *Journal of Consulting Psychology*, vol. 20, no. 5, pp. 343–350, 1956.

[20] C. K. Conners and M. Staff, *Conners' Continuous Performance Test II, (CPT II V. 5)*, Multi-Health Systems, North Tonawanda, NY, USA, 2000.

[21] S. M. Silverstein, G. Light, and D. R. Palumbo, "The sustained attention test: a measure of attentional disturbance," *Computers in Human Behavior*, vol. 14, no. 3, pp. 463–475, 1998.

[22] J. Legge, *The I Ching*, 1882.

[23] M. Zuoqiu, W. Zhang, S. Guan, P. Ge, Z. Pei, and X. Chen, I Ching in Simple Chinese.

[24] A. Hilton and R. A. Armstrong, "Statnote 6: post-hoc ANOVA tests," *Microbiologist*, vol. 2006, pp. 34–36, 2006.

[25] H. Kwon, A. L. Reiss, and V. Menon, "Neural basis of protracted developmental changes in visuo-spatial working memory," *Proceedings of the National Academy of Sciences of the United States of America*, vol. 99, no. 20, pp. 13336–13341, 2002.

[26] L. van Leijenhorst, E. A. Crone, and M. W. van der Molen, "Developmental trends for object and spatial working memory: a psychophysiological analysis," *Child Development*, vol. 78, no. 3, pp. 987–1000, 2007.

[27] J. T. Coull and A. C. Nobre, "Where and when to pay attention: the neural systems for directing attention to spatial locations and to time intervals as revealed by both PET and fMRI," *The Journal of Neuroscience*, vol. 18, no. 18, pp. 7426–7435, 1998.

[28] H. J. Müller and P. M. A. Rabbitt, "Reflexive and voluntary orienting of visual attention: time course of activation and resistance to interruption," *Journal of Experimental Psychology*, vol. 15, no. 2, pp. 315–330, 1989.

[29] D. S. McNamara and J. L. Scott, "Working memory capacity and strategy use," *Memory and Cognition*, vol. 29, no. 1, pp. 10–17, 2001.

[30] J. T. Townsend and F. G. Ashby, "Methods of modeling capacity in simple processing systems," *Cognitive Theory*, vol. 3, pp. 200–239, 1978.

[31] F. I. M. Craik and E. Bialystok, "Cognition through the lifespan: mechanisms of change," *Trends in Cognitive Sciences*, vol. 10, no. 3, pp. 131–138, 2006.

[32] E. A. Crone, C. Wendelken, S. Donohue, L. van Leijenhorst, and S. A. Bunge, "Neurocognitive development of the ability to manipulate information in working memory," *Proceedings of the National Academy of Sciences of the United States of America*, vol. 103, no. 24, pp. 9315–9320, 2006.

[33] P. J. Olesen, J. Macoveanu, J. Tegnér, and T. Klingberg, "Brain activity related to working memory and distraction in children and adults," *Cerebral Cortex*, vol. 17, no. 5, pp. 1047–1054, 2007.

[34] P. C. M. P. Koolschijn, M. A. Schel, M. de Rooij, S. A. R. B. Rombouts, and E. A. Crone, "A three-year longitudinal functional magnetic resonance imaging study of performance monitoring and test-retest reliability from childhood to early adulthood," *Journal of Neuroscience*, vol. 31, no. 11, pp. 4204–4212, 2011.

[35] A. Reichenberg, A. Caspi, H. Harrington et al., "Static and dynamic cognitive deficits in childhood preceding adult schizophrenia: a 30-year study," *American Journal of Psychiatry*, vol. 167, no. 2, pp. 160–169, 2010.

[36] A. M. Clements-Stephens, S. L. Rimrodt, and L. E. Cutting, "Developmental sex differences in basic visuospatial processing: differences in strategy use?" *Neuroscience Letters*, vol. 449, no. 3, pp. 155–160, 2009.

Hindawi Publishing Corporation
Neural Plasticity
Volume 2013, Article ID 670254, 7 pages
http://dx.doi.org/10.1155/2013/670254

Research Article

Enhanced Expression of NR2B Subunits of NMDA Receptors in the Inherited Glaucomatous DBA/2J Mouse Retina

Ling-Dan Dong,[1,2,3] Jie Chen,[1,2,3] Fang Li,[1,2,3] Feng Gao,[1,3,4] Jihong Wu,[1,3,4] Yanying Miao,[1,2,3] and Zhongfeng Wang[1,2,3,4]

[1] *Institutes of Brain Science, Fudan University, 138 Yixueyuan Road, Shanghai 200032, China*
[2] *Institute of Neurobiology, Fudan University, 138 Yixueyuan Road, Shanghai 200032, China*
[3] *State Key Laboratory of Medical Neurobiology, Fudan University, 138 Yixueyuan Road, Shanghai 200032, China*
[4] *Eye & ENT Hospital, Fudan University, 83 Fenyang Road, Shanghai 200031, China*

Correspondence should be addressed to Yanying Miao; yymiao@fudan.edu.cn and Zhongfeng Wang; zfwang@fudan.edu.cn

Received 8 July 2013; Accepted 14 August 2013

Academic Editor: Sheng Tian Li

DBA/2J mouse has been used as a model for spontaneous secondary glaucoma. Here, we investigated changes in expression of NMDA receptor (NMDAR) subunits and Cdk5/p35/NMDAR signaling in retinas of DBA/2J mice using Western blot technique. The protein levels of NR1 and NR2A subunits in retinas of DBA/2J mice at all ages (6–12 months) were not different from those in age-matched C57BL/6 mice. In contrast, the protein levels of NR2B subunits, in addition to age-dependent change, significantly increased with elevated intraocular pressure (IOP) in DBA/2J mice at 6 and 9 months as compared with age-matched controls. Moreover, expression of Cdk5, p35 and ratio of p-NR2A^{S1232}/NR2A progressively increased with time in both strains, suggestive of activated Cdk5/p35 signaling pathway. However, the changes in these proteins were in the same levels in both strain mice, except a significant increase of p35 proteins at 6 months in DBA/2J mice. Meanwhile, the protein levels of Brn-3a, a retinal ganglion cell (RGC) maker, remarkably decreased at 9–12 months in DBA/2J mice, which was in parallel with the changes of NR2B expression. Our results suggest that elevated IOP-induced increase in expression of NR2B subunits of NMDARs may be involved in RGC degeneration of DBA/2J mice.

1. Introduction

Glaucoma, the second leading cause of blindness worldwide, is a neurodegenerative disease characterized by apoptotic death of retinal ganglion cells (RGCs) and progressive visual field loss [1, 2], which is often associated with high intraocular pressure (IOP). Whilst the mechanisms of RGC death in glaucoma still remain a mystery, glutamate excitotoxicity triggered by overactivation of the N-methyl-D-aspartate receptors (NMDARs) may be a potential risk factor for retinal malfunction in glaucoma [3–5]. Indeed, delivery of NMDA channel blockers has been shown to effectively reduce RGC apoptosis in experimental rat glaucoma models [3, 6–8]. Our recent work also showed that cyclin-dependent kinase 5 (Cdk5)/p35-induced elevation of phosphorylated NR2A subunit of NMDARs at S1232 site (p-NR2A^{S1232}) may contribute to RGC apoptotic death in experimental glaucomatous rats [9].

DBA/2J mouse is a spontaneous model of glaucomatous neurodegeneration, which develops a progressive form of pigmentary angle-closure glaucoma [10–13]. In these mice, IOPs become elevated by 6 months of age, and continued intraocular hypertension results in progressive RGC degeneration [12–17]. This is similar to what is observed in primary open angle glaucoma, which makes the DBA/2J mice represent a useful model to study mechanisms of RGC death of human glaucoma [1, 11]. Previous studies have demonstrated that NMDAR antagonist memantine treatment significantly increased RGC survival in DBA/2J mice by inhibiting mitochondrial OPA1 and cytochrome c release, decreasing Bax gene expression and increasing Bcl-2 gene expression, suggesting that overactivation of NMDARs in the glaucomatous DBA/2J retina may lead to a distinct mitochondria-mediated RGC death pathway [15, 18]. However, whether expression of NMDARs is changed in DBA/2J retina is largely unknown. The only evidence for this is that

no changes in expression of NMDAR subunits were seen in DBA/2J mice by immunohistochemistry in retinal slices [19]. In the present work, we aimed to examine changes in expression of NMDAR subunits and Cdk5/p35/NMDAR signaling in retinas of DBA/2J mice at various ages (3, 6, 9, and 12 months) using Western blot technique.

2. Material and Methods

2.1. Animals. Male DBA/2J mice, obtained from The Jackson Laboratory (Bar Harbor, ME, USA), and age-matched C57BL/6 mice, obtained from SLAC Laboratory Animal Co. Ltd (Shanghai, China), were housed on a 12 h light/dark schedule, with standard food and water provided *ad libitum*. All experimental procedures described here were carried out in accordance with the National Institutes of Health (NIH) guidelines for the Care and Use of Laboratory Animals and the guidelines of Fudan University on the ethical use of animals. During this study, all possible efforts were made to minimize the number of animals used and their suffering.

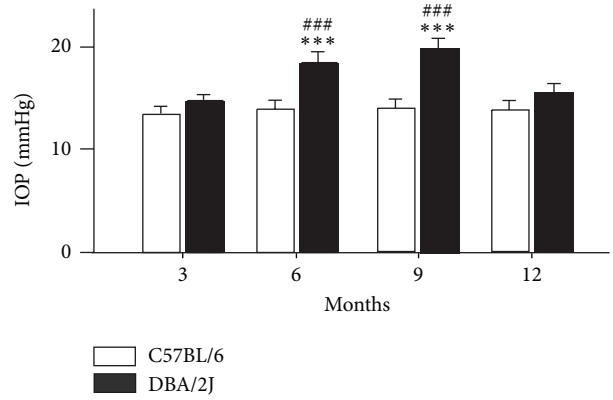

Figure 1: *Changes of IOPs in C57BL/6 and DBA/2J mice at various ages.* Bar chart showing changes of the average IOPs in C57BL/6 and DBA/2J mice at ages of 3 ($n = 24$), 6 ($n = 18$), 9 ($n = 12$) and 12 ($n = 6$) months. All data are presented as mean ± S.E.M. $^{***}P < 0.001$ versus 3-month-old C57BL/6 mice; $^{###}P < 0.001$ versus age-matched C57BL/6 mice.

2.2. IOP Measurement. IOPs of both eyes in DBA/2J mice and age-matched C57BL/6J mice were measured using a hand-held digital tonometer (TonoLab, TioLat, Finland) under general and local anesthesia as described previously [9, 20]. The average value of five consecutive measurements with a deviation of less than 5% was accepted. All measurements were performed in the morning to avoid possible circadian difference.

2.3. Western Blot Analysis. Western blot analysis was conducted as previously described with some modifications [9, 20]. DBA/2J mice or age-matched C57BL/6 mice in different ages (3, 6, 9, and 12 months) were deeply anesthetized with 25% urethane (1.25 g/kg, i.p.). The retinas were removed quickly and snap frozen in liquid nitrogen and then stored at −80°C for further use. Retinas were homogenized in RIPA lysis buffer (50 mM Tris-Cl, 150 mM NaCl, 1% Triton X-100, 0.1% aprotinin, 1 mM phenylmethylsulfonyl fluoride, 1 mM sodium orthovanadate, and 25 mM sodium fluoride, pH 7.4), supplemented with protease and phosphatase inhibitor cocktail (Roche, Mannheim, Germany). The concentration of total proteins was measured using a standard bicinchoninic acid (BCA) assay kit (Pierce Biotechnology, IL, USA). The extracted protein samples (20 μg, 15 μL in volume) were resolved by 8% or 15% SDS-PAGE gel and electroblotted onto PVDF membranes (Immobilon-P, Millipore, Billerica, MA, USA) using Mini-PROTEAN 3 Electrophoresis System and Mini Trans-Blot Electrophoretic Transfer System (Bio-Rad, Hercules, CA, USA). After blocking in 5% nonfat milk at room temperature for 1 h, the membranes were incubated overnight at 4°C with primary antibodies. The primary antibodies used in the present work include anti-NR1 (#05432, 1 : 500, Millipore, Billerica, MA, USA), anti-p-NR2A^{S1232} (#2056, 1 : 500, Tocris Bioscience, MO, USA), anti-NR2A (#320600, 1 : 500, Invitrogen, Carlsbad, CA, USA), anti-Brn-3a (sc-8429, 1 : 1000, Santa Cluz, Biotechnology, CA, USA), anti-Cdk5 (#20502, clone DC17, 1 : 1000, Millipore), anti-NR2B (#06600, 1 : 500, Millipore), anti-p35/p25 (sc-820, 1 : 1000; Santa Cruz Biotechnology), β-actin antibody (A5316, 1 : 2000, Sigma, Saint Louis, MO, USA), and anti-GAPDH (1 : 1000, Cell Signal Technology, MA, USA). After washing in Tris-buffered saline-Tween 20, the membranes were incubated with horseradish-peroxidase-(HRP-) conjugated donkey anti-mouse or donkey anti-rabbit secondary antibody (Thermo Scientific, Rockford, IL, USA) at a 1 : 2500 dilution for 1 h at room temperature. The blots were then incubated with chemifluorescent reagent ECL (Thermo Scientific, Rockford, IL, USA) and exposed to X-ray film in the dark. The experiments were performed in triplicate, and the protein bands were quantitatively analyzed with NIH Image J Analysis software.

2.4. Statistical Analysis. All data are presented as mean ± S.E.M. Statistical analysis was performed by using the Graphpad Prism software (version 5.0; Graphpad Software, San Diego, CA, USA). A one-way or two-way analysis of variance (ANOVA) with nonparametric test (Kruskal-Wallis test), Bonferroni's post hoc test (multiple comparisons), and Mann-Whitney test (comparisons between two groups) was used as appropriate. A value of $P < 0.05$ was considered significant.

3. Results

3.1. Changes in Expression of NMDAR Subunits in DBA/2J Mice at Various Ages. We first monitored changes in IOPs of DBA/2J mice with time. As shown in Figure 1, the average IOP of DBA/2J mice was 14.8 ± 0.5 mm Hg ($n = 24$) at age of 3 months, which was comparable to that of age-matched C57BL/6 control mice (13.6 ± 0.6 mm Hg) ($n = 24$). The average IOP of control mice kept this level at ages of 6, 9, and 12 months, while that of DBA/2J mice significantly increased to 18.5 ± 0.9 mm Hg ($n = 18$, $P < 0.001$) and 19.9 ± 1.0 mm Hg ($n = 12$, $P < 0.001$) at ages of 6 and 9 months, respectively,

and then declined to 15.6 ± 0.8 mm Hg ($n = 6$, $P > 0.05$) at age of 12 months (Figure 1). In the present study, all of the DBA/2J mice showed progressive elevated IOPs. Therefore, our data included all animals.

Expression of NR1 subunit of NMDARs was unchanged at the age of 6 months both in DBA/2J and C57BL/6 mice (101.0 ± 13.2% and 95.0 ± 8.1% of that at age of 3 months (control), $n = 6$, $P > 0.05$) (Figures 2(a) and 2(b)). While expression of this protein increased to 133.4±11.2% of control at age of 9 months in DBA/2J mice ($n = 6$, $P < 0.01$), following by a decline to 90.1 ± 19.2% of control at age of 12 months, it was not different from that of age-matched C57BL/6 mice (128.2 ± 17.1% of control, $P < 0.01$ for 9 months; 110.2 ± 12.1% of control, $P > 0.05$ for 12 months, resp.) (Figures 2(a) and 2(b)). Expression of NR2A subunit was elevated at ages of 9 and 12 months in DBA/2J mice (135.3 ± 14.1% and 148.2 ± 17.2% of control, resp., $n = 6$, all $P < 0.001$), which was comparable to age-matched C57BL/6 mice (125.3 ± 16.1% ($n = 6$, $P < 0.01$) and 140.0 ± 12.1% of control ($n = 6$, $P < 0.001$), resp.) (Figures 2(a) and 2(c)). Meanwhile, the ratio of p-NR2A^{S1232}/NR2A showed a remarkable increase at ages of 6 and 9 months in DBA/2J mice (145.4 ± 16.0% ($n = 6$, $P < 0.001$) and 128.0 ± 17.0% of control ($n = 6$, $P < 0.001$), resp.), and at the age of 6 months in age-matched C57BL/6 mice (134.5 ± 19.0% of control, $n = 6$, $P < 0.01$) (Figures 2(a) and 2(d)). However, the ratio of p-NR2A^{S1232}/NR2A did not show significant difference between DBA/2J and age-matched C57BL/6 mice at all ages. Expression of NR2B subunit was quite different (Figure 2(a)). The average level of NR2B proteins increased to 166.0±19.1% ($n = 6$, $P < 0.05$), 446.3 ± 15.0% ($n = 6$, $P < 0.001$), and 541.4 ± 19.3% of control ($n = 6$, $P < 0.001$) in C57BL/6 mice at ages of 6, 9, and 12 months. Expression of NR2B proteins in DBA/2J mice showed a dramatic increase, with average protein levels being 287.0 ± 29.4% ($n = 6$, $P < 0.001$ versus control and $P < 0.001$ versus age-matched C57BL/6 mice), 517.3 ± 62.0% ($n = 6$, $P < 0.001$ versus control and $P < 0.001$ versus age-matched C57BL/6 mice) and 540.4 ± 58.1% of control ($n = 6$, $P < 0.001$) at ages of 6, 9, and 12 months, respectively (Figures 2(a) and 2(e)).

3.2. Changes in Expression of Cdk5 and p35 in DBA/2J Mice at Various Ages. Since the expression of p-NR2A^{S1232} was at high level (Figure 2), we examined changes of its activator Cdk5 and coactivator p35/p25 [9]. As shown in Figure 3(a), the protein level of Cdk5 progressively increased with time in DBA/2J mice, with the average protein density being 148.1 ± 17.0% ($n = 6$, $P < 0.001$), 169.7 ± 18.1% ($n = 6$, $P < 0.001$), and 165.8 ± 18.0% of control ($n = 6$, $P < 0.001$) at ages of 6, 9, and 12 months, respectively (Figure 3(b)). However, there was no significant difference between DBA/2J mice and age-matched C57BL/6 mice at all ages (Figures 3(a) and 3(b)). Similarly, the p35 protein level gradually increased to 168.7 ± 21.1% ($n = 6$, $P < 0.01$), 229.7 ± 26.3% of control ($n = 6$, $P < 0.001$) in DBA/2J mice at ages of 6 and 9 months, and then slightly declined to 191.3±25.1% of control ($n = 6$, $P < 0.001$) at the age of 12 months (Figures 3(a) and 3(c)). Except at age of 6 months ($n = 6$, $P < 0.001$ versus age-matched C57BL/6 mice), the p35 protein levels at all other ages were comparable to those of age-matched C57BL/6 mice (Figures 3(a) and 3(c)). At the same time, p25 protein, a truncated form of p35, was not detected both in DBA/2J and C57BL/6 mice.

3.3. Changes in Expression of Brn-3a in DBA/2J Mice at Various Ages. We finally examined changes in expression of Brn-3a, a RGC marker, to evaluate RGC damage. Figure 4(a) shows representative Western blot results. The protein level of Brn-3a in DBA/2J mice was higher than that of control mice at ages of 3 and 6 months (127.6 ± 4.8% and 129.9 ± 5.4% of control, $n = 4$, all $P < 0.05$), whereas it decreased to 83.3 ± 2.7% ($n = 4$, $P < 0.05$ versus control and age-matched C57BL/6 mice; $P < 0.01$ versus DBA/2J mice at age of 3 months) and 86.7 ± 1.8% of control ($n = 4$, $P < 0.05$ versus control and age-matched C57BL/6 mice; $P < 0.01$ versus DBA/2J mice at age of 3 months) at ages of 9 and 12 months (Figure 4(b)).

4. Discussion

In the present study, we found that expression of NR2B subunits of NMDARs in retinas of the DBA/2J mice was gradually enhanced with time. Progressive elevated IOP-induced increase in NR2B expression may be associated with RGC degeneration in this glaucomatous model.

Glutamate excitotoxicity has been implicated in glaucomatous RGC death, which is primarily mediated by NMDARs [3, 21]. As a spontaneous glaucomatous model, overactivation of NMDARs by glutamate may be also involved in RGC degeneration of DBA/2J mice. This was supported by the experimental results. First, it was reported that vitreal glutamate content measured with HPLC in DBA/2J mice was higher than that of age-matched controls, and glutamate transporters GLAST and GLT-1v expression in DBA/2J mice showed a decrease by Western blotting [19]. Secondly, blocking NMDARs by memantine inhibited RGC apoptosis and increased RGC survival in DBA/2J mice [15, 18]. It should be noted that time-dependent loss of RGCs in DBA/2J mice started at 6 months of age [16], in parallel with progressive elevation of IOPs and changes of glutamate transporters and glutamate concentration [19].

Previous work has demonstrated that expression of both NMDAR and AMPA receptor (AMPAR) subunits did not show age-dependent change in the retinas of DBA/2J mice by immunohistochemistry [19]. Consistent with this, our results revealed that there was no significant change in expression of NR1 subunits in the retina of DBA/2J mice as compared with age-matched C57BL/6 mice by Western blot analysis. In human glaucomatous eyes, however, NR1 levels showed a decrease [22]. Even though there was no difference between DBA/2J mice and age-matched C57BL/6 mice in the expression of NR2A subunits at all ages, age-dependent increase in NR2A expression was observed at 9 and 12 months in both DBA/2J and C57BL/6 mice (Figure 2(c)). A major finding in this work is that, in addition to age-dependent change, expression of NR2B subunits significantly

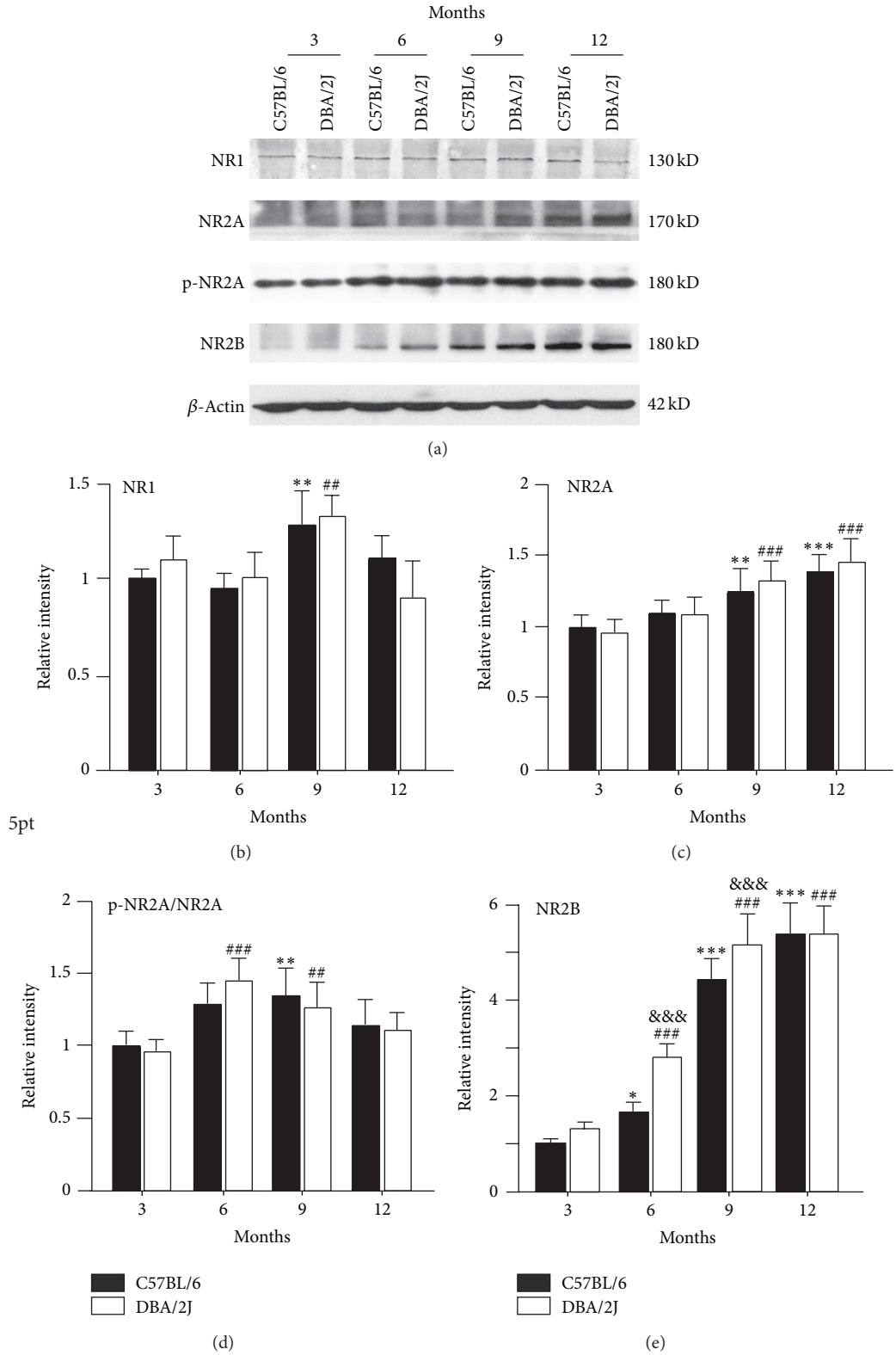

5pt

Figure 2: *Changes in expression of NMDA receptor subunits of DBA/2J mice at various ages.* (a) Representative immunoblots showing the changes of NR1, NR2A, p-NR2A^{S1232}, NR2B levels in DBA/2J and C57BL/6 mice at ages of 3, 6, 9, and 12 months. (b)–(e) Bar chart showing the average densitometric quantification of immunoreactive bands of NR1 (b), NR2A (c), p-NR2A^{S1232}/NR2A (d), and NR2B (e) in DBA/2J and C57BL/6 mice at ages of 3, 6, 9, and 12 months, respectively. $^{*}P < 0.05$, $^{**}P < 0.01$ and $^{***}P < 0.001$ versus 3-month-old C57BL/6 mice; $^{\#\#}P < 0.01$ and $^{\#\#\#}P < 0.001$ versus 3-month-old DBA/2J; $^{\&\&\&}P < 0.001$ versus age-matched C57BL/6 mice.

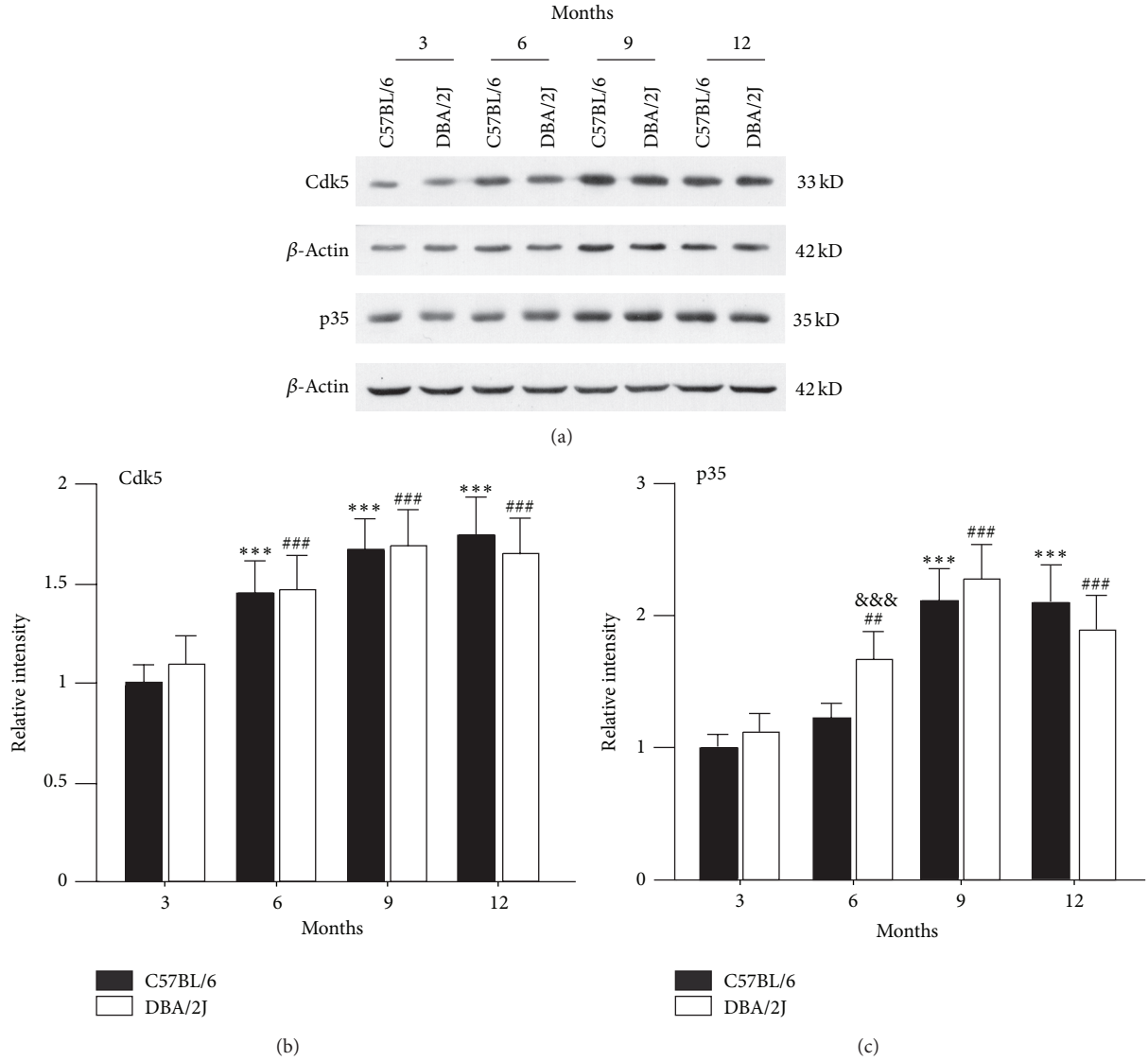

FIGURE 3: *Changes in expression of Cdk5, p35 of DBA/2J mice at various ages.* (a) Representative immunoblots showing the changes of Cdk5 and p35 levels in DBA/2J and C57BL/6 mice at ages of 3, 6, 9, and 12 months. ((b), (c)) Bar chart showing the average densitometric quantification of immunoreactive bands of Cdk5 (b) and p35 (c) in DBA/2J and C57BL/6 mice at ages of 3, 6, 9, and 12 months, respectively. $^{***}P < 0.001$ versus 3-month-old C57BL/6 mice; $^{\#\#}P < 0.01$ and $^{\#\#\#}P < 0.001$ versus 3-month-old DBA/2J; $^{\&\&\&}P < 0.001$ versus age-matched C57BL/6 mice.

increased accompanyied with elevated IOPs in DBA/2J mice (Figure 2(e)). It was recently reported that NMDARs located at the synapse stimulate cell survival pathways, while extrasynaptic receptors signal for cell death [23–26]. NR2B subunits are commonly associated with extrasynaptic locations at the synapse, thus involving in neurologic diseases and some neurodegenerative disorders [24–30]. In the retina, it was reported that NR2A and NR2B subunits were expressed predominantly synaptically and perisynaptically respectively [31]. Therefore, we deduced that excessive glutamate may stimulate the overexpressed extrasynaptic NR2B subunits in DBA/2J mice, thus triggering cell death signals. Consistently, Brn-3a expression was decreased following the changes of NR2B expression (Figure 4), indicating a correlation between overexpression of NR2B and RGC damage. Although Brn-3a expression was highly related to increase of NR2B expression, it is noteworthy that overactivation of NMDARs is not a sole factor for RGC degeneration in DBA/2J mice. Moreover, Brn-3a expression in DBA/2J mice was higher than control at ages of 3 and 6 months. It is possible that as a transcript factor, Brn-3a protein levels could not accurately reflect the number of RGCs, which is worthwhile to be further explored.

Our previous work found that Cdk5/p35 signaling pathway was activated in a rat experimental glaucoma model, and the activated Cdk5/p35 signaling in turn induced an elevation of p-NR2A^{S1232} expression, which contributed to rat RGC apoptotic death [9]. Indeed, we found that the expression of Cdk5, p35 and the ratio of p-NR2A^{S1232}/NR2A progressively

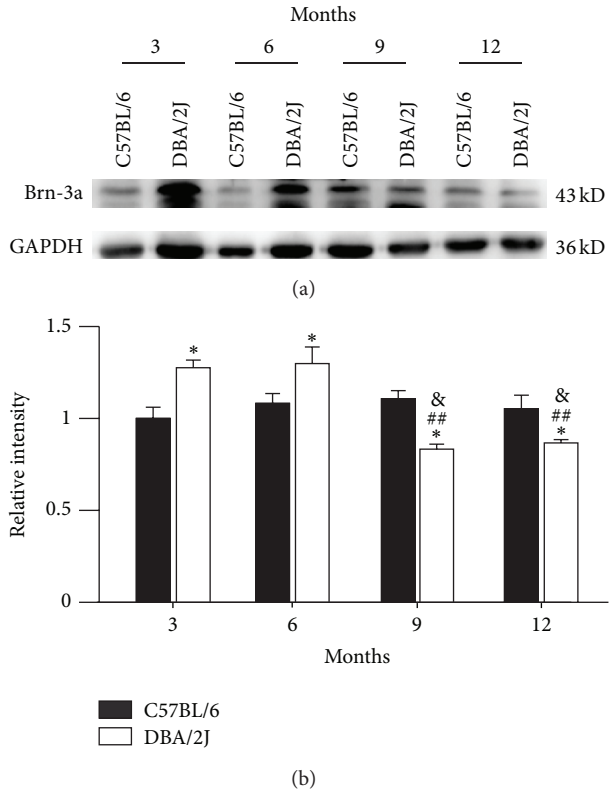

Figure 4: *Changes in expression of Brn-3a of DBA/2J mice at various ages.* (a) Representative immunoblots showing the changes of Brn-3a levels in DBA/2J and C57BL/6 mice at ages of 3, 6, 9, and 12 months. (b) Bar chart showing the average densitometric quantification of immunoreactive bands of Brn-3a in DBA/2J and C57BL/6 mice at ages of 3, 6, 9, and 12 months, respectively. $^{*}P < 0.05$ versus 3-month-old C57BL/6 mice; $^{\#\#}P < 0.01$ versus 3-month-old DBA/2J mice; $^{\&}P < 0.05$ versus age-matched C57BL/6 mice.

increased with time in retinas of DBA/2J mice, suggestive of activated Cdk5/p35 signaling pathway. However, the changes in these protein levels were comparable to those in age-matched C57BL/6 mice, except a significant increase in p35 expression of DBA/2J mice at age of 6 months. These results suggest that progressive moderate elevation of IOP in DBA/2J mice is unlikely a primary factor for activation of Cdk5/p35/NMDAR signaling pathway. Aging plays an important role in activating this signaling pathway. On the other hand, activated Cdk5/p35 signaling pathway may modulate NR2B subunits and increase their expression in DBA/2J mice since it was reported that Cdk5 may indirectly regulate NR2B [32].

In conclusion, our results suggest that NMDARs may be involved in RGC degeneration of DBA/2J mice through two pathways: IOP elevation-induced increase in expression of NR2B subunits and age-dependent activation of Cdk5/p35/NMDAR signaling pathway.

Conflict of Interests

There is no conflict of interests.

Acknowledgments

This work was supported by grants from the National Program of Basic Research sponsored by the Ministry of Science and Technology of China (2013CB835101; 2011CB504602), the Natural Science Foundation of China (30930034; 31070966; 31271173), and the Key Research Program of Science and Technology Commissions of Shanghai Municipality, China (11JC1401200).

References

[1] L. Guo, S. E. Moss, R. A. Alexander, R. R. Ali, F. W. Fitzke, and M. F. Cordeiro, "Retinal ganglion cell apoptosis in glaucoma is related to intraocular pressure and IOP-induced effects on extracellular matrix," *Investigative Ophthalmology & Visual Science*, vol. 46, no. 1, pp. 175–182, 2005.

[2] R. A. Hitchings, "Selective ganglion cell death in glaucoma," *British Journal of Ophthalmology*, vol. 84, no. 7, pp. 678–679, 2000.

[3] L. Guo, T. E. Salt, A. Maass et al., "Assessment of neuroprotective effects of glutamate modulation on glaucoma-related retinal ganglion cell apoptosis in vivo," *Investigative Ophthalmology & Visual Science*, vol. 47, no. 2, pp. 626–633, 2006.

[4] L. A. Levin, "Retinal ganglion cells and neuroprotection for glaucoma," *Survey of Ophthalmology*, vol. 48, no. 2, supplement, pp. S21–S24, 2003.

[5] M. Seki and S. A. Lipton, "Targeting excitotoxic/free radical signaling pathways for therapeutic intervention in glaucoma," *Progress in Brain Research*, vol. 173, pp. 495–510, 2008.

[6] J. I. Calzada, B. E. Jones, P. A. Netland, and D. A. Johnson, "Glutamate-induced excitotoxicity in retina: neuroprotection with receptor antagonist, dextromethorphan, but not with calcium channel blockers," *Neurochemical Research*, vol. 27, no. 1-2, pp. 79–88, 2002.

[7] W. A. Hare, E. WoldeMussie, R. N. Weinreb et al., "Efficacy and safety of memantine treatment for reduction of changes associated with experimental glaucoma in monkey, II: structural measures," *Investigative Ophthalmology & Visual Science*, vol. 45, no. 8, pp. 2640–2651, 2004.

[8] E. WoldeMussie, E. Yoles, M. Schwartz, G. Ruiz, and L. A. Wheeler, "Neuroprotective effect of memantine in different retinal injury models in rats," *Journal of Glaucoma*, vol. 11, no. 6, pp. 474–480, 2002.

[9] J. Chen, Y. Miao, X. H. Wang, and Z. Wang, "Elevation of p-NR2AS1232 by Cdk5/p35 contributes to retinal ganglion cell apoptosis in a rat experimental glaucoma model," *Neurobiology of Disease*, vol. 43, no. 2, pp. 455–464, 2011.

[10] M. G. Anderson, R. S. Smith, N. L. Hawes et al., "Mutations in genes encoding melanosomal proteins cause pigmentary glaucoma in DBA/2J mice," *Nature Genetics*, vol. 30, no. 1, pp. 81–85, 2002.

[11] S. W. M. John, R. S. Smith, O. V. Savinova et al., "Essential iris atrophy, pigment dispersion, and glaucoma in DBA/2J mice," *Investigative Ophthalmology & Visual Science*, vol. 39, no. 6, pp. 951–962, 1998.

[12] R. T. Libby, M. G. Anderson, I. H. Pang et al., "Inherited glaucoma in DBA/2J mice: pertinent disease features for studying the neurodegeneration," *Visual Neuroscience*, vol. 22, no. 5, pp. 637–648, 2005.

[13] C. L. Schlamp, Y. Li, J. A. Dietz, K. T. Janssen, and R. W. Nickells, "Progressive ganglion cell loss and optic nerve degeneration in DBA/2J mice is variable and asymmetric," *BMC Neuroscience*, vol. 7, article 66, 2006.

[14] B. P. Buckingham, D. M. Inman, W. Lambert et al., "Progressive ganglion cell degeneration precedes neuronal loss in a mouse model of glaucoma," *The Journal of Neuroscience*, vol. 28, no. 11, pp. 2735–2744, 2008.

[15] F. Schuettauf, K. Quinto, R. Naskar, and D. Zurakowski, "Effects of anti-glaucoma medications on gangion cell survival: the DBA/2J mouse model," *Vision Research*, vol. 42, no. 20, pp. 2333–2337, 2002.

[16] F. Schuettauf, R. Rejdak, M. Walski et al., "Retinal neurodegeneration in the DBA/2J mouse—a model for ocular hypertension," *Acta Neuropathologica*, vol. 107, no. 4, pp. 352–358, 2004.

[17] D. Reichstein, L. Ren, T. Filippopoulos, T. Mittag, and J. Danias, "Apoptotic retinal ganglion cell death in the DBA/2 mouse model of glaucoma," *Experimental Eye Research*, vol. 84, no. 1, pp. 13–21, 2007.

[18] W. K. Ju, K. Y. Kim, M. Angert et al., "Memantine blocks mitochondrial OPA1 and cytochrome c release and subsequent apoptotic cell death in glaucomatous retina," *Investigative Ophthalmology & Visual Science*, vol. 50, no. 2, pp. 707–716, 2009.

[19] F. Schuettauf, S. Thaler, S. Bolz et al., "Alterations of amino acids and glutamate transport in the DBA/2J mouse retina; possible clues to degeneration," *Graefe's Archive for Clinical and Experimental Ophthalmology*, vol. 245, no. 8, pp. 1157–1168, 2007.

[20] M. Ji, Y. Miao, L. D. Dong et al., "Group I mGluR-mediated inhibition of Kir channels contributes to retinal muller cell gliosis in a rat chronic ocular hypertension model," *The Journal of Neuroscience*, vol. 32, no. 37, pp. 12744–12755, 2012.

[21] X. G. Luo, K. Chiu, F. H. S. Lau, V. W. H. Lee, K. K. L. Yung, and K. F. So, "The selective vulnerability of retinal ganglion cells in rat chronic ocular hypertension model at early phase," *Cellular and Molecular Neurobiology*, vol. 29, no. 8, pp. 1143–1151, 2009.

[22] R. Naskar, C. K. Vorwerk, and E. B. Dreyer, "Concurrent downregulation of a glutamate transporter and receptor in glaucoma," *Investigative Ophthalmology & Visual Science*, vol. 41, no. 7, pp. 1940–1944, 2000.

[23] S. T. Li and J. G. Ju, "Functional roles of synaptic and extrasynaptic NMDA receptors in physiological and pathological neuronal activities," *Current Drug Targets*, vol. 13, no. 2, pp. 207–221, 2012.

[24] G. E. Hardingham, Y. Fukunaga, and H. Bading, "Extrasynaptic NMDARs oppose synaptic NMDARs by triggering CREB shut-off and cell death pathways," *Nature Neuroscience*, vol. 5, no. 5, pp. 405–414, 2002.

[25] A. M. Kaufman, A. J. Milnerwood, M. D. Sepers et al., "Opposing roles of synaptic and extrasynaptic NMDA receptor signaling in cocultured striatal and cortical neurons," *The Journal of Neuroscience*, vol. 32, no. 12, pp. 3992–4003, 2012.

[26] G. E. Hardingham and H. Bading, "Synaptic versus extrasynaptic NMDA receptor signalling: implications for neurodegenerative disorders," *Nature Reviews Neuroscience*, vol. 11, no. 10, pp. 682–696, 2010.

[27] S. Li, M. Jin, T. Koeglsperger, N. E. Shepardson, G. M. Shankar, and D. J. Selkoe, "Soluble A β oligomers inhibit long-term potentiation through a mechanism involving excessive activation of extrasynaptic NR2B-containing NMDA receptors," *The Journal of Neuroscience*, vol. 31, no. 18, pp. 6627–6638, 2011.

[28] R. Rönicke, M. Mikhaylova, S. Rönicke et al., "Early neuronal dysfunction by amyloid β oligomers depends on activation of NR2B-containing NMDA receptors," *Neurobiology of Aging*, vol. 32, no. 12, pp. 2219–2228, 2011.

[29] C. Tackenberg, S. Grinschgl, A. Trutzel et al., "NMDA receptor subunit composition determines beta-amyloid-induced neurodegeneration and synaptic loss," *Cell Death and Disease*, vol. 4, p. e608, 2013.

[30] A. Frasca, M. Aalbers, F. Frigerio et al., "Misplaced NMDA receptors in epileptogenesis contribute to excitotoxicity," *Neurobiology of Disease*, vol. 43, no. 2, pp. 507–515, 2011.

[31] J. Zhang and J. S. Diamond, "Subunit- and pathway-specific localization of NMD a receptors and scaffolding proteins at ganglion cell synapses in rat retina," *The Journal of Neuroscience*, vol. 29, no. 13, pp. 4274–4286, 2009.

[32] S. Zhang, L. Edelmann, J. Liu, J. E. Crandall, and M. A. Morabito, "Cdk5 regulates the phosphorylation of tyrosine 1472 NR2B and the surface expression of NMDA receptors," *The Journal of Neuroscience*, vol. 28, no. 2, pp. 415–424, 2008.